mRNA Localization and Turnover in Mutants of the Small GTPase Arf1p of *Saccharomyces cerevisiae*

Inauguraldissertation

zur

Erlangung der Würde eines Doktors der Philosophie

vorgelegt der

Philosophisch-Naturwissenschaftlichen Fakultät

der Universität Basel

von

Cornelia Kilchert

aus Berlin, Deutschland

Basel, 2010

creative commons

Attribution-Noncommercial-No Derivative Works 2.5 Switzerland

---

You are free:

to Share — to copy, distribute and transmit the work

Under the following conditions:

Attribution. You must attribute the work in the manner specified by the author or licensor (but not in any way that suggests that they endorse you or your use of the work).

Noncommercial. You may not use this work for commercial purposes.

No Derivative Works. You may not alter, transform, or build upon this work.

- For any reuse or distribution, you must make clear to others the license terms of this work. The best way to do this is with a link to this web page.
- Any of the above conditions can be waived if you get permission from the copyright holder.
- Nothing in this license impairs or restricts the author's moral rights.

Your fair dealing and other rights are in no way affected by the above.

This is a human-readable summary of the Legal Code (the full license) available in German:
http://creativecommons.org/licenses/by-nc-nd/2.5/ch/legalcode.de

Disclaimer:
The Commons Deed is not a license. It is simply a handy reference for understanding the Legal Code (the full license) — it is a human-readable expression of some of its key terms. Think of it as the user-friendly interface to the Legal Code beneath. This Deed itself has no legal value, and its contents do not appear in the actual license. Creative Commons is not a law firm and does not provide legal services. Distributing of, displaying of, or linking to this Commons Deed does not create an attorney-client relationship.

Quelle: http://creativecommons.org/licenses/by-nc-nd/2.5/ch/deed.en Datum: 3.4.2009

Genehmigt von der Philosophisch-Naturwissenschaftlichen Fakultät
auf Antrag von

Prof. Dr. Anne Spang und Prof. Dr. Martin Spiess

Basel, den 22. Juni 2010

Prof. Dr. Martin Spiess

Table of contents

Chapter 1

Introduction

1.1 Protein sorting in the cell

A yeast cell expresses more than 5,000 different proteins. Roughly half of them are sorted to membrane-bound organelles (Lodish et al., 2003). Newly synthesized membrane proteins are transported from the endoplasmic reticulum (ER) to the Golgi apparatus where they are routed to the cell surface or to other organelles of the endomembrane system. Transport along the secretory pathway is mediated by vesicles, small membrane-bound carriers that bud from the donor compartment and fuse with an acceptor organelle (Schekman & Orci, 1996; Rothman & Wieland, 1996). Specific coat proteins help to recruit cargo and locally deform the membrane, a process which eventually leads to vesicle budding (Schekman & Orci, 1996). Among the known coat complexes, COPII mediates protein transport from the ER to the Golgi, Clathrin coat is needed to shuttle cargo from the trans-Golgi network (TGN) to the plasma membrane (Bonifacino & Glick, 2004), and COPI-coated vesicles are responsible for retrograde transport from the *cis*-Golgi to the ER and for transport between Golgi stacks (Lee et al., 2004; Figure 1.1). In addition, more specialized coats have been described (Trautwein et al., 2006; Wang et al., 2006). The small GTPase ADP-ribosylation factor 1 (Arf1), which recruits COPI coat and clathrin adaptors, facilitates cargo selection and packaging. It is a crucial determinant in the formation of all types of vesicles at the Golgi as well as in the maintenance of Golgi structure (D'Souza-Schorey & Chavrier, 2006).

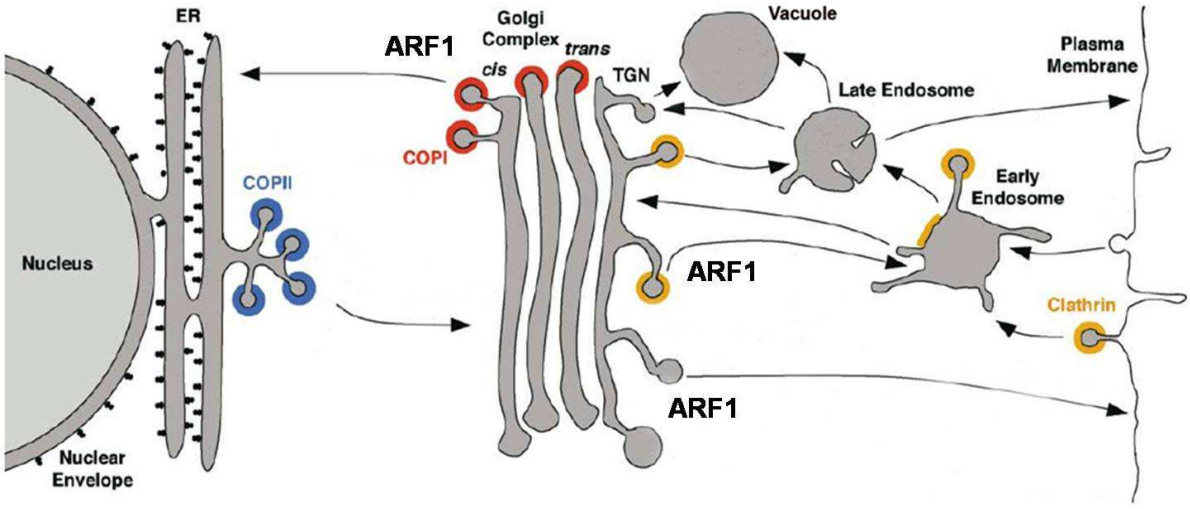

Figure 1.1: The secretory pathway in *S. cerevisiae*(adapted from Bonifacino & Glick, 2004). Arf1p regulates transport at the Golgi, including generation of COPI vesicles that mediate retrograde transport to the ER, and transport from the TGN to various secretory compartments. Each arrow represents a vesicle-mediated transport step, and colored patches represent different vesicular coats.

1.2 The small GTPase Arf1p

ARF proteins function as molecular switches. They exist in a GDP-bound form (inactive) and a membrane-associated GTP-bound form (active; Figure 1.2). Transition from one state to the other requires two different classes of proteins: The first type, guanine nucleotide exchange factors (GEFs), governs the exchange of GDP with GTP, and a conserved Sec7 domain is required for GEF activity (Chardin et al., 1996). In yeast, four ARF-GEFs have been characterized: Gea1p/Gea2p, Sec7p, and Syt1p, which act at different compartments (Franzusoff et al., 1992; Jones et al., 1999; Spang et al., 2001). The second type, GTPase-activating proteins (GAPs), are negative regulators of Arf1p and stimulate its GTPase activity. A zinc-finger motif is required for GAP activity. In yeast, four ARF-GAPs have been described: Glo3p, Gcs1p, Age1p, and Age2p (Poon et al., 1999).

Three different ARF proteins are present in *S. cerevisiae*: Arf1p, Arf2p und Arf3p. Yeast strains with single deletions of *ARF1* or *ARF2* are viable. The double deletion, however, is lethal. Deletion of *ARF1* as well as dominant-active variants of *ARF1* or brefeldin A treatment, which inhibits nucleotide exchange on ARF proteins, lead to a phenotype with a severely disturbed organelle structure (Gaynor et al., 1998). Deletion of *ARF2* does not cause any obvious phenotype. Arf3p is a Class III Arf protein and is not involved in vesicular transport at the Golgi. It is important for cell polarity and the organization of the actin cytoskeleton, but not essential for cell survival (Huang et al., 2003; Lambert et al., 2007; Tsai et al., 2008).

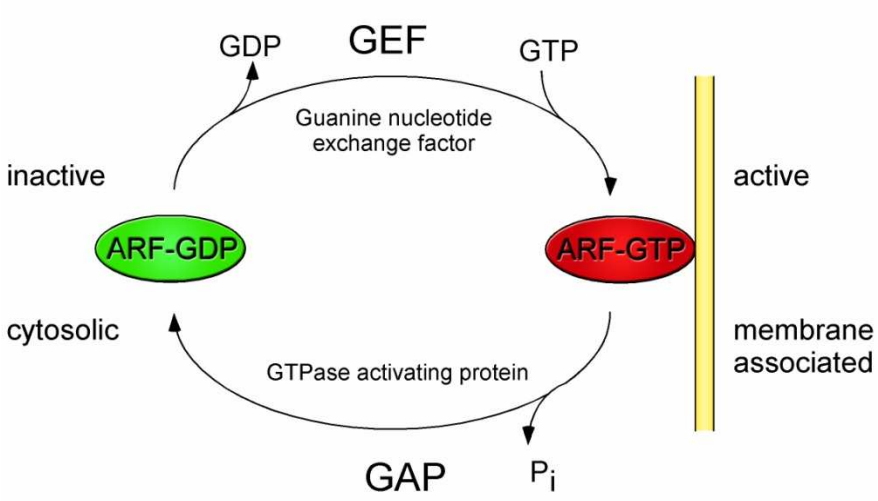

Figure 1.2: The GTPase cycle of Arf1p (adapted from Trautwein, 2004).
Cytosolic, GDP-bound Arf1p is activated with the help of a guanine nucleotide exchange factor (GEF) and becomes associated with Golgi membranes. At the Golgi, recruitment of effector proteins eventually leads to vesicle budding. Inactivation of Arf1p is mediated by GTPase activating proteins (GAPs).

Recently, a differential affinity chromatography screen for novel interactors of Arf1p was carried out in the lab. Using dominant-active and dominant-inactive forms of the small GTPase, the poly(A)-binding protein Pab1p was identified as specific interactor of activated Arf1p (Trautwein et al., 2004). Pab1p is essential, although the capacity to bind poly(A) tails may be dispensable for growth (Burd et al., 1991). It stabilizes mRNAs and is the major translational activator in the cell (Tarun & Sachs, 1995; Figure 1.3).

The interaction between Pab1p and Arf1p was RNase-sensitive. In addition, Arf1p-Pab1p ribonucleoprotein complexes (mRNPs) could be immunoprecipitated from yeast lysates, and vesicular coat components were also part of the complex. Furthermore, the Arf1p-Pab1p-complex was associated with purified COPI vesicles that had been generated from Golgi membranes *in vitro* (Trautwein et al., 2004). From this evidence, it seemed compelling that Arf1p plays a role in mRNA transport and might be involved in post-transcriptional gene regulation.

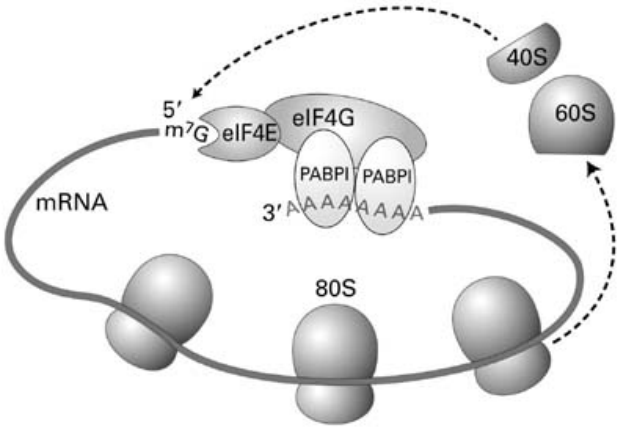

Figure 1.3: The role of Pab1p in translation (Source: Lodish et al., 2003).
Mutliple copies of Pab1p cover the poly(A) tail of an mRNA. Artificial tethering of Pab1p to a tail-less transcript is sufficient to promote mRNA stability, indicating that the major function of the poly(A) tail is recruitment of Pab1p **(Coller et al., 1998)**. During translation, the bridging factor eIF4G brings Pab1p and the cap-binding protein eIF4E into close proximity. The ensuing circularization of the transcript greatly enhances translation efficiency.

1.3 Post-transcriptional gene regulation and mRNA stability

1.3.1 General concepts

mRNA is the universal link between the information encoded in the genome and its expression as a functional protein. It serves as an intermediary between nucleus and cytoplasm, and every step in its life cycle is tightly controlled. Already during transcription, the nascent mRNA becomes associated with RNA-binding proteins (RBPs), and throughout its existence, it will remain part of an mRNP. In fact, more than 10% of all yeast proteins are annotated or predicted RBPs (Hogan et al., 2008). 5' and 3' end processing, splicing, nuclear export, cytoplasmic transport, anchoring, translation, and decay - all of these are regulated processes and important determinants of protein expression. Together, they constitute what is known as post-transcriptional gene regulation (Frey, 2002).

The natural frequency of mRNAs in the cytoplasm is very low. Even ADH1 mRNA, a rather abundant transcript coding for alcohol dehydrogenase, is present in only ~260 copies in an average yeast cell, while PAB1 mRNA frequency has been reported to be as low as ~1.5 molecules per cell on average (Gygi et al., 1999). These numbers are opposed to an estimated 200,000 molecules of Adh1p or 30,000 molecules of Pab1p per cell. Generally, correlation between transcript and protein abundance is weak, and translation efficiencies can vary broadly (Gygi et al., 1999; Arava et al., 2003), which suggests that translation can be modulated at the level of the individual transcript.

For a long time, steady-state levels of mRNAs were believed to be governed predominantly by variations in transcription rates; accordingly, many of the roughly 300 transcription factors present in *S. cerevisiae* have been studied in great detail (Zewail, 2008). However, some evidence indicated that mRNA decay is also closely controlled, e.g. the observation that half-lives for different members of the same protein complex often matched (Wang et al., 2002).

Recently it has become apparent that gene expression is regulated to a large part at the level of mRNA stability. In yeast, decay rates of a multitude of transcripts are altered under high salt conditions (Molin et al., 2009), after diauxic shift (García-Martínez et al., 2005), after oxidative stress (Molina-Navarro et al., 2008), or under osmotic shock (Romero-Santacreu et al., 2009). In human cells, it has been estimated that 50% of all stress genes are regulated through modulation of mRNA half-lives (Fan et al., 2002). As a consequence, García-Martínez et al. (2005) have postulated the existence of "decay regulons", groups of genes that are coordinately regulated at the level of mRNA stability, a hypothesis that calls for the existence of "protein tags" that recognize functionally related transcripts and target them either for decay or for preferential translation (see also Gerber et al., 2004). An increasing number of these proteins have been identified in yeast and other species. This incudes the Puf proteins, e.g. Puf3p, which preferentially binds mRNAs that code for mitochondrial proteins and is required for mitochondrial biogenesis (Gerber et al., 2004; Ulbricht & Olivas, 2008;

García-Rodríguez et al., 2007), and Puf5p, that represses MAP kinase signaling by negatively regulating signal protein mRNAs in the absence of stimuli (Prinz et al., 2007); Pub1p, which affects stability of 10% of all transcripts in yeast (Duttagupta et al., 2005); ARE-binding proteins, which recognize AU-rich elements and are regulated by MAP kinases (Vasudevan & Peltz, 2001); the cell wall stress protein Ssd1p that preferentially associates with mRNAs coding for cell wall-modulating enzymes and is targeted to mRNA-degrading granules upon phosphorylation following cell wall stress (Jansen et al., 2009; E. Weiss, personal communication); and more. Often, mRNAs are bound by multiple RBPs, and may well be subject to combinatorial regulation (Hogan et al., 2008). When Hogan et al. identified transcripts bound to 40 of the total of 600 RBPs present in yeast, 70% of all yeast mRNAs associated with at least one of these proteins, indicating that regulation through RBPs acts on a very broad scale.

1.3.2 Regulation of general translation by reversible phosphorylation o eIF2α

Yeast as a free-living unicellular eukaryote is an excellent model to study translation regulation. Its survival as a species critically depended on quick adaptation to an ever-changing environment, a need that has led to the evolution of several stress response pathways, all of which rely on the relative swiftness of translational control.

Of all stresses, starvation has been best studied with regards to translation regulation. Eukaryotic cells respond to starvation by a general attenuation of protein synthesis and concurrent enhanced translation of specific mRNAs that encode stress-responsive factors like Gcn4p, a transcription factor (Hinnebusch, 2005). In the starved state, nucleotide exchange on the translation initiation factor eIF2 is inhibited by eIF2α phosphorylation, which leads to a decrease in eIF2-GTP-Met-tRNAi, the ternary complex that is rate-limiting for translation initiation (Figure 1.4). As a result, scanning ribosomes can bypass the start codons of upstream ORFs (uORFs) in the leader sequence of GCN4 mRNA which prevent translation initiation at the correct start codon under non-starved conditions (Hinnebusch, 2005). Similarly, mRNAs with internal ribosomal entry sites (IRES) may escape translation attenuation (Fernandez et al., 2002), a process which can require recruitment of Pab1p to A-rich regions (Gilbert et al., 2007). The bulk of transcripts that is released from translation becomes part of silencing mRNPs that aggregate into cytoplasmic processing bodies, or P bodies (PBs).

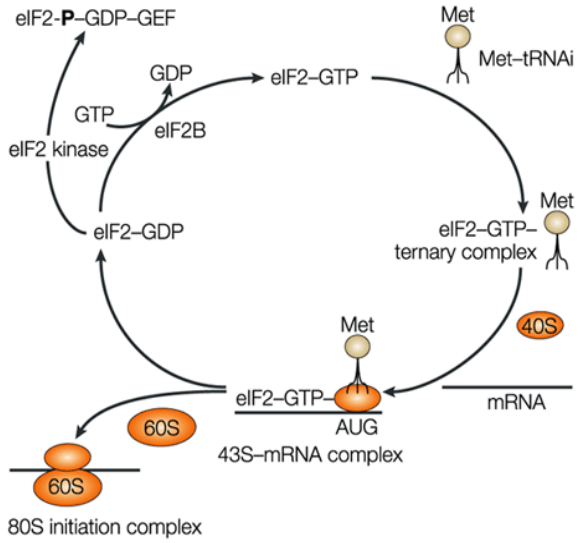

Figure 1.4: The role of eIF2 in translation initiation (Source: Kaufman et al., 2002). In the first step of protein synthesis, the ternary complex of eIF2, GTP and initiator Met–tRNA associates with the 40S ribosomal subunit. Subsequently, mRNA binds, and the 60S ribosomal subunit joins to form the 80S initiation complex. Concomitantly, GTP on eIF2 is hydrolyzed to GDP. For eIF2 to promote another round of initiation, GDP must be exchanged for GTP in a reaction that is catalyzed by the eIF2-GEF eIF2B. Phosphorylation of eIF2α stabilizes the eIF2–GDP–eIF2B complex and prevents GDP–GTP exchange. Because eIF2B concentrations are limiting, the exchange process is inhibited when only a fraction (20-30%) of eIF2α is phosphorylated and in an inactive complex with eIF2B. Phosphorylation of eIF2α therefore immediately reduces the level of functional eIF2, and limits initiation events on all cellular mRNAs within the cell, providing the cell with an efficient and rapid means to respond to various different stress stimuli.

1.3.3 P bodies

PBs are cytoplasmic granules that have been implicated in silencing and decay (Sheth & Parker, 2003). The overall structure of PBs is conserved from yeast to man. They contain extraction-resistant, i.e. protein-bound mRNA that is mostly deadenylated (Sheth & Parker, 2003; Aragon et al., 2006). Proteins linked to PBs sediment to the heavy mRNP fraction in sucrose gradients, but are also found associated with translating ribosomes (Mangus & Jacobson, 1999; Hu et al., 2010). One typical feature of PBs is their inducibility. In yeast, PBs are induced upon a variety of stresses, including starvation, osmotic stress, and oxidative stress (Teixeira & Parker, 2007). In neurons, PBs have been found in close proximity to synapses, indicating a possible role in synaptic plasticity (Zeitelhofer et al., 2008). In short, PBs abound when gross changes in the proteome have to be orchestrated. Supposedly, there are several subpopulations of PBs that vary in their composition, but so far no exhaustive study has been carried out to discern between different types of granules.

PBs had first been shown to contain general decay factors and proteins of the nonsense-mediated decay pathway, which is responsible for the clearance of transcripts that contain premature termination codons (Sheth & Parker, 2003; Sheth & Parker, 2006). In additional experiments, they were demonstrated to contain decay intermediates, to accumulate mRNAs when the major 5'->3' ribonuclease was depleted, and to vanish if mRNAs were protected from decay by stalling them on translating ribosomes (Sheth & Parker, 2003). Thus, PBs were long considered to be mere sites of decay that served a cell-protective function by sequestering the mRNA degradation machinery away from the general cytoplasm (Sheth & Parker, 2003; Cougot et al., 2004; Sheth & Parker, 2006).

By now, the scope of described PB functions has expanded considerably. It was quickly established that transcripts can leave PBs again (Brengues et al., 2005). Thus, mRNAs targeted to PBs are not immediately degraded but can be recycled when the stress is discontinued, especially since removal of the poly(A) tail is often inhibited during stress (Hilgers et al., 2006). This additional role of PBs as sites of mRNA silencing was corroborated when they were found to contain a plethora of translational repressors (Parker & Sheth, 2007), such that, by now, any RBP that is targeted to PBs will be considered a repressor of translation. When a large array of expression datasets was analyzed comparatively, the rapidity of gene induction correlated strongly with the degree of mRNA destabilization(Elkon et al., 2010), indicating that PBs might have an important function in modulating gene expression.

In species capable of RNA interference (RNAi), PBs are the site of miRNA-mediated gene silencing. They harbor the RNAi machinery and are involved in the storage of miRNA-repressed mRNAs (Jakymiw et al., 2005; Liu et al., 2005; Pillai et al., 2005). Viruses and retrotransposons can hi-jack these conserved structures to ensure efficient packaging (Beliakova-Bethell et al., 2006; Checkley et al., 2010). Neuronal RNPs contain many PB components and are essential for long range transport of silenced mRNAs (Kiebler & Bassell, 2006; Barbee et al., 2006). In addition, specialized PBs have been described, e.g. the yeast TAM body (temporal asymmetric MRP body), a single granule where CLB2 mRNA is degraded in telophase and that is asymmetrically localized to the daughter cell (Gill et al., 2006).

1.3.3.1 P body components in yeast

The number of proteins identified as PB components is still expanding. However, by now, the core decay machinery is well characterized (Figure 1.5). In yeast, it comprises the decapping complex Dcp1p/Dcp2p that removes the 5' guanyl cap from deadenylated transcripts, which then become a substrate for 5' to 3' decay by the exonuclease Xrn1p(Decker & Parker, 1993; Muhlrad et al., 1994; Beelman et al., 1996; Dunckley & Parker, 1999).

Alternatively, mRNAs can be eliminated by the exosome, a cytoplasmic multi-protein complex specialized in 3' to 5' decay that does not localize to PBs and targets only a minority of transcripts in yeast (Belostotsky, 2009).

5' to 3' decay is modulated by the decapping promoting factor Edc3p (Kshirsagar & Parker, 2004) and by Dhh1p, a DExD/H-box helicase that promotes mRNA decapping and translational repression (Coller et al., 2001). A second complex, the Lsm-Pat1 complex, is recruited to the 3' end of the mRNA. It shows an inherent affinity to deadenylated mRNA sequences and is required for efficient decapping (Bouveret et al., 2000; Tharun et al., 2000; Tharun & Parker, 2001; Tharun et al., 2005; Chowdhury et al., 2007). Eukaryotic Sm-like (Lsm) proteins form hetero-heptameric complexes that encircle mRNA and have various functions in RNA metabolism, including in splicing and nuclear

RNA processing (Khusial et al., 2005). The cytoplasmic Lsm1-7 complex specifically recruits proteins involved in decapping-dependent degradation and is often stably complexed with the translational repressor Pat1p (Bonnerot et al., 2000; He & Parker, 2000; Salgado-Garrido et al., 1999; Decker et al., 2007; Franks & Lykke-Andersen, 2008; Reijns et al., 2008).

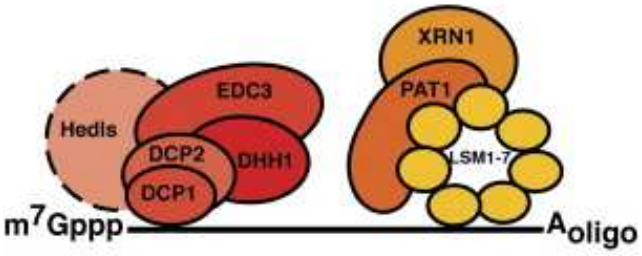

Figure 1.5: Core components of the P body. (Source: Parker & Sheth, 2007).
Two complexes are recruited to mRNAs targeted for degradation: The 5' end is bound by the decapping complex including Dcp1p/Dcp2p, the enhancer of decapping Edc3p, and the helicase Dhh1p. The deadenylated 3' end recruits the Lsm-Pat1 complex that is associated with the exonuclease Xrn1p.

Yeast strains lacking Pat1p show the strongest defects in decapping of any mutant besides those targeting the decapping enzyme Dcp1p/Dcp2p directly (Bonnerot et al., 2000; Bouveret et al., 2000). Cells deleted for *PAT1* and *DHH1* have a decreased number of PBs but show a corresponding increase in polysome-associated mRNA, indicating that decay and translation are balanced and may compete with each other (Coller & Parker, 2005). In general, yeast lacking components of the major mRNA decay pathway, e.g. deleted for *DCP1* or *LSM1*, are deficient in translation repression in response to starvation, in spite of reduced ternary complex levels (Holmes et al., 2004). Conversely, PB formation seems to correlate with defects in translation initiation (Eulalio et al., 2007; Parker & Sheth, 2007). Thus, Parker et al. (2005) have proposed PBs to be in dynamic equilibrium with the polysome fraction of the cell, such that any attenuation of translation initiation would result in a concomitant increase in PBs (Figure 1.6).

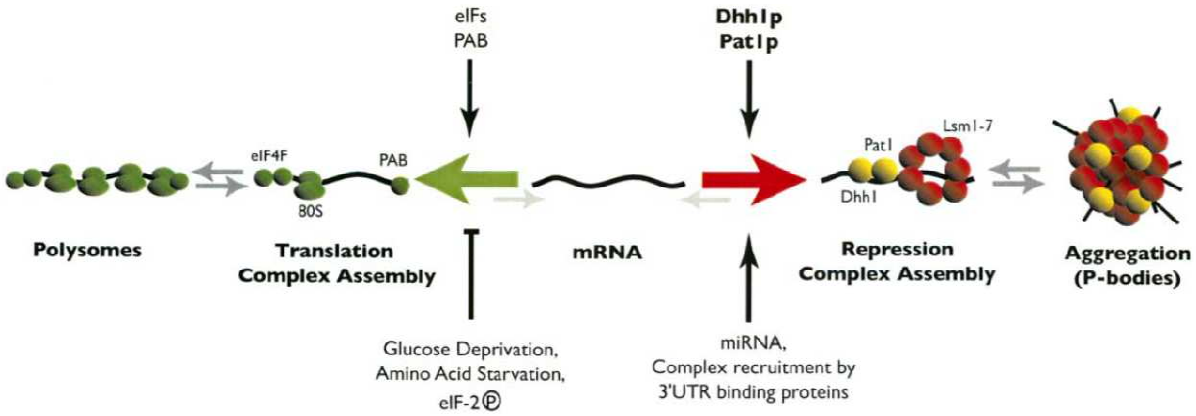

Figure 1.6: The dynamic equilibrium model of translation and repression (Source: Coller & Parker, 2005).
According to this model, a general repression machinery is in constant competition with translation. mRNAs are partitioned between the two competing states and can either associate with the translation machinery and be present in polysomes, or aggregate in a silenced state in P bodies. This equilibrium can be shifted towards PBs by general translation repression (eIF2α phosphorylation) or recruitment of translational repressors to specific mRNAs.

1.3.3.2 PB aggregation

To date, no single protein subunit of the PB has been found to be essential for PB assembly (Teixeira & Parker, 2007). Formation of macroscopic PBs can be prevented by concomitant deletion of Edc3p, which contains a self-interaction domain (YjeF), and the C-terminus of Lsm4p. Both components harbor prion-like glutamine/asparagine-rich domains that can mediate aggregation (Decker et al., 2007; Reijns et al., 2008). Interestingly, the process of aggregation itself does not seem to be required for PB function; it impacts neither on efficient decay of a reporter mRNA nor on general translation repression under starvation conditions (Decker et al., 2007). Similarly, in mammalian cells, RNA-mediated gene silencing does not require aggregation of macroscopic PBs (Eulalio et al., 2007). However, although its significance is not understood, PB aggregation is a conserved feature of eukaryotic cells (Balagopal & Parker, 2009).

Interestingly, 107 proteins in yeast contain prion-like domains (Michelitsch & Weissman, 2000) and roughly half of them are involved in mRNA transport, translation, or degradation, and other aspects of RNA metabolism (Decker et al., 2007). Many PB components contain Q/N-rich regions, and so do all yeast Puf proteins, which regulate specific mRNAs by directly repressing translation and inducing deadenylation (Wickens et al., 2002; Decker et al., 2007; Chritton & Wickens, 2010). Thus, aggregation into macroscopic granules might be a general feature of mRNA metabolism and masking/unmasking Q/N-rich domains a potential mechanism of targeting proteins to PBs

1.3.3.3 Subcellular localization of P bodies

The subcellular localization of PBs does not appear to be strongly conserved across species. In mammalian cells, macroscopic PBs are anchored on microtubules (MTs) and might rely on them for long range transport; so far, no association with membrane-bound organelles has been reported (Aizer et al., 2008). In *Drosophila* oocytes, Trailer hitch, a homolog of the yeast PB component Scd6p, induces the assembly of an endoplasmic reticulum (ER)-associated mRNP that is required for ER exit site function (Wilhelm et al., 2005). *C. elegans* P granules, specialized mRNA-containing bodies that are only present in the germ line and share components with PBs, are the principal sites of mRNA export from the nucleus and localize next to the nuclear membrane; they behave like liquid droplets that condense and disperse (Brangwynne et al., 2009; Sheth et al., 2010).

There is conflicting data on the localization of PBs in yeast: Sweet at al. demonstrated that a temperature-sensitive (ts) allele of α-tubulin (*tub1*) or treatment with benomyl, an MT-depolymerizing agent, induces PBs. Under these conditions, Tub1p colocalized with PBs. Also, a putative tubulin tyrosine ligase, Ybr094wp, relocated to PBs upon glucose starvation. However, disruption of microtubules affected neither translation nor general mRNA stability (Sweet et al., 2007). Conversely, Chang et al. (2008) found Myo2p, one of two class V myosins of *S. cerevisiae*, in a

large mRNP containing PB components. A temperature-sensitive allele of *myo2* delayed PB disassembly but did not affect their formation nor altered their distribution; and, after disruption of actin cables with latrunculin A, PBs were lost from the cell cortex and aggregated in the cytoplasm (Chang et al., 2008). The asymmetric presence of the yeast TAM body in daughter cells is dependent on the other class V myosin, Myo4p (Gill et al., 2006). Taken together, a connection of yeast PBs to the cytoskeleton is very likely. No association with membrane-bound organelles has been described.

1.3.4 Stress granules

Yeast also contains stress granules (SGs; Buchan et al., 2008; Grousl et al., 2009), which had earlier been described as EGP ("eIF4E, eIF4G, and Pab1p-containing") bodies (Hoyle et al., 2007). Like PBs, SGs are induced in response to stress and serve as mRNA storage sites. In contrast to PBs, SGs do not contain any of the major decay factors but translation initiation factors, translational activators, ribosomal subunits, and mRNA that is mostly polyadenylated and might be stalled in translation (Buchan & Parker, 2009).

There is some evidence that PBs mature into SGs under certain conditions (Buchan et al., 2008), however, it might also be that SGs can assemble independently. Their function is, as of yet, poorly defined, largely because their composition is more variable than has been observed for PBs and very much dependent on the stress that induced them (Hoyle et al., 2007; Buchan et al., 2008; Grousl et al., 2009). In other species, SGs are often considerably larger than PBs, and the two types of bodies have been observed to dock, opening the possibility that they exchange protein factors and/or mRNA (Wilczynska et al., 2005; Kedersha et al., 2005; Figure 1.7).

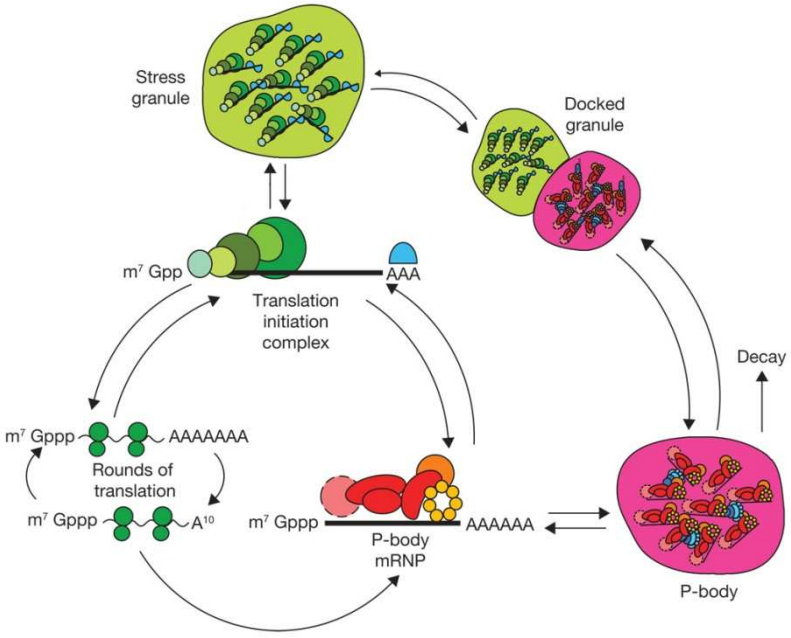

Figure 1.7: Model of the mRNA cycle (adapted form Hilliker & Parker, 2008).
mRNA can exist in at least three different states in the cytoplasm – in polysomes, P bodies (PBs), and stress granules (SGs).
During stress, mRNAs exit the translating pool to enter SGs and PBs, and recruitment of repressors like the Lsm-Pat1 complex can facilitate conversion into the silenced state. mRNPs that aggregate in PBs or SGs can be remodelled and either re-enter translation via different pathways, or become committed for decay.

At this point, it cannot be excluded that the classification of cytoplasmic granules into fixed categories like PBs and SGs is an oversimplification. Instead, the various mRNPs might be snapshots taken from a continuum of different mRNPs that are constantly being remodelled (Buchan & Parker, 2009). Some observations speak for this notion: The composition of the different bodies, especially of SGs, is very variable and dependent on the stress condition that induced them (Kedersha et al., 1999; Stoecklin et al., 2004; Serman et al., 2007); also, SGs seem to "ripen" and change over time (Kedersha et al., 2005; Mollet et al., 2008). Finally, for both types of granules, colocalization between different markers is often incomplete (Tourrière et al., 2003; Tsai et al., 2008), making it tempting to speculate that these bodies follow a maturation pathway, similar to membrane-bound organelles of the Golgi/endosomal system. So far, a time-resolved study of these granules under different stress conditions is lacking.

1.3.5 A link between vesicular transport and translation regulation?

How movement of mRNA to cytoplasmic granules is coordinated is unclear, but transport certainly takes place in form of mRNPs. The cytoskeleton may be involved, but it is quite conceivable that additional carriers are required.

Interestingly, several proteins have been implicated in both PB function and vesicular transport: Dhh1p, the DEAD-box RNA helicase, is required for decapping and frequently used as a marker for PBs, but its deletion also leads to an aberrant vacuolar morphology as well as to defects in α-factor secretion and sorting of carboxypeptidase Y and proteinase A (Fischer & Weis, 2002; Bonilla et al., 2002). In *Drosophila*, the Dhh1p homologue Me31B is required for the silencing of bicoid mRNA, which in turn has been shown to bind to a homologue of Vps36p, a member of the ESCRT-II complex required for vacuolar protein sorting, via its 3'UTR (Nakamura et al., 2001; Irion & St Johnston, 2007).

Scd6p, an RNA-binding, Sm-like protein of unknown function that also localizes to PBs, was first detected in a screen for multicopy suppressors of clathrin heavy chain deficiency (Nelson & Lemmon, 1993; Decker & Parker, 2006) and shows a negative genetic interaction with *SEC28*, a subunit of the COPI coat (Costanzo et al., 2010). In addition, mutations in the *C. elegans* Scd6p-homologue Car-1 lead to a disturbance in ER dynamics (Squirrell et al., 2006). Finally, Trailer hitch, the *Drosophila* homolog of Scd6p, induces the assembly of an mRNP that is required for ER exit site function, where cargo is incorporated into COPII vesicles (Wilhelm et al., 2005).

In the light of all this, it seemed interesting to look at changes in PB morphology in secretory mutants.

1.4 mRNA localization

1.4.1 General mechanisms

Many cases of mRNAs that undergo cytoplasmic transport and acquire a defined subcellular localization have been reported. Until recently, the prevailing view was that localized mRNAs are the exception to the rule, with mRNA transport affecting only select transcripts(Holt & Bullock, 2009). However, when Lécuyer et al. (2007) did a global analysis on mRNA localization in *Drosophila* oocytes and early embryos, a striking 70% of all transcripts displayed some type of subcellular localization. In this study, the authors could distinguish dozens of distinct patterns (Lécuyer et al., 2007). Similarly, in yeast, several classes of localized transcripts have been described: mRNAs are specifically transported to the tip of the growing bud (Takizawa et al., 1997), to the surface of mitochondria (Marc et al., 2002), to the nucleus (Andoh et al., 2006), or to peroxisomes (Zipor et al., 2009).

Generally, mRNA transport occurs in a silenced state in large mRNPs that control movement along cytoskeletal tracks and mediate translational repression (Besse & Ephrussi, 2008). Proteinaceous, "trans-acting" factors are recruited to specific sequence elements in the mRNA ("in cis") either already in the nucleus, e.g. during splicing, or once the transcript has been exported to the cytoplasm (Mili & Macara, 2009). In many cases, the nuclear history is a requirement for correct targeting (Giorgi & Moorem, 2007).

Movement in the cytoplasm is often mediated by motor proteins (for review, see Bullock, 2007). In many cases, mRNAs are transported by dynein and/or kinesin along microtubule tracks. In yeast, asymmetric localization of ASH1 mRNA requires the actin/myosin system (Takizawa et al., 1997). Alternative modes of localization include diffusion combined with local entrapment or local protection from degradation (St Johnston, 2005; see Figure 1.8).

Efficient mechanisms are in place to relieve translational repression once the destination has been reached, e.g. phosphorylation of the translational repressor at the target site. This has been reported for mammalian ZBP1, which transports β-actin mRNA until it becomes phosphorylated by Src (Hüttelmaier et al., 2005), and for Khd1p, that silences ASH1 mRNA and is phosphorylated by Yck1p at the yeast bud tip (Paquin et al., 2007).

To prevent diffusion from the target site, mRNAs are often anchored. Sometimes, specific anchoring factors are involved. In the case of ASH1, anchorage requires translation of the message (Gonzalez et al., 1999)

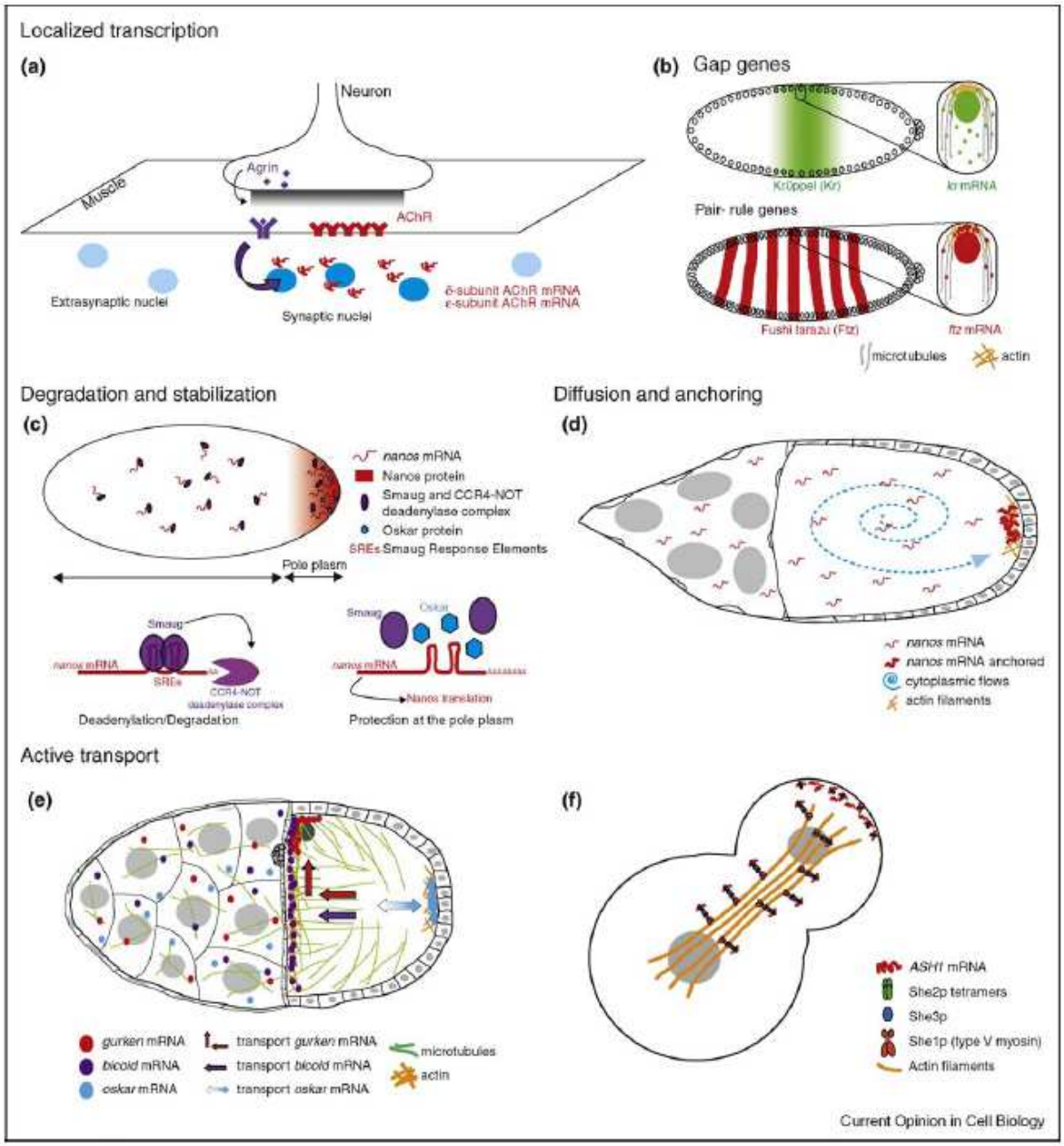

Figure 1.8: A survey of the different mechanisms of mRNA localization (Source: Meignin & Davis, 2010).
(**a, b**) **Localized transcription.** (**a**) Local transcription of AChR mRNA in synaptic nuclei at the activated neuromuscular junction. (**b**) Local transcription followed by active transport in the *Drosophila* syncytial blastoderm embryo. The expression of Gap and Pair-rule genes are both restricted to particular regions of the blastoderm embryo. While transcripts of the Gap gene krüppel are not localized in relation to the peripheral nuclei, mRNAs of the Pair-rule gene fushi tarazu are anchored apically after transport on microtubules. (**c**) **Degradation and stabilization**. In *Drosophila* embryos, Smaug binds SREs (Smaug Response Elements) in nanos mRNA and recruits the CCR4-NOT deadenylase complex to delocalized transcripts, which are then degraded. At the pole plasm, recruitment of Smaug to nanos mRNA is inhibited by Oskar and translation can occur. (**d**) **Diffusion and anchoring**. During *Drosophila* late oogenesis, contraction of the nurse cells creates a cytoplasmic flow that facilitates diffusion of nanos mRNA. nanos mRNAs is anchored at the posterior pole in an actin-dependent manner. (**e, f**) **Active transport.** (**e**) During *Drosophila* mid-oogenesis, localization of gurken, bicoid and oskar mRNA is microtubule-dependent. Arrows represent the transport of these mRNAs. gurken and bicoid mRNA require dynein and localize in two steps or a single step, respectively. The localization of oskar mRNA is kinesin-dependent; it moves randomly with a slight posterior bias. (**f**) In budding yeast, ASH1 mRNA is transported by myosin along actin filaments into the daughter cell.

1.4.2 Significance of mRNA localization

Intracellular mRNA sorting can serve multiple purposes. First, it is a way to achieve cell polarity. There are frequent examples where mRNA localization is employed to set up a protein gradient that induces cell polarization, e.g. in the case of bicoid and oskar, two morphogens needed for correct axis formation during *Drosophila* embryogenesis (Berleth et al., 1988; Kim-Ha et al., 1991). In yeast, asymmetric expression of Ash1p induces a mating type switch only in the daughter cell (Takizawa et al., 1997). In mammalian cells, β-actin mRNA is targeted to the sites of polarized growth. Subsequent localized translation of the message results in polarization of the migrating cell (Condeelis & Singer, 2005). In general, restricting synthesis of a protein to a specific subcellular location allows cells to side-step potential harmful effects that its ectopic expression might have. On-site storage permits a fast local activation of translation in response to extrinsic cues, a mechanism that is especially important in large cells, such as neurons, where many cases of axonal mRNA transport have been described (Holt & Bullock, 2009).

mRNA localization does not always correlate with the localization of its protein product. It has been suggested that proteins translated from localized mRNAs can have unique properties that distinguish them from the same protein synthesized elsewhere (Mili & Macara, 2009). For example, Elk-1, a neuronal transcription factor, can mediate cell death when its translation occurs in dendrites, but not when it is synthesized in the cell soma, a difference that might be due to distinct posttranslational modifications in the different subcellular environments (Barrett et al., 2006).

In other cases, spatially coordinated translation of proteins may facilitate complex assembly. Peripherin, a component of intermediate filaments, forms insoluble particles; to prevent unproductive aggregation, peripherin filaments assemble cotranslationally from mRNPs anchored to microtubules (Chang et al., 2006). In some cases, mRNA targeting can be required for delivery of the encoded protein to the correct membrane. In yeast, for example, the mRNA for the plasma membrane proteolipid Pmp1p associates with the plasma membrane, which is presumably needed to efficiently insert the transmembrane domain into the lipid bilayer (Loya et al., 2008). Likewise, in *Drosophila* follicle epithelial cells, correct localization of crumbs mRNA is required in order to restrict the transmembrane protein Crumbs to the apical membrane (Li et al., 2008).

1.4.3 mRNA localization to membranes

Although *bona fide* vesicular mRNA transport has not been reported in any organism, some enveloped retroviruses are known to utilize the host's vesicular transport machinery to transport the viral genomic RNA to the cell surface (Cohen, 2005).

In addition, there is evidence that cells use membranous structures to localize specific mRNAs asymmetrically. Most examples come from the field of developmental biology and take place

when cell polarity is first established (for review, see Cohen, 2005). In order to efficiently localize mRNA, it seems to have proven advantageous to "hijack" existing transport systems, e.g. through coupling mRNA transport to the bulk movement of organelles. In addition, membrane-bound organelles are frequently used as anchoring sites to maintain an mRNA at its place once an asymmetric distribution has been achieved.

The ER appears to constitute an mRNA hub in that it serves as an anchorage site for localized mRNAs in several species. In *Xenopus* oocytes, vegetal cortex-localized mRNAs associate with ER membranes (Deshler et al., 1997). In budding yeast, asymmetrically localized mRNAs co-migrate with cortical ER into the incipient bud and their transport has been linked to the inheritance of ER to daughter cells (Estrada et al., 2003; Schmid et al., 2006). Similarly, in *Drosophila* oocytes, gurken mRNA is recruited to ER-associated mRNPs. These mRNPs are enriched in transcripts encoding ER exit site components and are required for proper ER exit site function (Wilhelm et al., 2005).

In dorsal root ganglia neurons, a subunit of the COPI coat promotes axonal transport of κ opioid receptor mRNA (Bi et al., 2007). Also in *S. cerevisiae*, the secretory system has been implicated in mRNA transport. As stated above, more than 30 different mRNAs are selectively transported into the bud, including ASH1 mRNA, the first asymmetrically localized mRNA to be described in a unicellular organism (Long et al., 1997; Shepard et al., 2003; Aronov et al., 2007). The directional transport of ASH1 mRNA occurs on ER tubules (Schmid et al., 2006) and involves a specialized actin-myosin transport system, the SHE machinery, which comprises at least five proteins (Jansen et al., 1996; Long et al., 2000; Böhl et al., 2000). Even though a functional SHE machinery is sufficient for the transport of ASH1 mRNA to the distal pole of the bud, additional factors are required for its efficient anchoring at the cortex, and genetic evidence points to vesicular transport as a prerequisite for maintenance of correct ASH1 mRNA localization. For example, deletion of *ARF1* leads to delocalization of ASH1 mRNA in a high percentage of budding yeast cells (Trautwein et al., 2004). Some temperature-sensitive *arf1* alleles exhibit a similar phenotype, although to a varying degree, while some *arf1* mutants with pronounced protein sorting defects do not display any ASH1 mRNA localization phenotype. ASH1 mRNA is also delocalized in other secretory mutants, including *sar1-D32G* and a *sec23-1* strain, both of which are deficient in COPII vesicle formation, and in several mutants of the late secretory pathway (Trautwein et al., 2004; Aronov & Gerst, 2004). In some, but not all, of these secretory mutants, a disruption of the actin cytoskeleton is the most likely cause for the observed delocalization of ASH1 mRNA (Aronov & Gerst, 2004).

Manifestly, not all essential components of vesicular transport are necessary for correct ASH1 mRNA localization, so does neither a *sec27-1* nor a *sec28-1* mutant, where the β' and the ε subunit of coatomer are dysfunctional, respectively, display an ASH1 mRNA localization phenotype

(Trautwein et al., 2004). How the secretory system contributes to successful ASH1 mRNA localization is not understood.

1.4.4 mRNAs at the ER

Apart from these specialized cases, there are instances of bulk transport of mRNA in the cytoplasm. The most prominent example is the signal recognition particle (SRP)-dependent delivery of transcripts encoding secreted or membrane-bound proteins to the ER, which ensures efficient cotranslational insertion of these proteins into the ER lumen (Walter & Blobel, 1981).

Many secreted proteins are essential. Still, yeast cells can adapt to the loss of the SRP pathway by inducing a response similar to the unfolded protein response (UPR; Mutka & Walter, 2001), indicating that additional mechanisms are in place which ensure that mRNAs that encode secreted proteins reach the ER. Cell fractionation experiments in yeast and human T-cells followed by microarray analysis revealed that many transcripts are enriched at the ER, including numerous mRNAs that encode cytosolic proteins (Diehn et al., 2000). Similar results were obtained in NIH3T3 cells with *in situ* hybridization, an approach that rules out fractionation artifacts (Lerner et al., 2003). Although at first this result was surprising, there is emerging evidence that ER association might be used to compartmentalize translation. For example, during UPR, general translation in the cytoplasm is attenuated, while translation on membrane-bound ribosomes is sustained (Stephens et al., 2005). The same was observed when mammalian cells were exposed to arsenite stress (Unsworth et al., 2010). Thus, there may be two distinct pools of polysomes that can be regulated differentially, one of them membrane-associated, one of them cytosolic. Shuffling mRNAs from one pool to the other might be a means to adjust their translational status.

The protein machinery involved in such a process has not been identified; however, the mRNA-binding protein Scp160p is associated with polysomes at the ER, but not enriched on cytosolic polysomes (Weber et al., 1997; Frey et al., 1997), and there might be more factors that similarly discriminate between different ribosomal pools.

Scp160p is known to form RNase-sensitive complexes with Pab1p. Although all types of polyadenylated mRNA are found in Scp160p-mRNPs, Scp160p shows preferential association with a subset of transcripts and has been implicated in translational regulation (Li et al., 2003; Hogan et al., 2008). Interestingly, there are numerous links between Scp160p and Arf1p-mediated vesicular transport: Scp160p interacts physically with the ARF-GEF Gea1p and acts as multicopy suppressor of at least one known *GEA1* mutation, gea1-4 Δgea2 (Peyroche & Jackson, 2001). Scp160p-mRNPs contain Bfr1p, that also coimmunoprecipitates with Arf1p (Lang & Fridovich-Keil, 2000; Trautwein et al., 2004). Bfr1p was detected as a multicopy suppressor that confers resistance to brefeldin A, an inhibitor of Arf1p activation (Jackson & Képès, 1994; Peyroche et al., 1999). Moreover, a double deletion of *ARF1* und *BFR1* is lethal (Trautwein et al., 2004). Since Arf1p-Pab1p-mRNPs were found

on purified COPI vesicles and these are bound for the ER, we hypothesized that specific mRNA can "hitch a ride" on the surface of COPI vesicles, which could provide a mechanism how transcripts can be moved from one ribosomal "compartment" to the other.

1.5 The model system: temperature-sensitive *arf1* alleles

In this project, an array of temperature-sensitive *arf1* alleles in a *Δarf2* background is used (Yahara et al., 2001). Although Arf1p is by far the most abundant Arf protein and represents 90% of the total cellular Arf content, *ARF2* deletions are employed in order to rule out the influence of Arf2p, since Arf1p and Arf2p are 96% identical and functionally redundant (Stearns et al., 1990). Thus, in the strains used, Arf function is solely provided by the temperature-sensitive *arf1* allele.

All mutants show divergent sorting defects and belong to different intragenic complementation groups, which indicates that different functions of Arf1p are compromised. Under non-permissive conditions, *arf1-11* has severe defects in retrograde vesicular trafficking between Golgi and the ER. In *arf1-18*, vesicles accumulate in the cytoplasm, probably due to an impairment of intra-Golgi transport (Yahara et al., 2001). Both strains are unable to asymmetrically localize ASH1 mRNA after temperature shift (Trautwein et al., 2004). A third mutant, *arf1-17*, missorts proteins to the vacuole and the plasma membrane and is defective in retrograde transport to the ER (Yahara et al., 2001); in this mutant, asymmetric mRNA localization is not affected (Trautwein et al., 2004).

Chapter 2

Aim of this study

The small ras-like GTPase Arf1p, a Golgi-localized and vesicle-associated protein, plays a pivotal role in membrane trafficking. It regulates budding of COPI vesicles and certain types of clathrin-coated vesicles in *S. cerevisiae*. Recently, it has been shown that Arf1p is part of an mRNP complex that contains Pab1p, the poly(A)-binding protein, and that this complex is recruited to the surface of COPI vesicles that mediate Golgi to ER transport. This finding raised the interesting possibility that Arf1p has additional functions in mRNA transport and/or translation regulation.

It has lately become apparent that subcellular localization is of tremendous importance in mRNA metabolism. Depending on the physiological state of the cell, specific mRNAs are shuttled to and away from certain cytoplasmic locations, which strongly influences their translational status. How movement of mRNA to these different locations is coordinated is unclear, but transport certainly takes place in form of mRNPs, and we wanted to establish whether vesicular transport was involved.

Chapter 3

Intracellular signals regulate P-body number in *S. cerevisiae* in response to stress

3.1 Defects in the secretory pathway and high Ca^{2+} induce multiple P-bodies

The following manuscript was submitted to Molecular Biology of the Cell and was accepted for publication on May 17, 2010. The following authors have contributed to the manuscript:

Cornelia Kilchert performed the experiments represented in the following figures: Fig. 1 A, B, D, and E; Fig. 2 A-D, H, and I; Fig. 3 B, D, and F; Fig. 4; Fig. 5 A -D; Fig. 6 A-F; Fig. 7 A, B, and E; Suppl. Figs. 1, 2 A, and 3. She wrote parts of the manuscript and provided critical comments on the rest.

Julie Weidner constructed the strains *arf1-11 cmd1-3*, *arf1-11 ⊿gcn2*, and *arf1-11 ⊿ire1*. She performed all experiments on stress granules, including strain construction, i.e. Figs. 1 C, 2 F and G, and Suppl. Fig. 2 B, and provided critical comments on the manuscript.

Cristina Prescianotto-Baschong did the EM analysis on PBs (Fig. 7 C and Suppl. Fig. 4).

Anne Spang did several experiments on PB rescue and analyzed the EM data. She contributed the following figures: 3 A and C, 5 A; Fig. 6 A and Fig. 7 D. She wrote the manuscript.

The figure numbering was adapted to fit into this work.

Defects in the secretory pathway and high Ca^{2+} induce multiple P-bodies

Cornelia Kilchert, Julie Weidner, Cristina Prescianotto-Baschong, and Anne Spang
Biozentrum, Growth and Development, University of Basel, Klingelbergstrasse 70, CH-4056 Basel, Switzerland

Corresponding author:
Anne Spang
Biozentrum
University of Basel
Klingelbergstrasse 70
CH-4056 Basel
Switzerland

Email: anne.spang@unibas.ch

Keywords: processing bodies, stress granules, mRNA, *ARF1*, osmotic stress, secretory pathway, Calcium, calmodulin, mRNA metabolism, signaling pathways

Running title: Ca^{2+}-induced P body formation

Abstract

mRNA is sequestered and turned over in cytoplasmic processing bodies (PBs), which are induced by various cellular stresses. Unexpectedly, in *S. cerevisiae*, mutants of the small GTPase Arf1 and various secretory pathway mutants induced a significant increase in PB number, as compared to PB induction by starvation or oxidative stress. Exposure of wild-type cells to osmotic stress or high extracellular Ca^{2+} mimicked this increase in PB number. Conversely, intracellular Ca^{2+}-depletion strongly reduced PB formation in secretory mutants. In contrast to PB induction through starvation or osmotic stress, PB formation in secretory mutants and by Ca^{2+} required the PB components Pat1 and Scd6, and calmodulin, indicating that different stressors act through distinct pathways. Consistent with this hypothesis, when stresses were combined, PB number did not correlate with the strength of the translational block, but rather with the type of stress encountered. Interestingly, independent of the stressor, PBs appear as spheres of about 40-100 nm connected to the endoplasmic reticulum (ER), consistent with the idea that translation and silencing/degradation occur in a spatially coordinated manner at the ER. We propose that PB assembly in response to stress occurs at the ER and depends on intracellular signals that regulate PB number.

Introduction

Cells adapt to stress by varying their proteome. These changes in protein expression can be achieved through transcriptional and translational control or through changes in protein stability. Stress causes attenuation of general translation, while the translation of a subset of mRNAs is upregulated. Many mRNAs are sequestered in P bodies (PBs) or stress granules (SG) in response to stress. In SGs, mRNAs are stored until the stress is alleviated and the mRNAs can return to the cytosol (Coller & Parker, 2005). PBs on the other hand, are sites of mRNA storage and turn-over. The stress conditions that result in either PB or SG formation are only partially overlapping. Recent evidence suggests that PB formation could precede stress granule formation, and PBs could mature either into stress granules or into mRNA-degrading PBs (Buchan et al., 2008). However, SGs could potentially also form independently from PBs. While the mechanism of SG assembly still remains elusive, more is known about PB assembly. According to the current model, two separate complexes bind the mRNA, the decapping complex at the 5' end and the Lsm-Pat1 complex at the 3' end of the mRNAs, to promote interaction between different mRNPs to allow PB assembly (Decker et al., 2007; Franks & Lykke-Andersen, 2008; Reijns et al., 2008). Thus, loss of one complex may reduce the efficiency with which PBs are formed. In yeast, the decapping complex contains the decapping proteins Dcp1 and Dcp2 and the decapping promoting factor Edc3. The 3'-binding Lsm-Pat1 complex consists of Sm and Sm-like proteins (Lsm), which form two heptameric rings that encircle the RNA (Salgado-Garrido et al., 1999) and to which the decapping activator Pat1 is recruited. The Lsm-Pat1 complex shows an inherent affinity to deadenylated mRNA sequences (Bouveret et al., 2000; Tharun et al., 2000; Tharun & Parker, 2001; Tharun et al., 2005; Chowdhury et al., 2007). PB formation seems to correlate with defects in translation initiation, while translation elongation problems do not cause PBs to form (Eulalio et al., 2007; Parker & Sheth, 2007). Despite what is known about PB assembly, it is still debated if PBs are merely aggregations of 'unused' mRNA or whether PB assembly is regulated through distinct signals.

Components of the secretory pathway are responsible for the transport of proteins and lipids between cellular compartments as well as to the cell surface. Intracellular trafficking components have been implicated in mRNA transport (Aronov & Gerst, 2004; Trautwein et al., 2004; Bi et al., 2007). Interestingly, Deloche et al. (Deloche et al., 2004) showed that in yeast at least a subset of secretory transport mutants failed to properly initiate translation. This translation attenuation is likely a

consequence of membrane stress caused by blocks along the secretory pathway. Given that blocked translation initiation can lead to PB formation (Eulalio et al., 2007; Parker & Sheth, 2007), we asked whether mutants in the secretory pathway also promote PB formation in *S. cerevisiae*. We found that many more PBs were formed in secretory transport mutants than after induction of PBs upon starvation in wild-type cells. The PBs observed in secretory mutants and upon starvation were indistinguishable by size or by Dcp2-myc and Dhh1-myc content, as judged by immuno electron microscopy. Dcp2-myc and Dhh1-myc formed sphere-like structures 40-100 nm in diameter. The multiple PB phenotype was also induced in wild-type cells by the application of hyperosmotic shock or by increasing extracellular Ca^{2+} levels. The induction of numerous PBs in response to membrane stress required functional calmodulin and the PB components Scd6 and Pat1. Interestingly, mutations in calmodulin or deletion of *PAT1*, or *SCD6*, did not interfere with PB induction through starvation or hyperosmotic shock. The effect of inducing PBs under starvation and Ca^{2+} was additive since the block in translation initiation was much stronger when stresses were combined, but nevertheless multiple PBs were induced. Our results demonstrate that distinct signaling pathways are in place to induce PB production depending on the stress encountered and hence PB formation is more than just the mere consequence of a block in translation initiation. In this study we uncover that PB assembly is not the result of aggregation, but induced through distinct pathways, one of which requires calmodulin.

Results

P body number is increased in *arf1* mutants

Several mutants in the secretory pathway lead to attenuation of translation (Deloche et al., 2004). In addition, specific mutant alleles of the small GTPase Arf1 are defective in the asymmetric distribution of ASH1 mRNA, and these defects are not caused by disturbances of the actin cytoskeleton (Trautwein et al., 2004). Therefore, we wondered whether *arf1* mutants induce PBs, which provide a storage and degradation location for mRNAs in response to translational arrest. As a marker for PBs we used Dcp2 (**dec**apping **p**rotein 2), which is required for decapping of mRNAs and PB formation (Dunckley & Parker, 1999; Sheth & Parker, 2003; Teixeira & Parker, 2007). We chromosomally appended Dcp2 with GFP and determined the number of PBs in control and temperature-sensitive *arf1* mutant cells (Figure 3.1 A). As expected, few PBs were observed in wild-type cells or in *arf1* mutants at the permissive temperature with Dcp2-GFP largely distributed throughout the cytosol. Strikingly, a large increase in PB number (9-10 on average) was observed in *arf1* mutant alleles upon shift to 37℃ (Figure 3.1 A and B). The temperature shift represents considerable stress for the wild type, but does not induce a block in translation, and only 1-2 PBs were present in wild-type cells at 37℃ (Figure 3.1 A and B).

We have previously shown that *arf1-11* and *arf1-18* but not *arf1-17* failed to localize ASH1 mRNA to the bud tip of yeast cells (Trautwein et al., 2004). Strikingly, the *arf1-17* mutation also caused a dramatic increase in PB number similar to that detected in *arf1-11* and *arf1-18*, indicating that mislocalization of mRNAs that are dependent on the SHE machinery is not the cause of multiple PB formation (Figure 3.1 A and B).

The Dcp2 foci we observed in *arf1* mutants likely represent PBs and not SGs (or EGP-bodies) because, generally, SGs do not contain Dcp2 (Kedersha et al., 2005; Anderson & Kedersha, 2006; Hoyle et al., 2007). To provide corroborating evidence, we appended another PB component, the helicase Dhh1, with GFP, which behaved similarly to Dcp2-GFP in the *arf1* strains (Suppl. Fig. 1[1]). Moreover, deletion of an essential SG component, *PUB1* (Buchan et al., 2008; Swisher & Parker, 2010) did not interfere with the formation of Dcp2-GFP-positive structures (Suppl. Fig. 2 A). Finally, the SG marker eIF4G2 fused to GFP did not accumulate in foci in *arf1-11* at 37℃ (Figure 3.1 C).

[1] Supplementary Figures are included at the end of the manuscript (p. 43)

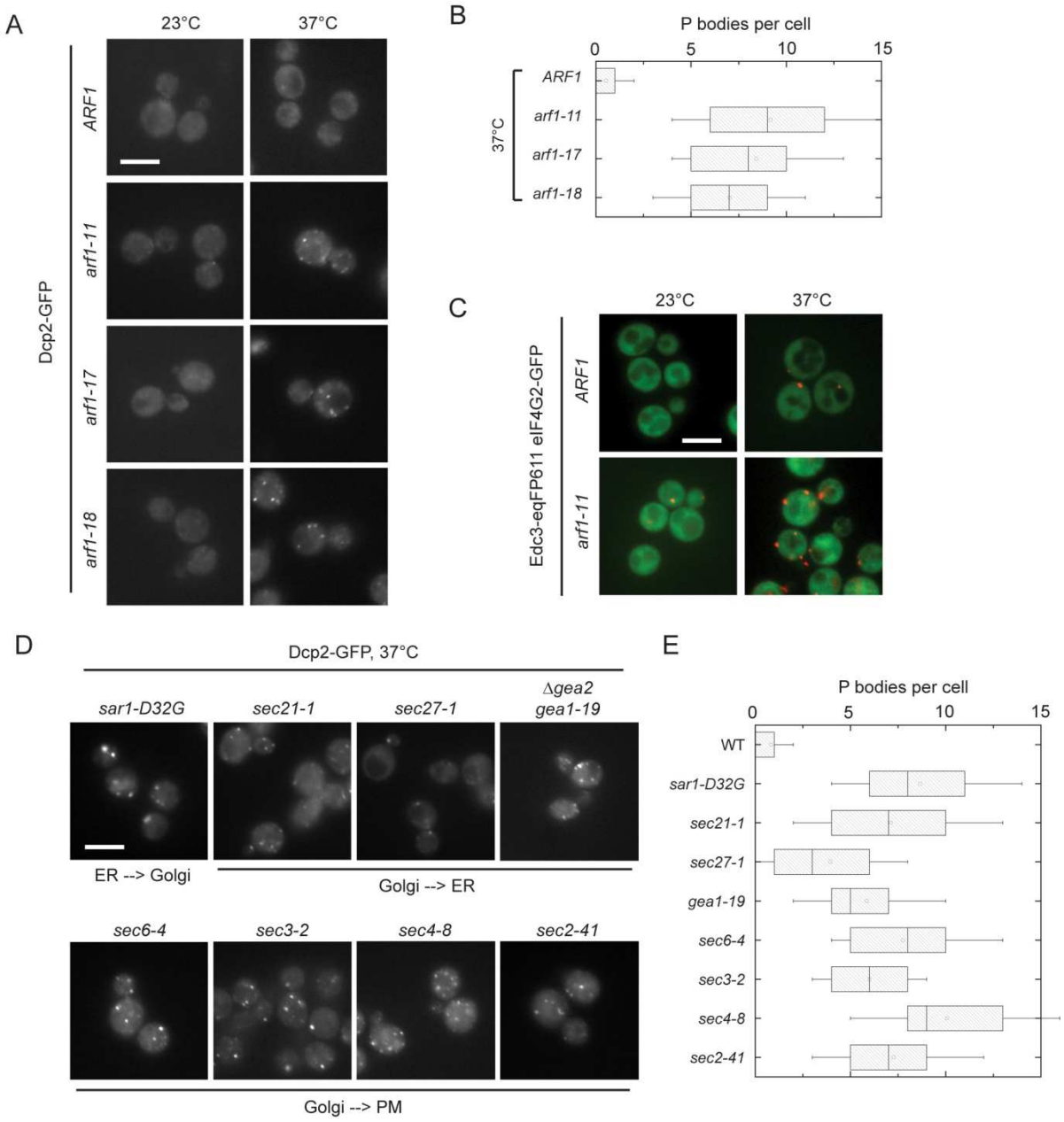

Figure 3.1: *arf1* and secretory pathway mutants have multiple PBs. (**A**) The PB marker Dcp2 was chromosomally tagged with GFP in the control strain and in several temperature-sensitive *arf1* mutants. At the permissive temperature (23℃), no PBs are observed, and Dcp2-GF P is dispersed throughout the cytoplasm. Upon shift to the non-permissive temperature (37℃) for 1 h, PB for mation is induced in all strains. The increase in PB number is more pronounced in *arf1* mutants than in the control. (**B**) Quantification of the multiple PB phenotype in *arf1* mutants at non-permissive temperature. A minimum of a hundred cells from at least two independent experiments was counted for each condition. The size of the box is determined by the 25th and 75th percentiles, the whiskers represent the 5th and 95th percentiles, the horizontal line and the little square mark the median and the mean, respectively. (**C**) Wild-type and *arf1-11* mutant cells expressing the PB marker Edc3-eqFP611 and the SG marker eIF4G2-GFP were shifted to 37℃ for 1 h. While multi ple PBs were formed in the *arf1-11* mutant, we observed no induction of SGs in the mutant or the control strain. (**D**) The number of PBs in different temperature-sensitive mutants in components of the secretory pathway was determined after shift for 1 h to 37℃. All secretor y mutants we analyzed displayed a multiple PB phenotype to a varying degree. (**E**) Quantification of the multiple PB phenotype in secretory mutants after a shift to the non-permissive temperature. See Figure 3.1 A for details on the representation. The white bars in Figures A, C, and D represent 5 µm.

PB number is increased in a variety of secretory transport mutants

Since the major function of Arf1p is to initiate COPI- and clathrin-coated vesicle budding events, we asked whether the increase in PBs is a common feature in secretory transport mutants. We monitored Dcp2-GFP in various temperature-sensitive secretory transport mutants covering ER->Golgi, Golgi->ER and post-Golgi trafficking steps and determined the number of PBs after a shift for 1 h to the non-permissive temperature (Figure 3.1 D). Interestingly, most of the mutants showed an increase in PB number similar to *arf1* mutants (Figure 3.1 E), indicating that this multiple PB phenotype is most likely related to a general defect in secretion.

Hyperosmotic stress led to numerous PBs

How do secretory transport mutants induce multiple PBs? It is unlikely that this phenotype occurs in response to general cellular stress. As has been reported before (Teixeira et al., 2005), PB formation is induced by starvation and under oxidation/redox conditions (Figure 3.2 A). However, neither starvation nor ox/redox stress led to a similar increase in PB number in wild type cells as observed for the *arf1* or secretory pathway mutants, therefore, these mutants appear to trigger a different type of PB response. Secretory pathway mutants may cause ER stress, which in turn would activate the unfolded protein response (UPR). Alternatively, secretory transport mutants may prevent the correct targeting of proteins to the plasma membrane and hence cause cell wall and osmotic stress. First, we tested whether UPR is coupled to the formation of multiple PBs. The hallmark for the activation of UPR is splicing of the transcriptional activator HAC1 mRNA (Sidrauski & Walter, 1997). Shift of *arf1-11* to the restrictive temperature induced UPR as indicated by the cleavage of the HAC1 mRNA, which was also true for *arf1-18*, albeit to a lesser extent, but not for wild type and *arf1-17* (Figure 3.2 B), indicating that there is no direct correlation between UPR and PB formation. Moreover, deletion of *IRE1*, the endonuclease that splices HAC1 transcript at the ER and senses unfolded proteins in the ER (Cox & Walter, 1996; Kimata et al., 2007), or *GCN2*, the single eIF2α kinase, which has been implicated in UPR (Patil et al., 2004), did not affect multiple PB formation in *arf1-11* (Figure 3.2 C and D). In contrast, when we challenged control or wild-type cells with cell wall stress, we detected an upregulation of PB formation. More importantly, after application of osmotic stress by incubating the cells for a short period of time (15 min) in 0.5 M NaCl, a similar increase in the number of PBs was observed as in the *arf1* mutants (Figure 3.2 A and E). We also examined SG formation under the same conditions to determine if these stresses were specific for assembling multiple PBs. Only 1-2 SG were induced under various stresses, except for robust heat stress (46℃), using Pub1-GFP, eIF4G2-GFP, and eIF3B-GFP as markers (Figure 3.2 F, Suppl. Fig. 2 B), indicating that this stress is PB specific. The foci formed at 46℃ represent SG because eIF3 localizes to SGs after robust heat shock (Grousl et al., 2009). These data could indicate that in *arf1* mutants the response to osmotic or cell wall stress is activated, and that this specific stress response increases PB number. Our data are consistent with the possibility that components of the cell wall or plasma membrane constituents do not reach the plasma membrane efficiently in *arf1* and most secretory pathway mutants at the non-permissive temperature, and that the cells become more susceptible to osmotic stress. If this hypothesis was true, preventing signaling in the osmo-response pathway should rescue the multiple PB phenotype in *arf1-11* mutants.

Neither the HOG nor the cell wall integrity pathways are required for the increase in PB number in *arf1* mutants

The major pathway activated in response to osmotic stress is the HOG MAP kinase signaling pathway (Van Wuytswinkel et al., 2000; Hohmann, 2002). The HOG pathway is at least partially repressed by addition of ethanol to the growth medium (Hayashi & Maeda, 2006). Strikingly, a very strong reduction in PB number was observed when *arf1-11* cells were shifted to the restrictive temperature in the presence

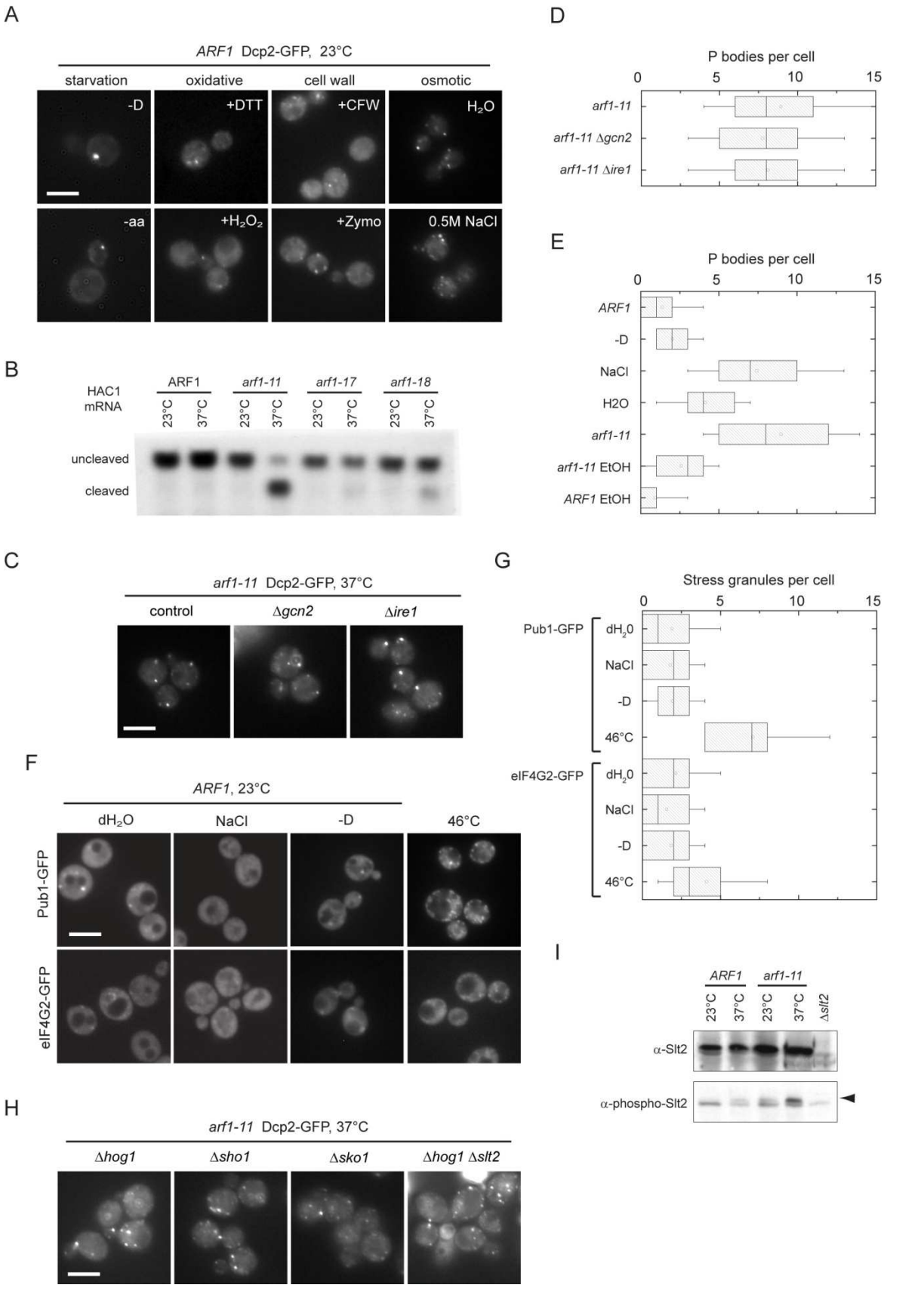

Figure 3.2: Different stresses lead to induction of a different number of PBs. (**A**) Osmotic stress induces an increase in PB number in wild-type cells. Wild-type cells expressing Dcp2-GFP were grown in rich medium to early log phase at 23℃. Starvation was induced by i ncubating cells in medium either lacking a carbon source (-D) or amino acids (-aa) for 15 min. To induce reductive or oxidative stress, 10 mM DTT or 0.4 mM H_2O_2 were added to the cultures for 1 h. Spheroplasting by enzymatic digest (+Zymo) or treatment with calcofluor white (CFW) were

used to induce cell wall stress. To induce osmotic stress, cells were harvested and either incubated in H_2O or rich medium containing 0.5 M NaCl for 15 min. All stresses were applied at 23℃. While cell wall stress did cause an increase in PB number, osmotic stress induced a strong multiple PB phenotype similar to *arf1* mutants. (**B**) UPR is not generally activated in *arf1* mutant alleles. Northern blot with a probe against HAC1 mRNA on total RNA extracted from *ARF1* and *arf1* cells grown at 23℃ or shifted to 37℃ for 1 h. Th e HAC1 cleavage product indicative of an active UPR is only observed in two of the mutant alleles. (**C**) The UPR components Gcn2 and Ire1 are not required for assembly of multiple PBs in *arf1-11*. Cells expressing Dcp2-GFP were deleted for either *GCN2* or *IRE1* and shifted to 37℃ for 1 h. (**D**) Quantification of PBs in *arf1-11* deleted for *GCN2* or *IRE1* after a shift to the non-permissive temperature. See Figure 3.1 A for details on the representation. (**E**) Quantification of the multiple PB phenotype in cells under osmotic stress and in the presence of ethanol. For the ethanol experiment, wild-type or *arf1-11* cells expressing Dcp2-GFP were shifted to 37℃ for 1 h in the presence or absence of 1.6 M EtOH. No effect was observed for wild-type, while the multiple PB phenotype in *arf1-11* was rescued in the presence of EtOH. See Figure 3.1 A for details on the representation. (**F**) Wild-type cells expressing the stress granule markers Pub1-GFP or eIF4G2-GFP were grown in rich medium early log phase at 23℃ to and then either incubated in H_2O, rich medium containing 0.5 M NaCl, or medium lacking a carbon source (-D) for 15 min, or subjected to high heat shock (10 min at 46℃). We did not observe a marked induction of stress granules under conditions that induce multiple PBs; however, Pub1-GFP containing stress granules were induced by heat shock. (**G**) Quantification of SGs in the wild-type induced by various stresses. See Figure 3.1 A for details on the representation. (**H**) Plasma membrane stress signaling pathways are not required for the assembly of multiple PBs. Key components of different signaling pathways were deleted in *arf1-11* cells expressing Dcp2-GFP. None of the mutants resulted in a reduction of PBs in *arf1-11* at 37℃. See Table 3.1 for quantification of all mutations tested. (**I**) Lysates were generated from wild-type or *arf1-11* cells after a 1 h shift to 37℃ and analyzed by immunoblot to detect total Slt2 and Slt2 phosphorylated in response to cell wall integrity signaling. The band marked with the arrowhead corresponds to phospho-Slt2. A lysate of a strain deleted for *SLT2* was loaded as a reference. The white bars in Figs. A, C, F, and H represent 5 µm**.**

Table 3.1: PB phenotype of various mutants.

	Supernumerary PBs				PBs induced	
	in *arf1-11* at 37℃		in *ARF1* + Ca^{2+}		by starvation	
	+/-	PB per cell	**+/-**	PB per cell	**+/-**	PB per cell
No deletion	**+**	9.15 ± 4.16	**+**	8.89 ± 3.50	**+**	2.16 ± 1.01
Δhog1	**+**	8.07 ± 3.50	**+**	7.51 ± 3.38	n.d.	n.d.
Δsho1	**+**	7.66 ± 3.62	**+**	5.52 ± 2.37	n.d.	n.d.
Δsko1	**+**	7.72 ± 3.32	**+**	5.43 ± 2.55	n.d.	n.d.
Δslt2	**+**	5.96 ± 4.47	**+**	7.64 ± 3.28	n.d.	n.d.
Δhog1 Δslt2	**+**	6.80 ± 5.18	**+**	7.48 ± 2.72	n.d.	n.d.
Δsli2	**+**	7.65 ± 4.05	**+**	6.90 ± 3.45	n.d.	n.d.
Δcnb1	**+**	6.41 ± 2.48	**+**	6.71 ± 2.74	n.d.	n.d.
Δcmk1 Δcmk2	**+**	7.65 ± 3.45	**+**	6.27 ± 2.85	n.d.	n.d.
Δcmk1 Δcmk2 Δcnb1	**+**	7.72 ± 4.05	**+**	6.81 ± 2.80	n.d.	n.d.
Δhog1 Δslt2 Δcnb1	**+**	7.97 ± 4.75	**+**	8.32 ± 3.35	n.d.	n.d.
Δpat1	**-**	1.93 ± 1.79	**-**	2.02 ±2.42	**+**	1.20 ± 0.99
Δscd6	**-**	2.04 ± 1.81	**-**	1.08 ±1.27	**+**	2.41 ± 1.28
cmd1-3	**-**	4.09 ± 2.72	**-**	2.02 ± 1.84	**+**	2.16 ± 1.07

+/- designates whether PBs are induced under this condition. Given is the average number of PBs counted per cell, ± one standard deviation. A minimum of hundred cells from at least two independent experiments was counted for each strain. (n.d.) not determined.

of ethanol (Figure 3.2 B), suggesting that the HOG pathway may be activated in the *arf1-11* mutant. Hog1 is not essential, and therefore we could test the requirement for HOG signaling pathway in PB formation directly by deleting *HOG1* in *arf1-11*. Surprisingly, the number of PBs was unchanged upon loss of Hog1p in *arf1-11* at 37℃ (Figure 3.2 G, Table 3.1). Moreover, deletion of the osmosensor *SHO1* or the HOG-dependent osmoresponsive transcription factor *SKO1* did not interfere with PB formation in *arf1-11* (Figure 3.2 G, Table 3.1). The results indicate that Hog1 is not involved in PB assembly in secretory mutants. This is in agreement with recent data suggesting that Hog1 may play a role in PB disassembly, and that PBs are formed in Δ*hog1* cells under mild and severe osmotic shock (Romero-Santacreu et al., 2009).

Another signaling pathway acting at the plasma membrane is the cell wall integrity pathway, which plays a role in the progression through the cell cycle. The MAP kinase Slt2p, also referred to as Mpk1p, is central to the cell wall integrity pathway (Lee et al., 1993) and is phosphorylated in response to cell wall stress. We observed the phosphorylation of Slt2 in *arf1-11* cells after shift to the non-permissive temperature (Figure 3.2 H). A low level of phosphorylation is already observable in *arf1-11* cells at 23℃ and in wild-type cells at 37℃, but these levels may be too low to drive numerous PB formation. Similar to Hog1, Slt2 is not essential and we could determine the number of PBs in an *arf1-11* Δ*slt2* strain at 37℃ (Table 3.1). As in the case of loss of Hog1, deletion of *SLT2* did not reduce PB number in *arf1-11* cells, showing that under these conditions neither the HOG nor the cell wall integrity pathway is involved in PB formation. Moreover, the two pathways do not cooperate in PB induction, because a deletion of both *HOG1* and *SLT2* did not reduce PB number in *arf1-11* cells (Figure 3.2 G, Table 3.1). Finally, we deleted the serine/threonine kinase Sli2p (also referred to as Ypk1p), which is involved in the cell integrity and sphingolipid-mediated signaling pathway (Schmelzle et al., 2002). Again, deletion of *SLI2* had no effect on PB number in *arf1-11* cells (Table 3.1). Similarly, treating *arf1-11* cells with chlorpromazine, a membrane permeable molecule that binds anionic lipids such as poly-phosphoinositides and leads to translation attenuation (De Filippi et al., 2007) did not change the amount of PBs (data not shown). Taken together, these results argue that the increase in PB number seen in *arf1* or secretory mutants is independent of the major plasma membrane signaling pathways.

Ca^{2+} induces numerous PBs

Since hyperosmotic shock leads to a transient increase in intracellular Ca^{2+} (Batiza et al., 1996; Matsumoto et al., 2002) and a Ca2+/calcineurin-regulated response is required for growth under high osmolarity and cell wall stress (Heath et al., 2004), we asked next whether Ca^{2+} is required for the formation of multiple PBs. Incubation of wild-type cells with Ca^{2+} induced rapid PB formation, to the same extent as hyperosmotic shock, within 10 min after $CaCl_2$ addition (Figure 3.3 A and B). Moreover, the effect was specific to Ca^{2+} because adding $MgCl_2$ had no effect on PB formation (Figure 3.3 A and B). If formation of multiple PBs depends on increased Ca^{2+} levels, *arf1-11* cells should not accumulate PBs in the presence of Ca^{2+}-chelating agents. To test this hypothesis, we precultured the strains in the presence of low concentrations of BAPTA prior to and during the temperature shift. Under these conditions, only 1-2 PBs were observed in *arf1-11* (Figure 3.3 C and D). Moreover, Ca^{2+} was less potent in inducing PBs in *ARF1*. Similar results were also observed in the gamma-COP mutant *sec21-1* and the exocyst component mutant *sec6-4* upon growth in BAPTA and shift to 37℃ (Figure 3.3 C and D), indicating that the increase in PB number in secretory mutants is dependent on a change in intracellular Ca^{2+}. Interestingly, in contrast to the PBs formed under glucose starvation or NaCl, Ca^{2+} induced PBs disappear rapidly over time, and after about 30 min only a few, if any, PBs could be detected (Figure 3.3 E and F). Most likely transporters are expressed at the plasma membrane, which extrude excess Ca^{2+} to maintain ion homeostasis. This effect is not observed in secretory pathway mutants, in which PBs persisted, even

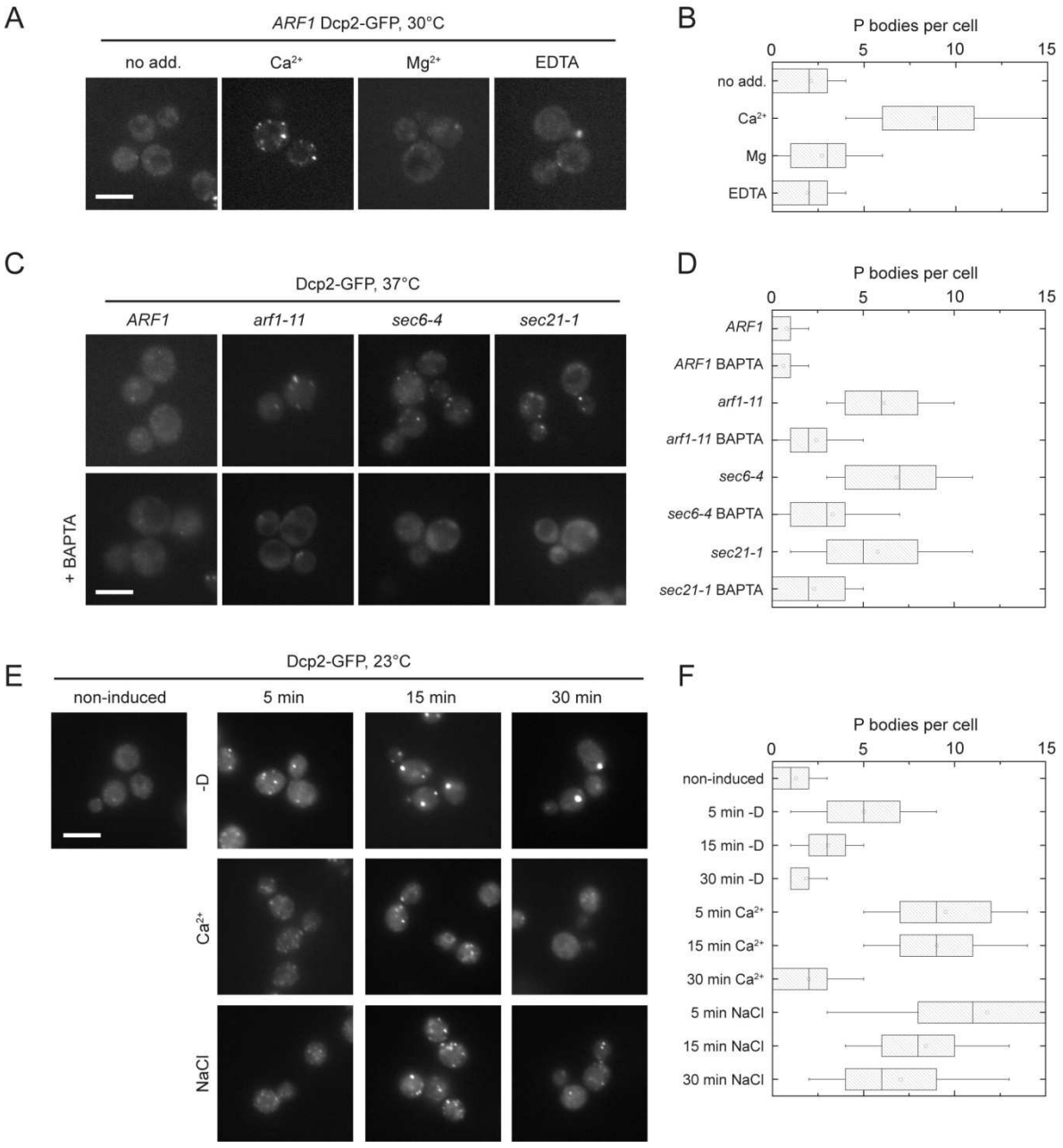

Figure 3.3: Ca^{2+} induces PB assembly to a similar extent than a secretion block. (**A**) Wild-type cells expressing Dcp2-GFP were treated with 200 mM $CaCl_2$, $MgCl_2$ or 12.5 mM EDTA for 15 min at 30℃, washed and inspected under the microscope. Only Ca^{2+} treatment induced multiple PBs. (**B**) Quantification of PBs in wild-type cells treated with Ca^{2+}, Mg^{2+} or EDTA. See Figure 3.1 A for details on the representation. (**C**) The Ca^{2+}-chelator BAPTA prevents formation of multiple PBs in secretory transport mutants. Cells expressing Dcp2-GFP were pre-cultured in the presence or absence of 0.6 mM BAPTA and shifted to 37℃ for 1 h prior to inspection under the microscope. PB induction was strongly reduced. (**D**) Quantification of PBs in secretory mutants treated with BAPTA after shift to the non-permissive temperature. See Figure 3.1 A for details on the representation. (**E**) Time-course analysis of PB induction under various conditions. Wild-type cells expressing Dcp2-GFP were either harvested and resuspended in rich medium without a carbon source (-D), or treated with 200 mM $CaCl_2$ or 0.5 M NaCl. After various time-points, samples were removed, fixed with formaldehyde, and analyzed under the microscope. PB response to Ca^{2+} appears to be transient, while PBs induced by osmotic stress or starvation persist longer. (**F**) Quantification of PBs in the time-course experiment. See Figure 3.1 A for details on the representation. The white bars in Figures A, C, and E represent 5 µm.

after a prolonged shift to the non-permissive temperature (Figure 3.1 D). This observation is expected as delivery of transporters to the plasma membrane is blocked in these mutants.

Elevated Ca^{2+} levels and starvation lead to translation attenuation and PB formation through different pathways

Secretory pathway mutants cause translation attenuation at the non-permissive temperature (Deloche et al., 2004) and induction of PBs is thought to correlate with translation attenuation (Sheth & Parker, 2003). The hallmark of translation attenuation is a loss of translating polysomes and a concomitant increase in the monosome (80S) fraction in the cell. First, we established that *arf1-11* cells indeed attenuate translation by determining their polysome profile after shift to 37℃ (Figure 3.4 A and B). Next we asked whether the number of PBs in the cell could be correlated with the strength of translational block because Parker and Sheth (Parker & Sheth, 2007) proposed a model in which the rates of translation and degradation of mRNAs would be governed by a dynamic equilibrium between polysomes and mRNPs in PBs. Therefore, we recorded polysome profiles of wild-type cells that were either starved for glucose or incubated with Ca^{2+} or a combination of both stresses (Figure 3.4 B and C). As shown previously (Ashe et al., 2000), glucose starvation causes a pronounced shift of ribosomes from the polysome fraction towards monosomes. A similar change was observed in cells that were treated with Ca^{2+} or NaCl and in *arf1-11*, albeit to a lesser extent (Figure 3.4). According to the dynamic equilibrium model, the weak translational repression induced by high Ca^{2+}, NaCl or the *arf1-11* mutant would yield multiple PBs, while the strong translational repression observed upon starvation would result in 1-2 PBs. It is conceivable that the multiple PBs we observe would coalesce to 1-2 PBs that contain more RNA or represent more densely packed, matured PBs, if translational repression was stronger. If this hypothesis was correct, combining starvation and high Ca^{2+} should lead to the formation of 1-2 PBs. However, combining high Ca^{2+} or NaCl with starvation led to the almost complete absence of polysomes, and even the monosomes seemed to partially disassemble, but multiple PBs were observed under these conditions (Figure 3.4 C). These results indicate that dynamic equilibrium might not be sufficient to explain different PB numbers observed under starvation and high Ca^{2+} and suggest the presence of at least two distinct pathways to generate PBs, one of which functions in sensing low glucose levels while the other responds to an increase in Ca^{2+} levels.

Calmodulin is required for the induction of PBs in secretory pathway mutants

The next question was how the cell would sense the potential intracellular Ca^{2+} changes. A major player in Ca^{2+} signaling is calmodulin (Cmd1), which contains 4 EF hands, 3 of which can coordinate Ca^{2+}. The temperature-sensitive *cmd1-3* mutant does not bind Ca^{2+} (Geiser et al., 1991). Therefore, to test whether calmodulin is involved in signaling to PBs, we replaced *CMD1* by the *cmd1-3* mutation in our Dcp2-GFP expressing wild-type and asked if cells would still accumulate PBs in the presence of Ca^{2+}. The *cmd1-3* mutant blocked formation of numerous PBs (Figure 3.5 A), demonstrating that PB induction upon elevated Ca^{2+} levels requires functional calmodulin. But is calmodulin also required for PB induction by other stresses? To address this question, we analyzed PB assembly after induction by glucose starvation or NaCl addition, but detected no difference between wild type and *cmd1-3* cells (Figure 3.5 A and B). Similarly, when we introduced the *cmd1-3* allele into the *arf1-11* mutant, induction of multiple PBs was reduced at the non-permissive temperature (Figure 3.5 C and D), indicating that the PBs formed in the secretory mutants do indeed correspond to PBs induced by Ca^{2+}, but differ from those induced by hyperosmotic stress, although they are indistinguishable by light microscopy.

To determine if one of the established Ca^{2+} signaling pathways is required for PB induction, we screened through mutants in the phosphatase calcineurin and in calmodulin-dependent kinases Deletion of the catalytic subunit of calcineurin, *CNB1*, or of the calmodulin-dependent kinases *CMK1* and

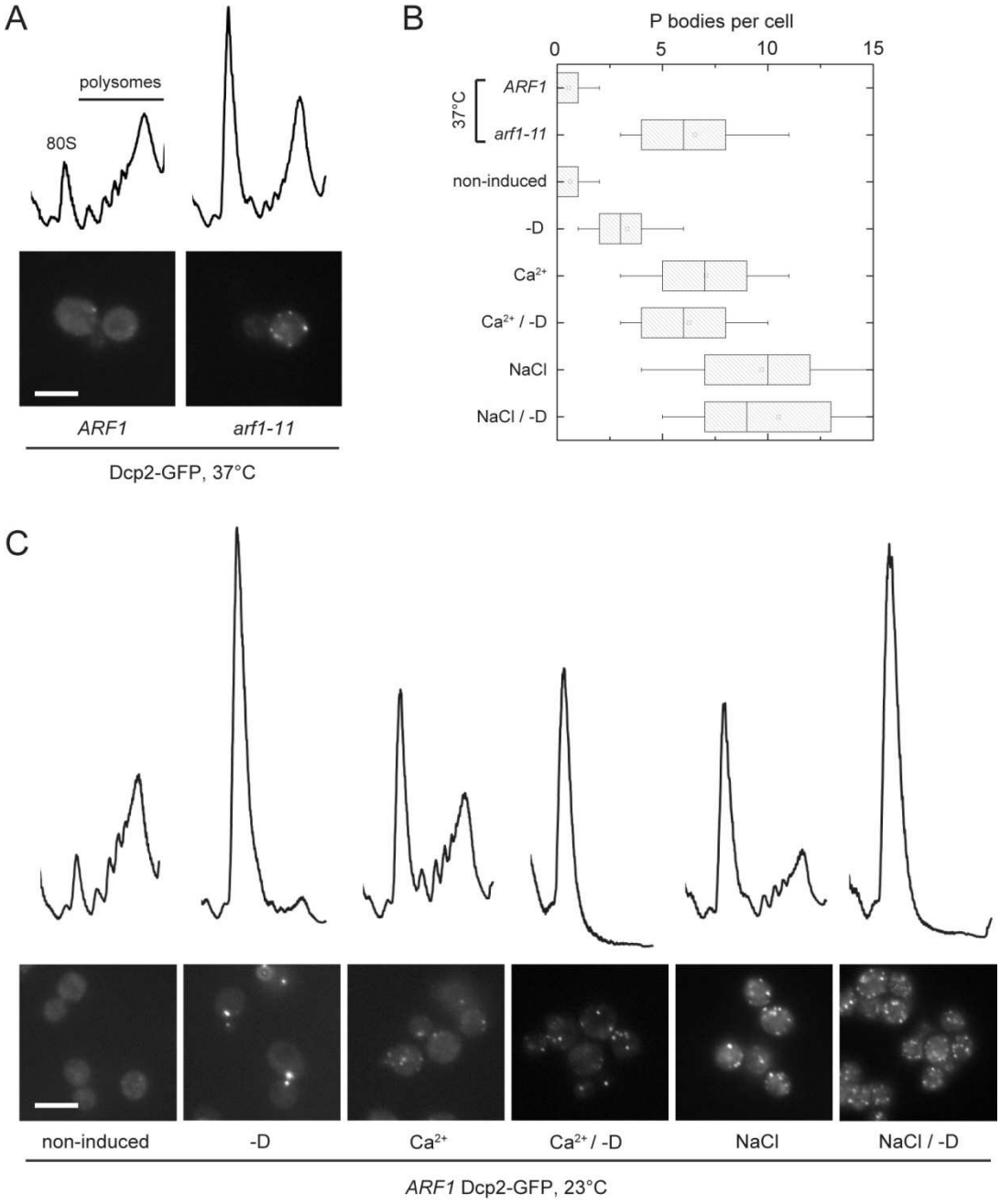

Figure 3.4: Translation attenuation and PB induction in response to different stresses (**A**) Wild-type or *arf1-11* cells expressing Dcp2-GFP were grown to early log phase at 23℃ and the shifted to 37℃ for 1 h. Cells were either inspected under the microscope or subjected to polysome profile analysis. In *arf1-11* cells, translation is attenuated. (**B**) Quantification of the PBs observed in A and C. See Figure 3.1 A for details on the representation. (**C**) Cells expressing Dcp2-GFP were grown in rich medium to early log phase at 23℃. Starvation was induced by resuspending cells into medium lacking a carbon source (-D). Alternatively, cells were incubated in rich medium containing 0.5 M NaCl or 200 mM $CaCl_2$, or subjected to combinations of these stresses. After 15 min incubation at 23℃, cells were either inspected under the microscope or subjected to polysome profile analysis. While starvation resulted in a marked increase in the monosome/polysome ratio and induction of few PBs, wild-type cells under osmotic stress or in the presence of Ca^{2+} displayed an intermediate increase in the monosome/polysome ratio and had multiple PBs, as was observed in the *arf1-11* mutant shifted to 37℃ for 1 h. When starvation was combined with either osmotic stress or Ca^{2+} treatment, polysomes were almost completely abolished, but cells had multiple PBs. The white bars in Figures A and C represent 5 µm.

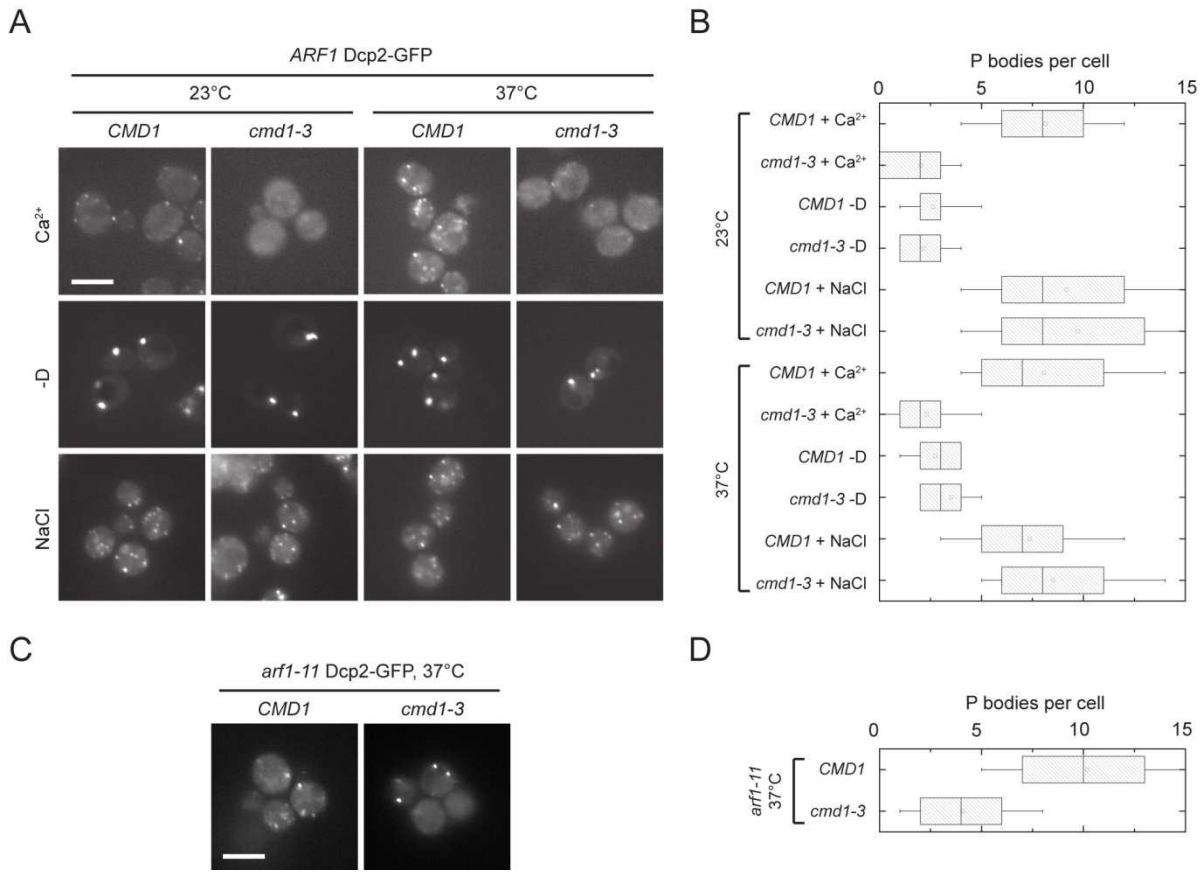

Figure 3.5: Calmodulin is required for the assembly of multiple PBs in the presence of Ca^{2+} and in secretory mutants. (**A**) PBs were induced in wild-type and *cmd1-3* mutant cells expressing Dcp2-GFP by treatment with 200 mM $CaCl_2$, 0.5 M NaCl, or incubation in rich medium lacking a carbon source (-D) for 15 min at 23℃, or after a 1 h shift to 37℃. While PB inductio n by osmotic stress or starvation was not affected in the *cmd1-3* mutant, a strong reduction of PB number was observed in the mutant after Ca^{2+} treatment. (**B**) Quantification of PBs in the *ARF1 cmd1-3* mutant induced either at 23℃ or after a shift to 37℃ for 1 h. See Figure 3.1 A for details on the representation. (**C**) *arf1-11* cells expressing Dcp2-GFP that were deleted for *CMD1* but carried a plasmid containing the *cmd1-3* allele were shifted to 37℃ for 1 h. PB number was r educed if compared to *arf1-11* alone. (**D**) Quantification of PBs in the *arf1-11 cmd1-3* mutant induced at 37℃. See Figure 3.1 A for details on the representation. The white bars in Figures A and C represent 5 µm.

CMK2 in *arf1-11* mutant or wild-type cells had no effect on PB induction by temperature-shift or Ca^{2+} treatment, respectively. Even concomitant loss of both calmodulin-dependent kinases and the regulatory subunit of calcineurin *(Δcmk1 Δcmk2 Δcnb1*), or of *HOG1*, *SLT2* and *CNB1 (Δhog1 Δslt2 Δcnb1*), did not inhibit formation of numerous PBs in *arf1-11* cells at 37℃ or in *ARF1* cells in the presence of Ca^{2+} (Table 3.1). Taken together these data indicate that the classical Ca^{2+} signaling pathways are not involved in inducing PB production, suggesting that calmodulin might act on PBs by an unknown mechanism.

Calmodulin is an abundant protein that performs a plethora of functions in the cell, and is localized to sites of polarized growth and the spindle pole body (Ohya & Botstein, 1994; Spang et al., 1996). When we appended Cmd1 with GFP in *arf1-11* and wild-type cells and induced PBs by temperature-shift or Ca^{2+}, respectively, we did not observe accumulation of Cmd1-GFP into multiple foci, indicating that Cmd1 is not a bona fide component of PBs. It is important to note that under these PB-inducing conditions Cmd1-GFP was lost from the site of polarized growth, the small bud tip, providing corroborating evidence that Ca^{2+} levels might be elevated in secretory mutants (Suppl. Fig. 3).

Pat1 and Scd6 are required for PB assembly in secretory pathway mutants

The above data indicate the existence of multiple parallel pathways by which PB formation can occur. The assembly of PBs has been best characterized under starvation conditions (Parker & Sheth, 2007; Teixeira & Parker, 2007; Franks & Lykke-Andersen, 2008). Interestingly, no single known component of PBs was solely responsible for PB formation (Teixeira & Parker, 2007). Thus, if different pathways exist that lead to PB formation, one might be able ot identify PB components that are required for PB formation only under specific conditions. To test this hypothesis, we tested two PB components that are not strictly involved in PB formation under starvation, namely Pat1 and Scd6 (Teixeira & Parker, 2007). We chose Pat1 because it contains an EF-hand, which might coordinate a Ca^{2+} ion. Pat1 binds, together with the Lsm1-7 complex, to the 3' region of mRNAs, and is involved in PB formation. However, PBs are still formed in Δ*pat1* cells upon glucose starvation (Teixeira & Parker, 2007). Scd6 is a Sm-like (LSM) protein most likely involved in the regulation of mRNA translation and/or degradation in PBs (Decker & Parker, 2006), and was first described as a multicopy suppressor of a membrane transport defect (Nelson & Lemmon, 1993). Deletion of *PAT1* or *SCD6* in wild-type cells strongly suppressed PB assembly induced by Ca^{2+} (Figure 3.6 A and B).

In agreement with previously published data, deletion of *PAT1* or *SCD6* did not influence PB formation upon glucose starvation of hyperosmotic shock, indicating that both proteins are required specifically for the formation of Ca^{2+}-dependent PBs (Figure 3.6 A and B). Next, we investigated the effect of *PAT1* or *SCD6* deletion in *arf1-11* and *sec6-4* after shift to the non-permissive temperature. As expected, these cells did not form multiple PBs (Figure 3.6 C and D), however, most cells did contain a single PB, reinforcing the idea that PB assembly is not strictly dependent on Pat1 or Scd6. When we appended Pat1 or Scd6 with GFP in wild type and *arf1-11* mutant cells and subjected them to Ca^{2+} treatment or shift to 37℃, respectively, the GFP signal remained mostly cytoplasmic. However, multiple GFP foci formed under these conditions, indicating that both proteins are components of the PBs we observe (Figure 3.6 E).

Taken together, our data provide evidence that the multiple PB phenotype in secretory pathway mutants is due to changes in intracellular Ca^{2+} and that Pat1 and Scd6 are involved in translating these changes into PB assembly.

PBs are in the vicinity of the ER

PB formation in secretory pathway mutants requires Scd6. The Lsm Scd6 homologue in *C.elegans*, CAR-1, is required for ER organization (Squirrell et al., 2006). The *Drosophila* homologue, trailer hitch, is localized close to ER exit sites, and is required for normal ER-exit site formation (Wilhelm et al., 2005). We therefore hypothesized that PBs induced in secretory mutants localize to the ER. To test this hypothesis, we examined the colocalization of Dcp2-GFP foci with an ER marker, Sec63-RFP, and found that they were in close proximity to the ER, in both wild-type and *arf1* mutant cells shifted to 37℃ (Figure 3.7 A). Immuno-electron microscopy confirmed this observation (Figure 3.7 C), and gold particles were found next to the ER in both mutant and wild-type cells after shift to 37℃ or in wild-type cells under starvation. The labeling was specific, because no gold particle accumulations were found in an untagged strain (Suppl. Fig. 4). Neither Scd6 nor Pat1 were required for the juxtaposition of PBs and ER (Figure 3.7 B).

We observed that the Dcp2-myc signal was organized in ring-like structures, which had in all cases a diameter of about 40 nm to 100 nm (Figure 3.7 D). Therefore, surprisingly, the PBs induced under various conditions share a strikingly similar organization. To confirm this result, we determined the localization of another PB component, the helicase Dhh1, which is not essential for PB formation (Teixeira & Parker, 2007). Interestingly, Dhh1 accumulated in similar size foci, again close to the ER, suggesting that Dcp2 and Dhh1 are part of the same spherical structure (Figure 3.7 C) independent of the induction condition or the strain background used. A spherical structure for PBs has

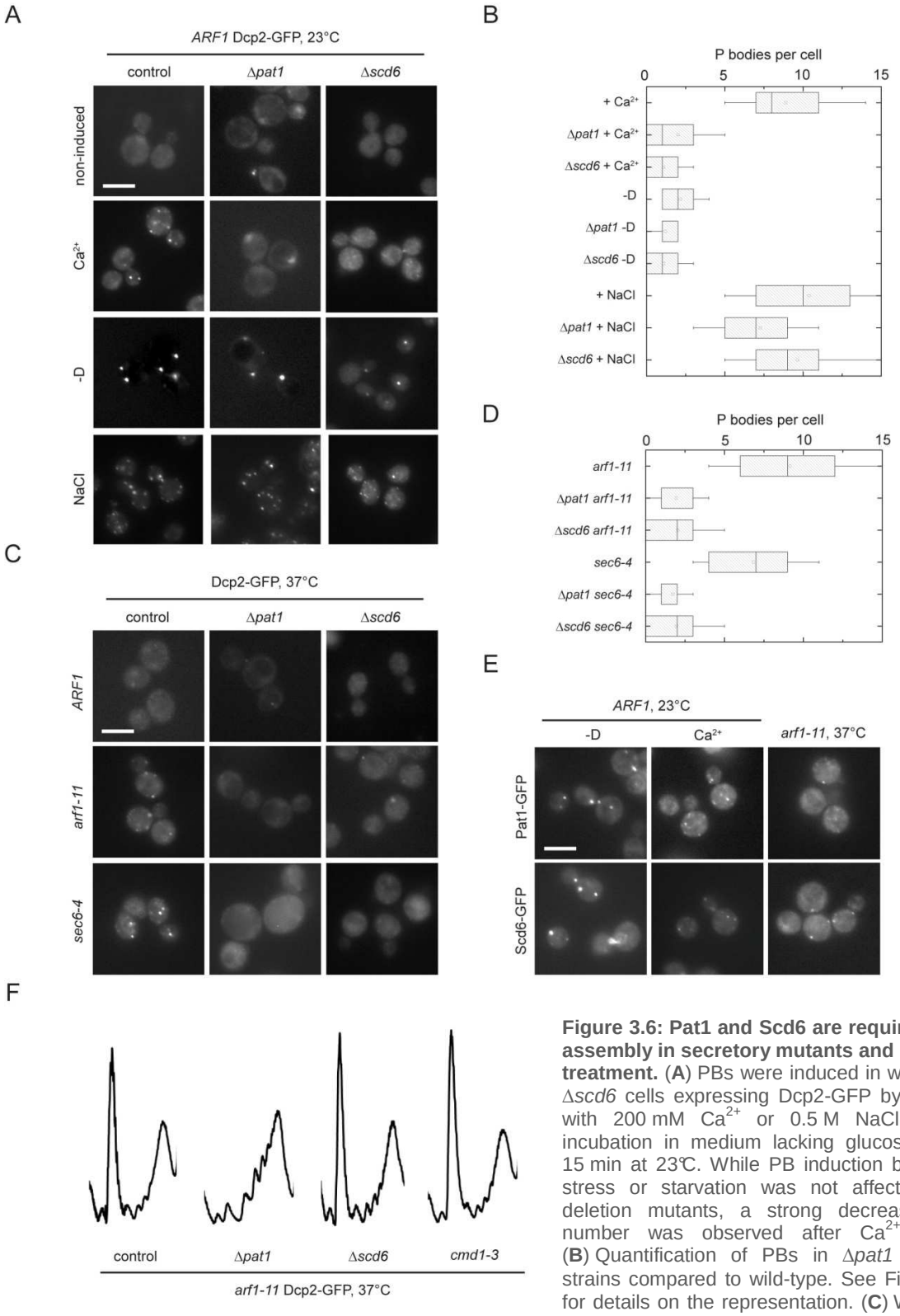

Figure 3.6: Pat1 and Scd6 are required for PB assembly in secretory mutants and upon Ca^{2+} treatment. (**A**) PBs were induced in wt, Δ*pat1* or Δ*scd6* cells expressing Dcp2-GFP by treatment with 200 mM Ca^{2+} or 0.5 M NaCl, or after incubation in medium lacking glucose (-D) for 15 min at 23℃. While PB induction by osmotic stress or starvation was not affected in the deletion mutants, a strong decrease in PB number was observed after Ca^{2+} addition. (**B**) Quantification of PBs in Δ*pat1* or Δ*scd6* strains compared to wild-type. See Figure 3.1 A for details on the representation. (**C**) Wt, *arf1-11 and sec6-4* ex-pressing Dcp2-GFP and deleted for *PAT1* or *SCD6* were shifted to 37℃ for 1 h. Deletion ofof *PAT1* or *SCD6* abolished the multiple PB phenotype in secretion mutants. (**D**) Quantification of PBs in secretory mutants deleted for *PAT1* or *SCD6* after shift to 37℃. See Figure 3.1 A for details on the representation. (**E**) PBs were induced in wt or *arf1-11* expressing Pat1-GFP or Scd6-GFP by incubation in medium lacking glucose (-D), treatment with 200 mM $CaCl_2$ for 15 min at 23℃, or shift to 37℃ for 1 h. Both Pat1-GFP and Scd6-GFP behaved simi larly to Dcp2-GFP and were found in multiple PBs after Ca^{2+} treatment or if the mutant was shifted to 37℃. (**F**) *arf1-11* cells deleted for *PAT1* or *SCD6*, or carrying the *cmd1-3* allele, were shifted to 37℃ for 1 h and their pol ysome profile recorded. Although all three strains do not induce multiple PBs under this condition, translation is derepressed only in the strain deleted for *PAT1.*
The white bars in Figures A, C, and E represent 5 µm.

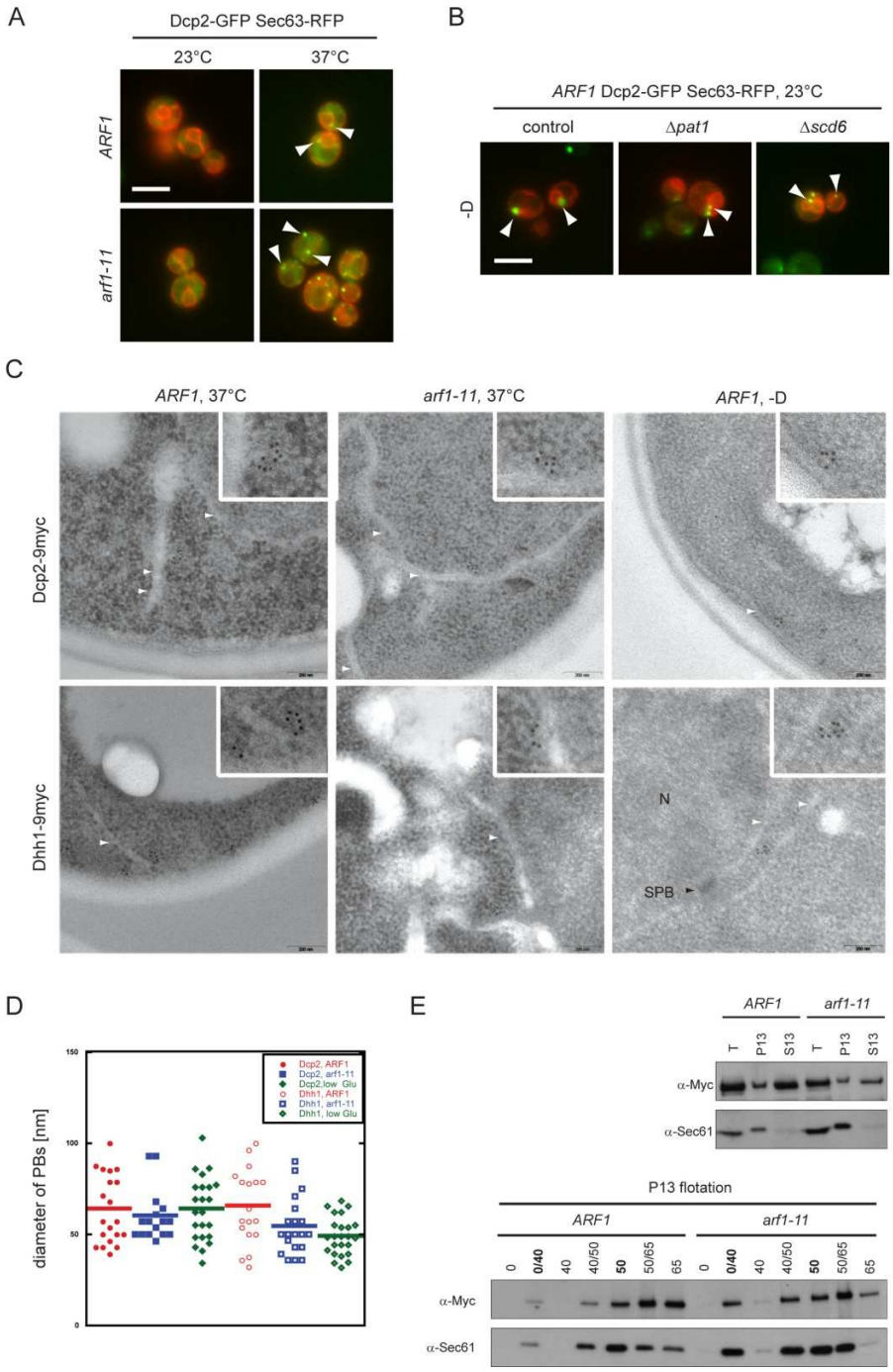

Figure 3.7: PBs associate with the ER. (**A**) Wt and *arf1-11* cells expressing Dcp2-GFP and the ER marker Sec63-RFP were shifted to 37℃ for 1 h. In both cases, PBs were observed next to the ER. White arrowheads point towards a selection of PBs. (**B**) PBs were induced in cells expressing Dcp2-GFP and the ER marker Sec63p-RFP deleted for either *PAT1* or *SCD6* by incubating cells in medium without glucose for 15 min. Both in the control and the deletion strains, PBs were observed in proximity to the ER. White arrowheads point towards a selection of PBs. (**C**) Dcp2 and Dhh1 are part of spherical structures in proximity to the ER. Wt and *arf1-11* cells expressing either Dcp2-9myc or Dhh1-9myc were shifted to 37℃ for 1 h or incubated in medium without a carbon source for 15 min (-D) at 23℃. Cells were fixed and analyzed by immuno-EM for myc. Clusters of gold particles localized next to ER membranes. The black bar represents 200 nm. The inlet is a 2x magnification of the area surrounding PBs. White arrowheads point to the ER; N marks a nucleus and SPB with a black arrowhead points to a spindle pole body. (**D**) Determination of the appr. diameter of PBs. The largest distance between two gold particles in a cluster was determined in wt and *arf1-11*. The size of the clusters did not change significantly between different conditions for the two markers. Each dot represents an individual PB, the line marks the average. (**E**) PBs are physically connected to the ER. Yeast lysates of wt and *arf1-11* expressing Dcp2-9myc were prepared after a shift to 37 ℃ for 1 h and separated into 13,000 g pellet (P13) and corresponding supernatant (S13). The pellet was subjected to buoyant density centrifugation. A fraction of Dcp2-9myc cosedimented with the ER in the P13 fraction and floated with Sec61p to the 0/40% sucrose interphase. Dcp2-9myc behaved similar in wt and *arf1-11* lysates. The white bars in Figures A and B represent 5 µm.

been previously proposed (Kedersha et al., 2005; Teixeira et al., 2005; Wilhelm et al., 2005), however, the data underlying this hypothesis were obtained by light microscopy. Given the size of 40-100 nm of PBs, the resolution of a standard light microscope does not allow a precise measurement. Interestingly, the size of the PBs was similar in wild type and *arf1-11* (Figure 3.7 D). Therefore, PB number could potentially be correlated to the amount of mRNA that has to be silenced and/or to be degraded.

PBs are tightly associated with the ER

The close proximity of PBs to the ER prompted us to test whether PBs are bound to the ER. First, we performed a differential centrifugation of total yeast cell lysate (Figure 3.7 E), and found the PB marker Dcp2-myc segregated into the P13 and the S13 fraction. We would not expect all Dcp2 to be efficiently depleted from the soluble pool, because we always observed cytoplasmic Dcp2-GFP under the microscope. The accumulation of a PB component in the P13 fraction could be explained either by its membrane association or simply by sedimentation of PBs at medium speed because of their large size and mass. To distinguish between these possibilities, we performed a buoyant density centrifugation with the P13 fraction (Figure 3.7 E). Membrane particles would float while large protein complexes should remain in the bottom of the tube. A fraction of Dcp2 floated to the same position in the gradient as the translocon component Sec61p, indicating that PBs do not only localize close to the ER but are physically associated with the membrane (Figure 3.7 E, 0/40 interphase). This localization of PBs to the ER suggests the intriguing possibility that translation of mRNA on one hand and mRNA silencing and degradation on the other hand occur in a spatially coordinated manner at the ER.

Discussion

We have characterized a pathway through which PBs are induced in response to a block in secretion. This pathway is different from PB induction under starvation. Moreover, we found that not all stresses elicit assembly of PBs to the same extent. While we observed only 1-4 PBs/cell upon starvation or exposure to oxidative stress, numerous PBs were formed in response to secretion defects or treatment with Ca^{2+} (average 9-10). Although appearance of multiple PBs could also be induced by osmotic stress, this pathway was independent from Ca^{2+}.

Thus far, no specific signaling pathway has been implicated in the formation of PBs. The common view is rather that a number of stresses cause attenuation of translation initiation, and, as a consequence, mRNAs accumulate in the cytoplasm and passively aggregate into PBs (Andrei et al., 2005; Coller & Parker, 2005; Ferraiuolo et al., 2005). However, when we combined stresses, PB number did not correlate with the strength of the translational block, but rather with the type of stress encountered, indicating that PB number is regulated by an upstream signal dependent on the stressor, but less dependent on the translational response. Interestingly, when other labs studied PB induction under starvation, loss of Dhh1 and Pat1 decreased the number of PBs but corresponded with increased polysome-associated mRNA (Coller & Parker, 2005), implying that an equilibrium between translation initiation and PB formation could exist. When secretory mutants were deleted for *PAT1*, we observed a similar phenomenon. However, when we deleted *SCD6* or introduced *cmd1-3* into *arf1-11*, PB induction was strongly reduced, but the attenuation of translation initiation remained unchanged, indicating an uncoupling of translation initiation and PB formation. Therefore, mRNA release from polysomes might not be the driving force for PB formation in secretory mutants.

The PBs induced in secretory transport mutants were very similar to PBs formed under starvation or heat stress as judged by immuno electron microscopy. Thus the increase in number of PBs would suggest that more mRNA might have to be silenced and eventually be degraded, if the stress persisted over longer periods. In mammalian cells, PBs appear to be highly dynamic structures in that they can quickly exchange a subset of the constituents with the cytoplasm (Andrei et al., 2005; Kedersha et al., 2005). It is therefore conceivable that the composition of PBs might vary depending on the particular stress that induced their assembly.

Individual PB proteins may also have different exchange rates and vary in the extent to which they can be exchanged. In fact, Dcp2 seems to be one of the less exchangeable PB constituents (Aizer et al., 2008). Thus Dcp2 and Dhh1 levels may not change dramatically between different PB subtypes, which may therefore be indistinguishable by immuno electron microscopy approach. Since Ca^{2+}-induced PBs are much shorter lived than the starvation-induced PBs, it is plausible that also a maturation pathway for PBs exists. The hallmarks of such a pathway would first be mRNA storage and later mRNA degradation.

The data we present here challenge the current prevailing model of PB assembly on various levels. First, different stresses lead to a different number of PBs independent of the level of translation attenuation (Figure 3.2 and Figure 3.4). Second, the diameters of Dcp2-myc and Dhh1-myc rings -which we assume represent PBs- do not significantly change under various stresses (Figure 3.7). If PBs were mere mRNP aggregates, why would they be uniform in size? Third, the formation of PBs after secretory transport block required functional calmodulin, while Dcp2-GFP foci were still observed in starved *cmd1-3* mutant cells subjected to starvation or osmotic stress (Figure 3.5). Finally, the Lsm-associated protein Pat1 and the Lsm homologue Scd6 were essential for PB formation in secretory pathway mutants or in Ca^{2+}-treated wild type cells, but not during starvation or NaCl treatment (Figure 3.6). Therefore our data indicate that parallel pathways for PB induction must exist, and those pathways may modulate the extent to which PBs are formed.

Here, we identified three novel modulators of the PB response, calmodulin, Scd6, and Pat1. The interaction partner for calmodulin in PB assembly remains elusive, but calmodulin does not seem to act through CaM kinases, as the concomitant loss of CaM kinase 1 and 2 (Δ*cmk1* Δ*cmk2*) had no effects on PB formation.

Whether Cmd1, Scd6, and Pat1 act in parallel or whether Cmd1 is upstream of Scd6 and Pat1 remains unclear. The EF-hand contained in Pat1 does not seem to be directly involved in Ca^{2+}-sensing; in a strain in which we mutated the putative Ca^{2+} coordinating residues, multiple PBs were still induced in response to Ca^{2+} (unpublished results). We envision a pathway in which secretory pathway mutants would trigger a change in intracellular Ca^{2+}, and this change would be sensed by calmodulin. Calmodulin might then either directly, or through Scd6 and Pat1, promote PB formation. The assembly of PBs induced by starvation or other stresses would follow a different, calmodulin-independent route.

Materials and Methods

Yeast methods

Standard genetic techniques were employed throughout (Sherman, 1991). All modifications were carried out chromosomally, with the exceptions listed below. Chromosomal tagging and deletions were performed as described (Knop et al., 1999; Gueldener et al., 2002). The temperature-sensitive alleles *sec21-1, sec27-1*, and *cmd1-3* were transferred into the YPH499 or NYY0-1 background according to Erdeniz et al. (Erdeniz et al., 1997). The *cmd1-3* allele was introduced into the *arf1-11* background using plasmid pHS47 (*URA3*) that was kindly provided by E. Schiebel. After plasmid transformation, the wild-type allele *CMD1* was deleted on the chromosome. The *sec6-4* allele was integrated into the *SEC6* locus using the pRS406 vector (Sikorski & Hieter, 1989). The *sar1-D32G* allele was introduced into YPH499 on plasmid pMYY3-1 (*TRP1*), that was a gift from A. Nakano. For ER co-staining, cells were transformed with pSM1959 (*LEU2*) or pSM1960 (*URA3*), high-copy plasmids carrying Sec63-RFP, which were kindly provided by S. Michaelis.

Fluorescence microscopy

Yeast cells were grown in YPD to early log phase and shifted for 1 h to 37℃ or subjected to various stresses where indicated; *arf1-11* Δ*slt2* required additional osmotic support for growth and was cultured in medium containing 1 M sorbitol. The cells were taken up in HC-complete medium (without glucose or supplemented with $CaCl_2$ or NaCl, where indicated) and immobilized on ConA-coated slides.

Fluorescence was monitored with an Axiocam mounted on an Axioplan 2 fluorescence microscope (Carl Zeiss) using Axiovision software. Image processing was performed using Adobe Photoshop CS2. For counting, pictures were exported to Photoshop, inverted, and the tonal range adjusted using the levels dialog box to facilitate counting; all pictures from the same experiment were treated equally. A minimum of one hundred cells from at least two independent experiments was counted for each condition. In the quantification graphs, the size of the box is determined by the 25th and 75th percentiles, the whiskers represent the 5th and 95th percentiles, the horizontal line and the little square mark the median and the mean, respectively.

Denaturing Yeast Extracts and Western Blot

15 ml of yeast culture were grown to early log phase (OD_{600} 0.5–0.7) and shifted for 1 h to 37℃ where indicated. The cells were harvested and lysed with glass beads in 150 µl lysis buffer (20 mM Tris/HCl, pH 8.0, 5 mM EDTA) in the presence of 1 mM dithiothreitol and protease inhibitors. The lysates were incubated at 65℃ for 5 min, and unlysed cells subsequently removed by centrifugation. The protein concentration was determined using the DC Protein Assay (Bio-Rad), and the equivalent of 30 µg of total protein analyzed by SDS-PAGE and immunoblotting. Total Slt2 was detected using goat anti-Mpk1 antibody (yN-19, Santa Cruz Biotechnology) and phospho-Slt2 using rabbit antiphospho-p44/42 MAP kinase (Thr202/Tyr204) antibody (Cell Signaling) with horseradish peroxidase-conjugated secondary antibodies (Pierce) and ECL reagent (GE Healthcare).

Polysome Profile Analysis

Polysome preparations were performed as described previously (de la Cruz et al., 1997) on 4-47% sucrose gradients prepared with a Gradient Master (Nycomed Pharma). Gradient analysis was performed using a gradient fractionator (Labconco) and the Äcta FPLC system (GE Healthcare) and continuously monitored at A_{254}.

Immuno-electron microscopy

Cells expressing Dcp2-9myc or Dhh1-9myc were grown to early log-phase at 23℃ and then shifted to 37℃ for 1 h or transferred to a medium lacking a carbon source for 15 min. Cells were fixed and treated for immuno-electron microscopy as described in (Prescianotto-Baschong & Riezman, 2002). 10 nm gold particles coupled to goat anti-rabbit IgG (BBInternational) were used to detect the binding of polyclonal rabbit anti-myc antibodies (Abcam).

Flotation of PBs

Flotation of ER membranes was performed according to (Schmid et al., 2006). The equivalent of 50 OD_{600} units was converted into spheroplasts at 37℃ and lysed by dounce homogenization in 3 ml of lysis buffer (20 mM Hepes/KOH, pH 7.6, 100 mM sorbitol, 100 mM KAc, 5 mM $Mg(Ac)_2$, 1 mM EDTA, 100 µg /ml cycloheximide) in the presence of 1 mM DTT and protease inhibitors. After removal of cellular debris (5 min, 300 g), membranes were pelleted by centrifugation (10 min, 13,000 g), resuspended in 2 ml of lysis buffer containing 50% sucrose, and layered on top of 2 ml 65% sucrose in lysis buffer. Two additional 5 ml and 2 ml cushions (40% and 0% sucrose) were layered on top. The step gradient was spun in a TST41.14 rotor for 16 h at 28,000 g. After centrifugation, 1 ml fractions were collected from each of the cushions and the interphases and TCA precipitated. The samples were analyzed by SDS-PAGE and immunoblotting using monoclonal mouse anti-myc antibodies (9E10, Sigma) and polyclonal rabbit anti-Sec61 antibodies (a gift from R. Schekman).

Northern Blot

Yeast cells were grown in YPD to early log phase and shifted for 1 h to 37℃ where indicated. Cells were lysed in lysis buffer by grinding in liquid nitrogen. RNA was extracted from the P13 pellet using TriZOL reagent (Invitrogen), and 15 µg of RNA were resolved on agarose gels containing formaldehyde. The RNA was transferred onto Hybond N+ (Amersham Biosciences) and subsequently hybridized to HAC1 probes, which were

generated using an AlkPhos direct labeling kit (GE Healthcare). The probes were detected using the CDP-Star reagent (GE Healthcare) according to the manufacturer's recommendations.

Acknowledgements

We are grateful to E. Schiebel, A. Diepold and members of the Spang lab for discussions, and to E. Hartmann and I.G. Macara for critical comments on the manuscript. S. Michaelis is acknowledged for providing the Sec63-RFP plasmid, and we thank T. Davis, M. Hall, A. Nakano, R. Schekman and E. Schiebel for reagents. This work was supported by the Boehringer Ingelheim Fonds (C.K.), the Werner Siemens Foundation (J.W.), the Swiss National Science Foundation, and the University of Basel.

Supplementary Figures

Suppl. Figure 1: Wild-type or *arf1-11* cells expressing Dhh1-GFP were shifted to 37℃ for 1 h. While multiple foci were observed in *arf1-11*, only 0-2 PBs/cell were induced in wild-type cells.

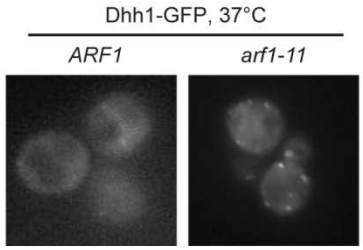

Suppl. Figure 2: (**A**) *arf1-11* cells expressing Dcp2-GFP and deleted for *PUB1* were shifted to 37℃ for 1 h. Multiple foci are still observed in this strain. (**B**) Wild-type cells expressing the SG marker eIF3B-GFP were shifted to 37℃ for 1 h or to 46℃ for 10 min. There was a marked induction of eIF3B-GFP containing granules after high heat shock. When cells were stressed by incubation in H_2O, rich medium containing 0.5 M NaCl, or medium lacking a carbon source (-D) for 15 min, no SG formation was observed with this marker.

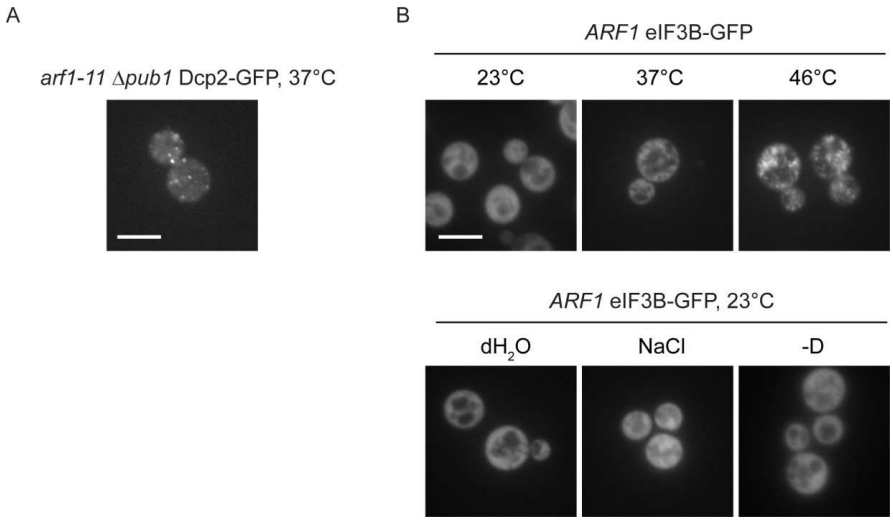

Suppl. Figure 3: Calmodulin is lost from the small bud tip in *arf1-11* and after Ca2+ treatment. Wild-type or *arf1-11* cells expressing Cmd1-GFP were shifted to 37℃ for 1 h or treated with 200 mM $CaCl_2$ for 15 min at 23℃. White arrowheads point towards small bud tips. The white bar represents 5 µm.

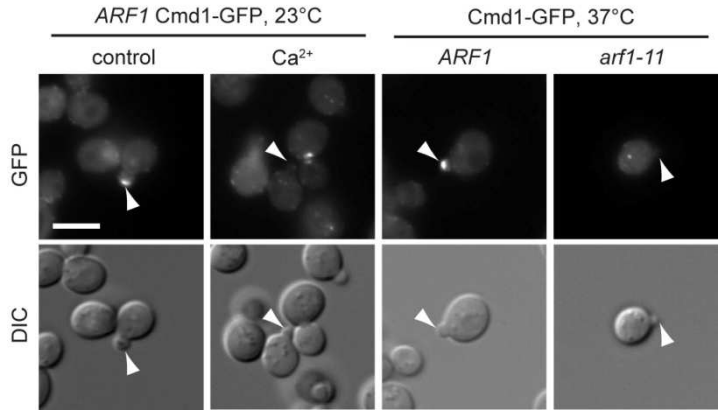

Suppl. Figure 4: The immuno-gold labeling is specific. Wild-type cells were prepared for thin section electron microscopy. Thin sections were labeled with myc-antibody and secondary antibodies coupled to gold. A few gold particles were observed scattered throughout the cell. The arrowheads point to individual gold particles. No gold clusters as in Figure 3.7 C were observed. The bar in the images represent 0.5 µm
.

3.2 Additional PB data

3.2.1 No differential recruitment of Scd6p and Edc3p to PBs under starvation or Ca^{2+} treatment

There is evidence in the literature that the *Drosophila* homologs of Edc3p and Scd6p, EDC3 and Trailer Hitch, compete for binding to Me31B, a homolog of the helicase Dhh1p, via their central FDF motif and may serve as a scaffold to recruit additional effectors like the translational repressor CUP (Tritschler et al., 2008; Tritschler et al., 2009). These protein-protein interactions appear to be conserved in *Xenopus* and *C. elegans* (Audhya et al., 2005; Decker & Parker, 2006; Tanaka et al., 2006).

Since we found that Scd6p is specifically required for the formation of Ca^{2+} induced PBs, but not for PBs induced by glucose starvation, we wondered whether Edc3p or Scd6p might be differentially recruited to PBs induced under specific conditions. Thus, we appended Edc3p and Scd6p with GFP in wild-type and *arf1-11* mutant. When PBs were induced in in these strains by glucose starvation or Ca^{2+} treatment, both markers localized to PBs regardless of the stress applied (Figure 3.8 A). Both Scd6-GFP and Edc3-GFP accumulated in foci in *arf1-11* shifted to the non-permissive temperature for 1 h.

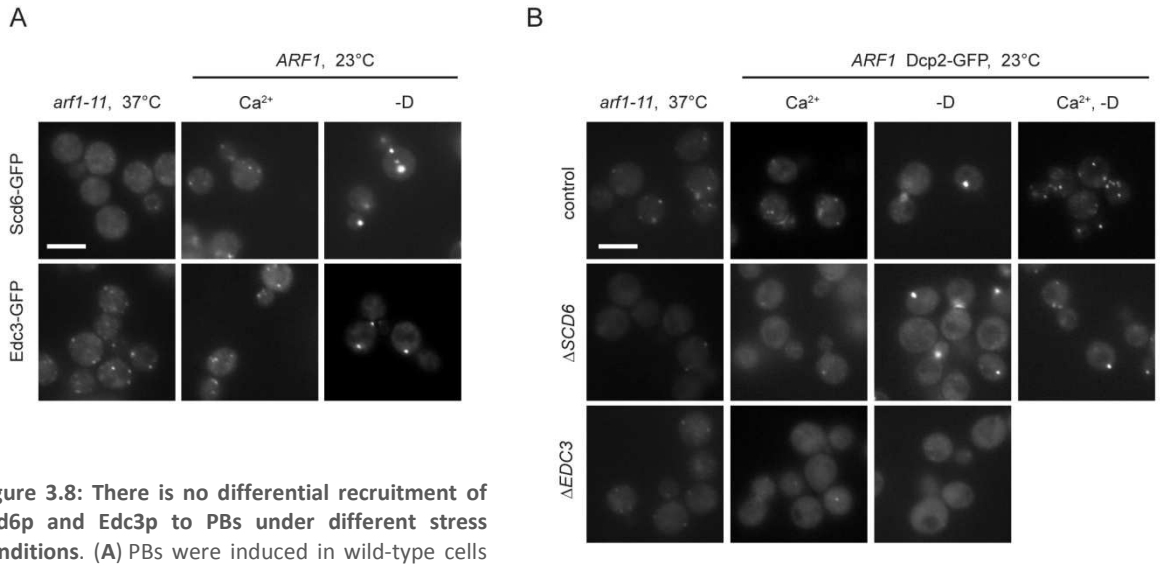

Figure 3.8: There is no differential recruitment of Scd6p and Edc3p to PBs under different stress conditions. (**A**) PBs were induced in wild-type cells expressing Scd6-GFP or Edc3-GFP by treatment with 200 mM Ca^{2+} or incubation in medium lacking a carbon source for 15 min. Alternatively, *arf1-11* was shifted to the non-permissive temperature for 1 h. Both proteins localize to PBs regardless of the stress condition that induced them. (**B**) PBs were induced in wild-type cells expressing Dcp2-GFP that were deleted for *SCD6* or *EDC3* by treatment with 200 mM Ca^{2+}, incubation in medium lacking a carbon source, or a combination of both stresses. Alternatively, *arf1-11* was shifted to the non-permissive temperature for 1 h. Deletion of *EDC3* reduced the formation of all types of PBs. Similarly, deletion of *SCD6* to did not fully restore PB numbers to levels observed under glucose starvation when a combination of Ca^{2+} treatment and glucose starvation was applied. The white bars in A and B represent 5 μm.

When cells were deleted for *EDC3,* Ca^{2+} treatment failed to elicit PB formation as judged by Dcp2-GFP, but so did glucose starvation (Figure 3.8 B), suggesting that there is a general requirement for Edc3p in PB aggregation, independently of the stressor, which is in approximate agreement with published data (Decker et al., 2007).

Similarly, deletion of *SCD6* did not fully restore PB number to the level observed under glucose starvation when a combination of Ca^{2+} treatment and glucose starvation was applied (Figure 3.8 B). Taken together, these data clearly show that differential recruitment of the two scaffold proteins is not what discriminates between the different types of PBs we observe.

3.2.2 Purification of PBs

Although we observed a striking difference in PB morphology on the light microscopic level if cells were starved for glucose or treated with Ca^{2+}, none of the PB markers we tested showed any specificity towards PBs induced under a certain stress. Thus, to identify proteins that might be recruited specifically to PBs induced in secretion mutants, we decided to purify PBs and to analyze the proteins associated with them by mass spectrometry. Because we hoped to also identify membrane-bound proteins that might anchor PBs to the ER, we subjected cells to formaldehyde cross-linking followed by a fully denaturing purification (Tagwerker et al., 2006). In short, wild-type or *arf1-11* mutant cells expressing Dcp2 appended with a C-terminal 6xHis-biotin-6xHis-tag (Dcp2-HBH) were shifted to the non-permissive temperature for 1 h to induce PB formation, fixed with a low concentration of formaldehyde, lysed, and a fraction enriched in ER membranes purified on Ni-NTA and streptavidin beads. Proteins were digested directly on the beads and the peptides analyzed by LC-MS/MS. The list of identified peptides was filtered against the untagged control and all hits present in purifications of unrelated HBH-tagged proteins that had previously been carried out in the lab (Table 3.2).

Besides Dcp2p, several *bona fide* PB components co-purified, including Edc3p, Scd6p (wild-type only), and Lsm1p (mutant only). In addition, multiple RNA-binding proteins were detected, among these Puf5p, which plays a role in cell wall integrity (Stewart et al., 2007); Vts1p, which is a homolog of *Drosophila* Smaug, a key regulator of maternal mRNA destabilization in maternal-to-zygotic transition, and stimulates mRNA degradation *in vitro* (Tadros et al., 2007; Rendl et al., 2008); the RNA helicases Dbp2p and Dbp3p; and Lhp1p, a La homolog originally implicated in RNA biogenesis, which is required for growth under conditions that induce UPR and has been shown to specifically bind to HAC1 mRNA (Inada & Guthrie, 2004, wild-type only). Interestingly, Arf1p was also detected in Dcp2-HBH-mRNPs in *arf1-11*. Only one ER-resident transmembrane protein co-purified, Zrg17p, which was present with only one peptide in the mutant, and was not analyzed any further; later, it was found in the untagged control of an unrelated purification, indicating that Zrg17p was a contaminant.

Table 3.2: Proteins associated with purified Dcp2-HBH-complexes.

Gene name	Description (Source: Proteome)	Number of peptides	
		ARF1	*arf1-11*
DCP2*	DCP2 decapping enzyme, an mRNA 5'-UTR binding ribonuclease that mediates deadenylation-dependent decapping of nuclear-transcribed mRNA, regulates mRNA stability, may play a role in nonsense-mediated mRNA catabolism	20	17
MHP1	Microtubule-interacting protein, functions in stabilization of microtubules	9	10
CYR1	Cyclic AMP requirement 1, functions as an adenylyl cyclase, generates cAMP in response to ras activation	6	6
RRP5	Ribosomal RNA processing 5, required for processing of pre-rRNA to 18S and 5.8S rRNA, component of the 80S U3 snoRNA complex (SSU processome) that is required for 18S rRNA biosynthesis	6	1
YCK2	Yeast casein kinase 2, exhibits multiple kinase activities and regulates a variety of cellular events	4	5
DOT6	Disruptor of telomeric silencing 6, functions in telomere silencing	4	2
PUF5	Multicopy suppressor of pop2 (two) 5, an RNA-binding "Puf" protein involved in mRNA degradation, also required for recovery from alpha-factor arrest, regulation of HO expression, normal life span, and inhibition of filamentous growth	3	4
EDC3*	Enhancer of mRNA decapping 3 homolog, an mRNA-decapping complex associated protein that is required for removal of the 5-prime cap from mRNA during mRNA degradation, exhibits homodimerization activity	4	1
YOL087C	Protein containing three WD domain G-beta repeats, which may mediate protein-protein interactions, has low similarity to uncharacterized C. pseudotropicalis Yol087p	4	3
RPA190	RNA polymerase A 190, RNA polymerase I largest subunit	4	-
TyB protein	TyB protein - yeast (Saccharomyces cerevisiae) retrotransposon Ty912	3	3
YBR238C	Protein with high similarity to S. cerevisiae Rmd9p, which may be involved in meiotic nuclear division, or respiration	3	3
ROM2	RHO1 multicopy suppressor 2, a GEF for Rho1p that is activated by cell wall defects, involved in ethanol tolerance and in the cAMP-mediated response to stress	3	3
VTS1	VTi1-2 suppressor 1, an RNA-binding protein that destabilizes SRE (Smg recognition element)-containing transcripts, confers allele-specific suppression of a vti1-2 mutation upon overproduction	2	3
DBP3	ATP-dependent RNA helicase CA3, member of the DEAD-box family of RNA helicases	2	1
MMT2	Protein involved in mitochondrial iron accumulation, member of a family of transition metal transporters	2	2
HTA1	Histone h two A 1, a chromatin binding protein that functions in chromatin related events	2	-
DBP2	ATP-dependent RNA helicase of the DEAD-box family	2	1
PFS2	Polyadenylation factor I subunit 2 required for mRNA 3'-end processing, bridges two mRNA 3'-end processing factors, has WD (WD-40) repeats	1	-
SIK1	Suppressor of IkappaB 1, a component of box C/D snoRNPs that are necessary for 2'-O-methylation of rRNAs, a component of the 80S U3 snoRNA complex (SSU processome) hat is required for 18S rRNA biosynthesis, also required for nucleolus morphology	1	1
INO2	Inositol requiring 2, a basic helix-loop-helix (bHLH) transcription factor required for derepression of phospholipid synthetic genes	1	3
IMP2	Inner membrane protease 2, the catalytic subunit of the mitochondrial inner membrane protease Imp, acts in complex with Imp1p but has different substrate specificity for removal of signal peptides	1	1
RRP12	Ribosomal-RNA binding protein required for nuclear export of 40S and 60S ribosomal subunits, possibly involved in rRNA processing	1	-
MMT1	Protein involved in mitochondrial iron accumulation	1	1
HMO1	High mobility group protein 1, a protein with HMG-box DNA-binding domain involved in rDNA transcription, may coordinate rDNA with ribosomal protein gene expression, interacts with FK506-binding protein Fpr1p	1	-
MAM3	Protein required for normal mitochondrial structure	1	-
VNX1	Vacuolar Na+/H+ exchanger 1, functions as a vacuolar monovalent cation/H+ antiporter to likely regulate ion homeostasis and cellular pH	1	2
YPL260W	Protein of unknown function, has high similarity to uncharacterized C. glabrata Cagl0h09108gp	1	1
NOP7	Nucleolar protein 7, an essential protein required for 60S ribosomal subunit biogenesis and transport, may regulate cell cycle progression	1	-

Gene name	Description (Source: Proteome)	Number of peptides	
		ARF1	*arf1-11*
GPD2	Glycerol-3-phosphate dehydrogenase (NAD+) 2, involved in glycerol production converting glycerol-3-phosphate and NAD+ to dihydroxyacetone phosphate and NADH	1	2
VTC3	Vacuolar transporter chaperone 3, a subunit of the vacuolar transporter chaperone (Vtc) complex (Vtc1p, Vtc2p, Vtc3p, Vtc4p), required for the final step of vacuolar fusion, involved in vacuolar polyphosphate accumulation	1	-
AMD1	AMP deaminase, converts AMP to IMP and ammonia	1	4
NOP13	Nucleolar protein with similarity to Nsr1p, has two RNA recognition (RRM) domains	1	-
MOT2	Modulator of transcription 2, a zinc finger transcriptional repressor and component of the CCR4-Not complex, involved in G protein-mediated pheromone signal transduction and decapping some mRNAs, catalyzes ubiquitination of the EGD complex with Ubc4p	1	-
LHP1	La homologous protein 1, protein homolog to human La autoantigen which binds to and stabilizes pre-tRNA for 3' endonucleolytic cleavage, has an RNA recognition (RRM) domain	1	-
PWP1	Protein containing three WD domain G-beta repeats, has high similarity to uncharacterized C. glabrata Cagl0a04037gp	1	1
PSP2	High-copy suppressor of temperature-sensitive mutations in DNA polymerase alpha	1	1
SCD6*	Multicopy suppressor of inviable strains of clathrin heavy chain deficient yeast	1	-
YDJ1	Yeast DnaJ homolog 1, exhibits ATPase stimulator activity, functions in mitochondrial and ER protein import, protein folding, and response to heat and stress	1	1
UTP14	U3 protein 14, a component of the 80S U3 snoRNA complex (SSU processome) that is required for 18S rRNA biosynthesis	1	-
YER067W	Protein of unknown function, has high similarity to uncharacterized S. cerevisiae Yil057p	1	1
SSP120	Protein of unknown function, has high similarity to uncharacterized C. glabrata Cagl0h03597gp; localizes to the cis Golgi	1	1
PRP43	Pre-mRNA processing 43, an RNA helicase of the DEAH-box family with ATPase activity, required for release of the lariat-intron from the spliceosome and for processing precursor RNAs of the small and large ribosomal subunits	1	-
YDR210W	Protein of unknown function	1	5
NOP58	Nucleolar protein 5, a component of box C/D snoRNPs that are necessary for 2'-O-methylation of rRNAs, a component of the 80S U3 snoRNA complex (SSU processome), also required for nucleolus morphology	1	-
HIS4	Histidine requiring 4, a phosphoribosyl-AMP cyclohydrolase, phosphoribosyl-ATP pyrophosphohydrolase and histidinol dehydrogenase that acts in the second, third, and tenth steps of histidine biosynthesis pathway	1	-
ARF1	ADP-ribosylation factor 1, a GTPase that regulates formation of nascent secretory vesicles from trans-Golgi network, inhibits ER to Golgi vesicular transport, induces phosphatidylinositol 4, 5-bisphosphate synthesis	-	4
CAR2	Ornithine aminotransferase (ornithine oxo-acid aminotransferase), acts in the degradation of arginine, citrulline and ornithine	-	2
YGR237C	Protein of unknown function, has moderate similarity to uncharacterized C. glabrata Cagl0f07975gp	-	2
XRN1*	KAR(-) enhancing mutation 1, a 5'-3' exonuclease for single-stranded RNA and DNA that degrades decapped mRNA, required for pseudohyphal and invasive growth, involved in the G1 to S phase transition	-	2
PRB1	Proteinase B 1, a serine protease of the subtilisin family with broad proteolytic specificity, mediates maturation of vacuolar alkaline phosphatase (Pho8p)	-	1
IRA2	Inhibitory Regulator of the RAS-cAMP pathway 2, a GAP for Ras1p and Ras2p that is required for normal sporulation and for glycogen and trehalose accumulation	-	1
PNC1	Pyrazinamidase and nicotinamidase 1, exhibits both pyrazinamidase and nicotinamidase activities, functions in rDNA silencing and determination of life span	-	1
SBP1*	Single-stranded nucleic acid-binding protein 1, associated with small nucleolar RNAs (snoRNAs), involved in glucose starvation-induced translation repression and PB formation	-	1
ZRG17	Zinc-regulated gene 17, member of the cation diffusion facilitator (CDF) family that mediates zinc uptake into the secretory pathway	-	1
PUB1	PolyU binding 1, a major polyadenylated RNA-binding protein of nucleus and cytoplasm that also binds AU-rich elements (ARE) and stabilizes ARE-containing transcripts, contains three RNA recognition (RRM) domains and three Gln/Asn-rich regions	-	1

The gene name, a short description of the protein function, and the number of individual peptides that were identified in the mass spectrometric analysis in wt or *arf1-11* are given. *Bona fide* PB components are marked with an asterisk. Mitochondrial, vacuolar, and nuclear proteins are designated in light gray. **Gene names high-lighted in bold were chosen for deletion analysis**. Gene names marked with an underscore code for transmembrane proteins. *Gene names in italics were later found in untagged control samples from unrelated purifications that were carried out in the lab.*

When we picked candidates for further analysis, we concentrated on potential regulators of PB formation; all proteins located to mitochondria, the vacuole, or the nucleus, or that were involved in ribosomal processing were considered to be contaminants and were disregarded (designated in gray in Table 3.2); Mhp1p was included although it had also been detected in an unrelated purification because it was the most abundant protein besides Dcp2-HBH itself.

We generated deletions in wild-type and *arf1-11* for all candidate ORFs (designated in bold in Table 3.2) and assayed PB induction after Ca^{2+}-treatment or temperature shift. None of the mutations prevented formation of multiple PBs; however, in the absence of *ROM2*, we observed an increase in PBs in the wild-type after temperature shift (data not shown). Several of the candidate ORFs were later detected in untagged control samples of other HBH-purifications that were carried out in the lab, including *ROM2* (designated in italics in Table 3.2), indicating that these proteins may have been contaminants and that an association with PBs does not take place. In the case of *ROM2*, deletion might result in a stress phenotype even under normal growth conditions that induces formation of PBs. This explanation would not require localization of Rom2p to PBs.

Some of the proteins that we identified were later found in additional purifications of Dcp2-HBH or Scd6-HBH that were carried out in the lab, which provides corroborating evidence that these proteins associate with PBs (Julie Weidner, unpublished data). Besides *bona fide* PB components, which always co-purified, these ORFs include *HTA1*, *DBP2*, *YPL260W*, *NOP7*, *PSP2*, and *ARF1*. Both the histone Hta1p and the nucleolar protein Nop7p localize to the nucleus; for them, a possible role in PB formation is hard to envision. However, the cytoplasmic proteins Dbp2p, Ypl260wp, and Psp2p could be additional regulators of PB function, and might merit further investigation.

3.2.3 Inference of mRNAs that could be contained in Ca^{2+}-induced PBs from published data.

To our understanding, the multiple PBs that we observed in secretory mutants should fulfill a discrete function: Either, they should clear away transcripts whose protein products would be deleterious under the stress encountered, or they should serve to stabilize mRNAs that encode for proteins that become essential under stress; alternatively, both may apply. In all cases, transcript abundances should be affected. Since – to our best knowledge – the multiple PB phenotype we observed in secretory mutants could be fully phenocopied by a short treatment with extracellular Ca^{2+} (see chapter 3.1), we used published expression data on the response to Ca^{2+} treatment and tried to infer which transcripts might be found in PBs induced in secretion mutants.

The Cyert lab has generated an extensive gene expression dataset on yeast treated with either Ca^{2+} or sodium chloride which they carefully analyzed with respects to the calcineurin dependency of the Ca^{2+} response (Yoshimoto et al., 2002). Since induction of PBs was not affected by deletion of calcineurin, we were mainly interested in those transcripts that respond to Ca^{2+}

treatment independently of calcineurin, presuming that this dataset would comprise genes regulated not by transcription but on the level of mRNA stability; thus, we reanalyzed their data accordingly.

We included all genes that were up- or downregulated at least three-fold after 15 min of Ca^{2+} treatment but were not strongly dependent on the presence of calcineurin in their response (less than 1.25-fold change). Of these 217 genes, more than 97% responded to Ca^{2+} at least twice as strongly as to NaCl treatment; in fact, only 8.3% of the ORFs showed more than a two-fold change upon NaCl treatment. Using FunSpec, a web-based analysis tool for yeast (Robinson et al., 2002), we mapped these genes to functional categories. Among the 109 transcripts that decreased upon Ca^{2+} treatment, ORFs implicated in rRNA processing; lipid, fatty acid and isoprenoid metabolism; or rRNA modification were enriched (MIPS Functional Classification; P-value cutoff 0.001, Table 3.3). Among the 108 transcripts that increased upon Ca^{2+} treatment, the following categories were overrepresented: oxidative stress response; protein fate (folding, modification, destination); secondary metabolism; and unfolded protein response (e.g. ER quality control) (P-value cutoff 0.001, Table 3.3). In both cases, some of the categories overlapped.

Table 3.3: MIPS Functional Classification categories enriched in ORFs increased or repressed after Ca^{2+} treatment.

Genes decreased upon Ca^{2+} treatment				
Category	**In Category from Cluster**	**k**	**f**	**p-value**
rRNA processing	KRR1 NOP1 NHP2 RRP1 ESF1 SNU13 ENP2 RPP1 GAR1 UTP21 RRP6 RRP12 DIM1 NOC4	14	169	5.853e-07
lipid, fatty acid and isoprenoid metabolism	YBR030W FEN1 SUR2 IZH1 ATF2 FAA3 AUR1 SHM2 SEC59 FAA4 IZH4	11	142	1.953e-05
rRNA modification	NOP1 NHP2 GAR1 DIM1	4	18	0.0001799

Genes increased upon Ca^{2+} treatment				
Category	**In Category from Cluster**	**k**	**f**	**p-value**
oxidative stress response	PRX1 UGA2 PST2 TSA2 GPX1 GAD1 GRE1	7	55	2.74e-05
PROTEIN FATE (folding, modification, destination)	SNO4 HSP33 HSP32	3	8	0.0002245
UNCLASSIFIED PROTEINS	RCR2 YDR391C IRC4 KRE29 YGR035C YGR042W YGR111W YHR140W CRG1 MPM1 MBB1 YJR008W YET1 YKL091C YJU3 YKL133C YKR011C YLR271W YML119W YMR027W YMR090W YMR181C YNL305C YOL048C YOL083W YOR052C YOR097C DCS2 AIM41 YOR352W SET6 PGC1	37	1378	0.0007884
secondary metabolism	COQ4 GRE3 YJR096W	3	12	0.0008409
unfolded protein response (e.g. ER quality control)	UBC5 HSP42 SHY1 SNO4 HSP33 HSP32	6	69	0.0008656

All genes that increased or decreased at least three-fold upon Ca^{2+} treatment but were independent of calcineurin (less than 1.25-fold change) were included into the analysis. All genes mapped to the respective category are given. (k) designates the number of genes mapped to the category from the cluster (f) designates the total number of genes found in each category. P-values are indicated. Data source: Yoshimoto et al., 2002. Clustering was carried out with FunSpec.

At the moment, we cannot predict which of the two sets of genes would be more likely to localize to Ca^{2+}-induced PBs, or whether both of them should. On one hand, PBs have been characterized as sites of mRNA decay; one would therefore expect mRNAs targeted to PBs to decrease in concentration. On the other hand, genome-wide analysis of decay rates under a similar stress condition, namely under hyperosmotic stress, has revealed a three-phasic response: During the first phase, which coincides with PB induction, the majority of transcripts became stabilized while transcription rates dropped, with only a few stress-responsive genes showing the opposite behavior; during the second phase, transcription rates surged, but transcripts were generally very unstable; finally, in the third phase, mRNA stability and transcription rates returned to unstressed levels (P. Cramer, B. Schwalb, personal communication). As stated above, appearance of PBs correlated with transcript stabilization. This suggests that – at least under stress – PBs are sites of mRNA storage rather than of decay. Whether aggregation into PBs might even be required for mRNA stabilization has not been examined. Thus, Ca^{2+}-induced PBs might also contain those mRNAs that are stabilized in response to the treatment. FISH/IF on candidate mRNAs in strains expressing Dcp2-GFP could show whether any of these transcripts are shuttled to PBs in reponse to Ca^{2+} treatment.

As we propose that secretory mutants have elevated calcium levels, and we know that at least some of them activate UPR (Figure 3.2 B), it is interesting to note that there was a significant induction of genes involved in UPR in response to Ca^{2+} treatment which didn't require calcineurin (Yoshimoto et al., 2002, see Table 4.7). If genes that are dependent on calcineurin were also considered, i.e. all 324 genes that increased at least three-fold after Ca^{2+} treatment were included in the analysis, three additional ORFs mapped to this category (P-value 0.0062); of these, two were in fact repressed by calcineurin. Of the total of nine genes involved in UPR that are upregulated after addition of Ca^{2+}, only one increased significantly in response to NaCl treatment, indicating that Ca^{2+} might be directly involved in UPR signaling. Indeed, it has been reported that ER stress triggers Ca^{2+} influx through the plasma membrane via the calcium channel Cch1/Mid1 (Bonilla & Cunningham, 2003). This response does not require Ire1p or Hac1p, but is dependent on the MAP kinase Slt2p and leads to activation of a calcineurin-dependent calcium cell survival pathway, which is not needed for UPR *per se*, but is necessary for long-term survival of yeast under ER stress (Bonilla et al., 2002).

Components of this pathway do not seem to be required for PB formation in secretory mutants, since deletion in *SLT2*, *CCH1*, *MID1*, or *CNB1*, the regulatory subunit of calcineurin, did not abolish the multiple PB phenotype (Table 3.1, data not shown). However, it may be that Ca^{2+} levels in secretion mutants are elevated independently from MAP kinase signaling and the plasma membrane calcium channel, but activate the same downstream effectors. In fact, the multiple PBs we observed may represent a part of the calcium cell survival pathway that is further downstream and might be activated directly by elevated Ca^{2+} levels. When we treated cells with the glycosylation inhibitor

tunicamycin for 1 h to induce ER stress, no multiple PBs were observed, although there was significant cleavage of HAC1 mRNA (data not shown); however, results from Bonilla and Cunningham (2003) indicate that intracellular Ca^{2+} levels rise only after prolonged treatment with tunicamycin (> 1 h), and they used a higher concentration for induction (2.5 µg/ml instead of 1 µg/ml). Thus, the conditions we employed might have been too mild to elicit a Ca^{2+} response. Additional experiments will have to be performed to asses whether induction of multiple PBs is connected to the calcium cell survival pathway that acts in response to ER stress. Furthermore, it would be interesting to know whether any of the UPR transcripts (s. Table 3.3) colocalize with PBs after Ca^{2+} treatment, and, if yes, whether Cmd1p or Pat1p are required for colocaliziation.

3.2.4 Repression of translation is not required for induction of PBs by Ca^{2+} treatment or in secretory mutants

According to the dynamic equilibrium model (Parker & Sheth, 2007), mRNAs passively aggregate into PBs when translation is repressed. In agreement with this, we observed an attenuation of protein translation under conditions that induced multiple PBs, namely in secretory mutants and after Ca^{2+} treatment, conditions which we consider to be equivalent (see chapter 3.1).

Deloche et al. (2004) have shown that translation attenuation requires the eIF2α kinase Gcn2p in some secretory mutants, and this was also true for *arf1-11* (see chapter 4.2.3). However, deletion of *GCN2* did not prevent induction of multiple PBs in *arf1-11* (Figure 3.2 C). Therefore, translation repression and PB induction were uncoupled in this strain, indicating that passive aggregation of mRNAs that are released from polysomes is not the cause for multiple PB formation.

Since Gcn2p is activated in response to UPR, we also analyzed a deletion of *IRE1*, an important sensor of ER stress. This mutation had a mild effect on translation attenuation but did not restore translation to wild-type levels; nor was PB induction rescued (Figure 3.9 A). When we analyzed the same deletions in wild-type cells treated with Ca^{2+}, the effect was the same: Although deletion of *GCN2* rescued translation attenuation, it did not affect PB number (Figure 3.9 B). Deletion of *IRE1* slightly enhanced general translation, but did not rescue PB induction. While we cannot exclude that Ca^{2+} treatment may induce UPR, which remains to be shown, these data clearly indicate that activation of Gcn2p upon elevated Ca^{2+} levels occurs independently of ER stress, since deletion of the stress sensor *IRE1* could not prevent translation attenuation, while deletion of *GCN2* fully restored translation to wild-type levels; thus, Ca^{2+} might directly activate Gcn2p through an unknown mechanism. Importantly, PB induction was independent of general translation attenuation in both cases, which suggests that Ca^{2+}-induced PBs do not accumulate random silenced transcripts, but contain specific mRNAs that might be selectively removed form translation.

In the future, additional experiments will show whether PB formation and translation attenuation can be equally uncoupled under hyperosmotic stress or glucose starvation, or whether

this is a unique feature of Ca^{2+}-induced PBs. In any case, this result shows that the dynamic equilibrium model (Coller & Parker, 2005) is not applicable to Ca^{2+}-induced PBs and has widespread implications for our understanding of the nature of PBs.

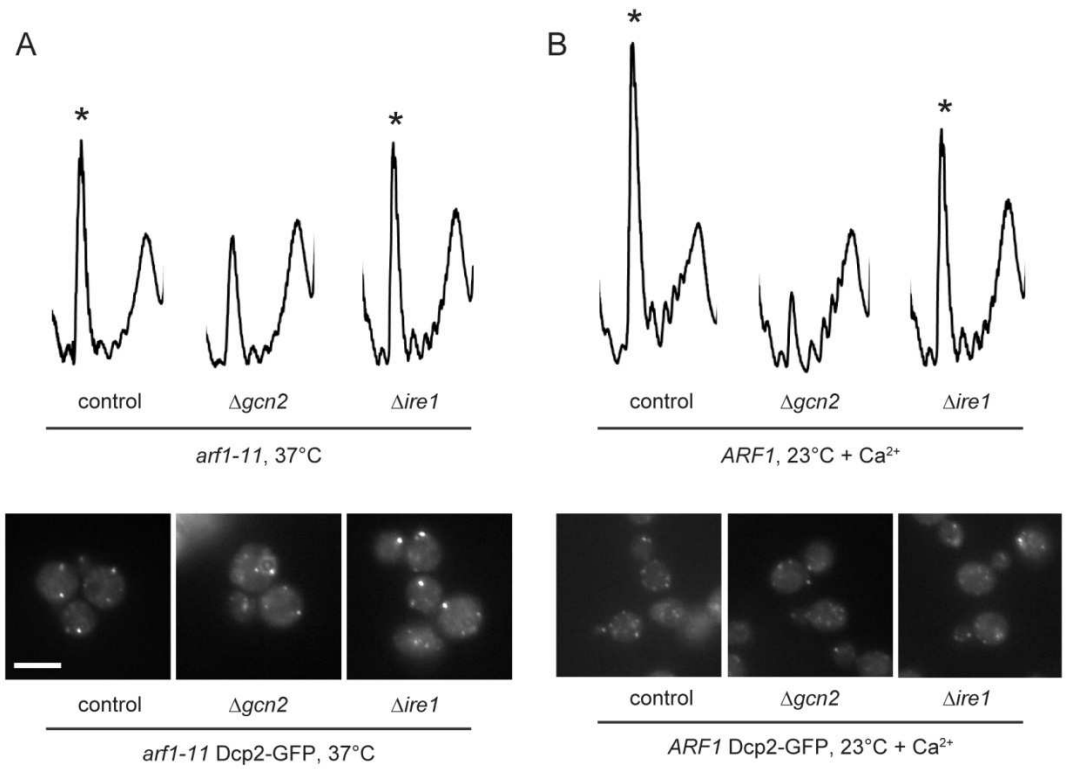

Figure 3.9: Translation repression and PB induction can be uncoupled. (**A** and **B**) Cells expressing Dcp2-GFP and deleted for *GCN2* or *IRE1* were both directly imaged under an epifluorescence microscope or lysates generated and polysome profiles recorded. Although deletion of *GCN2* rescued translational repression, multiple PBs were observed in all strains. (**A**) PBs were induced in *arf1-11* by a shift to the non-permissive temperature for 1 h. (**B**) PBs were induced in wild-type cells by treatment with 200 mM Ca^{2+} for 15 min. Polysome profiles indicative of attenuated translation are marked with an asterisk. The white bars in A and B represent 5 µm.

3.3 Section summary and open questions

We have found that multiple PBs are induced in secretion mutants or after Ca^{2+}-treatment (9 to 10 PBs per cell on average), a phenotype that is markedly different from PB induction after starvation, which leads to the aggregation of only 2 to 4 very bright Dcp2-GFP granules per cell. Formation of Ca^{2+}-induced PBs could be prevented by deletion of the PB components *SCD6* or *PAT1*, or by expressing *cmd1-3*, a mutant of calmodulin that is defective in Ca^{2+}-binding; in all three strains, PB induction by glucose starvation or hyperosmotic shock was not affected. Notably, the number of PBs did not just reflect the degree of translation attenuation because multiple PBs were still observed when Ca^{2+} treatment – which on its own results in only a weak translational inhibition – was combined with glucose starvation, which strongly blocks translation. Taken together, these data

indicate that there are several pathways that can lead to PB formation in response to stress, and these pathways also control PB number.

We believe that formation of multiple PBs in secretory mutants is regulated by Ca^{2+} because (i) treatment with $CaCl_2$ induced a similar number of PBs, (ii) PB induction in secretory mutants could be rescued by culturing them in a Ca^{2+}-chelating agent, and (iii) because formation of PBs required calmodulin and the PB components Scd6p and Pat1p in both cases, while PB formation under hyperosmotic stress, which also induced multiple PBs, was not affected. Additional evidence indicated that Ca^{2+} levels are elevated in secretory mutants: First, Cmd1-GFP disappeared from the small bud tip after addition of Ca^{2+} to the medium, but also in *arf1-11* upon temperature shift. Second, in Ca^{2+}-treated cells, ASH1 mRNA accumulated at the bud neck, as has been observed in many secretion mutants (Trautwein et al., 2004; data not shown). Third, translation was attenuated to a similar degree in *arf1-11* and after Ca2+ treatment; in both cases, translational repression could be fully rescued by deletion of *GCN2*.

Currently, we are ignorant of the mechanism by which Ca^{2+} enters the cell. It might passively leak into the cytoplasm from the extracellular milieu or escape vacuolar storage because the membrane structure is heavily compromised in secretory mutants. Alternatively, Ca^{2+} levels could rise as part of a signaling response and involve dedicated calcium channels. In general, Ca^{2+} influx and release have not been studied extensively in *S. cerevisiae*, with some notable exceptions (for review, see Bonilla & Cunningham, 2002). The plasma membrane calcium channel Cch1p has been reported to respond to stress within the secretory pathway (Bonilla & Cunningham, 2002), but deletion of *CCH1* did not abolish multiple PB formation (data not shown), indicating that other points of entry must exist. Interestingly, the existence of a calcium cell survival pathway has been postulated; this pathway becomes active after prolonged exposure to ER stress (Bonilla & Cunningham, 2003). It remains to be shown whether multiple PBs are induced under these conditions, and whether Ca^{2+}-induced PBs are a constituent of a general cell survival mechanism.

In addition, it would of course be interesting to know the nature of the transcripts that aggregate in Ca^{2+}-induced PBs. This would give a good impression of the final output of the stress response. Reverse transcription on isolated PBs and cDNA cloning may serve to sample PB-associated mRNAs and might allow the identification of consensus motifs; a similar approach has been used to characterize RNA-protein interactions in the pre-40S ribosomal subunit and has led to the successful identification of RBP-binding sites on mRNAs isolated from cross-linked samples (Hafner et al., 2010; Granneman et al., 2010).

Besides the specific mRNAs contained in PBs, it would be equally interesting to identify the machinery involved, i.e. the trans-acting factors that shuttle mRNAs to PBs in response to elevated Ca^{2+} levels, and to understand how these proteins are regulated. As we have seen in our

purifications, this is not an easy task, as the interaction of these factors with PBs may be very transient. This has been reported for other mRNA shuttling proteins, e.g. the essential nonsense-mediated decay factors Upf1p, Upf2p, and Upf3p, which are required for the efficient clearance of transcripts containing premature stop codons. Upf1-3 were identified in a screen using NMD reporters (Leeds et al., 1991), but their interaction with PBs could only be demonstrated once mRNA decay in PBs was blocked; after deletion of *DCP1*, *DCP2*, or the endonuclease *XRN1*, Upf1p, Upf2p, and Upf3p accumulated in PBs (Sheth & Parker, 2006). In our case, isolating Dcp2-HBH complexes from a strain deleted for *XRN1* might increase the likelihood of co-purifying the desired trans-acting factors. However, it may also be that the mRNAs are direct substrates for translational repressors like the Puf proteins (Chritton & Wickens, 2010). It would then be conceivable that the mRNAs are inactivated, e.g. by recruitment of a deadenylase complex, but only later aggregate into PBs, at a point in time when the translational repressor has left the complex. This would make an isolation of the repressor from PBs impossible. We do not consider this scenario very likely because it implies a passive aggregation of silenced complexes into PBs, and the PBs we observe after Ca^{2+} treatment show a behavior distinct from PBs induced by starvation, both in their apparent number and in their requirement for Pat1p and Scd6p, components which are present in both types of PBs.

Intriguingly, general translation repression was not required for the induction of multiple PBs by Ca^{2+} treatment. Thus, under these conditions, mRNAs do not aggregate into PBs because the translation machinery has been deactivated, but because they have been selectively removed from translation. This is in stark contrast to the current models (Coller & Parker, 2005). Overall, our understanding of the nature of PBs may have been obscured by the misconception that PBs behave the same under all conditions, although, in the end, stress-induced PBs may serve a different function from “house-keeping”, mRNA-degrading PBs.

There are good reasons to believe that this may be the case. For example, three major lines of evidence have served to characterize PBs as mRNA-degrading granules (Kulkarni et al., 2010), but not all of them apply during stress: First, PBs increase in size and number when mRNA decay is inhibited (Sheth & Parker, 2003), but it has not been shown whether this is also true for PBs induced by specific stresses. Second, mRNAs containing a polyG tract that is difficult to degrade accumulate in foci (Sheth & Parker, 2003); here, the same as above applies. Thirdly, if Ccr4p, the major cytoplasmic deadenylase, is deleted, PBs disappear, indicating that deadenylation, the first step in the 5’ decay pathway, is a prerequisite for PB formation (Sheth & Parker, 2003); however, under many conditions that induce PB formation, the Ccr4p/Pop2p/Notp complex is inactive (Hilgers et al., 2006). Thus, deadenylation may be necessary to accumulate mRNAs in house-keeping PBs, but is probably not a strict requirement for mRNA targeting to PBs under stress. In the end, it might turn out that,

depending on the condition that induced them, the properties of PBs can be very versatile, and that they play a more complex role in gene regulation than was previously thought.

In addition, we could show that PBs in yeast are stably associated with the ER, under glucose starvation as well as in secretory mutants or after osmotic shock (chapter 3.1; data not shown). Currently, we are optimizing the conditions for our PB purifications in order to identify the proteins that link PBs to the membrane.

.

Chapter 4

Global changes in the ER association of mRNAs in an *arf1* mutant

4.1 Mutations in *ARF1* repress general protein translation

Recent data from our group indicated that COPI vesicles might be involved in mRNA trafficking (Trautwein et al., 2004). As COPI vesicles are bound for the ER, the region with the highest ribosome density in a cell, we hypothesized that transcripts might "hitch a ride" on the surface of vesicles in order to augment the flux of transcripts in direction of the translation machinery. This might lead to a higher occupancy of ribosomes and thus to a significant increase in translation efficiency. If this assumption was true, disruption of COPI vesicular transport should lead to a decrease in translation. To test this, we grew wild-type or *arf1* mutant cells to logarithmic phase, shifted them to 37°C for 1 h, generated lysates and recorded their polysome profiles.

Indeed, for two *arf1* alleles, *arf1-11* and *arf1-18*, the polysome fraction decreased after a shift to the non-permissive temperature. At the same time, we observed a marked increase in non-translating monosomes, indicating that the level of translation is strongly reduced in these mutants (Figure 4.1 A). A third allele, *arf1-17*, did not show any signs of translational repression. This might reflect that a specific function of Arf1p needs to be compromised to elicit translation attenuation, and this function might still be operative in this mutant. Alternatively, *arf1-17* might represent a weaker allele.

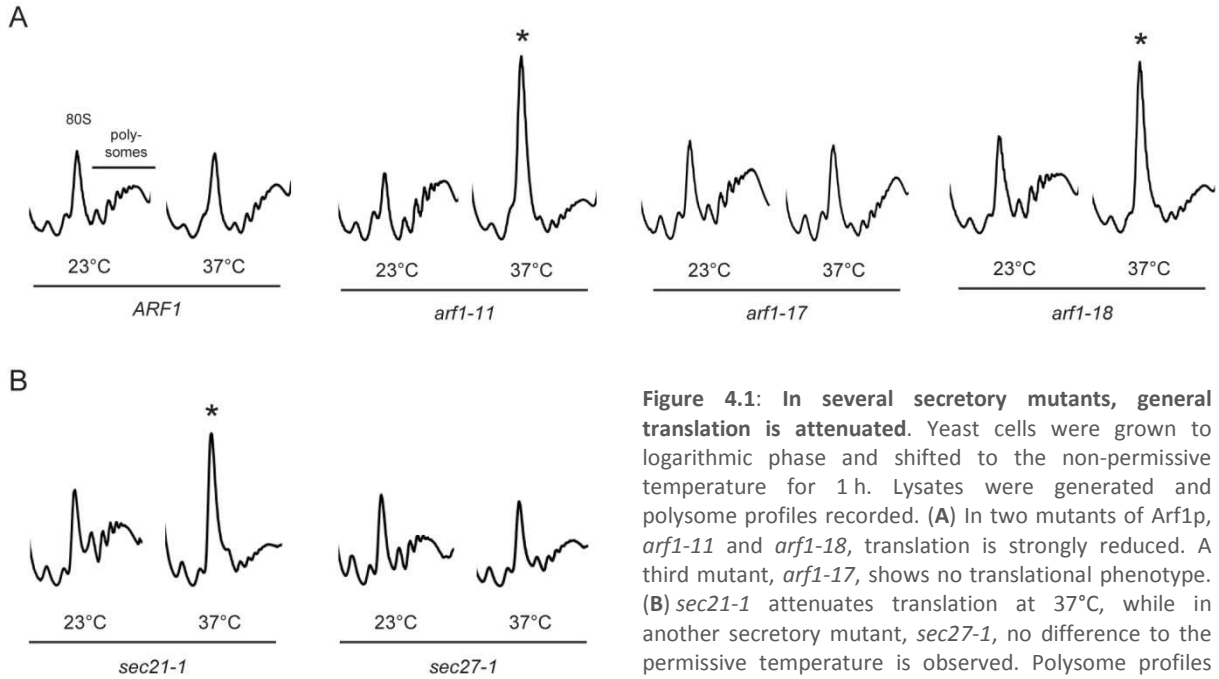

Figure 4.1: **In several secretory mutants, general translation is attenuated**. Yeast cells were grown to logarithmic phase and shifted to the non-permissive temperature for 1 h. Lysates were generated and polysome profiles recorded. (**A**) In two mutants of Arf1p, *arf1-11* and *arf1-18*, translation is strongly reduced. A third mutant, *arf1-17*, shows no translational phenotype. (**B**) *sec21-1* attenuates translation at 37°C, while in another secretory mutant, *sec27-1*, no difference to the permissive temperature is observed. Polysome profiles indicative of attenuated translation are marked with an asterisk.

Interestingly, we observed a reduction in translation efficiency only for *arf1* alleles that display an ASH1 mRNA delocalization phenotype (Trautwein et al., 2004). Many secretion mutants fail to correctly localize ASH1 mRNA, and it has been reported previously that other defects in membrane transport can lead to an attenuation of translation initiation (Trautwein et al., 2004; Aronov & Gerst, 2004; Deloche et al., 2004). This prompted us to ask whether the two phenotypes were correlated, and thus, we tested additional secretory mutants. Indeed, a *sec21-1* strain, which fails to localize ASH1 mRNA, also showed a strong attenuation of translation initiation, while the polysome profile of the *sec27-1* mutant, which displays no defect in asymmetric mRNA localization, was like wild-type (Trautwein et al., 2004; Figure 4.1 B).

4.2 Several RNA-binding proteins change their localization in *arf1* mutants

4.2.1 Bfr1p and Scp160p lose their ER association in *arf1* mutants

Translational attenuation in secretory mutants correlated with a reported disruption of ASH1 mRNA transport. The translational repressors Bfr1p and Scp160p are both required for the asymmetric distribution of ASH1 mRNA (Irie et al., 2002; Trautwein et al., 2004). In addition, both of them have been functionally linked to Arf1p. Under normal growth conditions, both proteins localize to the ER (Lang et al., 2001). We chromosomally appended Scp160p and Bfr1p with GFP in different *arf1* strains to test whether their ER association was affected by a block of Arf1p-mediated vesicular transport, which could provide evidence for an important role of Arf1p in mRNP localization.

The strains were grown to logarithmic phase, shifted to the non-permissive temperature for 1 h, and analyzed by epifluorescence microscopy. The ER association of both Scp160-GFP and Bfr1-GFP diminished in *arf1-11* and *arf1-18*, but not in *arf1-17* (Figure 4.2 A, data for Bfr1-GFP not shown). Again, loss of ER association of the two RBPs appeared to correlate with translation attenuation. When we altenatively repressed translation by glucose depletion, Bfr1p also acquired a cytoplasmic localization (Figure 4.2 B). Therefore, the altered localization of Bfr1p and Scp160p in *arf1* mutants could either be due to defective trafficking on the surface of COPI vesicles or a consequence of the translation attenuation we observe in these strains. However, since Scp160p-deficient strains as well as Bfr1p-deficient strains are unable to localize ASH1 mRNA correctly, it is interesting to note that in our *arf1* mutants ASH1 mRNA delocalization, translation attenuation, and reduced association of Bfr1p and Scp160p with the ER seem to coincide.

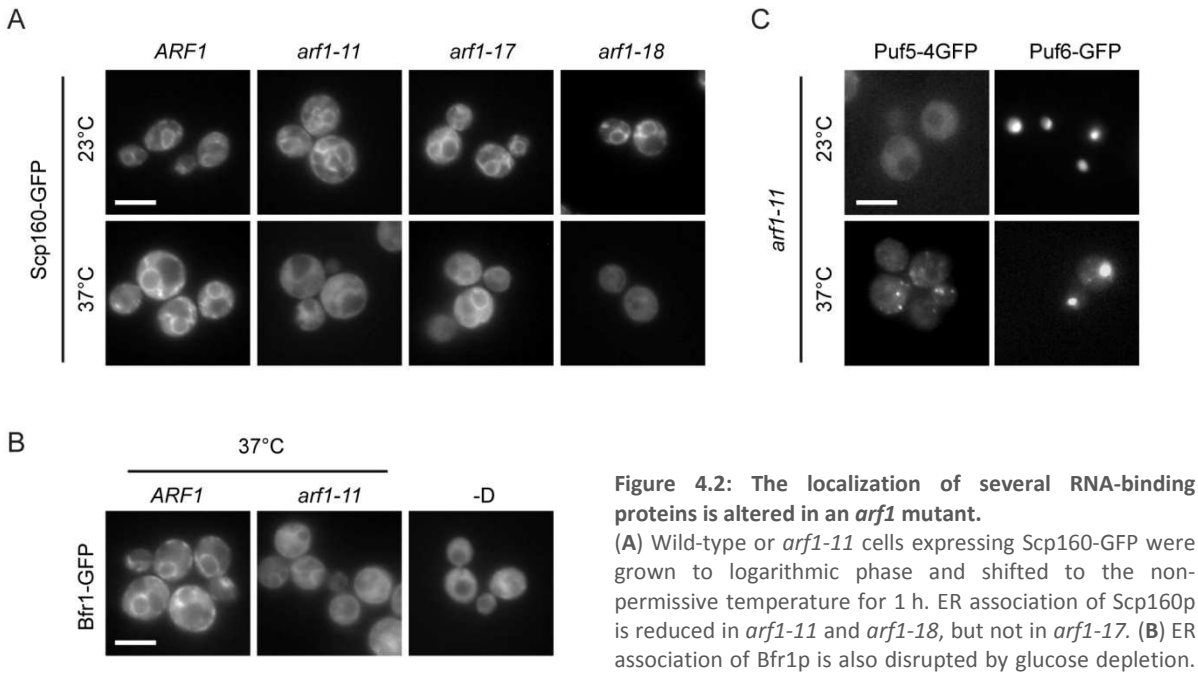

Figure 4.2: The localization of several RNA-binding proteins is altered in an *arf1* mutant.
(**A**) Wild-type or *arf1-11* cells expressing Scp160-GFP were grown to logarithmic phase and shifted to the non-permissive temperature for 1 h. ER association of Scp160p is reduced in *arf1-11* and *arf1-18*, but not in *arf1-17.* (**B**) ER association of Bfr1p is also disrupted by glucose depletion. Wild-type or *arf1-11* expressing Bfr1-GFP were grown to logarithmic phase and shifted to the non-permissive temperature for 1 h. Alternatively, the wild-type was incubated in medium lacking a carbon source for 15 min at RT. In the *arf1* mutant and under glucose starvation, Bfr1p acquires a cytoplasmic staining. (**C**) Distribution of Puf5p and Puf6p is altered in an *arf1* mutant. *arf1-11* cells expressing Puf5-4GFP or Puf6-GFP were grown to logarithmic phase and shifted to the non-permissive temperature for 1 h. At 37°C, Puf5-GFP accumulates in foci, while Puf6p loses its exclusively nucleolar staining and diffuses into the cytoplasm. The white bars represent 5 μm.

4.2.2 Puf5p and Puf6p show a divergent localization in *arf1-11*

Other RNA-binding proteins have been implicated in asymmetric mRNA transport, e.g. Puf5p and Puf6p, which are both required for correct localization of ASH1 mRNA (Tadauchi et al., 2001; Gu et al., 2004). Puf5p is a cytosolic protein that acts as a translational repressor and plays a role in cell wall integrity signaling and filamentous growth (Prinz et al., 2007; Bourens et al., 2009). Puf6p is concentrated in nucleoli under normal growth conditions and is directly involved in silencing of ASH1 mRNA-containing mRNPs (Deng et al., 2008). To see whether the localization of these RBPs was also affected in *arf1-11*, we generated fusions to one or, in the case of Puf5p, four copies of GFP. When *arf1-11* cells were shifted to the non-permissive temperature, the localization of both proteins changed: While Puf5-4GFP accumulated in foci, Puf6-GFP lost its exclusively nuclear localization and partially dissipated into the cytoplasm (Figure 4.2 C). For none of the two proteins, a link to the ER has been reported, but, nevertheless, we observed their redistribution in the *arf1-11* mutant. Thus, mutations in *ARF1* affect RNA metabolism on a much broader scale than we expected.

4.2.3 Translation attenuation in *arf1* mutants requires eIF2α kinase

From our analysis, relocalization of Bfr1p and Scp160p appeared to be coupled to a loss of translating polysomes. Translation attenuation has been observed in other secretory mutants; in some of them, signaling through the eIF2α kinase Gcn2p is required to decrease translation (Deloche et al., 2004).
In the light of these findings, it was plausible that the phenotypes we observed were a consequence of stress signaling rather than of a disruption of Arf1p-mRNP-dependent transport. To verify this, we generated deletions of *GCN2* in *arf1-11*. We grew cells to logarithmic phase, shifted them to 37°C for 1 h, generated lysates and recorded their polysome profiles. Deletion of *GCN2* completely rescued the translation attenuation observed in *arf1-11* (Figure 4.3). Thus, a stress pathway is activated in this mutant that shuts down translation via phosphorylation of eIF2α. It is very likely that the additional phenotypes we observe, i.e. relocalization of RBPs and disruption of ASH1 mRNA transport, are a consequence of this stress signaling, but we have not investigated their interrelationship any further.

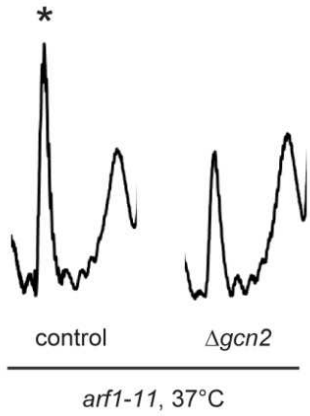

Figure 4.3: Deletion of *GCN2* rescues general translation attenuation in *arf1-11*.
Cells were grown to logarithmic phase and shifted to the non-permissive temperature for 1 h. Lysates were generated and polysome profiles recorded. Deletion of *GCN2* completely abolished translation attenuation in the *arf1* mutant. Polysome profiles indicative of attenuated translation are marked with an asterisk.

4.3 Microarray analysis of cytosolic and membrane-enriched fractions

Instead, we decided to take a novel, unbiased approach to investigate Arf1p-dependent mRNA transport. By performing RT-PCR on immunoprecipitated Arf1p-mRNPs, it had been shown that a variety of transcripts, including ASH1, ACT1, and ADH1 mRNA, is present in Arf1p-mRNPs (Trautwein et al., 2004). All mRNAs examined could be amplified from precipitated mRNPs, but since only eight individual mRNAs were tested, the analysis had by no means been exhaustive.

To identify mRNAs that undergo Arf1p-dependent transport to the ER, we used microarrays to characterize mRNAs that accumulate at the ER in an *arf1-11* mutant and compared them to wild-type. A membrane-enriched pellet containing the ER was generated from lysates by differential centrifugation (13,000 g), and RNA isolated from this fraction (P13) and the soluble supernatant (S13) was subsequently subjected to microarray analysis. In this manner, a membrane association score

(MAS) could be determined for each mRNA for both wild-type ($MAS_{wt} = P13_{wt}/S13_{wt}$) and *arf1* mutant ($MAS_{mut} = P13_{mut}/S13_{mut}$).

When MAS_{mut} was plotted against MAS_{wt} (Figure 4.4 A), the large majority of ORFs displayed a strictly linear correlation ($MAS_{mut} \approx MAS_{wt}$), indicating that the membrane association of a given mRNA did not change between wild-type and mutant. MA scores formed a continuum rather than that they clustered around pools of mRNAs that were either predominantly cytosolic or predominantly membrane-associated. It has to be stated, though, that the calculated MA scores are not quantitative. In the initial fractionation, roughly 10% of total RNA was found in the membrane pellet; still, an equal amount of RNA was used to generate cDNA from both fractions, and same amounts of cDNA were analyzed on each chip. Thus, an MA score of 1.0 does not mean that 50% of a given mRNA is associated with membranes. Likewise, when membrane recruitment is disrupted for a large fraction of mRNAs, MA scores will rise for all mRNAs that remain on the membrane. However, since we were mainly interested in relative changes, we could neglect this information.

When $S13_{mut}/S13_{wt}$ was plotted against $P13_{mut}/P13_{wt}$ (Figure 4.4 B), most ORFs clustered around the origin with a tendency to spread along the identity line. We focused on the transcripts that deviated from the diagonal line and were found either in the upper left quadrant (depleted from membranes in the mutant) or in the lower right quadrant (recruited to membranes in the mutant); ORFs present in the upper right or the lower left quadrant were not considered; they are up-regulated or downregulated, respectively, but do not change in membrane association when Arf1p-dependent vesicular transport is blocked.

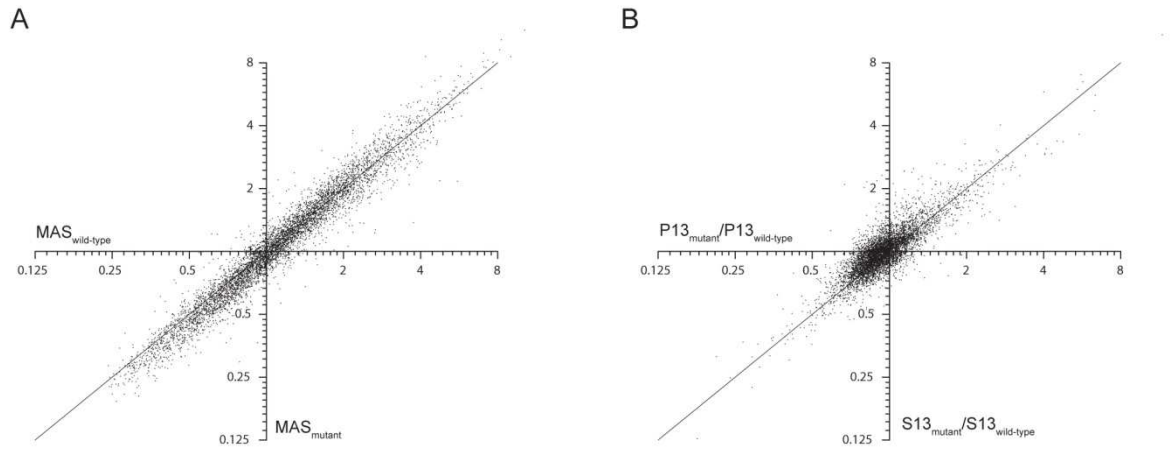

Figure 4.4: Result of the microarray analysis. (**A**) The membrane association score awarded to a given mRNA in the mutant was plotted against the membrane association score awarded in the wild-type. The majority of ORFs display a linear correlation. (**B**) Fold-change in the membrane fraction was plotted against fold-change in the cytosolic fraction (mutant/wild-type). The majority of ORFs was not affected. Some genes are overexpressed or downregulated, but do not change in membrane association (upper right and lower left quadrant, respectively). Few transcripts are either enriched on membranes in the mutant (lower right quadrant) or depleted from membranes (upper right quadrant). The identity line is shown for clarity.

To facilitate data analysis, we calculated a membrane recruitment shift coefficient MAS_{mut}/MAS_{wt}, which measures the change in membrane association between the mutant and the wild-type for a given mRNA (Table 7.1 and Table 7.2 in the Appendix). Values above 1.0 signify that an mRNA is enriched on membranes in the mutant, while values below 1.0 indicate depletion from membranes; a score of 1.0 signifies that the membrane association of a given mRNA remained unchanged. The data are based on three independent biological repeats. For 86% of the genes tested, the coefficient of variation between experiments was below 0.25; thus, the reproducibility was in a similar range as has been observed for comparable experimental setups (Melamed et al., 2008).

Many genes had MAS_{mut}/MAS_{wt} coefficients below one, which is indicative of a reduced membrane association of the mRNA in the *arf1* mutant and may be a direct consequence of a loss of vesicle-mediated transport to the ER. However, just as many mRNAs were specifically recruited to the membrane fraction in the *arf1* mutant. We hypothesized that this is part of a cellular stress response induced by the breakdown of vesicular transport. In accordance with this, many of the genes with a high MAS_{mut}/MAS_{wt} coefficient were located in the Hda1p-affected subtelomeric (HAST) region. Under normal growth conditions, HAST genes are significantly less active than genes present in other genomic regions, and they are thought to be activated primarily in response to environmental stress (Robyr et al., 2002).

To see whether specific pathways were affected, we mapped the ORFs of interest to functional categories using FunSpec (Robinson et al., 2002). Transcripts that were depleted from the membrane in the mutant ($MAS_{mut}/MAS_{wt} < 0.8$; 281 ORFs) were enriched in the following categories (MIPS Functional Classification; P-value cutoff 0.01, see also Table 4.1 and Table 7.1 in the Appendix): ribosomal proteins; rRNA processing; modification with sugar residues (e.g. glycosylation, deglycosylation); sugar transport. Among all transcripts that had a MAS_{mut}/MAS_{wt} coefficient above 1.3 (127 ORFs), the following categories were overrepresented (P-value cutoff 0.01; see also Table 4.1 and Table 7.2 in the Appendix): motor protein binding; intra-Golgi transport; cellular export and secretion; and actin cytoskeleton.

Because some of the enriched categories overlapped, we assembled functionally related gene groups into clusters using the Functional Annotation Clustering Tool offered by DAVID bioinformatics resources (Dennis et al., 2003; Huang et al., 2009); with this, we hoped to gain a better idea of the overarching biological processes that were represented in our dataset (Figure 4.5 and Figure 4.6). As had already been apparent from the functional classification, the prevailing theme for transcripts with a low MAS_{mut}/MAS_{wt} coefficient was ribosome biogenesis (Figure 4.5; clusters 1-3). It has been reported that ribosome biogenesis is downregulated at the level of transcription in response to failure in the secretory pathway (Nierras & Warner, 1999); this response requires the protein kinase Pkc1p and upstream regulators of the cell wall integrity pathway, but is independent

of Slt2p (Nierras & Warner, 1999; Li et al., 2000). Our finding that mRNAs encoding ribosomal constituents are depleted from membranes in *arf1-11* suggests that there might be a post-transcriptional component to the downregulation of ribosome biogenesis in secretion-defective strains. However, we did not analyze any mutants to show that the redistribution of ribosomal mRNAs is promoted by the same pathway, nor did we otherwise investigate this issue any further. Besides ribosomes, mRNAs depleted from membranes in *arf1-11* involve ER proteins (cluster 5), mitochondrial proteins (cluster 6), and processes related to glycosylation (cluster 7) and cell wall biosynthesis (cluster 9). Both these latter functions have been linked to the endomembrane system and are likely to be impaired in secretion mutants, suggesting that recruitment of these mRNAs to membranes might be disrupted as part of a specfic translational response which might directly involve Arf1p or be activated by a signaling pathway in response to membrane stress.

Even though the localization of Scp160p and some of the Puf proteins was altered in *arf1-11* (see chapters 4.2.1 and 4.2.2), mRNAs with a high or low MAS_{mut}/MAS_{wt} did not show a significant overlap with existing microarray data for mRNAs either enriched in Scp160p-mRNPs or associated with any of the six known members of the PUF family of RNA-binding proteins (Li et al., 2003; Gerber et al., 2004; Hogan et al., 2008). Of the 221 mRNAs that have been reported to associate wit hPuf5p (Gerber et al., 2004), three are found enriched on membranes in the mutant, while 13 are depleted from the pellet fraction, which corresponds to a random distribution; this result might have been expected, since there is no indication that Puf5p granules are ER-associated. In contrast, we had observed that the ER association of Scp160p is disrupted in *arf1-11* and would have expected to find Scp160p-bound mRNAs in our assay. However, Scp160p has a very broad mRNA specificity, and more than 1000 mRNAs were found enriched in mRNP purifications (Hogan et al., 2008); thus, the effect might be too general to be detected in our experimental setup. In accordance with this, when S. Frey (2002) compared a strain deleted for *SCP160* with wild-type, the ER-association of Scp160p-bound mRNAs was not altered, indicating that Scp160p might not play a major role in shuttling mRNAs between ER and cytoplasm.

Since we knew that translation in *arf1-11* was attenuated by the action of the eIF2α kinase Gcn2p (Figure 4.3), and it is well-established that some ORFs can escape eIF2α-mediated translation attenuation (Hinnebusch, 2005), we wondered how these transcripts behaved in our assay. There are five genes that contain uORFs and six published IRES-containing ORFs in *S. cerevisiae* (Hogan et al., 2008; Reineke et al., 2008). Among them, only one shifted significantly between membrane and cytosolic fraction (Ymr181c; MAS_{mut}/MAS_{wt} = 0.691). This finding is not surprising, since no requirement for membrane recruitment in IRES-mediated translation has been reported. However, it serves as a reminder that our experimental setup assays solely the localization of an mRNA, and not its translational status.

Table 4.1: MIPS Functional Classification categories enriched in ORFs with a MAS_{mut}/MAS_{wt} below 0.8 or above 1.3.

MAS_{mutant}/MAS_{wt} < 0.8				
Category	**In Category from Cluster**	**k**	**f**	**p-value**
ribosomal proteins	RRP7 MRP10 RPL41A MRPL1 RPL27B RPL37B RPL34A RPS26B RPL9A RPL27A RPL16A RPS22A RPL40B RSA3 MRPL15 RPL26A RPL31B MRPL3 RPL36A RPS10B MRP7 MRPL22 MRPL17 RPS10A RRP15	25	246	3.014e-05
UNCLASSIFIED PROTEINS	YAL063C-A YAL064W YAL067W-A MOH1 YBL095W TOS1 YBR182C-A YBR221W-A YCL002C YCL056C YCR108C YDL121C LRC1 YDR003W-A DOS2 FMP16 YDR169C-A YDR182W-A YDR357C APT2 HEH2 YDR532C YEL057C YEL075C CHZ1 ISD11 YER053C-A YER137C YER188C-A YFR039C YGL188C-A YGR035C YGR153W YGR169C-A YGR174W-A YGR204C-A SPG1 EFG1 YHR054C YIL002W-A YIL029C YIL134C-A YIL161W LOH1 AIM22 BIT61 YJL171C YAE1 YKL061W YKL068W-A YKL106C-A COS9 FCF2 YLR073C YLR162W-A YLR456W YML003W YML108W YMR181C YMR194C-B ICY1 EOS1 YNL122C YNL146C-A PGA2 MPP6 YNR062C YOL131W YOL159C-A YOL164W-A YOR152C YOR389W YOR390W CWC27 YPL216W YPL279C YPR159C-A	77	1378	0.002741
rRNA processing	POP7 RRP7 SAS10 RRP8 RRP17 SNU13 MRM2 LRP1 MRT4 UTP11 EBP2 FYV7 YOR287C NOP53 RRP15	15	169	0.004564
modification with sugar residues (e.g. glycosylation, deglycosylation)	GPI18 MNN11 MNN5 OST6	4	17	0.004617
sugar transport	HXT3 VRG4 HXT2 HXT11 HUT1	5	31	0.008558

MAS_{mutant}/MAS_{wt} > 1.3				
Category	**In Category from Cluster**	**k**	**f**	**p-value**
UNCLASSIFIED PROTEINS	05YAL064C-A YAR064W YBR056W-A RTN2 YDR034W-B YSP2 YEL076C-A YFL067W YFL068W DUG1 YGL006W-A YGR110W YHR022C-A YHR086W-A RTC3 YHR214C-E YJL047C-A IRC8 ICS3 YJL136W-A LAA1 YKL033W YKR015C YLL066W-B YLR154C-H MMR1 YLR307C-A YLR412C-A YLR422W YLR466C-B TCB3 YML083C AIM34 YMR196W YNL034W YNL144C YNL195C YNL208W YNL277W-A PRM1 PHM7 YOR161C-C FYV12 YOR387C YPL152W-A YPL277C YPR117W	47	1378	1.104e-05
motor protein binding	SAC6 CRN1 ABP140	3	5	6.443e-05
intra Golgi transport	VPS15 ARF2 VPS13 VPS27	4	33	0.003275
cellular export and secretion	BPH1 SAC6 GAL2 STT4	4	43	0.008543
actin cytoskeleton	ABP1 SAC6 WSC4 STT4 CRN1 ABP140	6	96	0.009451

All genes mapped to the respective category are given. (k) designates the number of genes mapped to the category from the cluster (f) designates the total number of genes found in each category. P-values are given

.

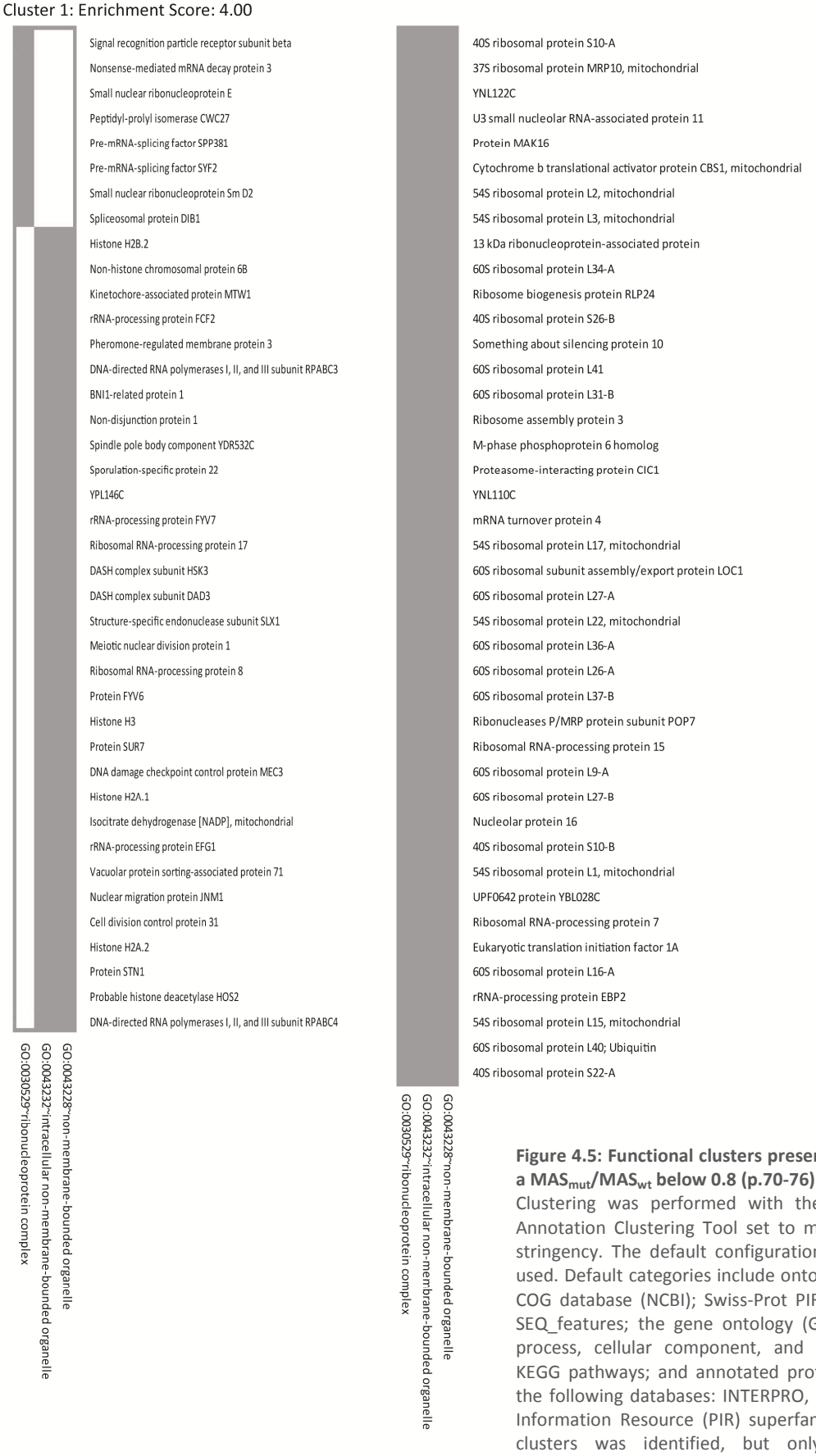

Figure 4.5: Functional clusters present among ORFs with a MAS_{mut}/MAS_{wt} below 0.8 (p.70-76).
Clustering was performed with the DAVID Functional Annotation Clustering Tool set to medium classification stringency. The default configuration for clustering was used. Default categories include ontology terms from the COG database (NCBI); Swiss-Prot PIR_keywords; uniprot SEQ_features; the gene ontology (GO) terms biological process, cellular component, and molecular function; KEGG pathways; and annotated protein domains within the following databases: INTERPRO, SMART, and Protein Information Resource (PIR) superfamilies. A total of 62 clusters was identified, but only clusters with a enrichment score above 1.0 were considered. Gray squares correspond to gene-term associations that have been positively reported. White squares correspond to gene-term associations that have not been reported yet.

Cluster 2: Enrichment Score: 3.16

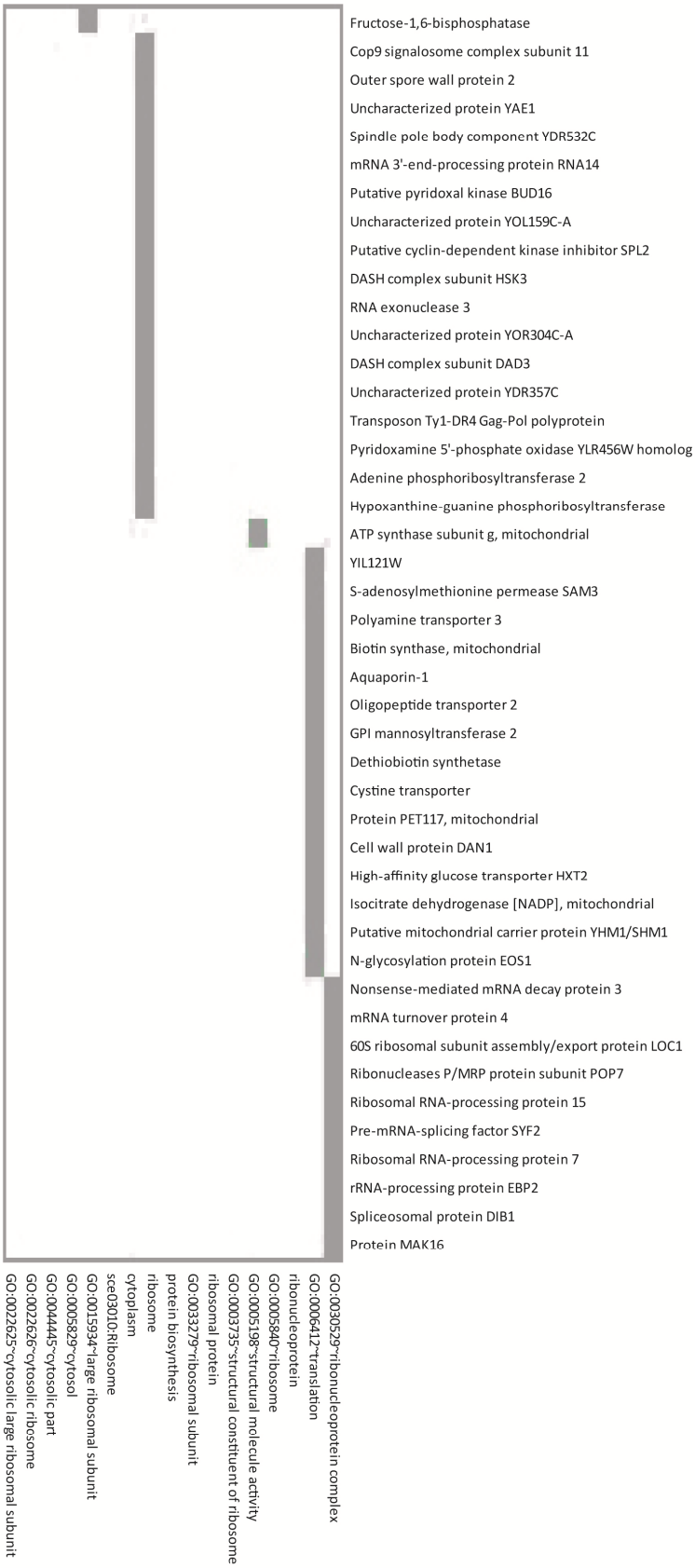

Cluster 2: Enrichment Score: 3.16 (continued)

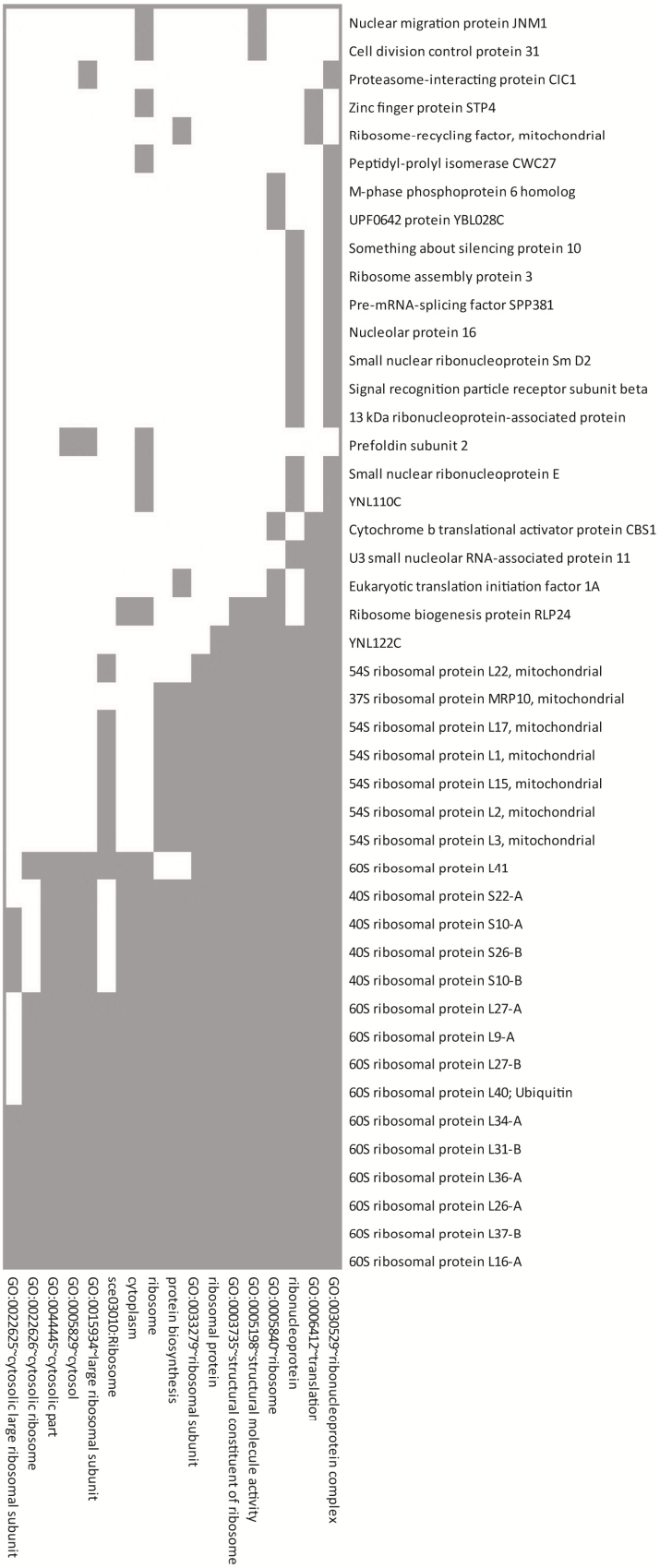

Cluster 3: Enrichment Score: 2.57

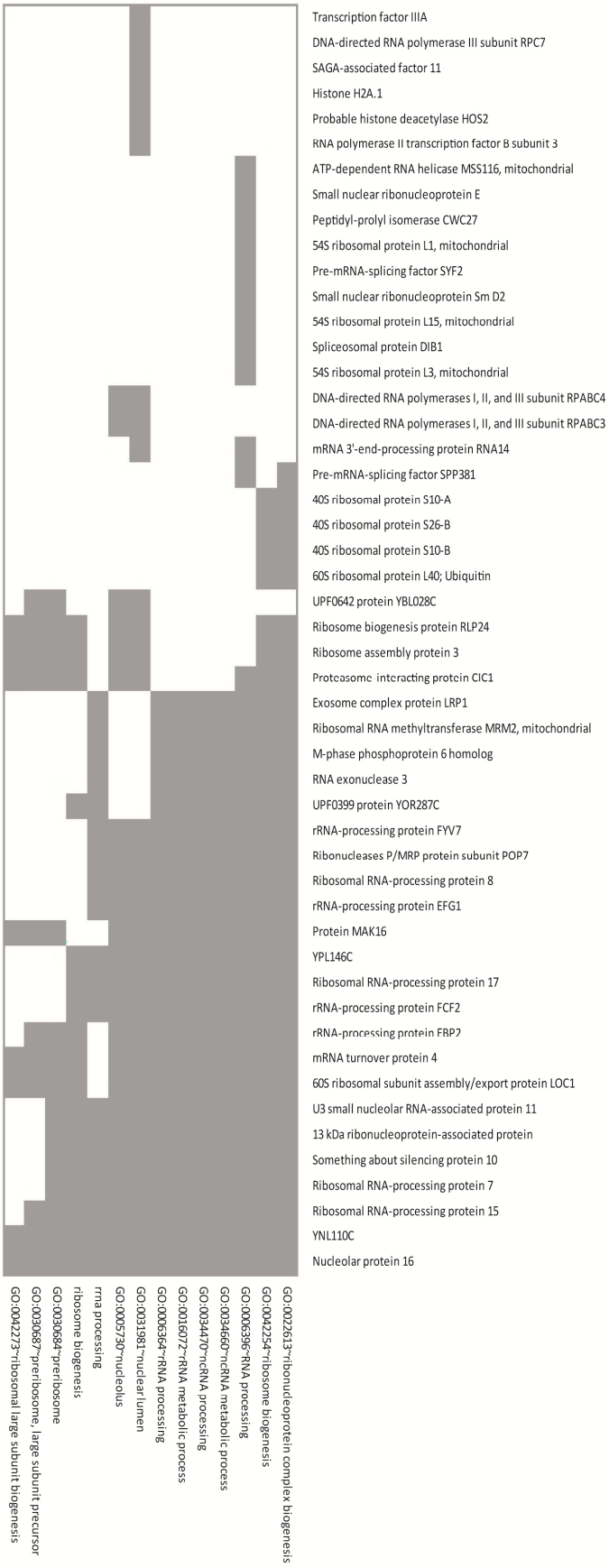

Cluster 4: Enrichment Score: 2.15

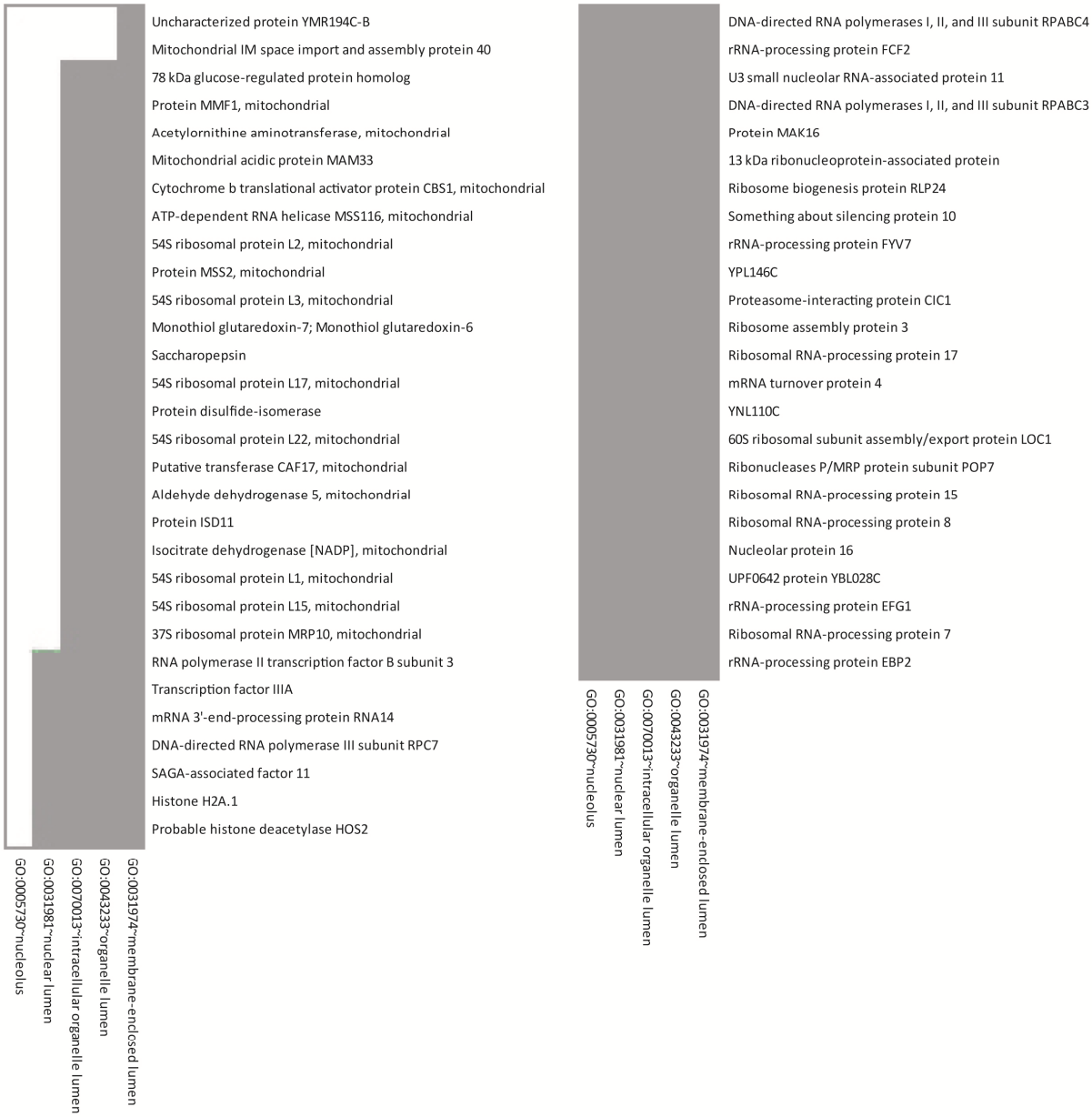

Cluster 5: Enrichment Score: 1.43

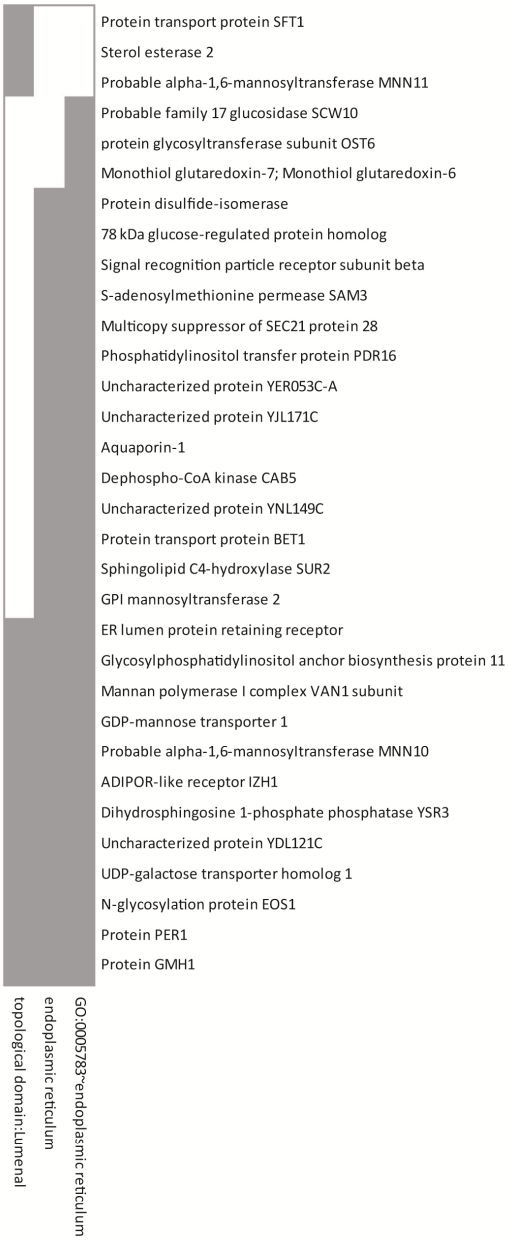

Cluster 6: Enrichment Score: 1.36

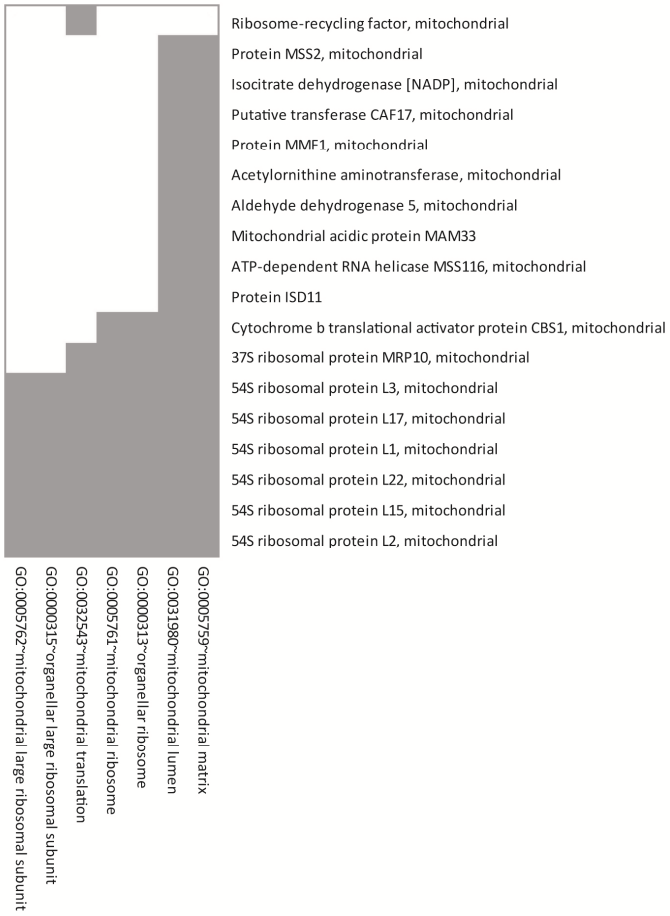

Cluster 7: Enrichment Score: 1.14

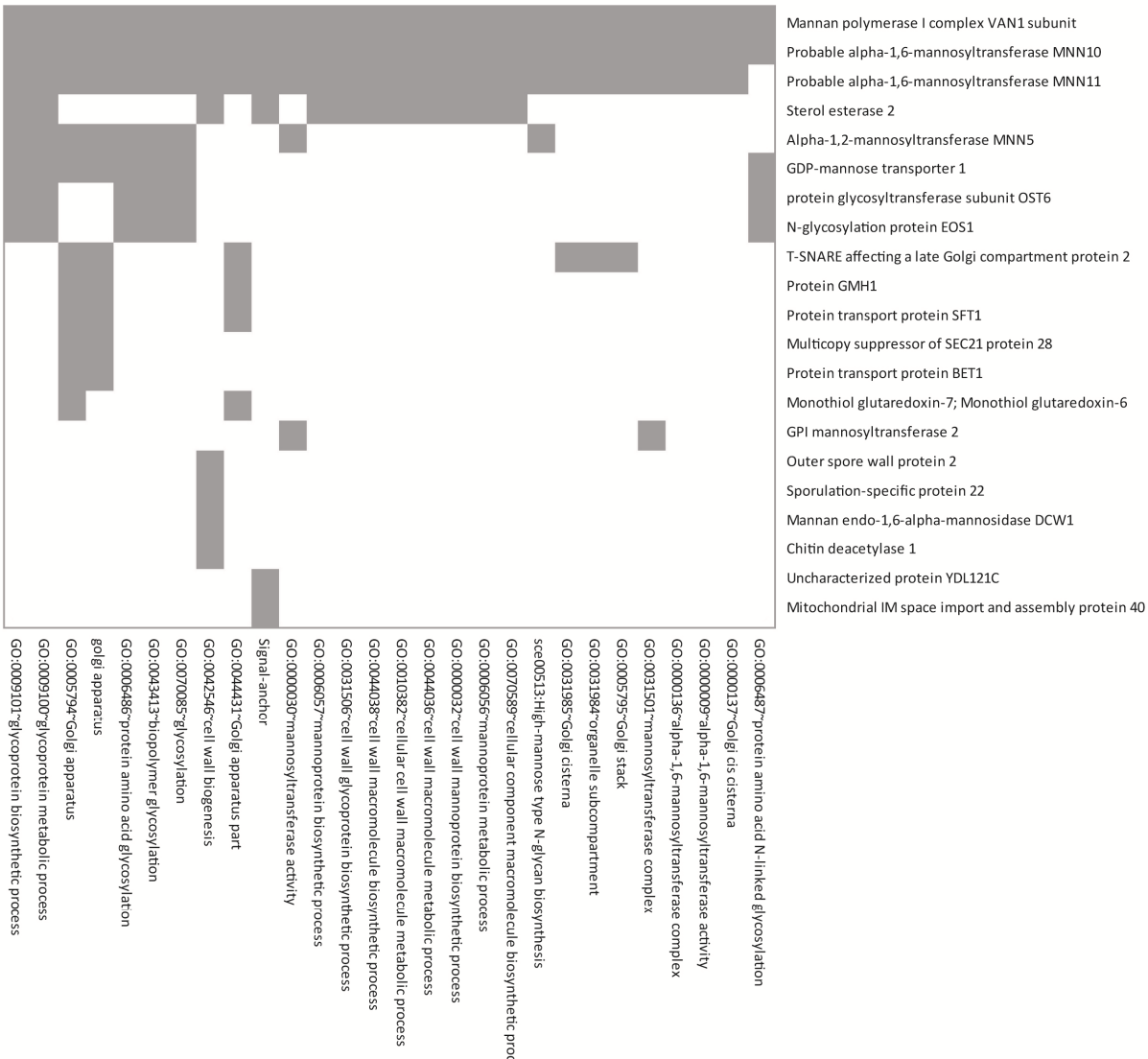

Cluster 8: Enrichment Score: 1.11

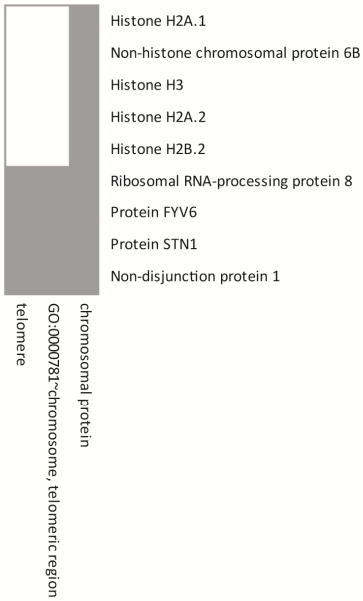

Cluster 9: Enrichment Score: 1.02

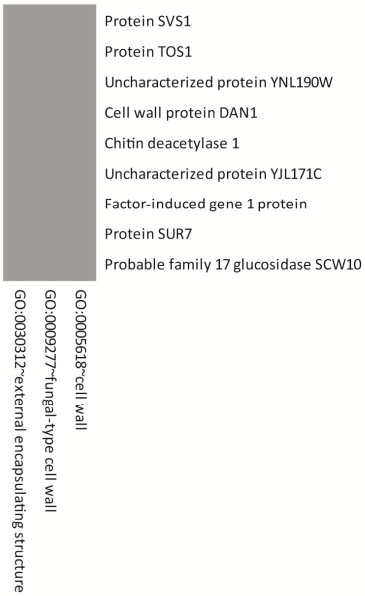

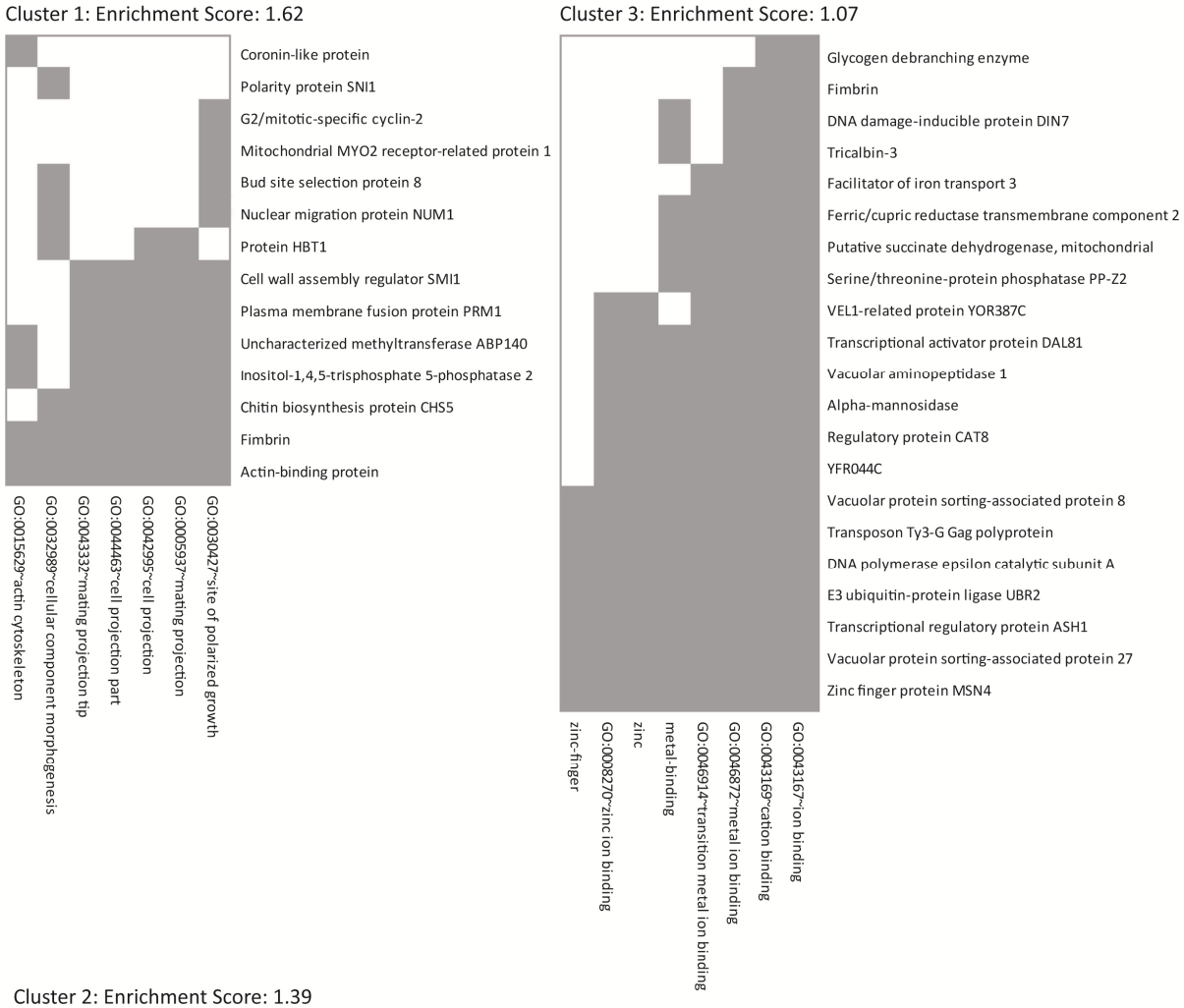

Figure 4.6: Functional clusters present among ORFs with a MAS_{mut}/MAS_{wt} above 1.3 (p. 77 & 78).
Clustering was performed with the DAVID Functional Annotation Clustering Tool set to medium classification stringency. The default configuration for clustering was used. Default categories include ontology terms from the COG database (NCBI); Swiss-Prot PIR_keywords; uniprot SEQ_features; the gene ontology (GO) terms biological process, cellular component, and molecular function; KEGG pathways; and annotated protein domains within the following databases: INTERPRO, SMART, and Protein Information Resource (PIR) superfamilies. A total of 40 clusters was identified, but only clusters with an enrichment score above 1.0 were considered. Gray squares correspond to gene-term associations that have been positively reported. White squares correspond to gene-term associations that have not been reported yet. ARF2 was manually removed from cluster 6 because it was deleted in our strain background.

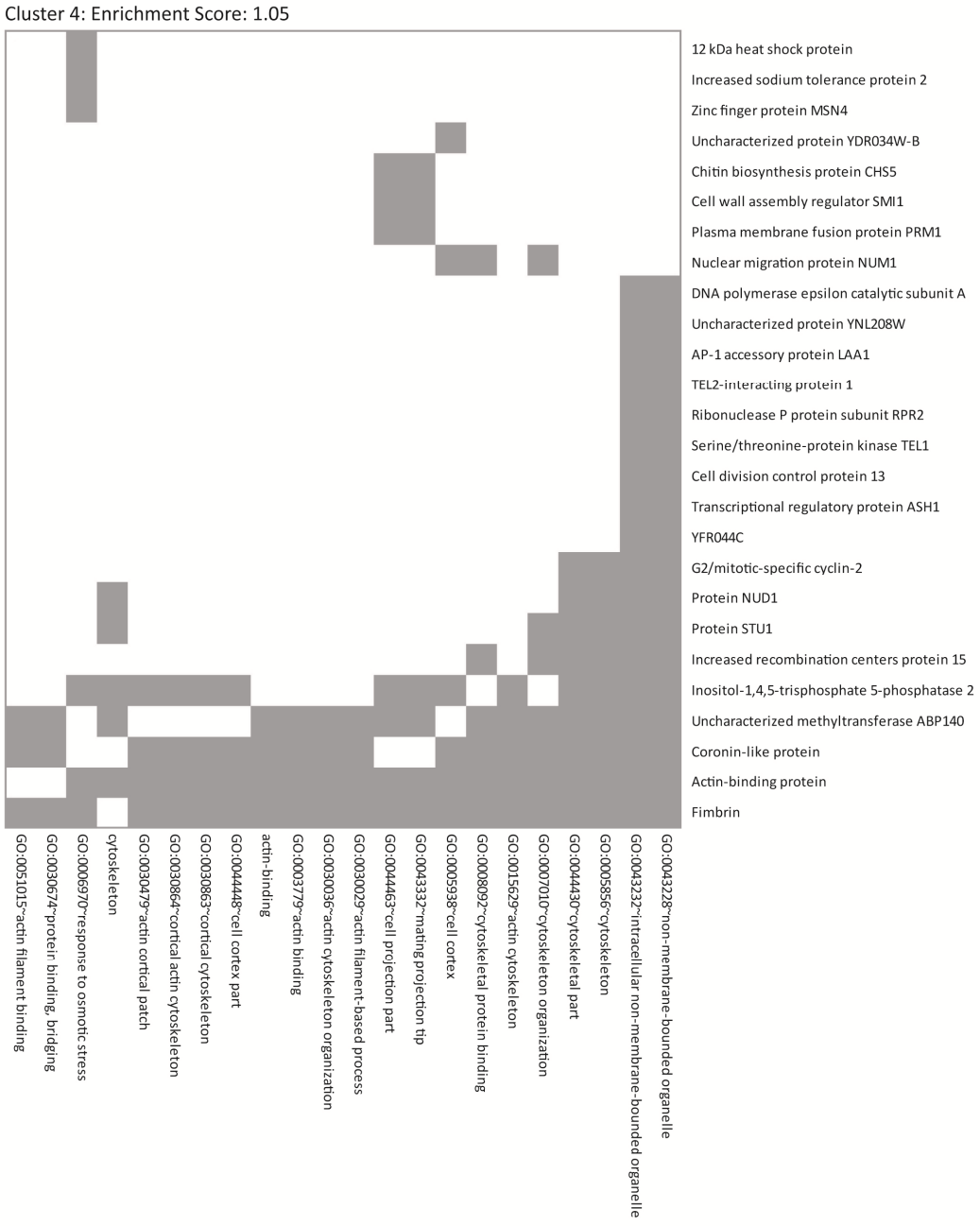
Cluster 4: Enrichment Score: 1.05
12 kDa heat shock protein
Increased sodium tolerance protein 2
Zinc finger protein MSN4
Uncharacterized protein YDR034W-B
Chitin biosynthesis protein CHS5
Cell wall assembly regulator SMI1
Plasma membrane fusion protein PRM1
Nuclear migration protein NUM1
DNA polymerase epsilon catalytic subunit A
Uncharacterized protein YNL208W
AP-1 accessory protein LAA1
TEL2-interacting protein 1
Ribonuclease P protein subunit RPR2
Serine/threonine-protein kinase TEL1
Cell division control protein 13
Transcriptional regulatory protein ASH1
YFR044C
G2/mitotic-specific cyclin-2
Protein NUD1
Protein STU1
Increased recombination centers protein 15
Inositol-1,4,5-trisphosphate 5-phosphatase 2
Uncharacterized methyltransferase ABP140
Coronin-like protein
Actin-binding protein
Fimbrin
GO:0051015~actin filament binding
GO:0030674~protein binding, bridging
GO:0006970~response to osmotic stress
cytoskeleton
GO:0030479~actin cortical patch
GO:0030864~cortical actin cytoskeleton
GO:0030863~cortical cytoskeleton
GO:0044448~cell cortex part
actin-binding
GO:0003779~actin binding
GO:0030036~actin cytoskeleton organization
GO:0030029~actin filament-based process
GO:0044463~cell projection part
GO:0043332~mating projection tip
GO:0005938~cell cortex
GO:0008092~cytoskeletal protein binding
GO:0015629~actin cytoskeleton
GO:0007010~cytoskeleton organization
GO:0044430~cytoskeletal part
GO:0005856~cytoskeleton
GO:0043232~intracellular non-membrane-bounded organelle
GO:0043228~non-membrane-bounded organelle

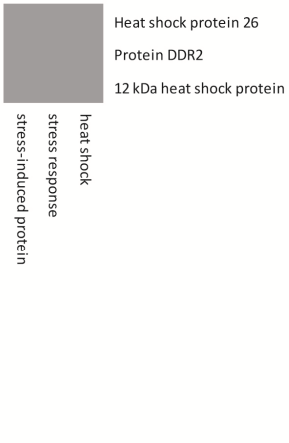
Cluster 5: Enrichment Score: 1.03
Heat shock protein 26
Protein DDR2
12 kDa heat shock protein
stress-induced protein
stress response
heat shock

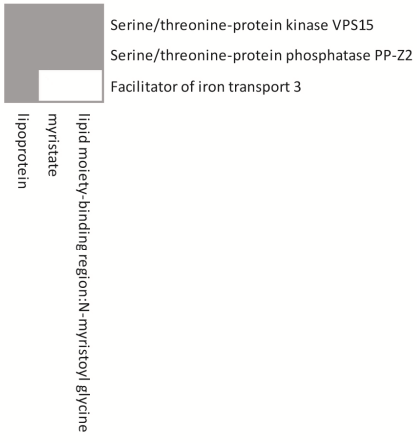
Cluster 6: Enrichment Score: 1.01
Serine/threonine-protein kinase VPS15
Serine/threonine-protein phosphatase PP-Z2
Facilitator of iron transport 3
lipoprotein
myristate
lipid moiety-binding region:N-myristoyl glycine

4.4 Validation of microarray hits by fluorescent *in situ* hybridization

We selected seventeen candidate genes which reproducibly displayed a very high or a very low MAS_{mut}/MAS_{wt} coefficient (designated in bold in Table 7.1 and Table 7.2 in the Appendix) and visualized the mRNAs in fixed cells using fluorescent *in situ* hybridization (FISH; Figure 4.7).

Surprisingly, we could not detect a difference in localization between wild-type and mutant for any of those mRNAs that were depleted from the membrane fraction in *arf1-11*; the signal strength, however, was generally very weak, and very few spots were visible (Figure 4.7, left panel), since we could not directly assess organelle association with FISH but had to infer it from the staining pattern, we cannot exclude that the ER association of these mRNAs is diminished in the mutant, but that we were not able to detect it with our assay. More importantly, for four out of ten mRNAs with a very high MAS_{mut}/MAS_{wt} coefficient, which corresponds to enhanced membrane association in the mutant, there was a striking redistribution of the FISH signal when *arf1-11* was shifted to the non-permissive temperature (Figure 4.7, right panel). As we would have predicted from our experimental setup, the staining that these four mRNAs acquired was reminiscent of the ER: Multiple small foci lined the cell periphery and sometimes appeared to encircle intracellular structures, which might represent nuclei. In the following, we investigated the behavior of these transcripts in more detail.

A short description of the functions assigned to the four ORFs is given in Table 4.2. Interestingly, two of the proteins are actin-associated, a category that was enriched among transcripts with a high MAS_{mut}/MAS_{wt} coefficient (Table 4.1), and while Ams1p and Chs5p have not been officially assigned to the MIPS category "cellular export and secretion", which was also enriched, Chs5p is required for export of chitin synthase to the plasma membrane, and Ams1p is a vacuolar enzyme (Baxter et al., 2005; Trautwein et al., 2006). Moreoever, when the ORFs with a high MAS_{mut}/MAS_{wt} were subjected to functional clustering (Dennis et al., 2003; Huang et al., 2009), two separate clusters of genes involved in cellular polarity were identified, and *CHS5*, *ABP1*, and *ABP140* were present in both (cluster 1 and 4; Figure 4.6). Cluster 2 contained genes involved in vacuolar transport, but AMS1 was present only in cluster 3 (metal-binding).

Table 4.2: Protein function assigned to the ORFs that displayed a redistribution in the *arf1-11* mutant. Source: Proteome

Protein function of the identified ORFs	
AMS1	Alpha-mannosidase 1, hydrolyzes terminal non-reducing alpha-D-mannose residues from alpha-D-mannosides and plays a role in the regulation of Ty3 retroretrotransposition
CHS5	Chitin synthase-related 5, a protein that is required for chitin synthase III activity, a component of the Chs5/6 complex that is involved in the transport of Chs3p from the trans-Golgi network to the plasma membrane
ABP1	Actin binding protein 1, functions in clathrin- and actin-mediated endocytosis, possibly in disassembly of the endocytic machinery
ABP140	Protein of unknown function, has high similarity to uncharacterized *C. glabrata* Cagl0j03780p

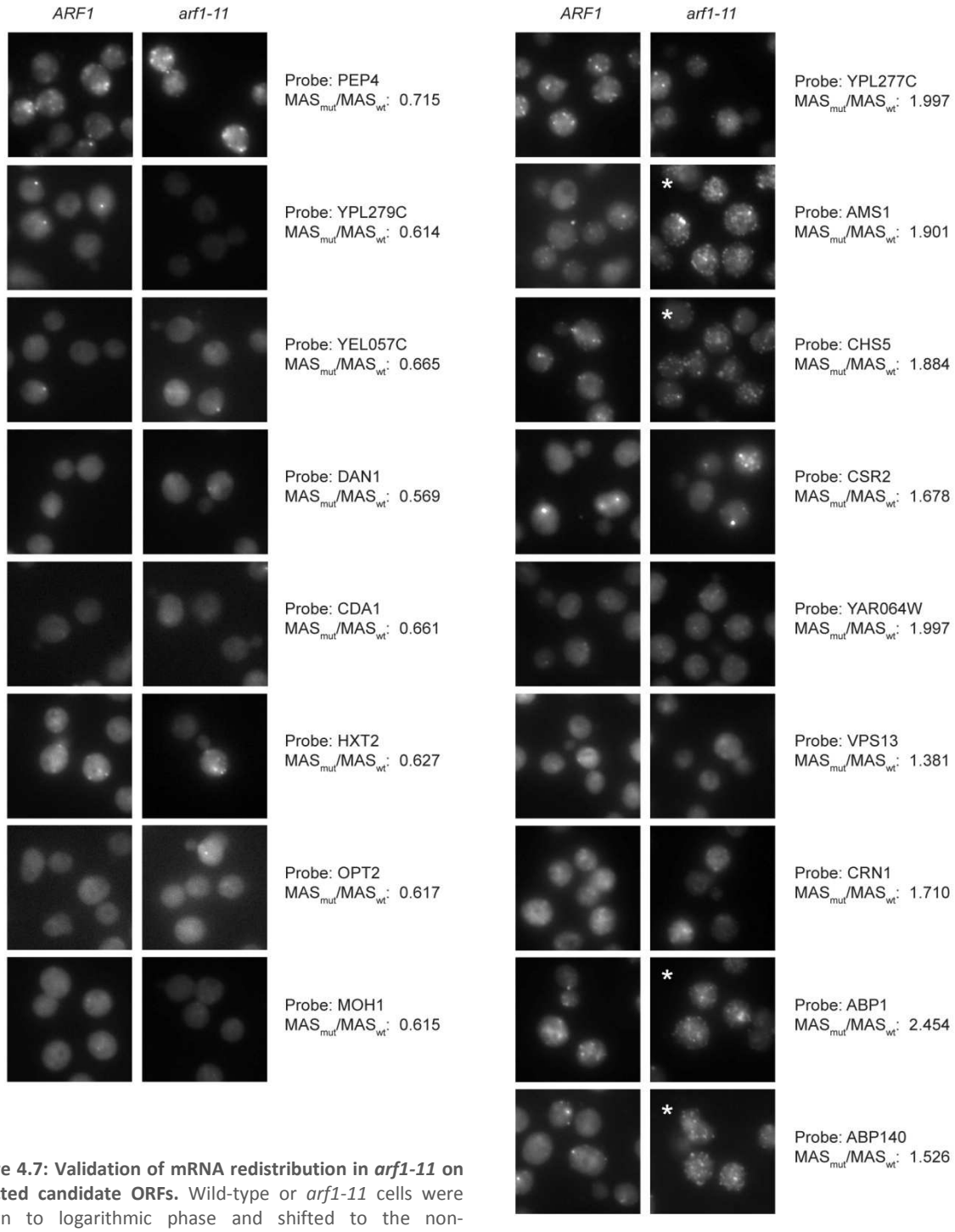

Figure 4.7: Validation of mRNA redistribution in *arf1-11* on selected candidate ORFs. Wild-type or *arf1-11* cells were grown to logarithmic phase and shifted to the non-permissive temperature for 1 h. Cells were fixed and analyzed by FISH with different anti-sense probes. The name of the gene and the corresponding MAS_{mut}/MAS_{wt} coefficient are indicated for each panel. For four of the genes, we observed a divergent mRNA localization in the mutant; these cases are marked with an asterisk. The black bar represents 5 μm.

4.5 Closer characterization of the identified ORFs

4.5.1 Protein abundance of all four ORFs is increased in *arf1-11*

According to the simplest view, the function of an mRNA is to serve as a template for protein translation. Thus, one would predict two possible outcomes to the redistribution we observed for the four candidate mRNAs: They could be targeted to the ER to be silenced, or to be available for preferential translation. In either case, the readout would be a change in protein abundance. Thus, we tested whether the levels of the proteins encoded by the four mRNAs were changed in the mutant.

Because we lacked specific antibodies, we chromosomally appended the genes with GFP in wild-type and *arf1-11* cells. As chromosomal tagging replaces the endogenous 3'UTR, where mRNA localization elements are often located, we first verified that the mRNAs of our constructs behaved like the non-tagged mRNA, which they did in principle (Figure 4.8 A).

We then generated denaturing lysates from cells shifted to 37°C for 1 h and analyzed them by immunoblot for GFP; Pgk1p was used as reference. For all four proteins, we observed an increase in abundance in the mutant while the Pgk1p content did not vary significantly between mutant and wild-type (Figure 4.8 B). Similar results were obtained when we used polyclonal antibodies raised against Chs5p and quantified protein levels in an untagged strain, which indicates that the endogenous 3'UTR is not required for the increase in Chs5p abundance observed in the mutant (data not shown). The increase in protein content was very variable. This variability was not due to the

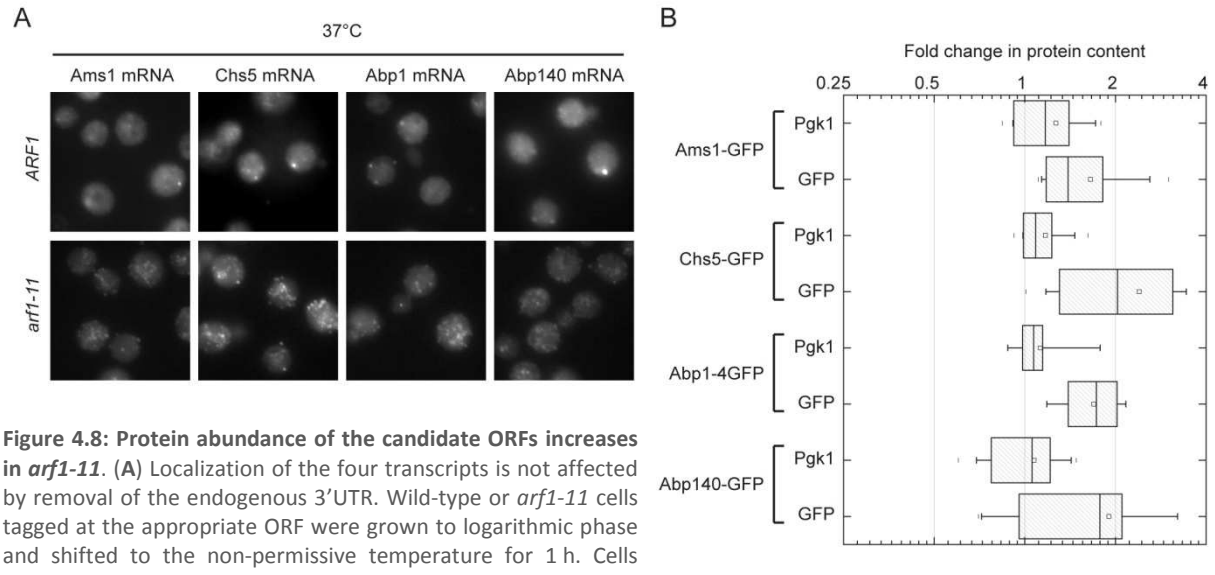

Figure 4.8: Protein abundance of the candidate ORFs increases in *arf1-11*. (**A**) Localization of the four transcripts is not affected by removal of the endogenous 3'UTR. Wild-type or *arf1-11* cells tagged at the appropriate ORF were grown to logarithmic phase and shifted to the non-permissive temperature for 1 h. Cells were fixed and analyzed by FISH with the corresponding probe. Relocalization of the mRNA was observed in all tagged strains. (**B**) Fold change in protein content (mutant/wild-type) is given. Wild-type or *arf1-11* cells expressing Ams1-GFP, Chs5-GFP, Abp1-4GFP, or Abp140-GFP were grown to logarithmic phase and shifted to the non-permissive temperature for 1 h. Lysates were generated and analyzed by immunoblot using antibodies against GFP or Pgk1p. Quantification of band intensities was performed with the LiCor Odyssey system.At least three independent blots of three independent experiments were quantified. In the graph, the size of the box is determined by the 25th and 75th percentiles, the whiskers represent the 5th and 95th percentiles, the horizontal line and the little square mark the median and the mean, respectively.

noisiness of the experimental procedure, since Pgk1p levels remained relatively stable between experiments; thus, the variability might be intrinsic to the biological process.

4.5.2 Translation attenuation in *arf1* mutants is more pronounced in the cytosol than at the ER

Although we cannot at the moment rule out that changes in protein stability play a role in the increase in protein abundance we observed, our data suggest that the four mRNAs could be translated more efficiently after their redistribution to the ER in the mutant. This is of particular interest because we observed a strong attenuation of general translation in *arf1-11* (Figure 4.1), and would imply that these transcripts are subjected to a special translational regime.

Intriguingly, Stephens et al. reported that ER-associated ribosomes are exempt from the general block in translation that is induced in response to ER stress, a condition that also elicits the unfolded protein response (UPR) (Stephens et al., 2005). To test whether translation attenuation is limited to the cytoplasm in secretory mutants, we grew *arf1-11* and *arf1-18* to logarithmic phase and shifted them to the non-permissive temperature for 1 h. After lysis, we separated cytosolic and membrane-enriched fractions and recorded individual polysome profiles (Figure 4.9 A).

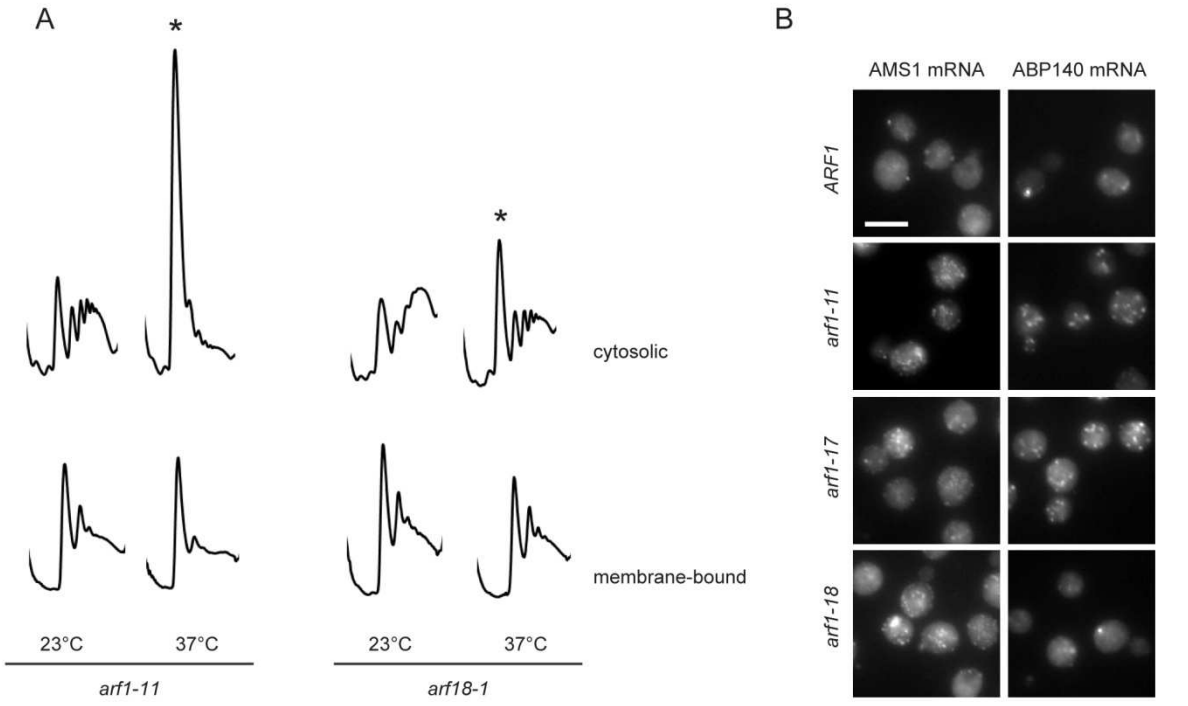

Figure 4.9: Translation attenuation in *arf1-11* and *arf1-18* is more pronounced in the cytosol than at the ER. (**A**) Cells were grown to logarithmic phase and shifted to 37°C for 1 h. Lysates were generated, cytosolic and membrane-enriched fractions seperated by centrifugation (13,000 g), and polysome profiles recorded from both fractions. Polysome profiles that show attenuated translation are marked with an asterisk. (**B**) FISH against AMS1 mRNA or ABP140 mRNA in wild-type or *arf1* mutants shifted to 37°C for 1 h. In *arf1-17* as well as in *arf1-11*, both mRNAs are redistributed after temperature shift. Localization of ABP140 mRNA is not altered in *arf1-18*. The black bar corresponds to 5 μm.

Indeed, translation was attenuated more strongly in the cytosolic fractions, although the difference was more pronounced in *arf1-18* than in *arf1-11*. Taken together, this suggests that recruitment of mRNAs to the ER could enhance their translation under these conditions.

To see whether a redistribution of the four candidate mRNAs also took place in other *arf1* alleles, we repeated the FISH experiment in *arf1-17* and *arf1-18* after a shift to the non-permissive temperature. AMS1 mRNA and ABP1 mRNA redistributed both in *arf1-11* and *arf1-18*, however, the same was true for the *arf1-17* allele (Figure 4.9 B; data for ABP1 mRNA not shown). This was surprising to us, because so far we had never observed any mRNA-related phenotype in this strain. While general translation is attenuated in *arf1-11* and *arf1-18*, no such effect is observed in *arf1-17* (see Figure 4.1 and Figure 3.2 B), suggesting that mRNA relocalization is not a consequence of the remodelled translational landscape, but a process that is regulated independently. Moreover, ABP140 mRNA did not redistribute in *arf1-18* (Figure 4.9 B), while relocalization of CHS5 mRNA was strong only in *arf1-11* (data not shown). The complexity of this pattern suggests that several RBPs might be involved in the observed redistribution of mRNAs to the ER, and that they operate in a modular fashion. Such a system has been suggested by Hogan et al. (2008).

4.5.3 Protein localization of two candidate mRNAs is disrupted in *arf1-11*

Disruption of mRNA targeting can cause mislocalization of the encoded protein (Chartrand et al., 2002). Thus, we used the GFP-tagged strains to assess whether the localization of the proteins was affected (Figure 4.10). In the wild-type, Ams1-GFP localized to foci juxtaposed to the vacuole that were very motile; in the mutant, these foci were brighter - which reflects the increase in protein abundance - but did not appear any different otherwise. In contrast, localization of Chs5-GFP, which generally localizes to the trans-Golgi network (TGN) where it is recruited by Arf1p (Trautwein et al., 2006), was disturbed in *arf1-11*; it now concentrated in large clumps that might still correspond to the TGN, but the diffuse signal in the cytoplasm was increased. Abp1p is an actin-binding protein that normally localizes to actin patches and thus to the sites of polarized growth (Drubin et al., 1988). When *arf1-11* cells were shifted to 37°C, Abp1-4GFP polarization was lost; instead, large fluorescent clusters were observed throughout the cell. Abp140p binds specifically to actin cables. After shift to 37°C, actin cable staining was markedly reduced in both wild-type and mutant, presumably due to heat-induced disassembly of actin cables. For Abp140-GFP, there was no apparent difference in localization between wild-type and mutant; however, already at permissive temperature, *arf1-11* is hypersensitive to the actin-depolymerizing drug latrunculin A, indicating that the structure of the actin cytoskeleton may well be compromised in this mutant (Mark Trautwein, unpublished data).

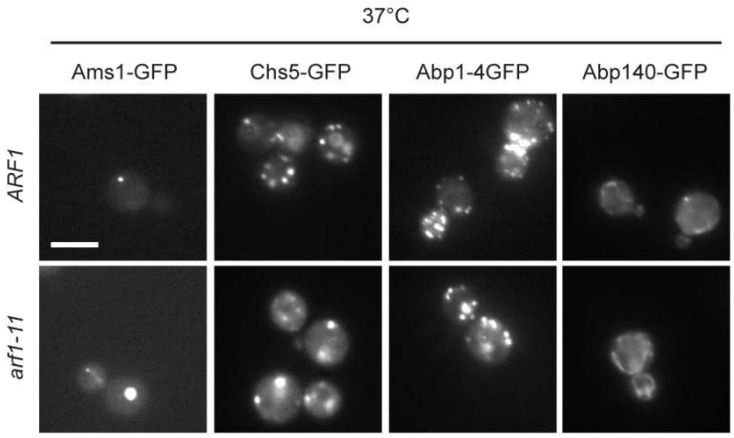

Figure 4.10: Localization of two of the candidate proteins is affected in *arf1-11*. Wild-type and *arf1-11* cells expressing Ams1-GFP, Chs5-GFP, Abp1-4GFP, or Abp140-GFP were grown to logarithmic phase and shifted to the non-permissive temperature for 1 h. GFP fluorescence was imaged under an epifluorescence microscope. The white bar corresponds to 5 µm.

In summary, for two out of four candidate mRNAs, the localization of the protein product is clearly altered in *arf1-11*, which might be a direct consequence of the redistribution of the mRNA. However, because the mRNA localization does not match the protein localization in wild-type it is quite likely that the mislocalization we observe reflects a disrupted organelle structure rather than defective protein targeting *per se*. In both cases, it would indicate that these proteins are compromised in their function, which would be compatible with the hypothesis that the mutant increases their translation as part of a specific response that is directed to alleviate symptoms of stress.

4.6 Section summary and open questions

In our microarray screen for transcripts with altered membrane association in an *arf1* mutant, we identified several candidate mRNAs. Relocalization of four of these could be validated by *in situ* hybridization. Upon shift, all of them were enriched on membranes and relocated to multiple foci in a configuration that was reminiscent of yeast ER. Concomitantly, we observed an increase in protein abundance. When we analyzed GFP fusions in live *arf1-11* cells, some of the proteins localized to organelles that were clearly disturbed in their structure.

We now propose a model in which a stress pathway is activated in response to certain defects in the mutant. As part of the stress response, specific mRNAs are targeted to the ER to be available for preferential translation, possibly to escape general translation attenuation in the cytoplasm. In agreement with this, in *arf1* mutants with decreased translation, ribosomes at the ER appear to be less affected. A similar compartmentalization of ribosomal populations had been observed when yeast were subjected to ER stress (Stephens et al., 2005); however, no signal-induced recruitment of mRNAs to one of these pools had been described. There have been reports that cells can specifically enhance translation of transcripts that do not contain IRES or other obvious features that would hallmark them for preferential translation, independently of their concentration (Fournier

et al., 2010). When Fournier et al. (2010) treated yeast cells with rapamycin and carried out transcriptome and proteome profiling over a period of 6 h, they identified 26 genes that increased in abundance at the protein level, but were unchanged or even decreased at the RNA level; so far, no mechanism has been described. In this work, we offer an idea how such a regulation might be possible.

At this stage, there are many open questions that need to be addressed, and some of them are quite central. First, it is not well documented that the membrane-like structures that our candidate mRNAs associate with indeed represent ER. We based our evidence on two observations: (i) the cortical staining in combination with internal ring-like structures strikingly resembled the typical yeast ER morphology and (ii) we found those mRNAs enriched in the P13 pellet of the mutant after temperature shift, thus in a fraction that is strongly enriched in ER membranes. However, a combined FISH/IF approach or live mRNA tracking (Lange et al., 2008) in a strain expressing an ER marker will be necessary to unambiguously judge whether these mRNAs are indeed redistributed to the ER in *arf1-11*, or whether they are targeted to yet another structure.

Secondly, our data suggest that translation of our candidate mRNAs is enhanced in the mutant; however, an increase in protein abundance is no definite proof. For this, sucrose gradient analysis followed by fractionation and RT-PCR should demonstrate that the mRNAs shift to heavier polysome fractions in the mutant. Possibly, an experimental setup that differentiates between cytosolic and membrane-bound ribosomes might provide additional insight.

Furthermore, we are missing the nature of the stress signal. From our studies we know that *arf1-11* suffers from a lot of stresses: It has activated UPR (as judged by HAC1 splicing; Figure 3.2 B), the cell wall integrity pathway is active (as judged by Slt2 phosphorylation; Figure 3.2 I), and these pathways have been shown to be coordinately regulated (Scrimale et al., 2009). However, the fact that a relocalization of the four candidate mRNAs also occured in *arf1-17*, where no HAC1 splicing is observed (Figure 3.2 I), suggests that these pathways do not play a decisive role in this process. Additionally, *arf1* mutants might well be presensitized to osmotic stress. Analysis of signaling mutants will reveal whether any of these stress signaling pathways is involved in mRNA redistribution in *arf1* mutants.

Finally, the nature of the protein factors involved in mRNA relocalization and of the protein components of the ER-associated mRNP is still elusive. Since we found induction of multiple PBs at the ER in *arf1-11* (Figure 3.1 A, Figure 3.7 A and C, see above), we tested whether our candidate mRNAs were recruited to these bodies. FISH in strains expressing Dcp2-GFP, a PB marker, did not reveal marked colocalization with the candidate mRNAs (data not shown). This lack of colocalization is in accordance with the observation that translation of the four mRNAs is enhanced, since PBs have been implicated in mRNA silencing and decay. To identify protein interactors, we have constructed a

plasmid that allows chromosomal integration of the PP7 stemloop into 3'UTRs; in combination with the stemloop-binding PP7 coat protein, which we have appended with an HBH tag, this system allows the efficient purification of mRNAs (Hogg & Collins, 2007). In the future, mRNA-IP followed by mass spectrometry of isolated complexes may help to identify the elusive trans-acting factors.

Chapter 5

Cotranslational transport of ABP140 mRNA to the distal pole of the mother cell

5.1 ABP140 mRNA localizes to the distal pole of the mother cell

When we verified our microarray hits by FISH, we quickly realized that ABP140 mRNA localizes in a peculiar fashion in wild-type cells or in the *arf1* mutant at the permissive temperature; namely, we detected one bright spot at the distal pole of the mother cell in a large percentage of cells (Figure 5.1 A), a localization that had not been described for any mRNA in yeast. The initial observation was corroborated by additional experiments, and we observed the same localization whether we used antisense probes complementary to nucleotides 39 to 746 or 936 to 1957 of the mRNA. Moreover, in a *Δabp140* strain, no signal was detected, indicating that our staining was specific (Figure 5.1 B). In the following FISH experiments, we used probe 936 to 1957, which gave the better signal.

For our research, we almost exclusively use haploid yeast strains because it is easier to generate mutants when only one copy of each gene is present. Haploid cells bud in an axial pattern, meaning that each new daughter buds proximal to the last budding event, opposite to the distal pole (Chang & Peter, 2003). We wondered whether ABP140 mRNA would always be found opposite to the current bud or whether some landmark was deposited during earlier budding events which would recruit ABP140 mRNA even if the cell repolarized. For this, we used a *Δbud5* strain that buds in a random pattern (Yang et al., 1997). As in the wild-type, ABP140 mRNA was found concentrated distal to the current bud in the *Δbud5* strain; we observed no random distribution along the cortex of the mother cell (Figure 5.1 C). The same was true for the diploid yeast BY4743, which buds bipolarly, i.e. polarity is reverted after each cell cycle, and for a *Δbud7/Δbud7* strain (Figure 5.1 C), a diploid yeast with a random budding pattern (Yang et al., 1997). From this data, it was apparent that ABP140 mRNA localization was governed by the current polarity axis of the cell.

5.1.1 ABP140 mRNA localization requires actin cables

Next, we wanted to know whether localization of ABP140 mRNA involved active transport along the cytoskeleton. In many organisms, microtubules have been implicated in mRNA localization (Czaplinski & Singer, 2006). In *S. cerevisiae*, the SHE machinery, an actin-myosin based system, was shown to transport mRNAs to the tip of the bud, where they are anchored (Long et al., 1997; Takizawa et al., 1997).

To test whether any of these cytoskeletal elements were needed for ABP140 mRNA localization, we first disrupted microtubules by treating cells with 30 µg/ml benomyl for 15 min; localization of ABP140 mRNA was not affected in treated cells (Figure 5.1 D). Next, we applied Latrunculin A (LatA), which prevents polymerization of actin (Coué et al., 1987). After only 10 min of treatment with 30 µg/ml LatA, the signal for ABP140 mRNA became disperse (Figure 5.1 D). To corroborate this data, we generated a *Δtpm1* strain that has no detectable actin cables (Liu &

Bretscher, 1989); absence of actin cables was verified by Rhodamine phalloidin staining (data not shown). As expected, in the *Δtpm1* strain, the FISH signal was diffuse and cytoplasmic (Figure 5.1 D).

These data clearly indicate that ABP140 mRNA is transported to the distal pole via actin cables; however, it also raises some questions. In *S. cerevisiae*, the actin cytoskeleton is polarized towards the bud, meaning that myosin-driven transport along cables is predominantly directed away from the distal pole (Yang & Pon, 2002). And indeed, if we deleted the unconventional myosin *MYO4*, which disrupts transport of mRNAs to the bud tip, ABP140 mRNA localized as in wild-type (data not shown). However, actin cables are no stationary entities. Insertion of actin monomers at the plus end results in a constant retrograde flow (Yang & Pon, 2002). It has been shown that mitochondria that

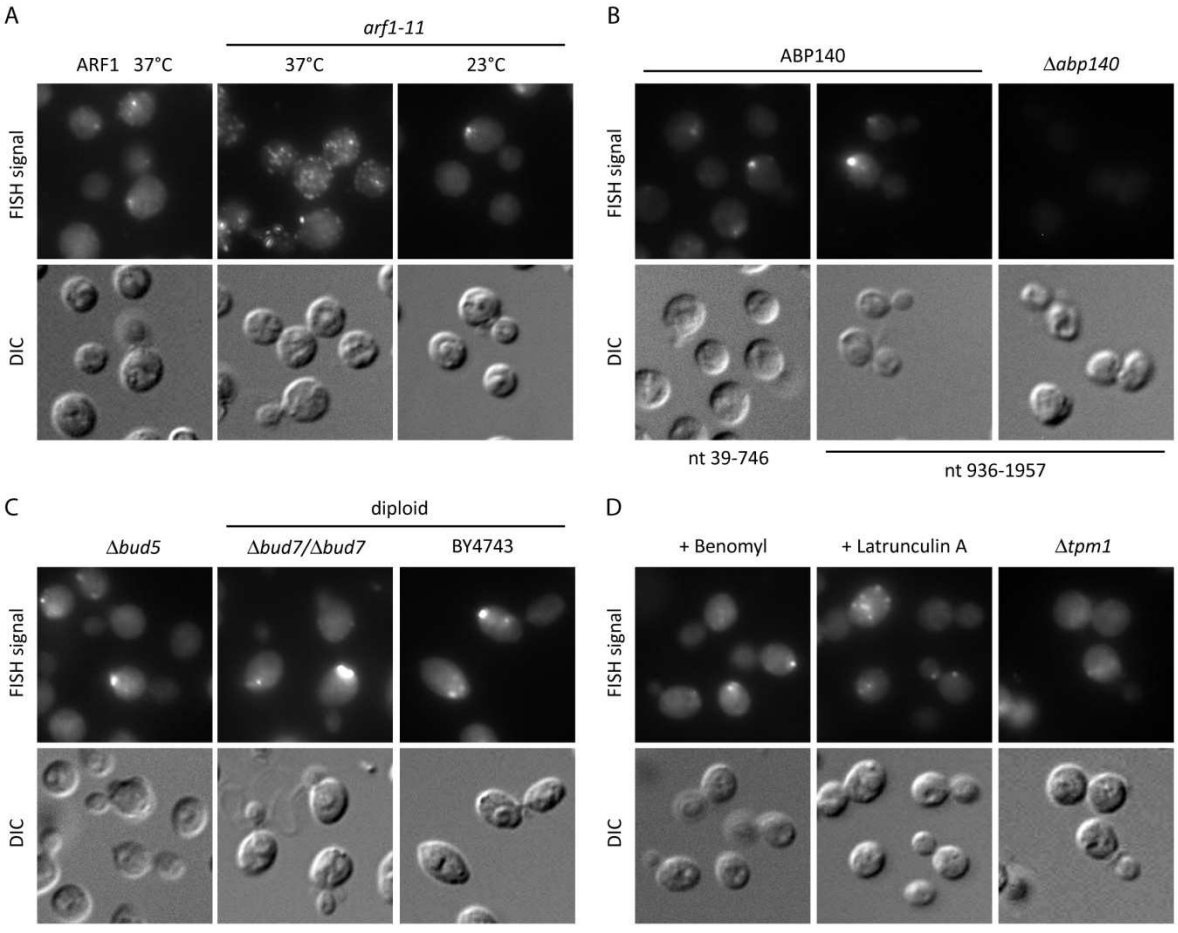

Figure 5.1: ABP140 mRNA localizes to the distal pole of the mother cell. (**A**) ABP140 mRNA localization is disrupted in the *arf1-11* mutant. Cells were grown to logarithmic phase and shifted to the non-permissive temperature for 1 h. Cells were fixed and subjected to FISH against ABP140 mRNA. While the mRNA localizes to the distal pole of the mother cell in wild-type cells or in *arf1-11* at the permissive temperature (23°C), mRNA localization becomes disperse when the mutant is grown at 37°C. (**B**) The FISH signal is specific. Anti-sense probes towards different regions of the mRNA give similar staining. No signal was detected in a strain deleted for *ABP140*. (**C**) **Localization is governed by the current polarity axis of the cell.** FISH against ABP140 mRNA in two mutants with a random budding pattern, *Δbud5* and *Δbud7/Δbud7*, and a diploid control. The mRNA was detected at the distal pole in all cases. (**D**) **ABP140 mRNA localization is dependent on actin.** FISH against ABP140 mRNA in cells either treated with either 30 µg/ml benomyl, which disrupts microtubules, or with 30 µg/ml latrunculin A, which prevents polymerization of actin cables, for 15 min or 10 min, repectively. Alternatively, a *Δtpm1* mutant, which has no detectable actin cables, was used. In the absence of actin cables, localization of ABP140 mRNA to the distal pole was lost.

are retained in the mother cell during cell division undergo actin-dependent retrograde movement at the speed of the flow, indicating that they are transported to the distal pole by stable linkage to actin cables (Boldogh et al., 2005).

We propose that ABP140 mRNA transport involves a similar mechanism. There is evidence in the literature that actin retrograde flow can be accelerated or slowed down by deleting *TPM2* or *MYO1*, respectively (Huckaba et al., 2006). In our hands, none of the mutations resulted in a marked increase or decrease of ABP140 mRNA localization; however, nor was the appearance of the tubular mitochondrial network altered in these mutants, indicating that retrograde transport might be very robust to variations in the rate of the flow (data not shown). Besides, our FISH analysis is not quantitative, and the percentage of cells which shows strong localization is subject to variations even in the wild-type; therefore, we would probably not be able to detect subtle differences in localization efficiency with this protocol.

5.1.2 ABP140 mRNA localizes to the end of actin cables

Abp140p localizes to actin cables and the protein has been used as *bona fide* marker to study actin cable dynamics in yeast (Yang & Pon, 2002). The mRNA of the GFP-tagged construct displayed wild-type localization to the distal pole (Figure 5.2 B). This allowed us to look at actin cables and ABP140 mRNA simultaneously with a joint FISH/immunofluorescence (FISH/IF) protocol. We used an overexpressing ADH1 promoter construct to further increase the signal.

Z stacks recorded on a confocal microscope revealed that ABP140 mRNA accumulations were almost exclusively found at the end of actin cables, preferentially at sites where several cables converged, further corroborating our previous data which strongly suggest that ABP140 mRNA is transported on the actin cytoskeleton (Figure 5.2 A).

5.1.3 The ORF sequence is sufficient to localize ABP140 mRNA to the distal pole

In many instances, mRNAs are localized with the help of trans-acting factors that recognize and bind sequences in the untranslated regions (UTRs) of the transcript, most often in the 3'UTR (Jambhekar & Derisi, 2007). In the FISH/IF experiment, we had used a strain where a strong ADH1 promoter was inserted in front of Abp140-GFP. For this, PCR-generated cassettes had been integrated into the chromosome upstream and downstream of the ORF by homologous recombination (Wach et al., 1994, Figure 5.2 C), and had replaced the endogenous sequences. Thus, when the endogenous 5'UTR was replaced by the ADH1 5'UTR, ABP140 mRNA localization to the distal pole was not affected; in fact, because the ADH1 promoter is stronger than the endogenous promoter, there was a marked increase in FISH signal at the distal pole, and crystals of the dye used for visualization could be detected in the DIC channel (Figure 5.2 B). Similarly, when the endogenous 3'UTR was replaced by fusing GFP followed by ADH1 3'UTR to the ABP140 ORF, ABP140 mRNA localized as in wild-type

(Figure 5.2 B). Furthermore, replacing 5' and 3'UTR at the same time had no effect on ABP140 mRNA localization, indicating that the ORF sequence is sufficient to localize the transcript (Figure 5.2 B).

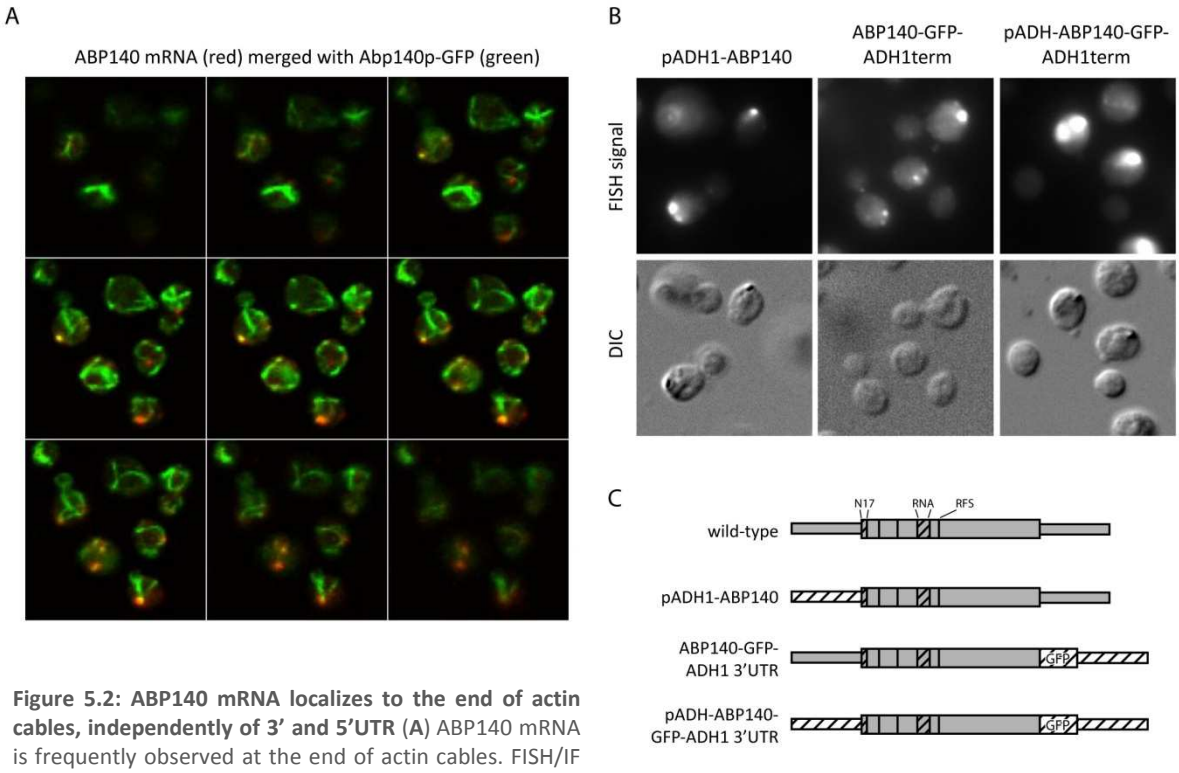

Figure 5.2: ABP140 mRNA localizes to the end of actin cables, independently of 3' and 5'UTR (**A**) ABP140 mRNA is frequently observed at the end of actin cables. FISH/IF against ABP140 mRNA and GFP protein in cells expressing Abp140-GFP under an ADH1 promoter. Z-stacks were recorded on a confocal microscope. (**B**) 5' or 3' UTR are not required for localization of ABP140 mRNA to the distal pole. FISH against ABP140 mRNA in strains where either the 5' UTR, the 3' UTR, or both were exchanged for the corresponding sequences from the *ADH1* locus. The mRNA was detected at the distal pole in all cases. (**C**) A sketch of the constructs used in B. Gray represents endogenous sequences, while hatched parts are taken from exogenous sources. The thick area corresponds to the ORF. Additional features of the protein are indicated: N17: actin-binding domain; RNA: putative RNA-binding domain; RFS: ribosomal frameshift site

5.1.4 Localization of Abp140p determines ABP140 mRNA localization

In the simplest case, the machinery responsible for ABP140 mRNA localization would consist of only one protein with two distinct features: An RNA-binding domain, which would be able to recruit ABP140 mRNA, and an actin-binding domain, which would stably link the mRNA to actin cables. Actin retrograde flow would then transport the mRNA towards the distal pole, where the mRNA would be deposited at sites where the actin cables disassembled.

One candidate meets both requirements and immediately came to our minds – Abp140p itself: It binds to actin cables with the 17 N-terminal amino acids and carries a putative RNA-binding domain (R. Wedlich-Söldner, personal communication), which was mapped to amino acids 205 to 249 using the optimal prediction mode of RNAbindR, a software for prediction of RNA binding residues in proteins (Terribilini et al., 2007).

We first wanted to test whether actin-binding of Abp140p was required for correct localization of ABP140 mRNA. We therefore constructed an N-terminal truncation where the first 17 amino acids

were replaced by GFP and placed it under an ADH1 promoter; as judged by GFP fluorescence, the resulting protein localized to the cytoplasm (ΔN17-GFP-Abp140; Figure 5.3 A and E). When we assessed ABP140 mRNA localization via FISH, the staining for the mRNA was also cytoplasmic, indicating that the actin-binding capacity of Abp140p was required for ABP140 mRNA localization to the distal pole (Figure 5.3 A).

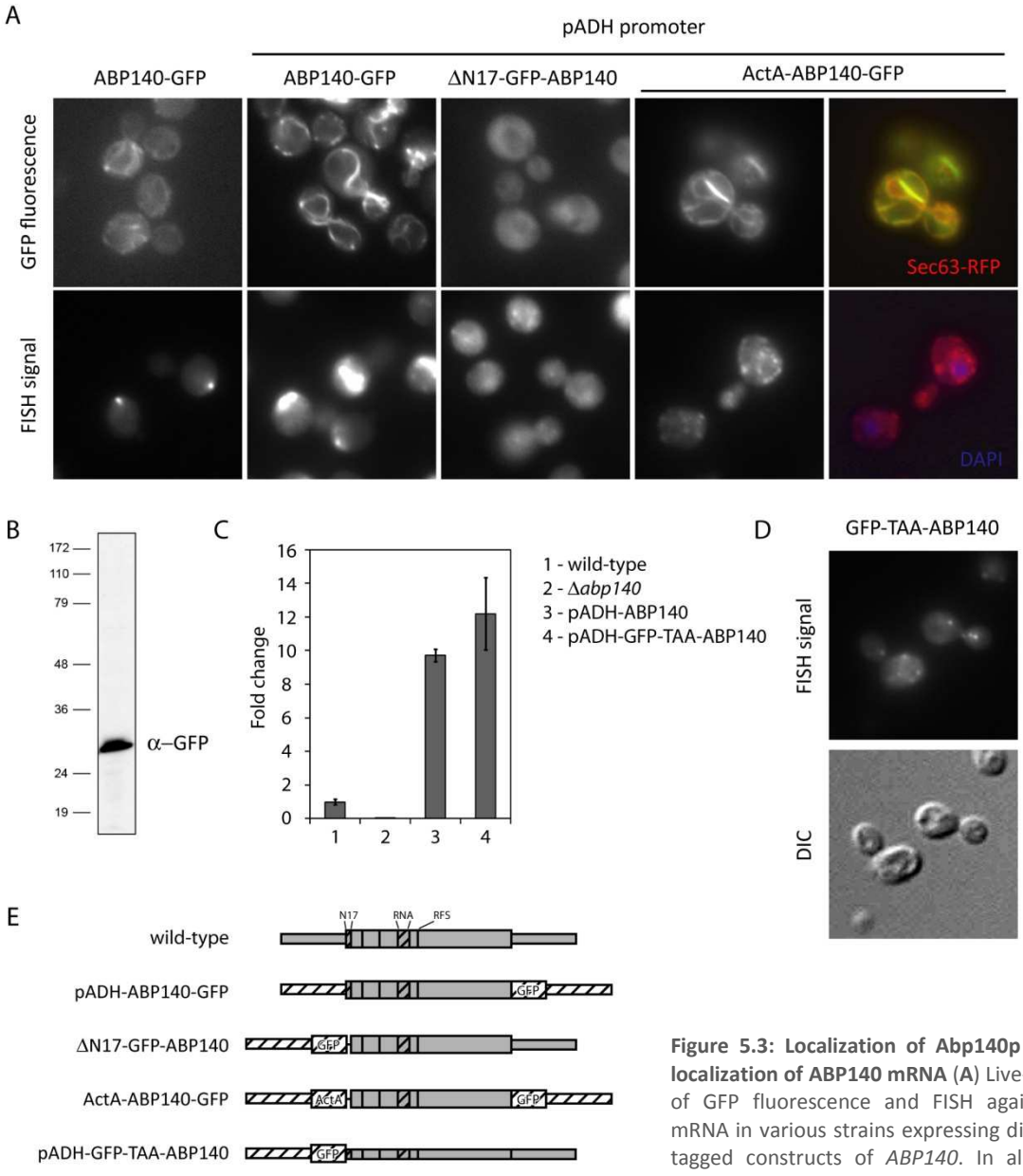

Figure 5.3: Localization of Abp140p determines localization of ABP140 mRNA (**A**) Live-cell imaging of GFP fluorescence and FISH against ABP140 mRNA in various strains expressing different GFP-tagged constructs of *ABP140*. In all cases, the localization of the mRNA follows the localization of the protein. Colocalization of ActA-Abp140-GFP with the ER was verified by coexpression of the ER marker Sec63-RFP. In FISH, nuclear DNA was stained with DAPI to delineate the perinuclear ER. (**B-D**) **Abp140p is required for ABP140 mRNA localization**. (**B** and **C**) Construct GFP-TAA-ABP140, which harbors an in-frame stop codon after the N-terminal GFP, is expressed. (**C**) Western blot for GFP on total lysate. (**D**) quantitative RT-PCR with primers specific for ABP140; PGK1 was used to normalize the samples. GFP-TAA-ABP140 is present in similar amounts as the wild-type transcript when placed under the same promoter (pADH1). (**E**) Expression of Abp140p is required for localization of ABP140 mRNA. FISH against ABP140 mRNA in a strain expressing GFP-TAA-ABP140. In the absence of Abp140p, ABP140 mRNA signal becomes disperse. (**B**) Sketch of the constructs used in A-D. See Figure 5.2 C for details on the representation.

Next, we wondered whether we would be able to force ABP140 mRNA into an ectopic localization if we redirected the protein to a different organelle. Therefore, we replaced the 17 N-terminal amino acids of Abp140p by the 27 C-terminal amino acids of the ActA protein from *Listeria monocytogenes*, which binds the outer mitochondrial leaflet in mammalian cells (Zhu et al., 1996), but targeted Abp140p to the ER in our strain background when fused to the N-terminus (ActA-ABP140; Figure 5.3 A and E). ER localization of ActA-Abp140p was confirmed by coexpression of a plasmid-borne ER marker coupled to red fluorescent protein (Sec63-RFP, Figure 5.3 A). As predicted, the mRNA of this construct localized to the cell periphery and encircled the nucleus, which was stained with DAPI, a structure typical for yeast ER (Figure 5.3 A). Colocalization of this construct's mRNA with the ER was verified by confocal microscopy using a combined FISH/IF protocol where we stained for the ER-marker HDEL-GFP (data not shown). From this data, it was apparent that Abp140p localization determines the localization of ABP140 mRNA, making it a good candidate for the trans-acting factor postulated above.

To prove that Abp140p expression is required to localize its own mRNA, we designed a construct in which we replaced the endogenous 5'UTR of ABP140 by the ADH1 promoter followed by a GFP including a TAA stop codon; the resulting transcript carries the full ORF, but only GFP is expressed (GFP-TAA-ABP140; Figure 5.3 B). Because of the artificially extended 3'UTR, we were afraid that this construct would be a substrate for nonsense-mediated decay (NMD), which affects transcripts that carry premature stop codons (Leeds et al., 1991). However, with immunoblot, we detected expression of GFP, and quantitative RT-PCR with primers specific for *ABP140* revealed that the mRNA was present in amounts comparable to the wild-type transcript when placed under the same promoter (Figure 5.3 C and D). As expected, the mRNA did not localize to the distal pole, but showed punctate staining throughout the cell (Figure 5.3 E), further strengthening our notion that Abp140p mediates the localization of its mRNA.

5.1.5 Active translation, but not the putative RNA-binding domain, is required for ABP140 mRNA localization

Next, we needed to prove that Abp140p satisfies the second requirement of a trans-acting factor – the capacity to bind ABP140 mRNA. We first wanted to know whether the putative RNA-binding domain of Abp140p was in fact required to localize ABP140 mRNA. We therefore deleted amino acids 205 to 249 on the chromosome ("*ΔRNA*") using the delitto perfetto method (Storici et al., 2001).

To our surprise, the mRNA of the *ΔRNA* mutant localized as in wild-type (Figure 5.4 A and E). From our previous data, we knew that under normal growth conditions localization of ABP140 mRNA followed the localization of Abp140p. Both protein localization domains we tested, the endo-genous actin-binding domain and the ER-targeting ActA peptide, were located at the very N-terminus of the protein, making them the first part of the protein to exit the ribosome during translation. It would

therefore be conceivable that ABP140 mRNA transport happened cotranslationally; this way, the translating ribosome would provide the missing link between protein and mRNA.

If this hypothesis were correct, we would expect that translation inhibition would disrupt transport of ABP140 mRNA to the distal pole. Indeed, whether we treated wild-type cells with the protein translation inhibitor Verrucarin A for 1 h or used the conditional allele *prt1-1,* a mutant deficient in translation initiation (Hartwell & McLaughlin, 1969), ABP140 mRNA signal became disperse (Figure 5.4 B). Loss of translating polysomes was confirmed by polysome profile analysis (Figure 5.4 B). From previous experiments, we knew that Abp140p was required for ABP140 mRNA localization. To exclude that we depleted the protein during the treatment, we detected the GFP-

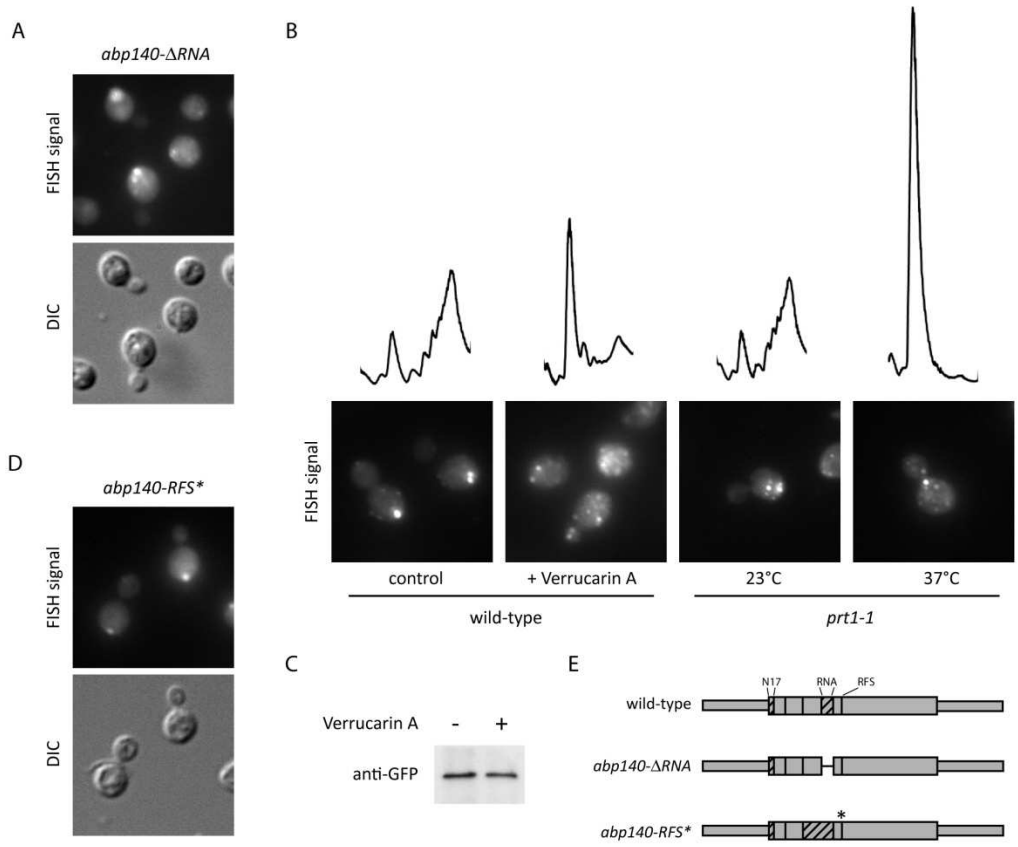

Figure 5.4: (A-C) Active translation, but not the putative RNA-binding domain is required for ABP140 mRNA localization to the distal pole. (**A**) FISH against ABP140 mRNA in a strain where the putative RNA-binding domain was deleted (*ΔRNA*). ABP140 mRNA localization to the distal pole is not affected in this strain. (**B**) Translation was blocked either by treatment of wild-type cells with 10 µg/ml Verrucarin A for 1 h or in a conditional translation initiation-deficient mutant that was shifted to the non-permissive temperature for 20 min. Cells were either processed for FISH against ABP140 mRNA, or their polysome profile recorded to verify the block in translation. In both cases, translation was greatly reduced; concomitantly, localization of ABP140 mRNA to the distal pole was lost. (**C**) Abp140p is not depleted during Verrucarin A treatment. Western blot against GFP on total lysate of cells expressing Abp140-GFP that were treated with 10 µg/ml Verrucarin A for 1 h. (**D**) **The ribosomal frameshift site does not contribute to ABP140-mRNA localization to the distal pole.** FISH against ABP140 mRNA in a strain where the ribosomal framehift site was mutated (*RFS**). ABP140 mRNA localization is not affected in this strain. (**E**)) Sketch of the constructs used in A and D. See Figure 5.2 C for details on the representation.

tagged protein by immunoblot; no decrease in Abp140p levels was detected (Figure 5.4 C), indcating that depletion of the protein was not responsible for the phenotype we observed.

Unfortunately, even after repeated attempts, we were not successful in tagging Abp140p in the *prt1-1* strain, thus we could not assess Abp140p stability in this mutant; however, since we only shifted the cells to the non-permissive temperature for 20 min, we do not consider a complete depletion of the protein very likely. Taken together, these experiments indicate that active translation of ABP140 mRNA is necessary for its localization, supporting the hypothesis that transport happens cotranslationally.

5.1.6 +1 ribosomal frameshift is not required for ABP140 mRNA localization

ABP140 mRNA carries a +1 ribosomal frameshift site at amino acid 831. The frameshifting mechanism involves a translational pause at a codon that is recognized very slowly; recognition of the first codon in the +1 frame by a highly abundant tRNA can then lead to a shift in the reading frame (Farabaugh et al., 2006). We hypothesized that this translational pause might be required to enable efficient cotranslational transport of the Abp140p-ribosome-mRNA complex. We therefore constructed a frameshift-corrected allele of *ABP140* by replacing the frameshift consensus site CUU-AGG-C by uug-GGC (similar to Morris & Lundblad, 1997). The mutated mRNA, however, localized as in wild-type (*abp140-RFS**; Figure 5.4 D and E), demonstrating that the frameshift site was not required for mRNA localization.

5.1.7 The first 67 amino acids of Abp140p are sufficient to localize ABP140 mRNA

As we had demonstrated that the N-terminal actin-binding domain was necessary for ABP140 mRNA localization but none of the salient features of the Abp140p C-terminus was required for efficient transport, we now asked ourselves whether appending the N-terminal actin-binding domain to any protein would be sufficient to localize the corresponding mRNA to the distal pole. We constructed a C-terminal truncation of Abp140p by fusing GFP directly to amino acids 1-17 of the protein; the resulting construct is an actin cable-localized GFP and, in fact, identical to the actin tracker Lifeact (Riedl et al., 2008). The mRNA of this construct failed to localize to the distal pole (Figure 5.5 A), indicating that there were additional requirements besides the N-terminal actin-binding domain.

In order to identify the minimal localizing fragment, we constructed a series of C-terminal truncations: (1-831)-GFP, which is truncated at the ribosomal frameshift site; (1-750)-GFP, which is truncated immediately after the putative RNA-binding domain; (1-612)-GFP, which is truncated immediately before the putative RNA-binding domain; and three shorter truncations (1-402)-GFP, (1-201)-GFP, and (1-67)-GFP. All truncations were expressed (Figure 5.5 B) and the protein product localized to actin cables for each of the constructs (data not shown). When we probed for the

corresponding mRNAs using a probe complementary to GFP, distal pole localization was detected for all truncation constructs, indicating that only a short fragment comprising the first 67 amino acids is required for efficient mRNA localization.

5.1.8 The N-terminal 67 amino acids of Abp140p sustain mRNA localization only if followed by a translatable sequence

If our hypothesis of cotranslational mRNA localization were correct, transport would occur only while the N-terminal actin-binding domain is exposed to the cytoplasm but protein and mRNA are still stably associated with the translating ribosome. During translation, around 40 amino acids are buried in the ribosomal protein-conducting channel (Matlack & Walter, 1995), and protein biosynthesis in *S. cerevisiae* progresses at a speed of approximately 20 amino acids per second (Frank, 2003).

In our truncation analysis, only 67 amino acids were required for efficient mRNA transport (Figure 5.5 A). Thus, the transport-competent complex with the N-terminal domain exposed would be stable for less than a second; however, all our truncation constructs were fused to GFP, which adds another 250 aa or approximately 12 s until translation terminates, which might be sufficient to sustain transport.

When we inserted a stop codon between amino acids 1-67 of Abp140p and the GFP sequence, mRNA localization to the distal pole was lost ((1-67)TAA-GFP; Figure 5.5 A). Thus, translation needs to continue for a certain time after the N-terminus has exited the ribosome in order to ensure proper localization of ABP140 mRNA, which would be in agreement with cotranslational transport.

There are two possible explanations why the first 17 amino acids fused to GFP are not sufficient to localize the mRNA: First, the total length of the construct might be insufficient to ensure cotransport of mRNA and protein on the ribosome; however, (1-17)-GFP consists of 267 aa, while (1-67)-GFP consists of 317 aa, which would translate into a predicted residence time on the ribosome of 13 s and 15 s, respectively, a relatively small difference which we feel would not be likely to generate the marked difference in localization we observe. Alternatively, some feature present in amino acids 18-67 or contained in bases 52-201 of the mRNA might promote cotranslational coupling. From what we know, the RNA sequence between 52 and 201 neither folds into a particularly stable secondary structure – as predicted by RNAfold, a resource for secondary structure prediction for single-stranded RNA (Gruber et al., 2008) – nor does it contain any codons that are notably rare in *S. cerevisiae* (Nakamura et al., 2000). Further analysis will be required to understand the role of this fragment in ABP140 mRNA localization.

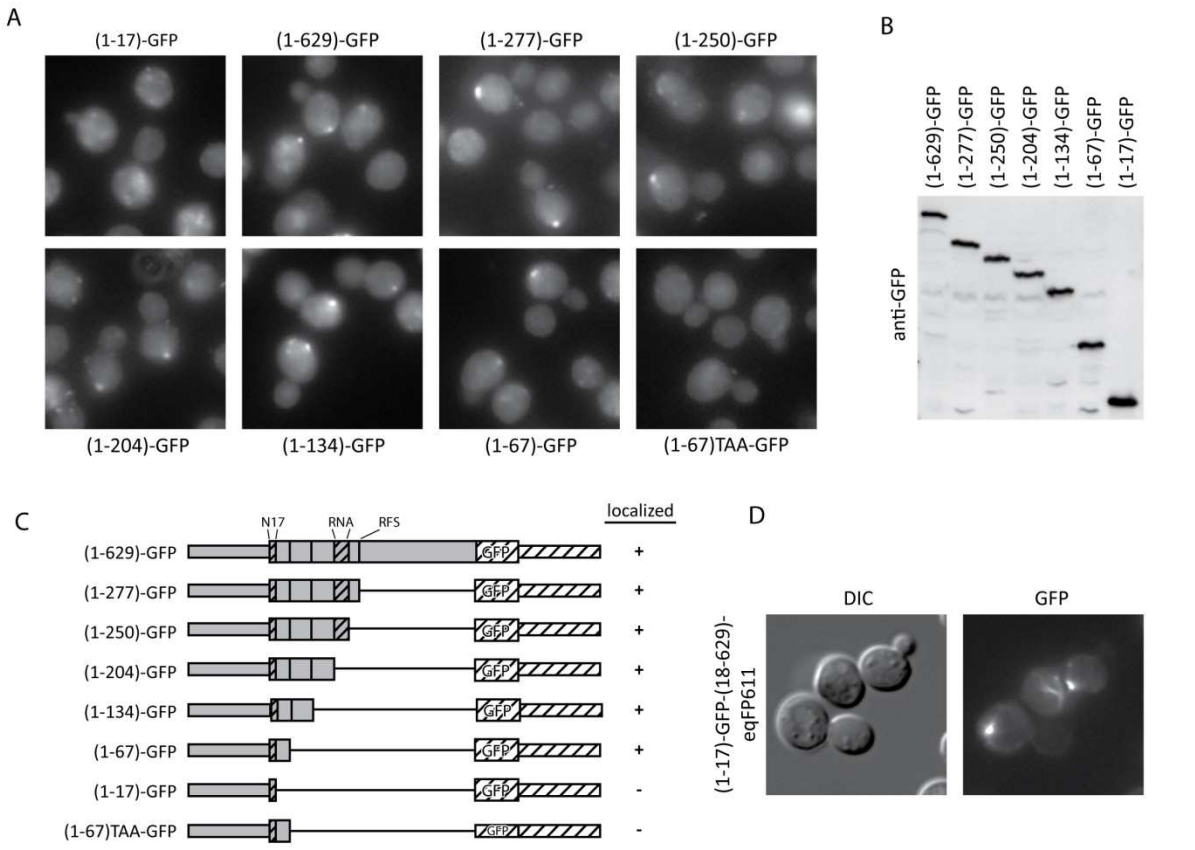

Figure 5.5: (A-C) The first 67 amino acids of Abp140p are sufficient to localize the mRNA to the distal pole if followed by a translatable sequence. (**A**) FISH against GFP in different GFP-tagged C-terminal truncations of *ABP140*. The first 67 amino acids are sufficient to localize the mRNA to the distal pole when fused to GFP; the first 17 amino acids, however, are not. If a stop codon is inserted between ABP140(1-67) and GFP, mRNA localization to the distal pole is lost. (**B**) Western blot against GFP on total lysates generated from the strains used in A. (**C**) Sketch of the constructs used in A and B. See Figure 5.2 C for details on the representation. (**D**) **Decreased protein motility leads to accumulation of Abp140p at the distal pole.** An aggregation-prone construct of Abp140p is concentrated at the end of actin cables.

5.1.9 An aggregation-prone construct of Abp140p localizes to the distal pole

There was one observation which we found rather puzzling: While ABP140 mRNA is deposited at the end of actin cables and remains there, Abp140p is associated with cables throughout the cell, with no visible accumulations at the distal pole. Yet, according to our model, both molecules are bound to actin cables via the same domain, either directly or indirectly. Our translation inhibitor experiment suggested that Abp140p is not turned over quickly, indicating that the protein is able to freely diffuse in the cell and rebind cables at the tip of the daugther cell.

We fused eqFP611, an aggregation-prone red fluorescent protein, C-terminally to Abp140p. Protein localization was monitored by fluorescence of GFP, which was inserted between amino acids 17 and 18 to leave actin-binding intact; insertion of GFP alone did not influence localization of the protein or the mRNA (data not shown). The resulting protein accumulated at the distal pole (Figure 5.5 D). Thus, interfering with the motility of an actin cable-bound macromolecule is sufficient to

concentrate it at the end of actin cables, indicating that ABP140 mRNA might be less diffusible than untagged Abp140p.

5.2 Section summary and open questions

We have identified ABP140 mRNA as a distal pole-localized transcript. In a series of experiments, the mode of transport was characterized in detail: We believe ABP140 mRNA to be transported cotranslationally, as part of the ternary complex of mRNA, translating ribosome, and nascent polypeptide with the N-terminal actin-binding domain exposed to the cytoplasm, by actin retrograde flow. Truncation analysis has revealed that a short construct consisting of amino acids 1-67 of Abp140p is sufficient to localize the mRNA if appended to a translatable sequence. Whether amino acids 18-67 are specifically required for cotranslational coupling and serve as a stop transfer signal remains to be determined. A construct in which this sequence is deleted has been generated and verified. In parallel, we appended the actin-binding motif with four copies of GFP to increase the total length of the ORF. Both constructs are expressed and localize to actin cables, and FISH on ABP140 will help to clarify the role of amino acids 18-67 in mRNA localization.

When diffusibility of Abp140p in the cytoplasm was constrained, it accumulated at the distal pole, which by analogy implies that the mRNA might not be very motile or even anchored on site to prevent diffusion. However, interfering with mRNA transport by disruption of actin cables or inhibition of protein translation quickly abolished its localization, making a stable association with an anchoring factor unlikely. Rather, translation might be required for anchoring, as is the case for ASH1 mRNA (Gonzalez et al., 1999), possibly because an actively translated mRNA that is – in the case of ABP140 – associated with 11 to 12 ribosomes (Arava et al., 2003), is simply to bulky to diffuse away.

Open questions remain. First of all, the function of Abp140 protein has remained frustratingly elusive. When Abp140p was first isolated, it was described as an actin filament-binding protein with weak actin-bundling activity (Asakura et al., 1998). The gene is not essential, and its deletion does not result in a growth defect. Likewise, cellular morphology and actin cable dynamics are not affected (Asakura et al., 1998). Bud site selection is not disrupted, and mating and sporulation occur normally (data not shown). *ABP140* shows negative genetic interactions with clathrin light chain (*CLC1*), the RhoGAP *RGD1*, the Rho GDP dissociation inhibitor *RDI1*, and *CDC3*, an essential component of the septin ring (Costanzo et al., 2010). Except for actin, no protein interactors have been described, although Abp140p may be a substrate for diverse kinases and for acetylation, as suggested by high-throughput analyses (Ptacek et al., 2005; Lin et al., 2009). At the very C terminus, Abp140p carries a putative methyltransferase domain orthologous to human METTL2B, a putative methyltransferase that interacts with presenilins, which have been implicated in Alzheimer's disease (Zhang et al., 2001); so far, no substrate has been identified.

In addition, the mRNA contains a +1 ribosomal frameshift site that has persisted in budding yeasts for 150 million years, suggesting that there was evolutionary pressure to maintain the gene functional (Farabaugh et al., 2006). Programmed frameshift sites are very rare; indeed, only one other non-transposon gene in *S. cerevisae*, *EST3*, employs a +1 frameshift site that obeys the same mechanism (Farabaugh et al., 2006). If frameshifting on Abp140 fails, translation is terminated at a stop codon immediately downstream of the frameshift site, which results in a C-terminally truncated protein that is easily distinguished from full-length Abp140p by immunoblot when an internal GFP-tag is inserted (data not shown). Interestingly, frameshifting efficiency of Ty1 retrotransposon, which carries an identical frameshift site, is largely dependent on the growth condition and increases after diauxic shift (Stahl et al., 2004). However, although the ratio between non-frameshifted, truncated Abp140p and the frameshifted full-length protein increased when cells entered stationary phase, expression of the frameshift mutant *abp140-RFS**, which produces only full-length Abp140p, had no deleterious effect when cells were grown on glycerol , indicating that differential frameshifting on Abp140p is not a major regulatory mechanism during diauxic shift.

Abp140p is the only protein in *S. cerevisiae* which stably binds to actin cables but is not associated with any other form of actin, making it a likely candidate to be involved in retrograde transport. However, when we tested different published retrograde cargo (Boldogh et al., 2005; Liu et al., 2010), none of them was dependent on Abp140p: After deletion of *ABP140*, the mitochondrial tubular network retained its wild-type morphology, and actin-dependent exclusion of heat-induced protein aggregates from daughter cells was not impaired (data not shown).

Without a clear idea of Abp140p function, the question whether ABP140 mRNA localization is of biological significance is moot. Other cases of cotranslational transport have been reported, firstly, ER-targeting of SRP-dependent mRNAs (Walter & Blobel, 1981), and secondly, ER recruitment of mammalian XBP1, an mRNA that is spliced in response to ER stress and is tethered to the membrane by hydrophobic regions contained solely in the unspliced protein product (Yanagitani et al., 2009). In both cases, cotranslational transport serves an important cellular function, indicating that, in the course of evolution, this mechanism has been purposefully employed.

At the moment, we do not understand why redistribution of ABP140 mRNA in *arf1-11* completely abolishes distal pole localization. In chapter 4, we hypothesized that relocalization of mRNAs to the ER might be a mechanism to ensure their preferential translation on ER-bound ribosomes under conditions when general translation in the cytoplasm is attenuated. It would be conceivable that ER-associated ribosomes cannot undergo retrograde transport because they are stably linked to the membrane, but that under theses conditions translation initiation in the cytoplasm occurs too rarely to sustain cotranslational transport. This explanation would, however, have additional implications: Since ABP140 mRNA is delocalized in *arf1-17*, but translation is not

attenuated in this mutant, this model would require a shuttling factor that represses translation on ABP140 mRNA in the cytoplasm until the complex has been recruited to the ER. So far, such a factor has not been described, and additional investigation will be necessary to fully understand this process.

Chapter 6

Conclusion

We had set out – somewhat naively, one might say – to characterize vesicle-mediated mRNA transport in *S. cerevisiae* using a mutant in the small GTPase Arf1p. What we have ended up with, is a more thorough understanding of the intricacies of post-transcriptional gene regulation in a yeast cell under stress.

When we performed a microarray-based screen to identify transcripts that undergo Arf1p-dependent transport to the ER, none of the ORFs qualified as a convincing cargo of vesicle-mediated transport. Instead, all promising candidates turned out to be part of what we now believe to be a stress response that recruits specific mRNAs to the ER to make them available for preferential translation.

When we discovered that one of the transcripts localized asymmetrically, we characterized its transport in greater detail. By now, we have a good understanding of how ABP140 mRNA is targeted to its unusual localization, the distal pole of the mother cell, by cotranslational coupling.

Finally, in a series of experiments, we have sought to define what distinguishes multiple PBs induced in secretory mutants from the few bright granules that are observed after glucose starvation. We could show that the appearance of multiple PBs is linked to Ca^{2+}, and we have identified a set of proteins that is strictly required for formation of Ca^{2+}-induced PBs but is dispensable for PB induction under other conditions. Moreover, we have indications that the different pathways for PB induction directly regulate PB number, because combination of stresses led to multiple PBs although starvation appeared to be the more potent stress when translation attenuation was used as readout.

Translation attenuation and PB induction in secretory mutants could be uncoupled by deletion of *GCN2.* This finding was very surprising, because it indicates that the mRNAs that aggregate in multiple PBs are not identical to the mRNAs that are released from polysomes after the block in translation, since relieving the translational inhibition did not decrease PB brightness or number. Thus, the common belief that PBs are a mere reservoir for translationally inactive mRNAs and that, *vice versa*, all silenced mRNAs passively aggregate into PBs is far too simple.

In addition, we could show that PBs are stably linked to the ER. Together with our microarry data, this indicates that the yeast ER serves an important platform for post-transcriptional gene regulation.

Chapter 7

Appendix

Table 7.1: List of genes with an average $MAS_{mutant}/MAS_{wild\text{-}type}$ coefficient below 0.8, indicating that the mRNA is depleted from the ER in *arf1-11*.

Synonyms	Gene Symbol	MAS_{mutant}/MAS_{wt}				Description
		Exp I	Exp II	Exp III	average	
YGR174W-A		0.570	0.339	0.663	**0.524**	Protein of unknown function
YGL188C-A		0.840	0.159	0.703	**0.568**	Protein of unknown function
YJR150C	**DAN1**	0.444	0.502	0.761	**0.569**	Cell wall mannoprotein induced during anaerobic growth, member of the seripauperin (PAU) family
YOL140W	ARG8	0.612	0.487	0.636	**0.578**	Arginine requiring 8, an acetylornithine aminotransferase in ornithine and arginine biosynthesis
YOL131W		0.486	0.639	0.655	**0.593**	Protein of unknown function
YPR156C	TPO3	0.736	0.200	0.843	**0.593**	Transporter of polyamines 3, a spermine transporter
YIL073C	SPO22	0.705	0.506	0.582	**0.598**	Sporulation 22, a tetratricopeptide repeat protein required for meiotic crossover/chiasma formation
YPL279C		0.810	0.257	0.775	**0.614**	Member of the CrcB-like family, which may be integral membrane proteins involved in chromatin condensation
YOL156W	HXT11	0.788	0.175	0.880	**0.614**	Low-affinity glucose permease, member of the hexose transporter family of the major facilitator superfamily
YBL049W	**MOH1**	0.698	0.442	0.704	**0.615**	Member of the yippee putative zinc-binding protein family
YPR194C	**OPT2**	0.800	0.422	0.628	**0.617**	Oligopeptide transporter, member of the oligopeptide transporter (OPT) family of membrane transporters
YMR011W	**HXT2**	0.837	0.448	0.595	**0.627**	High-affinity hexose transporter, member of the hexose transport family of the major facilitator superfamily
YKL061W		0.940	0.320	0.673	**0.644**	Protein of unknown function
YGR174W-A		0.640	0.554	0.758	**0.651**	Protein of unknown function
YLR307W	**CDA1**	0.809	0.484	0.691	**0.661**	Chitin deacetylase, responsible along with Cda2p for the synthesis of chitosan for the ascospore wall
YEL057C		0.853	0.442	0.700	**0.665**	Protein of unknown function
YDL184C	RPL41A	0.825	0.398	0.785	**0.669**	Ribosomal protein L41A, identical to Rpl41Bp
YLR054C	OSW2	0.716	0.712	0.593	**0.673**	Protein of unknown function
YLR107W	REX3	0.837	0.446	0.776	**0.686**	Member of the exonuclease family, similarity to *C. elegans* PQE-1, which protects neurons from polyQ neurotoxicity
YAL064W		0.777	0.442	0.844	**0.688**	Protein of unknown function
YDR003W-A		1.041	0.261	0.762	**0.688**	Protein of unknown function
YPR200C	ARR2	0.775	0.451	0.838	**0.688**	Arsenate reductase required for resistance to arsenic
YAR071W	PHO11	0.920	0.479	0.665	**0.688**	Acid phosphatase, secreted, nearly identical to Pho12p; subtelomerically encoded
YOR108W	LEU9	0.865	0.531	0.671	**0.689**	Alpha-isopropylmalate synthase II
YMR181C		0.642	0.742	0.688	**0.691**	Protein of unknown function
YGL183C	MND1	0.571	0.997	0.515	**0.694**	Meiotic nuclear divisions 1, required in meiosis
YIL159W	BNR1	1.033	0.210	0.842	**0.695**	Bni1 related 1, a protein involved in actin (Act1p) filament assembly and polarized cell growth
YCR108C		0.737	0.532	0.825	**0.698**	Protein of unknown function
YCR014C	POL4	0.890	0.520	0.711	**0.707**	Polymerase 4, a DNA polymerase that functions in double-strand break repair via nonhomologous end-joining
YBR233W-A	DAD3	0.849	0.554	0.723	**0.708**	Duo1p and Dam1p interacting 3 an essential protein localized to kinetochore, component of the DASH complex
YDL246C	SOR2	0.841	0.506	0.778	**0.708**	Protein almost identical to Sor1p sorbitol dehydrogenase
YBL101W-C		0.837	0.515	0.774	**0.709**	Protein of unknown function
YIL029C		0.931	0.268	0.932	**0.710**	Protein of unknown function
YJL054W	TIM54	0.900	0.545	0.686	**0.710**	Mitochondrial inner membrane protein involved in import of mitochondrial inner membrane proteins

Synonyms	Gene Symbol	MAS_{mutant}/MAS_{wt}				Description
		Exp I	Exp II	Exp III	average	
YKL195W	MIA40	0.886	0.471	0.779	**0.712**	Mitochondrial IMS import and assembly 40, an essential mitochondrial protein
YAL067W-A		0.787	0.712	0.637	**0.712**	Protein of unknown function
YPL063W	TIM50	0.800	0.716	0.623	**0.713**	Essential integral membrane protein that functions as part of the mitochondrial translocase complex
YLR447C	VMA6	0.820	0.505	0.814	**0.713**	Vacuolar membrane ATPase 6, , plays a role in vacuolar fusion
YPL146C	NOP53	0.762	0.467	0.910	**0.713**	Nucleolar protein 53, involved in 60S ribosomal subunit biogenesis, specifically rRNA processing
YKL068W-A		0.737	0.553	0.850	**0.713**	Protein of unknown function
YDR532C		0.881	0.397	0.863	**0.714**	Protein of the spindle pole body, forms a complex with Spc105p
YPL154C	**PEP4**	0.817	0.651	0.678	**0.715**	Carboxypeptidase Y-deficient 4, saccharopepsin that is required for activation of various degradative enzymes
YDR259C	YAP6	0.880	0.501	0.767	**0.716**	Transcription factor of the basic leucine zipper (bZIP) family, involved in salt tolerance
YDR297W	SUR2	0.911	0.499	0.743	**0.718**	Hydroxylase involved in sphingolipid metabolism
YML108W		0.962	0.309	0.883	**0.718**	Protein of unknown function
YKL138C-A	HSK3	1.035	0.339	0.783	**0.719**	Helper of Ask1p 3, component of the DASH or Dam1p complex, required for DASH complex integrity
YCR020W-B	HTL1	1.142	0.157	0.860	**0.720**	Protein involved with the RSC complex in regulating the G2/M transition of the cell cycle
YDR116C	MRPL1	0.772	0.651	0.740	**0.721**	Protein of the mitochondrial large ribosomal subunit, has similarity to prokaryotic ribosomal protein L1
YPR186C	PZF1	0.782	0.576	0.804	**0.721**	RNA polymerase III transcription initiation factor TFIIIA, has nine C2H2-type zinc fingers
YMR174C	PAI3	0.890	0.553	0.722	**0.721**	Protein of unknown function
YML003W		0.880	0.414	0.874	**0.723**	Protein of unknown function
YDR471W	RPL27B	0.902	0.535	0.733	**0.723**	Ribosomal protein L27, identical to Rpl27Ap
YMR195W	ICY1	0.918	0.572	0.681	**0.723**	Protein of unknown function
YBL003C	HTA2	1.076	0.448	0.648	**0.724**	Histone h two A 2, a chromatin binding protein that functions in chromatin related events
YOR390W		0.967	0.474	0.736	**0.725**	Member of the CrcB-like family, which may be integral membrane proteins involved in chromatin condensation
YDL010W	GRX6	0.736	0.750	0.690	**0.725**	Glutaredoxin 6, exhibits glutaredoxin transhydrogenase assay with glutathione and bis-(2-hydroxyethyl)-disulfide
YNL121C	TOM70	0.817	0.679	0.687	**0.728**	Mitochondrial specialized import receptor of the outer membrane, has tetratricopeptide (TPR) repeats
YGL194C	HOS2	0.767	0.625	0.792	**0.728**	HDA one similarity 2, component of Set3p complex that has histone deacetylase activity
YKL106C-A		0.696	0.784	0.705	**0.728**	Protein of unknown function
YDR399W	HPT1	0.834	0.528	0.824	**0.729**	Hypoxanthine-guanine phosphoribosyl transferase 1
YLR312W-A	MRPL15	0.847	0.568	0.772	**0.729**	Mitochondrial ribosomal protein L15, a component of the mitochondrial large ribosomal subunit
YER002W	NOP16	0.852	0.591	0.745	**0.729**	Protein involved in ribosome biogenesis, associated with nuclear pore complex, localizes to nucleus and nucleolus
YNL146C-A		0.976	0.432	0.782	**0.730**	Protein of unknown function
YFR039C		0.945	0.522	0.724	**0.730**	Protein of unknown function
YOR152C		0.754	0.670	0.768	**0.731**	Protein of unknown function
YPL027W	SMA1	0.699	0.665	0.829	**0.731**	Spore membrane assembly 1, binds phospholipase D (Spo14) and is required for prospore membrane formation
YJR122W	CAF17	0.921	0.574	0.699	**0.731**	Iron-sulfur cluster assembly factor for biotin synthase- and aconitase-like mitochondrial proteins
YGR169C-A		0.953	0.445	0.796	**0.731**	Protein of unknown function
YPR120C	CLB5	0.781	0.670	0.744	**0.732**	Cyclin B5, a B-type cyclin that associates with Kar9p, appears late in the G1 phase of the cell cycle

Synonyms	Gene Symbol	MAS_{mutant}/MAS_{wt}				Description
		Exp I	Exp II	Exp III	average	
YDL237W		0.908	0.642	0.646	**0.732**	Protein of unknown function that binds phosphoinositol 3-phosphate in vitro
YDR194C	MSS116	0.745	0.693	0.761	**0.733**	Mitochondrial splicing suppressor 116, an RNA helicase of the DEAD box family
YOR389W		0.928	0.502	0.777	**0.735**	Protein of unknown function
YHR136C	SPL2	0.895	0.552	0.763	**0.737**	Putative inhibitor of Pho80p-Pho85p cyclin-dependent protein kinase
YER188C-A		0.705	0.752	0.753	**0.737**	Member of the DUF468 protein of unknown function family
YKR094C	RPL40B	0.932	0.496	0.786	**0.738**	Fusion protein comprised of ubiquitin (N-terminal half) and ribosomal protein L40
YBR042C		0.870	0.624	0.721	**0.738**	Member of the phospholipid and glycerol acyltransferase family, which function in phospholipid biosynthesis
YJL183W	MNN11	0.896	0.641	0.680	**0.739**	Mannosyltransferase 11, a subunit of the Anp1p-Hoc1p-Mnn10-Mnn11p-Mnn9p mannosyltransferase complex
YOR293W	RPS10A	0.985	0.494	0.739	**0.739**	Ribosomal protein S10, nearly identical to Rps10Bp
YEL026W	SNU13	0.874	0.618	0.725	**0.739**	snRNP of 13 kDa, a component of the U4/U6.U5 snRNP, a component of the 80S U3 snoRNA complex
YIL070C	MAM33	0.852	0.591	0.775	**0.739**	Mitochondrial protein required for normal respiratory growth
YIL161W		0.886	0.601	0.733	**0.740**	Protein of unknown function
YIL071C	PCI8	0.992	0.294	0.934	**0.740**	Protein that binds to Prt1p and Rpg1p subunits of eIF3, may have regulatory role in transcription or translation
YMR024W	MRPL3	0.895	0.576	0.750	**0.740**	Mitochondrial ribosomal protein of the large subunit (YmL3)
YOL159C-A		0.971	0.460	0.790	**0.741**	Protein of unknown function
YGL136C	MRM2	0.876	0.573	0.773	**0.741**	Methyltransferase that methylates mitochondrial 21S rRNA
YLR377C	FBP1	0.643	1.025	0.555	**0.741**	Fructose-1,6-bisphosphatase 1, gluconeogenic enzyme, activity is inhibited by phosphorylation
YNL190W		0.755	0.687	0.782	**0.741**	Putative GPI-anchored protein that may be involved in cell wall maintenance, induced under hyperosmotic stress
YBL040C	ERD2	1.005	0.502	0.717	**0.742**	Endoplasmic reticulum defective 2, protein required for receptor-mediated retrieval of luminal ER proteins
YIL002W-A		1.010	0.435	0.782	**0.742**	Protein of unknown function
YPL171C	OYE3	0.708	0.703	0.815	**0.742**	NADPH dehydrogenase (old yellow enzyme), isoform 3
YBR167C	POP7	0.990	0.464	0.775	**0.743**	Protein subunit of both RNase P and RNAse MRP, which are needed for tRNA processing and 5.8S rRNA processing
YIL121W	QDR2	0.778	0.830	0.625	**0.745**	Quinidine resistance 2, a protein that confers increased resistance to the cisplatin and bleomycin
YPL148C	PPT2	0.814	0.600	0.823	**0.746**	Acyl carrier-protein synthase, phosphopantetheine protein transferase for Acp1p
YBR162C	TOS1	0.990	0.510	0.738	**0.746**	Protein weakly associated with the cell wall, has similarity to Aga1p
YER073W	ALD5	0.804	0.644	0.793	**0.747**	Mitochondrial aldehyde dehydrogenase
YJL171C		0.851	0.598	0.792	**0.747**	Putative GPI-protein with an GPI-attachment site at the C terminus
YJL034W	KAR2	0.839	0.673	0.731	**0.748**	Karyogamy 2, heat shock protein of the ER lumen; required for protein translocation across the ER membrane
YKL099C	UTP11	0.832	0.611	0.802	**0.748**	U3 protein 11, a component of the 80S U3 snoRNA complex that is required for 18S rRNA biosynthesis
YPL163C	SVS1	0.851	0.682	0.712	**0.748**	Serine- and threonine-rich protein required for vanadate resistance
YMR305C	SCW10	0.885	0.626	0.737	**0.749**	Putative glucanase or transglucosidase, involved in cell wall integrity
YGR153W		0.836	0.585	0.828	**0.750**	Protein of unknown function
YNL133C	FYV6	0.865	0.597	0.788	**0.750**	Protein required for viability following exposure to toxin
YMR260C	TIF11	0.996	0.490	0.764	**0.750**	Translation initiation factor 1 subunit 1 (eukaryotic translation initiation factor 1A)
YPL216W		0.823	0.546	0.882	**0.750**	Member of the DDT domain family, which may bind DNA,

Synonyms	Gene Symbol	MAS_{mutant}/MAS_{wt}				Description
		Exp I	Exp II	Exp III	average	
YKL006C-A	SFT1	0.969	0.454	0.828	**0.750**	V-SNARE-like protein required for vesicle traffic between Golgi compartments
YGR072W	UPF3	1.028	0.459	0.766	**0.751**	Up frameshift 3, a protein involved with Nam7p and Nmd2p in decay of mRNA containing nonsense codons
YCR075C	ERS1	0.864	0.736	0.654	**0.751**	Suppressor of erd1 mutation
YCL048W	SPS22	0.913	0.389	0.951	**0.751**	Protein with similarity to Ecm33p and Sps2p; Cell wall organization and biogenesis; PM
YDR083W	RRP8	0.932	0.482	0.841	**0.752**	Protein involved in cleavage at site A2 in pre-rRNA in the pathway of ribosomal RNA processing
YEL075C		0.915	0.547	0.794	**0.752**	Protein of unknown function, has very strong similarity to an ATP-dependent helicase
YKL172W	EBP2	0.791	0.580	0.886	**0.752**	Epstein-Barr nuclear antigen 1 binding protein 2, involved in pre-rRNA processing and ribosomal subunit assembly
YER131W	RPS26B	0.890	0.631	0.739	**0.753**	Ribosomal protein of the small subunit 26B, nearly identical to Rps26Ap
YBL028C		1.064	0.518	0.680	**0.754**	Protein of unknown function
YLR073C		0.695	0.834	0.733	**0.754**	Protein involved in the regulation of protein deubiquitination
YLR051C		0.889	0.528	0.846	**0.754**	Faf1p co-purifying factor 2, plays a role in the maturation of 18S rRNA from 35S pre-rRNA
YHR044C	DOG1	0.858	0.651	0.754	**0.754**	2-Deoxyglucose-6-phosphate phosphatase
YDL121C		1.100	0.505	0.658	**0.754**	Protein of unknown function that associates with the nuclear pore complex
YPR082C	DIB1	0.882	0.602	0.780	**0.755**	Component of the U4/U6.U5 snRNP, also required for mitotic spindle formation or function
YDR196C		0.922	0.570	0.772	**0.755**	Member of the dephospho-CoA kinase family
YDR245W	MNN10	0.894	0.656	0.716	**0.755**	Mannosyltransferase 10, subunit of the Anp1p-Hoc1p-Mnn10p-Mnn11p-Mnn9p mannosyltransferase complex
YOL164W-A		0.813	0.603	0.849	**0.755**	Protein of unknown function
YOL108C	INO4	0.859	0.605	0.802	**0.755**	Inositol requiring 4, a basic helix-loop-helix transcription factor involved in activation of phospholipid synthetic genes
YDL066W	IDP1	0.809	0.799	0.658	**0.755**	Isocitrate dehydrogenase (NADP+), mitochondrial
YDL198C	GGC1	0.865	0.617	0.785	**0.756**	GTP/GDP carrier in mitochondria, involved in mitochondrial iron homeostasis
YMR158C-A		0.961	0.328	0.978	**0.756**	Protein of unknown function
YKR053C	YSR3	0.893	0.884	0.491	**0.756**	Sphingoid base-phosphate phosphatase, putative regulator of sphingolipid metabolism and stress response
YCL031C	RRP7	0.838	0.541	0.889	**0.756**	Protein involved in pre-rRNA processing and ribosome assembly
YIL004C	BET1	0.756	0.625	0.887	**0.756**	Blocked early in transport 1, v-SNARE protein essential for ER to Golgi transport
YGR023W	MTL1	0.786	0.750	0.733	**0.756**	Protein that acts with Mid2p in signal transduction of cell wall stress during pheromone-induced morphogenesis
YDR070C		0.786	0.692	0.791	**0.757**	Protein possibly required for full induction of IME1 during early meiosis
YLR162W-A		0.806	0.872	0.594	**0.758**	Protein of unknown function
YNL177C	MRPL22	0.871	0.583	0.821	**0.758**	Mitochondrial ribosomal protein L22, a component of the mitochondrial large 39S ribosomal subunit
YER058W	PET117	0.885	0.674	0.718	**0.759**	Protein involved in assembly of cytochrome oxidase
YGR204C-A		1.013	0.529	0.736	**0.759**	Protein of unknown function
YDR182W-A		0.913	0.570	0.794	**0.759**	Protein of unknown function
YNL122C		1.076	0.410	0.791	**0.759**	Protein of unknown function
YHR010W	RPL27A	0.929	0.586	0.763	**0.759**	Ribosomal protein L27, identical to Rpl27Bp
YPR143W	RRP15	0.914	0.549	0.815	**0.759**	Member of the DUF1665 domain of unknown function family
YBR182C-A		0.924	0.673	0.681	**0.760**	Protein of unknown function

Synonyms	Gene Symbol	MAS_{mutant}/MAS_{wt}				Description
		Exp I	Exp II	Exp III	average	
YAL063C-A		1.075	0.361	0.843	**0.760**	Protein of unknown function
YJR067C	YAE1	0.999	0.470	0.810	**0.760**	Essential protein of unknown molecular function
YMR232W	FUS2	0.789	0.708	0.784	**0.760**	Cell fusion 2, protein required for cell fusion during mating, localizes to dots beneath the tip of mating projection
YMR194C-B		0.928	0.651	0.703	**0.760**	Protein of unknown function
YPL189W	GUP2	0.888	0.769	0.627	**0.761**	Putative glycerol transporter involved in active glycerol uptake
YGR272C		1.073	0.384	0.827	**0.761**	Protein of unknown function
YOR031W	CRS5	0.821	0.790	0.673	**0.762**	Metallothionein-like protein that binds Cu+, Cd2+, and Zn2+, provides copper and zinc resistance
YMR230W	RPS10B	1.096	0.378	0.813	**0.762**	Ribosomal protein S10, nearly identical to Rps10Ap
YNL005C	MRP7	0.818	0.684	0.785	**0.762**	Mitochondrial ribosomal protein of the large subunit (YmL2)
YNR024W		0.830	0.731	0.726	**0.762**	RNA binding protein involved in surveillance of pre-rRNA and pre-mRNA and degradation of non-coding RNAs
YCL002C		0.983	0.465	0.839	**0.762**	Protein of unknown function
YFR001W	LOC1	0.959	0.574	0.755	**0.763**	Localization of mRNA 1, binds double-stranded RNA, involved in localization of mRNA
YCL043C	PDI1	0.898	0.638	0.753	**0.763**	Protein disulfide isomerase 1, an enzyme that is localized to the ER and functions in protein folding
YGR271C-A		1.148	0.345	0.797	**0.763**	Protein of unknown function
YML019W	OST6	1.012	0.597	0.681	**0.763**	Oligosaccharyltransferase 6, member of a complex of ER proteins that transfers the core oligosaccharide
YIR032C	DAL3	0.668	0.980	0.642	**0.764**	Ureidoglycolate hydrolase; involved in utilization of purines as nitrogen sources
YJR016C	ILV3	0.795	0.758	0.741	**0.765**	Dihydroxyacid dehydratase (DAD), third step in valine and isoleucine biosynthesis pathway
YML081C-A	ATP18	0.922	0.558	0.814	**0.765**	Subunit i, or j, of the F0 subunit of ATP synthase-mitochondrial respiratory complex V
YDR073W	SNF11	0.857	0.667	0.774	**0.766**	Component of SWI-SNF global transcription activator complex, acts to assist gene-specific activators
YNR062C		0.820	0.737	0.741	**0.766**	Protein of unknown function
YOR193W	PEX27	0.838	0.627	0.835	**0.767**	Protein involved in regulating peroxisome size and number
YDR302W	GPI11	0.970	0.569	0.762	**0.767**	Protein involved in glycosylphosphatidylinositol (GPI) biosynthesis
YBR228W	SLX1	0.943	0.558	0.802	**0.768**	Synthetic lethal of unknown (X) function 1, functions in a complex with Slx4p as a 5' flap endonuclease
YGR035C		0.842	0.668	0.798	**0.770**	Probably plays a role in drug resistance
YPR192W	AQY1	0.591	0.961	0.758	**0.770**	Spore-specific aquaporin water channel protein, plays a role in spore fitness
YDL048C	STP4	0.845	0.716	0.750	**0.770**	Protein containing a zinc finger C2H2 type repeat, which bind nucleic acids
YER137C		0.784	0.700	0.827	**0.770**	Protein of unknown function
YLR009W	RLP24	0.834	0.644	0.836	**0.771**	member of the ribosomal L24e family, which are part of the large ribosomal subunit
YDR492W	IZH1	0.882	0.533	0.908	**0.774**	Protein that may be involved in zinc homeostasis
YJL046W		0.869	0.660	0.796	**0.775**	Protein containing a biotin or lipoate A or B protein ligase family domain
YMR194W	RPL36A	0.940	0.509	0.876	**0.775**	Ribosomal protein L36, nearly identical to Rpl36Bp
YBL002W	HTB2	0.950	0.597	0.779	**0.775**	Histone h two B 2, a chromatin binding protein that functions in chromatin related events
YOR159C	SME1	1.036	0.494	0.797	**0.776**	Spliceosomal snRNA-associated Sm core protein required for mRNA splicing
YEL029C	BUD16	0.900	0.574	0.854	**0.776**	Protein involved in budding, encodes pyridoxal kinase, synthesizes the biologically active form of vitamin B6
YBL095W		0.868	0.695	0.766	**0.776**	Protein of unknown function

Synonyms	Gene Symbol	MAS_{mutant}/MAS_{wt}				Description
		Exp I	Exp II	Exp III	average	
YDR068W	DOS2	0.844	0.629	0.858	**0.777**	Protein containing a BSD domain
YLR221C	RSA3	0.885	0.664	0.783	**0.778**	Nucleolar protein required for 60S ribosomal subunit biogenesis
YNL252C	MRPL17	0.927	0.631	0.776	**0.778**	Mitochondrial ribosomal protein of the large subunit (YmL30; YmL17)
YJL038C		0.999	0.660	0.675	**0.778**	Protein of unknown function
YDR043C	NRG1	0.838	0.657	0.839	**0.778**	Negative regulatory of glucose-controlled genes 1, a transcriptional repressor involved in glucose repression
YGL147C	RPL9A	0.920	0.557	0.857	**0.778**	Ribosomal protein of the large subunit 9A, a component of the ribosomal large subunit
YHR054C	RSC30	1.285	0.242	0.808	**0.778**	Component of the abundant RSC chromatin remodeling complex
YKL009W	MRT4	0.842	0.622	0.872	**0.778**	Protein involved in mRNA turnover
YBR221W-A		0.906	0.653	0.777	**0.779**	Protein of unknown function
YLR406C	RPL31B	0.933	0.545	0.858	**0.779**	Ribosomal protein L31, nearly identical to Rpl31Ap
YJL190C	RPS22A	0.995	0.566	0.776	**0.779**	Ribosomal protein S22 , nearly identical to Rps22Bp
YIL172C	FSP2	0.901	0.631	0.806	**0.779**	Protein with strong similarity to S. cerevisiae Ygr287p, which is an alpha glucosidase
YOR257W	CDC31	0.952	0.535	0.852	**0.779**	Centrin, calmodulin-like calcium-binding protein of spindle pole body
YCR107W	AAD3	1.033	0.383	0.923	**0.780**	Putative aryl alcohol dehydrogenase
YLR020C	YEH2	0.984	0.599	0.756	**0.780**	Steryl ester hydrolase of the plasma membrane
YLR344W	RPL26A	0.865	0.736	0.738	**0.780**	Ribosomal protein L26, nearly identical to Rpl26Bp
YBR152W	SPP381	0.962	0.670	0.707	**0.780**	Protein required for efficient pre-mRNA splicing, component of the U4/U6.U5 tri-snRNP complex
YNL151C	RPC31	0.841	0.699	0.800	**0.780**	RNA polymerase C 31, RNA polymerase III, small subunit, essential subunit, not shared
YLR275W	SMD2	0.993	0.465	0.883	**0.780**	Spliceosomal snRNA-associated Sm core protein
YJL058C	BIT61	0.994	0.445	0.903	**0.781**	Protein of unknown function
YLR456W		1.110	0.483	0.750	**0.781**	plays a role in determining cellular response to gliotoxin, a fungal metabolite with immunosuppressive properties
YKR030W	GMH1	1.013	0.506	0.826	**0.781**	Member of the UNC-50 family
YGR201C		0.883	0.679	0.784	**0.782**	Protein with similarity to translation elongation factors
YOR287C		0.783	0.798	0.765	**0.782**	Member of the DUF947 domain of unknown function family
YDR357C		1.107	0.394	0.845	**0.782**	Protein of unknown function
YBR003W	COQ1	0.890	0.645	0.811	**0.782**	Coenzyme Q 1, a hexaprenyl pyrophosphate synthetase that catalyzes the first step in coenzyme Q biosynthesis
YPL274W	SAM3	0.937	0.656	0.754	**0.782**	S-adenosylmethionine permease 3, a high affinity S-adenosylmethionine permease
YDR082W	STN1	0.981	0.503	0.864	**0.783**	Protein involved in telomere size regulation and in protecting telomeres from homologous recombination
YMR294W	JNM1	0.789	0.692	0.868	**0.783**	Just nuclear migration 1, a constituent of the dynactin complex
YCL056C		0.828	0.632	0.889	**0.783**	Protein of unknown function
YJR055W	HIT1	0.887	0.669	0.793	**0.783**	Protein required for growth at high temperature
YHR081W	LRP1	0.951	0.514	0.885	**0.783**	Like an rRNA processing protein 1, an exosome-associated protein required for 3' processing
YEL003W	GIM4	1.065	0.402	0.884	**0.783**	Gene involved in microtubule biogenesis 4 (prefoldin subunit 2)
YIL134C-A		0.842	0.619	0.892	**0.784**	Protein of unknown function
YDR345C	HXT3	0.875	0.680	0.798	**0.784**	Low-affinity hexose transporter

Synonyms	Gene Symbol	MAS_{mutant}/MAS_{wt}				Description
		Exp I	Exp II	Exp III	average	
YBR089C-A	NHP6B	0.998	0.535	0.821	**0.785**	Non-histone protein 6B, a protein with DNA-binding and DNA-bending activity
YAL025C	MAK16	0.980	0.517	0.858	**0.785**	Maintenance of killer 16, required for propagation of M1 double-stranded RNA (dsRNA) virus
YOL104C	NDJ1	1.020	0.558	0.776	**0.785**	Nondisjunction 1, a telomeric DNA binding protein
YDR441C	APT2	0.810	0.660	0.885	**0.785**	Adenine phosphoribosyltransferase (APRT)
YDR169C-A		0.880	0.524	0.952	**0.785**	Protein of unknown function
YMR271C	URA10	0.977	0.621	0.757	**0.785**	Orotate phosphoribosyltransferase 2, fifth step in pyrimidine biosynthesis pathway
YJR086W	STE18	1.033	0.520	0.803	**0.785**	Gamma subunit of the guanine nucleotide-binding protein that mediates signal transduction during mating
YKL154W	SRP102	0.808	0.847	0.701	**0.785**	Signal recognition particle receptor beta subunit
YAR033W	MST28	1.312	0.125	0.919	**0.785**	Protein that binds COPI and COPII complexes, suppresses some coatomer mutants
YJL186W	MNN5	0.949	0.690	0.719	**0.786**	Mannosyltransferase required for forming and extending the mannose branches of the outer chain mannans
YAL034W-A	MTW1	0.873	0.710	0.775	**0.786**	Essential kinetochore protein involved in mitosis
YPL047W	SGF11	0.852	0.681	0.826	**0.786**	Component of the SAGA histone acetyltransferase complex and SLIK (SAGA-like) complex
YLR288C	MEC3	0.865	0.615	0.880	**0.787**	Mitosis entry checkpoint 3, component of the checkpoint clamp complex
YDR412W		1.007	0.506	0.848	**0.787**	Protein that purifies with the nuclear pore complex
YBL003C	HTA2	0.925	0.642	0.793	**0.787**	Histone h two A 2, a chromatin binding protein that functions in chromatin related events
YOL027C	MDM38	0.726	0.896	0.740	**0.787**	Mitochondrial distribution and morphology 38, mediates K+ and H+ transport across the mitochondrial membrane
YHR143W-A	RPC10	1.024	0.502	0.836	**0.787**	RNA polymerase C subunit 10, shared subunit of RNA polymerases I, II, and III
YPL192C	PRM3	0.845	0.626	0.890	**0.787**	Nuclear membrane protein involved in karyogamy
YDR166C	SEC5	0.933	0.620	0.808	**0.787**	Component of exocyst complex, 107 kDa, required for exocytosis
YJL200C		1.077	0.518	0.770	**0.788**	Protein with similarity to aconitase, has potential mitochondrial transit peptide
YNL231C	PDR16	0.836	0.623	0.907	**0.788**	Phosphatidylinositol transfer protein, involved in regulation of phospholipase D
YHR038W	RRF1	0.816	0.741	0.809	**0.788**	Mitochondrial ribosome recycling factor
YNR057C	BIO4	0.817	0.794	0.755	**0.789**	Dethiobiotin synthase, component of the biotin biosynthesis pathway
YPR020W	ATP20	0.993	0.471	0.903	**0.789**	Subunit g of the F0 subunit of ATP synthase-mitochondrial respiratory complex V
YML052W	SUR7	0.862	0.759	0.746	**0.789**	Suppressor of rvs167 mutation, a component of eisosomes, which are sites of endocytosis
YKL041W	VPS24	0.871	0.751	0.748	**0.790**	Vacuolar protein sorting 24 homolog, binds to phosphoinositide, plays a role in protein targeting
YDL114W		0.554	0.937	0.878	**0.790**	Protein containing a short chain dehydrogenase domain
YER053C-A		1.180	0.426	0.764	**0.790**	Protein possibly involved in tolerance of high salt, osmotic stress, and low temperature conditions
YDL069C	CBS1	0.902	0.546	0.922	**0.790**	Translational activator of COB mRNA
YPR036W-A		0.887	0.625	0.859	**0.790**	Protein of unknown function
YOR087W	YVC1	1.032	0.597	0.743	**0.791**	Inward-rectifying voltage-gated calcium-activated vacuolar ion channel
YBR004C	GPI18	0.858	0.610	0.904	**0.791**	Functional homolog of human PIGV (alpha-1,6-mannosyltransferase)
YPR017C	DSS4	0.860	0.746	0.766	**0.791**	Guanine-nucleotide exchange factor for Sec4p
YML115C	VAN1	0.926	0.770	0.676	**0.791**	Vanadate resistance protein, component of mannan polymerase M-Pol I
YPL064C	CWC27	0.796	0.746	0.831	**0.791**	Protein possibly involved in pre-mRNA splicing

Synonyms	Gene Symbol	MAS_{mutant}/MAS_{wt}				Description
		Exp I	Exp II	Exp III	average	
YER030W		1.013	0.547	0.813	**0.791**	Chaperone for Htz1p - histone H2B 1, a histone-binding protein
YOL018C	TLG2	0.934	0.775	0.665	**0.791**	T-SNARE affecting a late Golgi compartment 2, involved in endocytosis and maintenance of proteins in the TGN
YPR159C-A		1.243	0.397	0.736	**0.792**	Protein of unknown function
YCR096C	HMRA2	1.015	0.566	0.795	**0.792**	Regulatory protein A2p (no known function); sequence is the same as the last 119 residues of Alpha2p
YGR129W	SYF2	0.815	0.825	0.737	**0.792**	Protein with possible involvement in pre-mRNA splicing
YDL153C	SAS10	0.891	0.645	0.841	**0.793**	Something about silencing 10, a protein that derepresses HMR, HML and telomeres
YNL192W	CHS1	0.888	0.535	0.955	**0.793**	Chitin synthase I, has a repair function during cell separation
YLR068W	FYV7	0.858	0.767	0.753	**0.793**	Protein of unknown function
YDR460W	TFB3	0.854	0.678	0.845	**0.793**	Component of RNA polymerase II transcription initiation TFIIH (factor b), 38 kDa subunit
YDR261C-D	EXG2	1.171	0.302	0.905	**0.793**	Exo-beta-1,3-glucanase (beta-1,3-D-glucanglucanohydrolase), minor isoform
YGR236C	SPG1	0.777	0.779	0.824	**0.793**	Stationary phase gene 1, a mitochondrial protein that interacts with Cdc7p during mitosis
YNL149C		1.049	0.592	0.739	**0.793**	Member of the DUF1531 domain of unknown function family
YOR304C-A		0.945	0.660	0.776	**0.794**	Protein of unknown function
YGL225W	VRG4	1.045	0.590	0.746	**0.794**	Golgi GDP-mannose transporter, member of the nucleotide-sugar transporter (NST) family
YHR052W	CIC1	0.960	0.589	0.833	**0.794**	Core interacting component 1, associated with the 26S proteasome
YBR010W	HHT1	0.952	0.679	0.751	**0.794**	Histone H3, identical to Hht2p
YBR040W	FIG1	0.971	0.543	0.869	**0.794**	Factor-induced gene 1, a protein regulating the low affinity Ca2+ influx system activated during the mating respons
YDL045W-A	MRP10	0.955	0.662	0.768	**0.795**	Mitochondrial ribosomal protein 10
YER056C-A	RPL34A	0.917	0.677	0.792	**0.795**	Ribosomal protein L34, nearly identical to Rpl34Bp
YKL219W	COS9	0.992	0.680	0.713	**0.795**	Member of the duplication (DUP) family
YCR044C	PER1	0.892	0.866	0.629	**0.795**	Protein required for Phospholipase A2 activity involved in modification of GPI anchors
YMR061W	RNA14	0.965	0.386	1.036	**0.796**	Pre-mRNA processing 14, a component of pre-mRNA cleavage and polyadenylation factor I
YDR500C	RPL37B	0.930	0.791	0.666	**0.796**	Ribosomal protein L37, nearly identical to Rpl37Ap
YIL051C	MMF1	0.911	0.751	0.725	**0.796**	Maintenance of mitochondrial function 1, plays a role in maintenance of mitochondrial DNA
YOR224C	RPB8	0.850	0.740	0.799	**0.796**	RNA polymerase B subunit 8, shared subunit of RNA polymerases I, II, and III
YGR286C	BIO2	0.790	0.810	0.788	**0.796**	Biotin synthetase, catalyzes the last step of the biotin synthesis pathway
YPL244C	HUT1	0.951	0.685	0.754	**0.796**	Protein involved in native disulfide bond formation in endoplasmic reticulum
YNL080C		0.943	0.674	0.773	**0.797**	Protein of the endoplasmic reticulum membrane that may be involved in protein N-glycosylation
YDR225W	HTA1	0.948	0.608	0.834	**0.797**	Histone h two A 1, a chromatin binding protein that functions in chromatin related events
YIL133C	RPL16A	0.893	0.690	0.810	**0.797**	Ribosomal protein L16, nearly identical to Rpl16Bp
YDL107W	MSS2	0.957	0.533	0.903	**0.798**	Protein involved in translocation of the Cox2p C-terminal end across the mitochondrial inner membrane
YER048W-A		0.943	0.456	0.995	**0.798**	Mitochondrial maxtrix protein that is required for Fe/S cluster biogenesis and cellular iron homeostasis
YNL110C	NOP15	0.926	0.589	0.879	**0.798**	Protein that functions in cytokinesis and pre-rRNA processing
YBR076W	ECM8	0.864	0.629	0.901	**0.798**	Protein possibly involved in cell wall structure or biosynthesis
YML041C	VPS71	0.992	0.734	0.670	**0.799**	Vacuolar protein sorting 71, component of the complex responsible for deposition of histone variant Htz1p

Synonyms	Gene Symbol	MAS_{mutant}/MAS_{wt}				Description
		Exp I	Exp II	Exp III	average	
YDR458C		1.008	0.644	0.744	**0.799**	Helix-extension-helix fold 2, a protein that localizes to the inner nuclear membrane
YKL046C	DCW1	0.913	0.727	0.759	**0.799**	Glycosylphosphatidylinositol (GPI)-anchored protein involved in cell wall biosynthesis

$MAS_{mutant}/MAS_{wild\text{-}type}$ coefficients for the three independent microarray experiments are given. A short description of the gene function is included (Source: Proteome). **Proteins localized to mitochondria or of unknown function are marked in gray.** **ORFs that were chosen for the initial round of FISH validation are designated in bold.**

Table 7.2: List of genes with an average $MAS_{mutant}/MAS_{wild\text{-}type}$ coefficient above 1.3, indicating that the mRNA is enriched on the ER in *arf1-11*.

Synonyms	Gene Symbol	MAS_{mutant}/MAS_{wt}				Description
		Exp I	Exp II	Exp III	average	
YCR088W	**ABP1**	4.642	1.504	1.215	**2.454**	ABP1
YOR387C		1.264	3.903	1.306	**2.158**	Protein of unknown function; Mitochondrial
YNL195C		2.154	2.650	1.274	**2.026**	Protein of unknown function; Mitochondrial
YPL277C		1.926	2.191	1.873	**1.997**	Protein of unknown function; membrane fraction
YFL068W		2.036	2.555	1.298	**1.963**	Protein that may bind phosphatidylinositol-4,5-bisphosphate; similar to other subtelomerically-encoded proteins
YOR183W	FYV12	1.979	2.704	1.022	**1.901**	Cell wall abnormal; Killer toxin sensitive
YGL156W	**AMS1**	1.976	2.206	1.522	**1.901**	Alpha-mannosidase; vacuole
YLR330W	**CHS5**	2.078	2.306	1.148	**1.844**	CHS5
YLR429W	**CRN1**	1.811	2.241	1.079	**1.710**	CRN1
YMR003W		3.633	0.584	0.895	**1.704**	mitochondrial
YLR307C-A		2.031	1.465	1.545	**1.680**	Protein of unknown function
YPR030W*	**CSR2**	1.408	2.307	1.319	**1.678**	Chs5 Spa2 rescue 2, Ion homeostasis; Cell wall organization and biogenesis; Galactose transport
YJL136W-A		1.166	2.426	1.407	**1.666**	Protein of unknown function
YFL067W		1.185	2.617	1.126	**1.642**	Protein of unknown function
YGR109W-A		1.418	2.435	1.041	**1.631**	Protein of unknown function
YJL051W*		2.418	1.562	0.891	**1.624**	Protein of unknown function
YBR148W	YSW1	1.466	2.311	1.057	**1.611**	Protein of unknown function
YFL010W-A	AUA1	1.598	2.198	0.982	**1.593**	Protein involved in ammonia regulation of Gap1p
YFL014W	HSP12	1.661	1.287	1.823	**1.591**	Heat shock protein of 12 kDa
YGL006W-A		1.723	1.852	1.132	**1.569**	Protein of unknown function
YDR326C		2.887	0.850	0.967	**1.568**	Mitochondrial protein involved in apoptosis induced by reactive oxygen species and intracellular acidification
YJL077C	ICS3	1.088	2.205	1.371	**1.555**	Protein required for normal resistance to copper, has a possible role in signal transduction
YLR190W*	MMR1	2.644	1.086	0.918	**1.549**	Protein that functions as a receptor for Myo2p on mitochondria and mediates mitochondrial transport into the bud
YPL201C		1.381	1.915	1.327	**1.541**	Protein of unknown function
YLL066W-B		0.919	2.805	0.889	**1.537**	Protein of unknown function
YBR208C	DUR1,2	1.520	1.894	1.197	**1.537**	Urea amidolyase, contains urea carboxylase and allophanate hydrolase activities
YLR412C-A		1.709	1.713	1.157	**1.526**	Protein of unknown function

Synonyms	Gene Symbol	MAS_{mutant}/MAS_{wt}				Description
		Exp I	Exp II	Exp III	average	
YOR239W	ABP140	2.586	1.031	0.961	**1.526**	ABP140
YLR353W	BUD8	2.101	1.474	0.987	**1.521**	Budding 8, required for bipolar budding
YDL247W	MPH2 /3	1.320	2.268	0.965	**1.518**	Protein with maltose permease activity, member of hexose transporter family of the major facilitator superfamily
YAR064W		1.408	1.789	1.355	**1.517**	Protein of unknown function
YBR072W	HSP26	1.215	1.748	1.581	**1.515**	Heat shock protein of 26 kDa
YKL185W*	ASH1	2.783	0.889	0.869	**1.514**	Asymmetric synthesis of HO 1, a GATA-type transcription factor that localizes preferentially to daughter cells
YLR142W	PUT1	1.234	2.055	1.247	**1.512**	Mitochondrial Proline oxidase (proline dehydrogenase), first step in synthesis of glutamate from proline
YBR136W	MEC1	1.500	1.784	1.245	**1.510**	Mitosis entry checkpoint 1, a protein kinase that is required for the telomere checkpoint; acts together with Tel1
YIL037C	PRM2	1.572	2.056	0.888	**1.505**	Pheromone Regulated Membrane protein 2, protein with putative functions in karyogamy and mating
YGR110W		1.174	2.241	1.069	**1.495**	Protein of unknown function
YNL034W		1.330	2.132	1.020	**1.494**	Protein of unknown function
YER129W	SAK1	1.827	1.489	1.104	**1.474**	Snf1p-activating kinase 1 (polymerase alpha kinase 1), a protein kinase acting together with Tel1
YJL047C-A		1.948	1.092	1.381	**1.473**	Protein of unknown function
YNL242W	ATG2	1.553	1.825	1.042	**1.473**	Protein involved in cytoplasm to vacuole targeting (Cvt), autophagy, peroxisomal degradation, and sporulation
YPR184W	GDB1	1.427	1.760	1.214	**1.467**	Glycogen debranching enzyme (4-alpha-glucanotransferase or oligo-1, 4 - 1, 4-glucantransferase)
YOL052C-A	DDR2	1.325	1.568	1.489	**1.460**	DNA damage responsive 2, a protein induced by different stresses
YDL085W	NDE2	1.293	2.070	1.001	**1.455**	Mitochondrial NADH dehydrogenase that catalyzes the oxidation of cytosolic NADH
YPR117W		1.523	1.358	1.483	**1.454**	Protein of unknown function
YPR119W*	CLB2	2.529	0.909	0.907	**1.448**	Cyclin B2, a G2/M-phase-specific cyclin that regulates cyclin-dependent protein kinase activity
YBL088C	TEL1	1.194	1.965	1.174	**1.444**	Telomere maintenance 1, a likely phosphatidylinositol 3-kinase ; acti with Mec1p in maintenance of genome stability
YEL076C-A	YRF1-1 7	1.540	1.754	1.022	**1.439**	subtelomeric Y'-helicase
YBL034C	STU1	2.003	1.264	1.038	**1.435**	Suppressor of beta-tubulin mutation that is required for assembly of the mitotic spindle
YKR015C		1.294	0.862	2.149	**1.435**	Protein of unknown function
YDL223C	HBT1	1.290	1.724	1.286	**1.433**	Target of Hub1p ubiquitination, involved in bud site selection and shmoo formation
YHR214C-E		1.648	1.269	1.371	**1.429**	Protein of unknown function
YOL084W	PHM7	1.665	1.676	0.942	**1.428**	Protein transcriptionally regulated by phosphate; vacuole, PM
YLR106C	MDN1	1.537	1.492	1.220	**1.416**	Nuclear protein involved in rRNA processing and nucle+I24ar export of 60S subunits
YPR026W	ATH1	1.686	1.502	1.057	**1.415**	Acid trehalase 1 (vacuolar acid trehalase), a secreted enzyme that converts alpha, alpha-trehalose to glucose
YHR087W		1.478	1.270	1.483	**1.410**	Protein of unknown function
YPR032W	SRO7	1.221	1.917	1.092	**1.410**	Suppressor of rho3 7, functions together with Sec9p in exocytosis downstream of the Rho3p
YAL002W	VPS8	1.477	1.698	1.047	**1.407**	Vacuolar protein sorting 8, component of the CORVET complex involved in endosome-vacuole biogenesis
YDL204W	RTN2	1.224	1.926	1.060	**1.403**	Reticulon 2, a protein that localizes almost exclusively to the peripheral endoplasmic reticulum
YOR161C-C		1.243	1.720	1.244	**1.403**	Protein of unknown function
YGR213C	RTA1	1.116	1.799	1.279	**1.398**	Protein involved in 7-aminocholesterol resistance
YOR383C	FIT3	1.438	1.648	1.102	**1.396**	Facilitator of iron transport 3, may play a role in iron uptake

Synonyms	Gene Symbol	MAS_{mutant}/MAS_{wt}				Description
		Exp I	Exp II	Exp III	average	
YNL277W-A		1.012	1.713	1.462	**1.396**	Protein of unknown function
YER065C	ICL1	1.196	1.863	1.124	**1.395**	Isocitrate lyase, carries out part of the glyoxylate cycle, required for gluconeogenesis
YLR305C	STT4	1.337	1.744	1.086	**1.389**	Staurosporine and temperature sensitivity 4, a phosphatidylinositol 4-kinase that functions in the MAPKKK cascade
YBR097W	VPS15	1.575	1.357	1.230	**1.387**	Vacuolar protein sorting 15, a serine/threonine protein kinase involved in vacuolar protein sorting
YDR129C	SAC6	1.889	1.199	1.066	**1.385**	Suppressor of actin mutations 6, an actin filament bundling protein essential for polarized secretion and endocytosis
YNL279W	PRM1	1.178	2.108	0.868	**1.385**	Protein that is involved in cell fusion and required for efficient mating
YML072C*	TCB3	1.836	1.374	0.939	**1.383**	Tricalbin 3, contains 3 calcium- and phospholipid-binding C2 domains and a transmembrane domain
YLL040C	**VPS13**	1.424	1.577	1.141	**1.381**	Protein involved in vacuolar sorting
YER105C	NUP157	1.567	1.455	1.121	**1.381**	Nuclear pore protein
YAL064C-A		1.472	1.359	1.308	**1.380**	Protein containing a PA14 domain, has strong similarity to a region of flocculin
YHR022C-A		0.843	2.343	0.952	**1.380**	Protein of unknown function
YPL085W	SEC16	1.138	2.024	0.971	**1.378**	Secretory 16, a hydrophilic protein required for autophagy and vesicle formation in ER to Golgi transport
YLR154C-H		1.158	1.544	1.430	**1.377**	Protein of unknown function
YHL028W	WSC4	1.070	2.203	0.834	**1.369**	Protein required for secretory protein translocation, maintenance of cell wall integrity, and stress response
YML083C		1.198	1.857	1.045	**1.367**	Protein of unknown function
YLR422W		1.467	1.532	1.089	**1.363**	Member of the dedicator of cytokinesis family, which may be guanine nucleotide exchange factors
YFR044C		1.349	1.347	1.389	**1.361**	Defective in utilization of glutathione 1, catalyzes the cleavage of the Cys-Gly dipeptide
YLR466C-B		1.184	2.125	0.773	**1.361**	Protein of unknown function
YDR263C	DIN7	1.279	1.778	1.021	**1.359**	Mitochondrial inner membrane nuclease with a role in stabilizing the mitochondrial genome,
YNL214W	PEX17	1.926	1.132	1.014	**1.358**	Peroxin 17, a peroxisomal peripheral membrane protein required for peroxisome biogenesis
YGR229C	SMI1	1.316	1.726	1.025	**1.356**	Suppressor of mar inhibitor 1, a protein that is required for efficient sporulation and functions in chitin metabolism
YGR046W*	TAM41	2.476	0.586	0.998	**1.353**	Translocator assembly and maintenance 41, peripheral membrane protein at the inner mitochondrial membrane
YNL144C		1.491	1.532	1.035	**1.353**	Protein of unknown function; mitochondrial
YGL089C	MFA2	1.060	1.129	1.850	**1.346**	Mating factor alpha 2, a form of the mating pheromone alpha-factor
YDL220C	CDC13	0.879	2.112	1.040	**1.344**	Cell division cycle 13, a telomere-binding protein involved in protection of the telomere
YKL220C	FRE2	1.071	1.880	1.076	**1.342**	Ferric reductase 2, and enzyme that exhibits ferric and cupric reductase activities, subject to regulation by iron
YGR121C	MEP1	1.236	1.675	1.116	**1.342**	Ammonia permease of high capacity and moderate affinity, membrane transporter
YGL184C	STR3	1.006	1.917	1.104	**1.342**	Protein containing a cysteine-methionine metabolism pyridoxal-phosphate-dependent enzyme domain
[YDL137W	ARF2	1.060	1.696	1.270	**1.342**	GTP-binding protein of the arf family involved in assembly of coated vesicles of the secretory system]
YMR280C	CAT8	1.172	1.532	1.319	**1.341**	Transcription factor required for derepression of gluconeogenic enzymes
YHR165C	PRP8	1.305	1.685	1.033	**1.341**	U5 snRNA-associated splicing factor, involved in association of U5 snRNP with U4/U6 snRNP
YCR081W	SRB8	1.394	1.480	1.149	**1.341**	Component of RNA polymerase II holoenzyme and Kornberg's mediator (SRB) subcomplex
YDR436W	PPZ2	1.405	1.571	1.047	**1.341**	Protein serine/threonine phosphatase involved in osmoregulation
YNL262W	POL2	1.352	1.502	1.149	**1.334**	DNA polymerase epsilon large subunit, catalytic subunit essential for DNA replication
YLR024C	UBR2	1.367	1.543	1.092	**1.334**	Ubiquitin protein ligase E3 component recognin 2

Synonyms	Gene Symbol	MAS_{mutant}/MAS_{wt}				Description
		Exp I	Exp II	Exp III	average	
YML118W	NGL3	1.022	1.899	1.067	**1.330**	Protein with possible DNAse/RNAse function
YLR081W	GAL2	1.072	1.754	1.162	**1.329**	Galactose metabolism 2, a galactose and glucose permease
YLR087C	CSF1	1.134	1.816	1.028	**1.326**	Protein required for normal growth rate and resistance to NaCl and H2O2
YMR196W		1.247	1.535	1.180	**1.321**	Protein of unknown function
YDR150W	NUM1	1.325	1.459	1.166	**1.317**	Nuclear migration 1, controls interaction of bud-neck cytoskeleton with G2; involved in membrane targeting
YNL208W		1.226	1.483	1.237	**1.315**	Protein of unknown function
YBL013W	FMT1	1.307	1.794	0.845	**1.315**	Mitochondrial methionyl-tRNA transformylase
YBR284W		0.948	1.806	1.191	**1.315**	Protein containing an adenosine and AMP deaminase domain
YPL152W-A		1.090	1.868	0.983	**1.314**	Protein of unknown function
YBR086C*	IST2	2.031	1.083	0.826	**1.313**	cortical endoplasmic reticulum; may be involved in sensitivity to NaCl
YKL103C	LAP4	1.174	1.508	1.254	**1.312**	Leucine aminopeptidase 4, plays an important role in cytosol to vacuole targeting
YIR023W	DAL81	1.225	1.629	1.079	**1.311**	Transcriptional activator for allantoin, 4-aminobutyric acid (GABA), and urea catabolic genes
YKL062W	MSN4	0.919	2.047	0.963	**1.310**	Multicopy suppressor of snf 4, transcriptional required for tolerance to heat shock, osmotic, and oxidative stress
YPR049C	ATG11	1.364	1.425	1.140	**1.310**	Autophagy related 11, required for the cytoplasm to vacuole targeting (cvt) pathway
YNL106C	INP52	1.477	1.438	1.010	**1.308**	Inositol polyphosphate 5-phosphatase 52, acts in actin cytoskeleton organization and endocytosis
YIR015W	RPR2	1.281	1.533	1.110	**1.308**	Subunit of RNase P, which is responsible for pre-tRNA processing
YPL017C		0.985	1.965	0.973	**1.308**	Protein containing a pyridine nucleotide-disulfide oxidoreductase domain
YDR034W-B		1.143	1.428	1.351	**1.307**	Protein of unknown function
YMR118C		1.016	1.893	1.012	**1.307**	Member of the succinate dehydrogenase cytochrome B subunit family
YOR373W	NUD1	1.123	1.588	1.208	**1.306**	Spindle pole body (SPB) protein required for nuclear division, regulates meiotic SPB inheritance
YBR056W-A		1.259	1.387	1.272	**1.306**	Protein of unknown function
YGR225W	AMA1	1.098	1.937	0.883	**1.306**	Activator for meiotic anaphase 1, associates with the anaphase promoting complex/cyclosome
YNL034W		1.390	1.313	1.212	**1.305**	Protein of unknown function
YHR086W-A		1.500	1.391	1.024	**1.305**	Protein of unknown function
YKL033W		1.212	1.722	0.980	**1.305**	Protein of unknown function
YNR006W	VPS27	1.443	1.412	1.059	**1.305**	Vacuolar protein sorting 27, functions in sorting of ubiquitinated membrane proteins for degradation
YML128C	MSC1	1.549	1.230	1.133	**1.304**	Protein that affects meiotic homologous chromatid recombination
YJL207C	LAA1	1.563	1.268	1.081	**1.304**	Large AP-1 accessory 1, a protein required for localization of the clathrin/AP-1 complex to vesicles
YMR316W	DIA1	1.276	1.492	1.138	**1.302**	Protein involved in invasive growth, mRNA abundance is reduced in a calcineurin-dependent manner
YCR032W	BPH1	1.353	1.293	1.252	**1.300**	Probable acetic acid export pump

$MAS_{mutant}/MAS_{wild\text{-}type}$ coefficients for the three independent microarray experiments are given. A short description of the gene function is included (Source: Proteome). Proteins localized to mitochondria or of unknown function are designated in gray. ARF2 is given in brackets because the ORF has been deleted in our strain background. **ORFs that were chosen for the initial round of FISH validation are designated in bold**. Genes whose mRNA is localized to the bud tip in a SHE-dependent manner are marked with an asterisk.

7.1 Materials and Methods

7.1.1 Media

LB medium:	10 g Bacto-tryptone (BD) 5 g Bacto yeast extract (BD) 10 g NaCl (Roth) ad 1 l dH_2O and autoclaved the same day
LB agar:	5 g Bacto-tryptone (BD) 2.5 g Bacto yeast extract (BD) 5 g NaCl (Roth) 10 g Bacto-agar (BD) ad 500 ml dH_2O and autoclaved the same day
SOC-medium	5 g yeast extract (BD) 20 g Bacto-peptone (BD) 20 g dextrose (Roth) 10 mM NaCl 2.5 mM KCl 10 mM MgSO4 ad 1 l dH_2O and autoclaved the same day
YP medium:	1% Bacto yeast extract (BD) 2% Bacto-Peptone (BD)
YP agar:	10 g Bacto-peptone (BD) 5 g yeast-extract (BD) 10 g Bacto-agar (BD) ad 450 ml $dH_2O$and autoclaved the same day. Complemented with 50 ml 20% (w/v) glucose before plates were poured.
5-FOA-plates:	0.34 g Yeast Nitrogen Base without amino acids (BD) 0.05 g 5-Fluoroorotic acid (Biovectra 1555) 1 g Dextrose (Glucose-monohydrate Roth 6780.2) 5 ml 10x HC-complete selection mixture ad 20 ml dH_2O and filter sterilized into 25 ml warm (55°C) sterile agar (1 g in 25 ml H_2O)

10 x HC-selection mixture:	0.2 mg/ml adenine hemi-sulfate 0.35 mg/ml uracil 0.8 mg/ml L-tryptophan 0.2 mg/ml L-histidine-HCl 0.8 mg/ml L-leucine 1.2 mg/ml L-lysine-HCl 0.2 mg/ml L-methionine 0.6 mg/ml L-tyrosine 0.8 mg/ml L-isoleucine 0.5 mg/ml L-phenylalanine 1.0 mg/ml L-glutamic acid 2.0 mg/ml L-threonine 1.0 mg/ml L-aspartic acid 1.5 mg/ml L-valine 4.0 mg/ml L-serine 0.2 mg/ml L-arginine-HCl autoclaved without the components to select for
10 x YNB:	33.5 g Yeast Nitrogen Base w/o amino acids (BD) ad 500 ml dH_2O wrapped in aluminum foil and autoclaved the same day.
HC medium:	800 ml dH_2O 100 ml 10x HC-XX (without the component to select for) 100 ml 10 x YNB
HC plates:	hot sterile agar (10 g Bacto-agar (BD) dissolved in 350 ml) 50 ml 20% dextrose 50 ml 10 x YNB 50 ml 10 x HC selection mixture

7.1.2 Commonly used solutions and buffers

7.1.2.1 Antibiotics

1000 x ampicillin	100 mg/ml in dH_2O, filter-sterilized
250 x kanamycin	10 mg/ml in dH_2O, filter-sterilized
100 x G418	20 mg/ml geneticin in dH_2O, filter-sterilized
2000 x ClonNAT	200 mg/ml nourseotricin in dH_2O, filter-sterilized

7.1.2.2 Inhibitors

40 x CFW	2 mg/ml in dH_2O; NaOH added dropwise to dissolve
1000 x tunicamycin	1 mg/ml tunicamycin in DMSO
333 x benomyl	10 mg/ml benomyl in DMSO
333 x LatA	10 mg/ml latrunculin A in DMSO
500 x chlorpromazine	45 mg/ml chlorpromazine in dH_2O
1000x Verrucarin A	10 mg/ml in chloroform
100 x PMSF	0.1 M in isopropanol

7.1.2.3 Solutions

1000 x Rhodamine B, hexyl ester:	0.1 M in DMSO
1000 x DTT	1 M DTTin dH_2O
Buffer P1:	50 mM Tris/HCl pH 8.0 10 mM EDTA 100 µg/ml RNase Stored at 4°C.
Buffer P2:	0.2 M NaOH 1% SDS
Buffer P3:	3 M KAc, pH 5.5
TE buffer:	10 mM Tris/HCl pH 7.5 1 mM EDTA
Carrier DNA for transformations:	200 mg Salmon Sperm DNA (Sigma D1626) ad 100 ml with TE buffer
6 x loading buffer for agarose gel-electrophoresis:	0.25% bromphenolblue 0.25% xylencyanole 30% glycerol

50 x TAE-buffer:	2 M Tris/HAc pH 7.7 5 mM EDTA
5 x Laemmli-buffer:	62.5 mM Tris/HCl pH 6.8 5% β-mercaptoethanol 10% glycerol 2% SDS 0.0025% bromophenolblue
20 x TBS:	60 g Tris/HCl pH 7.4 160 g NaCl 4 g KCl ad 1 l with dH_2O
TBST:	TBS with 0.1% Tween-20
20 x PBS:	46.6 g Na_2HPO_4 x 12 H_2O 4.2 g KH_2PO_4 175.2 g NaCl 44.8 g KCl ad 1 l with dH_2O
50 x Denhardt's reagent:	10 g Ficoll type 400 10 g BSA fraction V 10 g polyvinylpyrrolidone ad 1 l with dH_2O and filter-sterilized, stored at –20°C
20 x SSC:	3 M NaCl 0.3 M Na-citrate/NaOH pH 7.0
DEPC-H_2O:	1 l H_2O 1 ml DEPC stirred for > 1 h, then autoclaved

7.1.3 Strains, oligonucleotide primers, plasmids, antibodies, and web resources

7.1.3.1 Strains

Table 7.3: Yeast strains used in this study

Strain	Designation	Genotype	Source
YPH499	WT	*MAT a ade2-101 his3-200 leu2-1 lys2-801 trp-63 ura3-52*	P. Hieter
NYY0-1	*ARF1*	*MAT a ade2::ARF1::ADE2 arf1::HIS3 arf2::HIS3 ura3 lys2 trp1 his3 leu2*	A. Nakano
NYY11-1	*arf1-11*	*MAT a ade2::arf1-11::ADE2 arf1::HIS3 arf2::HIS3 ura3 lys2 trp1 his3 leu2*	A. Nakano
NYY17-1	*arf1-17*	*MAT a ade2::arf1-17::ADE2 arf1::HIS3 arf2::HIS3 ura3 lys2 trp1 his3 leu2*	A. Nakano
NYY18-1	*arf1-18*	*MAT a ade2::arf1-18::ADE2 arf1::HIS3 arf2::HIS3 ura3 lys2 trp1 his3 leu2*	A. Nakano
RSY1017	sec21-1	*MAT α pep4::URA3 ura3-52 his3Δ200*	R. Schekman
RSY1312	*sec27-1*	*MAT a leu2,3,-112 trp1 ura3-52*	R. Duden
YAS1184	*ARF1* Scp160-GFP	*MAT a ade2::ARF1::ADE2 arf1::HIS3 arf2::HIS3 ura3 lys2 trp1 his3 leu2 SCP160::SCP160-yeGFP-kanMX4*	This study
YAS1185	*arf1-11* Scp160-GFP	*MAT a ade2::arf1-11::ADE2 arf1::HIS3 arf2::HIS3 ura3 lys2 trp1 his3 leu2 SCP160::SCP160-yeGFP-kanMX4*	This study
YAS1186	*arf1-17* Scp160-GFP	*MAT a ade2::arf1-17::ADE2 arf1::HIS3 arf2::HIS3 ura3 lys2 trp1 his3 leu2 SCP160::SCP160-yeGFP-kanMX4*	This study
YAS1187	*arf1-18* Scp160-GFP	*MAT a ade2::arf1-18::ADE2 arf1::HIS3 arf2::HIS3 ura3 lys2 trp1 his3 leu2 SCP160::SCP160-yeGFP-kanMX4*	This study
YAS1271	*ARF1* Bfr1-GFP	*MAT a ade2::ARF1::ADE2 arf1::HIS3 arf2::HIS3 ura3 lys2 trp1 his3 leu2 BFR1::BFR1-yeGFP-kanMX*	This study
YAS1272	*arf1-11* Bfr1-GFP	*MAT a ade2::arf1-11::ADE2 arf1::HIS3 arf2::HIS3 ura3 lys2 trp1 his3 leu2 BFR1::BFR1-yeGFP-kanMX*	This study
YAS1273	*arf1-17* Bfr1-GFP	*MAT a ade2::arf1-17::ADE2 arf1::HIS3 arf2::HIS3 ura3 lys2 trp1 his3 leu2 BFR1::BFR1-yeGFP-kanMX*	This study
YAS1274	*arf1-18* Bfr1-GFP	*MAT a ade2::arf1-18::ADE2 arf1::HIS3 arf2::HIS3 ura3 lys2 trp1 his3 leu2 BFR1::BFR1-yeGFP-kanMX*	This study
YAS1194	*ARF1* Puf5-4GFP	*MAT a ade2::ARF1::ADE2 arf1::HIS3 arf2::HIS3 ura3 lys2 trp1 his3 leu2 PUF5::PUF5-4GFP-kanMX4*	This study
YAS1195	*arf1-11* Puf5-4GFP	*MAT a ade2::arf1-11::ADE2 arf1::HIS3 arf2::HIS3 ura3 lys2 trp1 his3 leu2 PUF5::PUF5-4GFP-kanMX4*	This study
YAS1180	*ARF1* Puf6-GFP	*MAT a ade2::ARF1::ADE2 arf1::HIS3 arf2::HIS3 ura3 lys2 trp1 his3 leu2 PUF6::PUF6-GFP-kanMX4*	This study
YAS1181	*arf1-11* Puf6-GFP	*MAT a ade2::arf1-11::ADE2 arf1::HIS3 arf2::HIS3 ura3 lys2 trp1 his3 leu2 PUF6::PUF6-GFP-kanMX4*	This study
YAS1583	*ARF1* Ams1-GFP	*MAT a ade2::ARF1::ADE2 arf1::HIS3 arf2::HIS3 ura3 lys2 trp1 his3 leu2 AMS1::AMS1-yeGFP-kanMX*	This study
YAS1584	*arf1-11* Ams1-GFP	*MAT a ade2::arf1-11::ADE2 arf1::HIS3 arf2::HIS3 ura3 lys2 trp1 his3 leu2 AMS1::AMS1-yeGFP-kanMX*	This study
YAS1652	*ARF1* Chs5-GFP	*MAT a ade2::ARF1::ADE2 arf1::HIS3 arf2::HIS3 ura3 lys2 trp1 his3 leu2 BFR1::BFR1-yeGFP-kanMX*	This study
YAS1653	*arf1-11* Chs5-GFP	*MAT a ade2::arf1-11::ADE2 arf1::HIS3 arf2::HIS3 ura3 lys2 trp1 his3 leu2 BFR1::BFR1-yeGFP-kanMX*	This study
YAS1362	*ARF1* Abp1-4GFP	*MAT a ade2::ARF1::ADE2 arf1::HIS3 arf2::HIS3 ura3 lys2 trp1 his3 leu2 ABP1::ABP1-4GFP-kanMX*	This study
YAS1208	*arf1-11* Abp1-4GFP	*MAT a ade2::arf1-11::ADE2 arf1::HIS3 arf2::HIS3 ura3 lys2 trp1 his3 leu2 ABP1::ABP1-4GFP-kanMX*	This study
YAS1648	*ARF1* Abp140-GFP	*MAT a ade2::ARF1::ADE2 arf1::HIS3 arf2::HIS3 ura3 lys2 trp1 his3 leu2 ABP140::ABP140-yeGFP-kanMX*	This study
YAS1586	*arf1-11* Abp140-GFP	*MAT a ade2::arf1-11::ADE2 arf1::HIS3 arf2::HIS3 ura3 lys2 trp1 his3 leu2 ABP140::ABP140-yeGFP-kanMX*	This study
YAS1843	*Δabp140*	*MAT a ade2::ARF1::ADE2 arf1::HIS3 arf2::HIS3 ura3 lys2 trp1 his3 leu2 ABP140::natNT2*	This study
YAS1842	*Δ bud5*	*MAT a ade2::ARF1::ADE2 arf1::HIS3 arf2::HIS3 ura3 lys2 trp1 his3 leu2 BUD5::LEU2 (K. lactis)*	This study
BY4743	BY4743	*MAT a/α his3Δ1/his3Δ1 leu2Δ0/leu2Δ0 lys2Δ0/LYS2 MET15/met15Δ0 ura3Δ0/ura3Δ0*	Euroscarf
YAS348	*Δ bud7/ Δ bud7*	*MAT a/α his3Δ1/his3Δ1 leu2Δ0/leu2Δ0 lys2Δ0/LYS2 MET15/met15Δ0 ura3Δ0/ura3Δ0 BUD7::kanMX4/BUD7::kanMX4*	R. Gauss
YAS1836	*Δtpm1*	*MAT a ade2::ARF1::ADE2 arf1::HIS3 arf2::HIS3 ura3 lys2 trp1 his3 leu2 TPM1::LEU2 (K. lactis)*	This study

Strain	Designation	Genotype	Source
Δmyo4	*Δmyo4*	*MAT a his3Δ1 leu2Δ0 lys2Δ0 ura3Δ0 MYO4::kanMX4*	Euroscarf
YAS1696	*Δtpm2*	*MAT a ade2::ARF1::ADE2 arf1::HIS3 arf2::HIS3 ura3 lys2 trp1 his3 leu2 TPM1::LEU2 (K. lactis)*	This study
YAS1697	*Δmyo1*	*MAT a ade2::ARF1::ADE2 arf1::HIS3 arf2::HIS3 ura3 lys2 trp1 his3 leu2 TPM1::LEU2 (K. lactis)*	This study
YAS1938	pADH-Abp140	*MAT a ade2::ARF1::ADE2 arf1::HIS3 arf2::HIS3 ura3 lys2 trp1 his3 leu2 ABP140::natNT2-pADH1-ABP140*	This study
YAS1965	pADH-Abp140-GFP	*MAT a ade2::ARF1::ADE2 arf1::HIS3 arf2::HIS3 ura3 lys2 trp1 his3 leu2 ABP140::natNT2-pADH1-ABP140-yeGFP-kanMX*	This study
YAS2480	DN17-GFP-ABP140	*MAT a ade2::ARF1::ADE2 arf1::HIS3 arf2::HIS3 ura3 lys2 trp1 his3 leu2 ABP140::natNT2-pADH1-GFP-ABP140(18-629)*	This study
YAS2489	ActA-Abp140-GFP	*MAT a ade2::ARF1::ADE2 arf1::HIS3 arf2::HIS3 ura3 lys2 trp1 his3 leu2 ABP140::natNT2-pADH-ActA-ABP140(18-629)-GFP- kanMX4*	This study
YAS1150	GFP-TAA-Abp140	*MAT a ade2::ARF1::ADE2 arf1::HIS3 arf2::HIS3 ura3 lys2 trp1 his3 leu2 ABP140::natNT2-pADH1-GFP-TAA-ABP140*	This study
YAS2317	*abp140-ΔRNA*	*MAT a ade2::ARF1::ADE2 arf1::HIS3 arf2::HIS3 ura3 lys2 trp1 his3 leu2 ABP140::abp140(Δ613-747)*	This study
prt1-1	*prt1-1*	*his prt1-1*	T. Wölfle
YAS1151	*abp140-RFS**	*MAT a ade2::ARF1::ADE2 arf1::HIS3 arf2::HIS3 ura3 lys2 trp1 his3 leu2 ABP140::abp140-rfs**	This study
YAS1940	(1-17)-GFP	*MAT a ade2::ARF1::ADE2 arf1::HIS3 arf2::HIS3 ura3 lys2 trp1 his3 leu2 ABP140::abp140(1-17)-yeGFP-kanMX*	This study
YAS2430	(1-67)-GFP	*MAT a ade2::ARF1::ADE2 arf1::HIS3 arf2::HIS3 ura3 lys2 trp1 his3 leu2 ABP140::abp140(1-67)-yeGFP-kanMX*	This study
YAS2431	(1-134)-GFP	*MAT a ade2::ARF1::ADE2 arf1::HIS3 arf2::HIS3 ura3 lys2 trp1 his3 leu2 ABP140::abp140(1-134)-yeGFP-kanMX*	This study
YAS1777	(1-204)-GFP	*MAT a ade2::ARF1::ADE2 arf1::HIS3 arf2::HIS3 ura3 lys2 trp1 his3 leu2 ABP140::abp140(1-204)-yeGFP-kanMX*	This study
YAS1779	(1-250)-GFP	*MAT a ade2::ARF1::ADE2 arf1::HIS3 arf2::HIS3 ura3 lys2 trp1 his3 leu2 ABP140::abp140(1-250)-yeGFP-kanMX*	This study
YAS1787	(1-277)-GFP	*MAT a ade2::ARF1::ADE2 arf1::HIS3 arf2::HIS3 ura3 lys2 trp1 his3 leu2 ABP140::abp140(1-277)-yeGFP-kanMX*	This study
YAS2478	(1-67)-TAA-GFP	*MAT a ade2::ARF1::ADE2 arf1::HIS3 arf2::HIS3 ura3 lys2 trp1 his3 leu2 ABP140::abp140(1-67)-TAA-yeGFP-kanMX*	This study
YAS2375	(1-17)-GFP-(18-629)-eqFP611	*MAT a ade2::ARF1::ADE2 arf1::HIS3 arf2::HIS3 ura3 lys2 trp1 his3 leu2 ABP140::abp140(1-17)-yeGFP-(18-629)-eqFP611-natNT2*	This study
YAS1031A	*ARF1* Dcp2-GFP	*MAT a ade2::ARF1::ADE2 arf1::HIS3 arf2::HIS3 ura3 lys2 trp1 his3 leu2 DCP2::DCP2-yeGFP-kanMX4*	This study
YAS1032A	*arf1-11* Dcp2-GFP	*MAT a ade2::arf1-11::ADE2 arf1::HIS3 arf2::HIS3 ura3 lys2 trp1 his3 leu2 DCP2::DCP2-yeGFP-kanMX4*	This study
YAS1033A	*arf1-17* Dcp2-GFP	*MAT a ade2::arf1-17::ADE2 arf1::HIS3 arf2::HIS3 ura3 lys2 trp1 his3 leu2 DCP2::DCP2-yeGFP-kanMX4*	This study
YAS1034A	*arf1-18* Dcp2-GFP	*MAT a ade2::arf1-18::ADE2 arf1::HIS3 arf2::HIS3 ura3 lys2 trp1 his3 leu2 DCP2::DCP2-yeGFP-kanMX4*	This study
YAS2428	*ARF1* Edc3-eqFP611 eIFG2-GFP	*MAT a ade2::ARF1::ADE2 arf1::HIS3 arf2::HIS3 ura3 lys2 trp1 his3 leu2 EDC3::EDC3-eqFP611-kanMX4 eIFG2:: eIFG2-yeGFP-TRP1 (K.lactis)*	J. Weidner
YAS2429	*arf1-11* Edc3-eqFP611 eIFG2-GFP	*MAT a ade2::arf1-11::ADE2 arf1::HIS3 arf2::HIS3 ura3 lys2 trp1 his3 leu2 EDC3::EDC3-eqFP611-kanMX4 eIFG2:: eIFG2-yeGFP-TRP1 (K.lactis)*	J. Weidner
YAS1681	*sar1-D32G* Dcp2-GFP	*MAT a ade2-101 his3-200 leu2-1 lys2-801 trp-63 ura3-52 SAR1::LEU2 (K. lactis) pMYY3-1(Ycp[sar1-D32G TRP1]) DCP2::DCP2-yEGFP-kanMX4*	This study
YAS1683	*sec21-1 (YPH499)*	*MAT a ade2-101 his3-200 leu2-1 lys2-801 trp-63 ura3-52 sec21-1*	This study
YAS1133	*sec21-1* Dcp2-GFP	*MAT αade2-101 his3-200 leu2-1 lys2-801 trp-63 ura3-52 sec21-1 DCP2::DCP2-yEGFP-kanMX4*	This study
YAS1682	*sec27-1 (YPH499)*	*MAT a ade2-101 his3-200 leu2-1 lys2-801 trp-63 ura3-52 sec27-1*	
YAS1134	*sec27-1* Dcp2-GFP	*MAT a ade2-101 his3-200 leu2-1 lys2-801 trp-63 ura3-52 sec27-1 DCP2::DCP2-yEGFP-kanMX4*	This study
APY 026	*Δgea2 gea1-19*	*MAT a ura3-52 leu2,3-112 his3-200 GEA2::HIS3 gea1-19*	C. Jackson

Strain	Designation	Genotype	Source
YAS1131	*Δgea2 gea1-19* Dcp2-GFP	*MAT a ura3-52 leu2,3-112 his3-200 GEA2::HIS3 gea1-19 DCP2::DCP2-yEGFP-kanMX4*	This study
YAS1064	*sec6-4 (YPH499)*	*MAT a ade2-101 his3-200 leu2-1 lys2-801 trp-63 ura3-52 sec6-4 CHS6::CHS6-9myc-TRP1 (K. lactis)*	M. Trautwein
YAS1135	*sec6-4* Dcp2-GFP	*MAT a ade2-101 his3-200 leu2-1 lys2-801 trp-63 ura3-52 sec6-4 CHS6::CHS6-9myc-TRP1 (K. lactis) DCP2::DCP2-yEGFP-kanMX4*	This study
YAS1449	*sec3-2 (YPH499)*	*MAT a ura3 leu2 trp1 sec3-2*	B. Zanolari
YAS1877	*sec3-2* Dcp2-GFP	*MAT a ura3 leu2 trp1 sec3-2 DCP2::DCP2-yEGFP-kanMX4*	This study
YAS1589	*sec4-8 (YPH499)*	*MAT a ura3 leu2 lys sec4-8*	B. Zanolari
YAS1880	*sec4-8* Dcp2-GFP	*MAT a ura3 leu2 lys sec4-8 DCP2::DCP2-yEGFP-kanMX4*	This study
YAS1405	*sec2-41 (YPH499)*	*MAT a ura3 leu2 his3 lys2 trp1 ade2 sec2-41*	B. Zanolari
YAS1878	*sec2-41* Dcp2-GFP	*MAT a ura3 leu2 his3 lys2 trp1 ade2 sec2-41 DCP2::DCP2-yEGFP-kanMX4*	This study
YAS2235	*ARF1* Pub1-GFP	*MAT a ade2::ARF1::ADE2 arf1::HIS3 arf2::HIS3 ura3 lys2 trp1 his3 leu2 PUB1::PUB1-yEGFP-kanMX4*	J. Weidner
YAS1945	*ARF1* Dcp2-GFP *Δhog1*	*MAT a ade2::ARF1::ADE2 ARF1::HIS3 ARF2::HIS3 ura3 lys2 trp1 his3 leu2 DCP2::DCP2-yEGFP-kanMX4 HOG1::LEU2 (K. lactis)*	This study
YAS1946	*arf1-11* Dcp2-GFP *Δhog1*	*MAT a ade2::arf1-11::ADE2 ARF1::HIS3 ARF2::HIS3 ura3 lys2 trp1 his3 leu2 DCP2::DCP2-yEGFP-kanMX4 HOG1::LEU2 (K. lactis)*	This study
YAS1685	*ARF1* Dcp2-GFP *Δsho1*	*MAT a ade2::ARF1::ADE2 ARF1::HIS3 ARF2::HIS3 ura3 lys2 trp1 his3 leu2 DCP2::DCP2-yEGFP-kanMX4 SHO1::LEU2 (K. lactis)*	This study
YAS1686	*arf1-11* Dcp2-GFP *Δsho1*	*MAT a ade2::arf1-11::ADE2 ARF1::HIS3 ARF2::HIS3 ura3 lys2 trp1 his3 leu2 DCP2::DCP2-yEGFP-kanMX4 SHO1::LEU2 (K. lactis)*	This study
YAS1947	*ARF1* Dcp2-GFP *Δsko1*	*MAT a ade2::ARF1::ADE2 ARF1::HIS3 ARF2::HIS3 ura3 lys2 trp1 his3 leu2 DCP2::DCP2-yEGFP-kanMX4 SKO1::LEU2 (K. lactis)*	This study
YAS1948	*arf1-11* Dcp2-GFP *Δsko1*	*MAT a ade2::arf1-11::ADE2 ARF1::HIS3 ARF2::HIS3 ura3 lys2 trp1 his3 leu2 DCP2::DCP2-yEGFP-kanMX4 SKO1::LEU2 (K. lactis)*	This study
YAS1967	*ARF1* Dcp2-GFP *Δslt2*	*MAT a ade2::ARF1::ADE2 ARF1::HIS3 ARF2::HIS3 ura3 lys2 trp1 his3 leu2 DCP2::DCP2-yEGFP-kanMX4 SLT2::LEU2 (K. lactis)*	This study
YAS1968	*arf1-11* Dcp2-GFP *Δslt2*	*MAT a ade2::arf1-11::ADE2 ARF1::HIS3 ARF2::HIS3 ura3 lys2 trp1 his3 leu2 DCP2::DCP2-yEGFP-kanMX4 SLT2::LEU2 (K. lactis)*	This study
YAS1986	*ARF1* Dcp2-GFP *Δhog1 Δslt2*	*MAT a ade2::ARF11::ADE2 ARF1::HIS3 ARF2::HIS3 ura3 lys2 trp1 his3 leu2 DCP2::DCP2-yEGFP-kanMX4 HOG1:: LEU2 (K. lactis) SLT2::URA3 (K. lactis)*	This study
YAS1987	*arf1-11* Dcp2-GFP *Δhog1 Δslt2*	*MAT a ade2::arf1-11::ADE2 ARF1::HIS3 ARF2::HIS3 ura3 lys2 trp1 his3 leu2 DCP2::DCP2-yEGFP-kanMX4 HOG1:: LEU2 (K. lactis) SLT2::URA3 (K. lactis)*	This study
YAS2092	*ARF1* Dcp2-GFP *Δhog1 Δslt2 Δcnb1*	*MAT a ade2::ARF1::ADE2 ARF1::HIS3 ARF2::HIS3 ura3 lys2 trp1 his3 leu2 DCP2::DCP2-yEGFP-kanMX4 HOG1::loxP SLT2::loxP CNB1::LEU2 (K. lactis)*	This study
YAS2292	*arf1-11* Dcp2-GFP *Δhog1 Δslt2 Δcnb1*	*MAT a ade2::arf1-11::ADE2 ARF1::HIS3 ARF2::HIS3 ura3 lys2 trp1 his3 leu2 DCP2::DCP2-yEGFP-kanMX4 HOG1::loxP SLT2::loxP CNB1::LEU2 (K. lactis)*	This study

Strain	Designation	Genotype	Source
YAS2575	*ARF1* Dcp2-GFP *Δypk1*	*MAT a ade2::ARF1::ADE2 ARF1::HIS3 ARF2::HIS3 ura3 lys2 trp1 his3 leu2 DCP2::DCP2-yEGFP-kanMX4 YPK1::LEU2 (K. lactis)*	This study
YAS2010	*arf1-11* Dcp2-GFP *Δypk1*	*MAT a ade2::arf1-11::ADE2 ARF1::HIS3 ARF2::HIS3 ura3 lys2 trp1 his3 leu2 DCP2::DCP2-yEGFP-kanMX4 YPK1::LEU2 (K. lactis)*	This study
YAS2021	*ARF1* Dcp2-GFP *Δcnb1*	*MAT a ade2::ARF11::ADE2 ARF1::HIS3 ARF2::HIS3 ura3 lys2 trp1 his3 leu2 DCP2::DCP2-yEGFP-kanMX4 CNB1::LEU2 (K. lactis)*	This study
YAS2051	*arf1-11* Dcp2-GFP *Δcnb1*	*MAT a ade2::arf1-11::ADE2 ARF1::HIS3 ARF2::HIS3 ura3 lys2 trp1 his3 leu2 DCP2::DCP2-yEGFP-kanMX4 CNB1::LEU2 (K. lactis)*	This study
YAS2088	*ARF1* Dcp2-GFP *Δcmk1 Δcmk2*	*MAT a ade2::ARF11::ADE2 ARF1::HIS3 ARF2::HIS3 ura3 lys2 trp1 his3 leu2 DCP2::DCP2-yEGFP-kanMX4 CMK1::LEU2 (K. lactis) CMK2::URA3 (K. lactis)*	This study
YAS2089	*arf1-11* Dcp2-GFP *Δcmk1 Δcmk2*	*MAT a ade2::arf1-11::ADE2 ARF1::HIS3 ARF2::HIS3 ura3 lys2 trp1 his3 leu2 DCP2::DCP2-yEGFP-kanMX4 CMK1::LEU2 (K. lactis) CMK2::URA3 (K. lactis)*	This study
YAS2090	*ARF1* Dcp2-GFP *Δcmk1 Δcmk2 Δcnb1*	*MAT a ade2::ARF1::ADE2 ARF1::HIS3 ARF2::HIS3 ura3 lys2 trp1 his3 leu2 DCP2::DCP2-yEGFP-kanMX4 CMK1::loxP CMK2::loxP CNB1::LEU2 (K. lactis)*	This study
YAS2091	*arf1-11* Dcp2-GFP *Δcmk1 Δcmk2 Δcnb1*	*MAT a ade2::arf1-11::ADE2 ARF1::HIS3 ARF2::HIS3 ura3 lys2 trp1 his3 leu2 DCP2::DCP2-yEGFP-kanMX4 CMK1::loxP CMK2::loxP CNB1::LEU2 (K. lactis)*	This study
YAS2586	*arf1-11* Dcp2-GFP *Δgcn2*	*MAT a ade2::arf1-11::ADE2 arf1::HIS3 arf2::HIS3 ura3 lys2 trp1 his3 leu2 DCP2::DCP2-yEGFP-kanMX4 GCN2::URA3 (K. lactis)*	J. Weidner
YAS2588	*arf1-11* Dcp2-GFP *Δire1*	*MAT a ade2::arf1-11::ADE2 arf1::HIS3 arf2::HIS3 ura3 lys2 trp1 his3 leu2 DCP2::DCP2-yEGFP-kanMX4 IRE1:: URA3 (K. lactis)*	J. Weidner
YAS2296	*ARF1 cmd1-3* Dcp2-GFP	*MAT a ade2::ARF1::ADE2 ARF1::HIS3 ARF2::HIS3 ura3 lys2 trp1 his3 leu2 DCP2::DCP2-yEGFP-kanMX4 CMD1::cmd1-3*	This study
YAS2580	*arf1-11 cmd1-3* Dcp2-GFP	*MAT a ade2::arf1-11::ADE2 arf1::HIS3 arf2::HIS3 ura3 lys2 trp1 his3 leu2 DCP2::DCP2-yEGFP-kanMX4 pHS47(cmd1-3 URA3) CMD1::kanMX4*	J. Weidner
YAS2294	*ARF1* Dcp2-GFP *Δpat1*	*MAT a ade2::ARF1::ADE2 ARF1::HIS3 ARF2::HIS3 ura3 lys2 trp1 his3 leu2 DCP2::DCP2-yEGFP-kanMX4 PAT1::LEU2 (K. lactis)*	This study
YAS2295	*arf1-11* Dcp2-GFP *Δpat1*	*MAT a ade2::arf1-11::ADE2 ARF1::HIS3 ARF2::HIS3 ura3 lys2 trp1 his3 leu2 DCP2::DCP2-yEGFP-kanMX4 PAT1::LEU2 (K.lactis)*	This study
YAS2297	*sec6-4* Dcp2-GFP *Δpat1*	*MAT a ade2-101 his3-200 leu2-1 lys2-801 trp-63 ura3-52 sec6-4 CHS6::CHS6-9myc-TRP1 (K. lactis) DCP2::DCP2-yEGFP-kanMX4 PAT1::LEU2 (K. lactis)*	This study
YAS1097	*ARF1* Dcp2-GFP *Δscd6*	*MAT a ade2::ARF1::ADE2 arf1::HIS3 arf2::HIS3 ura3 lys2 trp1 his3 leu2 DCP2::DCP2-yEGFP-kanMX4 SCD6::LEU2 (K. lactis)*	This study
YAS1098	*arf1-11* Dcp2-GFP *Δscd6*	*MAT a ade2::arf1-11::ADE2 arf1::HIS3 arf2::HIS3 ura3 lys2 trp1 his3 leu2 DCP2::DCP2-yEGFP-kanMX4 SCD6::LEU2 (K. lactis)*	This study
YAS2500	*sec6-4* Dcp2-GFP *Δscd6*	*MAT a ade2-101 his3-200 leu2-1 lys2-801 trp-63 ura3-52 sec6-4 CHS6::CHS6-9myc-TRP1 (K. lactis) DCP2::DCP2-yEGFP-kanMX4 SCD6::LEU2 (K. lactis)*	This study

Strain	Designation	Genotype	Source
YAS1294	*ARF1* Dcp2-9myc	*MAT a ade2::ARF1::ADE2 arf1::HIS3 arf2::HIS3 ura3 lys2 trp1 his3 leu2 DCP2::DCP2-9myc-TRP1 (K. lactis)*	This study
YAS1295	*arf1-11* Dcp2-9myc	*MAT a ade2::arf1-11::ADE2 arf1::HIS3 arf2::HIS3 ura3 lys2 trp1 his3 leu2 DCP2::DCP2-9myc-TRP1 (K. lactis)*	This study
YAS1693	*ARF1* Dhh1-9myc	*MAT a ade2::ARF1::ADE2 ARF1::HIS3 ARF2::HIS3 ura3 lys2 trp1 his3 leu2 DHH1::DHH1-9myc-TRP1 (K. lactis)*	This study
YAS1694	*arf1-11* Dhh1-9myc	*MAT a ade2::arf1-11::ADE2 ARF1::HIS3 ARF2::HIS3 ura3 lys2 trp1 his3 leu2 DHH1::DHH1-9myc-TRP1 (K. lactis)*	This study
YAS2576	*arf1-11* Pat1-GFP	*MAT a ade2::arf1-11::ADE2 arf1::HIS3 arf2::HIS3 ura3 lys2 trp1 his3 leu2 PAT1::PAT1-EGFP-TRP1 (K.lactis)*	This study
YAS2578	*arf1-11* Scd6-GFP	*MAT a ade2::arf1-11::ADE2 arf1::HIS3 arf2::HIS3 ura3 lys2 trp1 his3 leu2 SCD6: SCD6-yeGFP-kanMX4*	This study
YAS1153	*ARF1* Dhh1-GFP	*MAT a ade2::ARF1::ADE2 arf1::HIS3 arf2::HIS3 ura3 lys2 trp1 his3 leu2 DHH1::DHH1-yeGFP-kanMX4*	This study
YAS1154	*arf1-11* Dhh1-GFP *Dpub1*	*MAT a ade2::arf1-11::ADE2 arf1::HIS3 arf2::HIS3 ura3 lys2 trp1 his3 leu2 DHH1::DHH1-yeGFP-kanMX4*	This study
YAS2153	*ARF1* Cmd1-GFP	*MAT a ade2::ARF1::ADE2 arf1::HIS3 arf2::HIS3 ura3 lys2 trp1 his3 leu2 CMD1::CMD1-yeGFP-kanMX4*	This study
YAS2154	*arf1-11* Cmd1-GFP	*MAT a ade2::arf1-11::ADE2 arf1::HIS3 arf2::HIS3 ura3 lys2 trp1 his3 leu2 CMD1::CMD1-yeGFP-kanMX4*	This study
	ARF1 Scd6-GFP	*MAT a ade2::ARF1::ADE2 arf1::HIS3 arf2::HIS3 ura3 lys2 trp1 his3 leu2 SCD6: SCD6-yeGFP-kanMX4*	This study
YAS2238	*ARF1* Edc3-GFP	*MAT a ade2::ARF1::ADE2 arf1::HIS3 arf2::HIS3 ura3 lys2 trp1 his3 leu2 EDC3::EDC3-yeGFP-TRP1 (K. lactis)*	J. Weidner
YAS2239	*arf1-11* Edc3-GFP	*MAT a ade2::arf1-11::ADE2 arf1::HIS3 arf2::HIS3 ura3 lys2 trp1 his3 leu2 EDC3::EDC3-yeGFP-TRP1 (K. lactis)*	J. Weidner
YAS2300	*ARF1* Dcp2-GFP *Δedc3*	*MAT a ade2::ARF1::ADE2 arf1::HIS3 arf2::HIS3 ura3 lys2 trp1 his3 leu2 DCP2::DCP2-yeGFP-kanMX4 EDC3::LEU2 (K. lactis)*	This study
YAS2301	*arf1-11* Dcp2-GFP *Δedc3*	*MAT a ade2::arf1-11::ADE2 arf1::HIS3 arf2::HIS3 ura3 lys2 trp1 his3 leu2 DCP2::DCP2-yeGFP-kanMX4 EDC3::LEU2 (K. lactis)*	This study
YAS2585	*ARF1* Dcp2-GFP	*MAT a ade2::ARF1::ADE2 arf1::HIS3 arf2::HIS3 ura3 lys2 trp1 his3 leu2 DCP2::DCP2-yeGFP-kanMX4 GCN2::URA3 (K. lactis)*	J. Weidner
YAS2587	*arf1-11* Dcp2-GFP	*MAT a ade2::arf1-11::ADE2 arf1::HIS3 arf2::HIS3 ura3 lys2 trp1 his3 leu2 DCP2::DCP2-yeGFP-kanMX4 IRE3::URA3 (K. lactis)*	J. Weidner
YAS1936	*ARF1* Dcp2-HBH	*MAT a ade2::ARF1::ADE2 arf1::HIS3 arf2::HIS3 ura3 lys2 trp1 his3 leu2 DCP2::DCP2-HBH-TRP1 (K. lactis)*	This study
YAS1937	*arf1-11* Dcp2-HBH	*MAT a ade2::arf1-11::ADE2 arf1::HIS3 arf2::HIS3 ura3 lys2 trp1 his3 leu2 DCP2::DCP2-HBH-TRP1 (K. lactis)*	This study
YAS2068	*ARF1* Dcp2-GFP *Δmhp1*	*MAT a ade2::ARF1::ADE2 ARF1::HIS3 ARF2::HIS3 ura3 lys2 trp1 his3 leu2 DCP2::DCP2-yEGFP-kanMX4 MHP1::LEU2 (K. lactis)*	This study
YAS2069	*arf1-11* Dcp2-GFP *Δmhp1*	*MAT a ade2::arf1-11::ADE2 ARF1::HIS3 ARF2::HIS3 ura3 lys2 trp1 his3 leu2 DCP2::DCP2-yEGFP-kanMX4 MHP1::LEU2 (K. lactis)*	This study
YAS2070	*ARF1* Dcp2-GFP *Δcyr1*	*MAT a ade2::ARF1::ADE2 ARF1::HIS3 ARF2::HIS3 ura3 lys2 trp1 his3 leu2 DCP2::DCP2-yEGFP-kanMX4 CYR1::LEU2 (K. lactis)*	This study
YAS2071	*arf1-11* Dcp2-GFP *Δcyr1*	*MAT a ade2::arf1-11::ADE2 ARF1::HIS3 ARF2::HIS3 ura3 lys2 trp1 his3 leu2 DCP2::DCP2-yEGFP-kanMX4 CYR1::LEU2 (K. lactis)*	This study
YAS2066	*ARF1* Dcp2-GFP *Δyck2*	*MAT a ade2::ARF1::ADE2 ARF1::HIS3 ARF2::HIS3 ura3 lys2 trp1 his3 leu2 DCP2::DCP2-yEGFP-kanMX4 YCK2::LEU2 (K. lactis)*	This study
YAS2067	*arf1-11* Dcp2-GFP *Δyck2*	*MAT a ade2::arf1-11::ADE2 ARF1::HIS3 ARF2::HIS3 ura3 lys2 trp1 his3 leu2 DCP2::DCP2-yEGFP-kanMX4 YCK2::LEU2 (K. lactis)*	This study

Strain	Designation	Genotype	Source
YAS2072	*ARF1* Dcp2-GFP *Δdot6*	*MAT a ade2::ARF1::ADE2 ARF1::HIS3 ARF2::HIS3 ura3 lys2 trp1 his3 leu2 DCP2::DCP2-yEGFP-kanMX4 DOT6::LEU2 (K. lactis)*	This study
YAS2073	*arf1-11* Dcp2-GFP *Δdot6*	*MAT a ade2::arf1-11::ADE2 ARF1::HIS3 ARF2::HIS3 ura3 lys2 trp1 his3 leu2 DCP2::DCP2-yEGFP-kanMX4 DOT6::LEU2 (K. lactis)*	This study
YAS2076	*ARF1* Dcp2-GFP *Δ*Yol087c	*MAT a ade2::ARF1::ADE2 ARF1::HIS3 ARF2::HIS3 ura3 lys2 trp1 his3 leu2 DCP2::DCP2-yEGFP-kanMX4 YOL087C::LEU2 (K. lactis)*	This study
YAS2077	*arf1-11* Dcp2-GFP *Δ*Yol087c	*MAT a ade2::arf1-11::ADE2 ARF1::HIS3 ARF2::HIS3 ura3 lys2 trp1 his3 leu2 DCP2::DCP2-yEGFP-kanMX4 YOL087C::LEU2 (K. lactis)*	This study
YAS2074	*ARF1* Dcp2-GFP *Δ*Ybr238c	*MAT a ade2::ARF1::ADE2 ARF1::HIS3 ARF2::HIS3 ura3 lys2 trp1 his3 leu2 DCP2::DCP2-yEGFP-kanMX4 YBR238C::LEU2 (K. lactis)*	This study
YAS2075	*arf1-11* Dcp2-GFP *Δ*Ybr238c	*MAT a ade2::arf1-11::ADE2 ARF1::HIS3 ARF2::HIS3 ura3 lys2 trp1 his3 leu2 DCP2::DCP2-yEGFP-kanMX4 YBR238C::LEU2 (K. lactis)*	This study
YAS2064	*ARF1* Dcp2-GFP *Δrom2*	*MAT a ade2::ARF1::ADE2 ARF1::HIS3 ARF2::HIS3 ura3 lys2 trp1 his3 leu2 DCP2::DCP2-yEGFP-kanMX4 ROM2::LEU2 (K. lactis)*	This study
YAS2065	*arf1-11* Dcp2-GFP *Δrom2*	*MAT a ade2::arf1-11::ADE2 ARF1::HIS3 ARF2::HIS3 ura3 lys2 trp1 his3 leu2 DCP2::DCP2-yEGFP-kanMX4 ROM2::LEU2 (K. lactis)*	This study
YAS2080	*ARF1* Dcp2-GFP *Δssp120*	*MAT a ade2::ARF1::ADE2 ARF1::HIS3 ARF2::HIS3 ura3 lys2 trp1 his3 leu2 DCP2::DCP2-yEGFP-kanMX4 SSP120::LEU2 (K. lactis)*	This study
YAS2081	*arf1-11* Dcp2-GFP *Δssp120*	*MAT a ade2::arf1-11::ADE2 ARF1::HIS3 ARF2::HIS3 ura3 lys2 trp1 his3 leu2 DCP2::DCP2-yEGFP-kanMX4 SSP120::LEU2 (K. lactis)*	This study
YAS2078	*ARF1* Dcp2-GFP *Δira2*	*MAT a ade2::ARF1::ADE2 ARF1::HIS3 ARF2::HIS3 ura3 lys2 trp1 his3 leu2 DCP2::DCP2-yEGFP-kanMX4 IRA2::LEU2 (K. lactis)*	This study
YAS2079	*arf1-11* Dcp2-GFP *Δira2*	*MAT a ade2::arf1-11::ADE2 ARF1::HIS3 ARF2::HIS3 ura3 lys2 trp1 his3 leu2 DCP2::DCP2-yEGFP-kanMX4 IRA2::LEU2 (K. lactis)*	This study

7.1.3.2 Oligonucleotide primers

Table 7.4: Oligonucleotide primers used in this study

Primer	Designation	Sequence	Purpose
CK095	scp160-S2	GCCAAAATCTATATTGAAAAAAATTGGTTTCAAAGAGCTTGTCTAATCGATGAATTCGAGCTCG	C-terminal tagging (pYM); forward
CK096	scp160-S3	GGTGTCGAAAAGGCCGGTGAAATGGTTTTGAAATCCTTAAGAAGACGTACGCTGCAGGTCGAC	C-terminal tagging (pYM); revers
CK097	scp160-tagtestfor	TGTTGGTAGCGGTGGTCATA	tagging control, forward
CK098	scp160-tagtestrev	GAGGAATTTCGATTGGAGCA	tagging control, reverse
MT-A1	S3-BFR1	GAAAAAAGATTGAAAGAACAGGAAGAGTCTGAAAAAGATAAAGAAAATCGTACGCTGCAGGTCGAC	C-terminal tagging (pYM); forward
MT-A2	S2-BFR1	AGTAATGAAGAAAGATCAGGAGAAAAATTTTTTTCTACTTCAGGTATCGATGAATTCGAGCTCG	C-terminal tagging (pYM); reverse
MT-A42	BFR1-Tagtest	TCCAAAGGATGTCTCCAACC	tagging control, forward
CK087	puf5-S2	TTTGTACAGTAAGAAGGAAAGAAAAAGAAAGAAAAAAAAGTATTAATCGATGAATTCGAGCTCG	C-terminal tagging (pYM); forward
CK088	puf5-S3	ATGAATACCGCTAGAACATCTGATGAACTTCAATTCACTTTGCCACGTACGCTGCAGGTCGAC	C-terminal tagging (pYM); reverse
CK089	puf5-tagtestfor	ATCAAACGGAAGGTGCAAAC	tagging control, forward
CK090	puf5-tagtestrev	AAAAATGCTTGAGCGAATGG	tagging control, reverse
CK091	puf6-S2	AGATGCTTATATACCAAATATTGTGACTTTATCGTAGAAAATTTAATCGATGAATTCGAGCTCG	C-terminal tagging (pYM); forward
CK092	puf6-S3	GATGAAAGTAACAAAGGCTCTCAGCTTTTGGCTAAATTGTTAAAACGTACGCTGCAGGTCGAC	C-terminal tagging (pYM); reverse
CK093	puf6-tagtestfor	AGGCTCTCAGCTTTTGGCTA	tagging control, forward
CK094	puf6-tagtestrev	TCCTGTTCATCATTCGTGGA	tagging control, reverse
CK218	AMS1-S2	TTTGGGAGTGAGTGAATGTAAAAAACAGTGAGGGAGACAAACTCAATCGATGAATTCGAGCTCG	C-terminal tagging (pYM); forward
CK219	AMS1-S3	ATTAAATTGAGACCTTTTGAGATTGCCTCATTCAGGTTGTATTTCCGTACGCTGCAGGTCGAC	C-terminal tagging (pYM); revers
CK220	AMS1-tagtestfor	AACGCGAGACGAATCAAATC	tagging control, forward
CK221	AMS1-tagtestrev	TCTACTCGGGCCATTGGTAG	tagging control, reverse
RG066	CHS5-S3	AATAAGAAGAAGAATAAGAAGAATAAGAAGAAAGGGAAAAAGAAACGTACGCTGCAGGTCGAC	C-terminal tagging (pYM); forward
RG067	CHS5-S2	AAAAAATAAACGTGCGTCGTGGAACTCATTGAAGGCATCCATTAAATCGATGAATTCGAGCTCG	C-terminal tagging (pYM); reverse
RG041	CHS5-tagtestfor	GAGGCCTCTGCTTCTCTTGA	tagging control, forward
RG042	CHS5-tagtestrev	CGGCAAAAATAACGGGTAAA	tagging control, reverse
CK124	ABP1-S2	TTACGTAAGAATAATATAATAGCATGACGCTGACGTGTGATTCTAatcGATGAATTCGAGCTCG	C-terminal tagging (pYM); forward
CK125	ABP1-S3	GGCTCAAAAGGTCTCTTCCCCAGCAATTATGTGTCTTTGGGCAACcgtACGCTGCAGGTCGAC	C-terminal tagging (pYM); reverse
CK132	ABP1-tagtestfor	TGGGATGATGATGAAGACGA	tagging control, forward
CK133	ABP1-tagtestrev	AAGGGAAGGCTCGTGAAAGT	tagging control, reverse
CK128	ABP140-S2	GTTTTATGATGAGAGAGGAGGTGGTACTTGTCTCAGAACTTCCTAatcGATGAATTCGAGCTCG	C-terminal tagging (pYM); forward
CK129	ABP140-S3	AAAATGTACCGCTGCTGGGTACAAGCTGTGTTTGACGTTCCTCAAcgtACGCTGCAGGTCGAC	C-terminal tagging (pYM); reverse
CK134	ABP140-tagtestfor	GACGCAGAACCCGTTACAAT	596 bp before STOP
CK135	ABP140-tagtestrev	ATATGCGCGACGAGAAAACT	69 bp after STOP
CK282	ABP140-S1	ACAATTGTATACCAAATAAGCTATTACAAATTGATTTAAAATGCGTACGCTGCAGGTCGAC	N-terminal tagging (pYM); forward
CK279	BUD5-delfor	ATTAGCGGACCTCTTGAGCGGTGAGCCTCTGGCAAAGAAGAAAGAcagctgaagcttcgtacgc	deletion (pUG); forward
CK280	BUD5-delrev	TACAAGAAGCAAAAGGAAGTCATCTTTCTTTGAACAGTTCTGTTTgcataggccactagtggatctg	deletion (pUG); reverse
CK281	BUD5-deltestfor	TCAAAAACTGGGTTTCGAATAGA	101 before START

Primer	Designation	Sequence	Purpose
CK276	TPM1-delfor	TCTACATAGTAGAACTCACACCCCATACACACAAAAAAGGCAACAcagctgaagcttcgtacgc	deletion (pUG); forward
CK277	TPM1-delrev	CAGCGTGTTGGGGAAAAGAAAAAGAAAACAAAAAACAAAAGTAGAgcataggccactagtggatctg	deletion (pUG); reverse
CK266	TPM1-Ntagtestfor	CTTGGCAAGAAGAAGGTTCG	108 bp before START
CK254	Tpm2-delfor	TTTTCTCATGAGGTTGAGAAAGCATCTAAAATAGCAATTAGCAAAcagctgaagcttcgtacgc	deletion (pUG); forward
CK255	Tpm2-delrev	GTTTGTCGTTTGTATCTTCCGTAATTTTAGTCTTATCAATGGGAAgcataggccactagtggatctg	deletion (pUG); reverse
CK257	Tpm2-deltestfor	AGACTTGGCCTCCTTGGTCT	253 bp before START
CK252	Myo1-delfor	GGTTAGAAGATCATAACAAAGTTAGACAGGACAACAACAGCAATAcagctgaagcttcgtacgc	deletion (pUG); forward
CK253	Myo1-delrev	TAAATAAAGGATATAAAGTCTTCCAAATTTTTAAAAAAAAGTTCGgcataggccactagtggatctg	deletion (pUG); reverse
CK256	Myo1-deltestfor	CCCAAAAGGGTAATTGCGTA	187 bp vor START
CK282	ABP140-S1	ACAATTGTATACCAAATAAGCTATTACAAATTGATTTAAAATGCGTACGCTGCAGGTCGAC	N-terminal tagging (pYM); forward
CK298	ABP140-S4	TTCCTTTGAGATGCTTTCGAATTTCTTGATCAAATCTGCGACACCCATCGATGAATTCTCTGTCG	N-terminal tagging (pYM); reverse
CK264	ABP140-Ntagtestfor	CGTAGGATTGGACACGAGGT	110 bp vor START
CK497	ABP140-51-S4	TTTGAGAGGCTTTGATGAACTGTTTGTATCAACGGTAGCATCGCCCATCGATGAATTCTCTGTCG	N-terminal tagging (pYM), reverse; deletes first 51 bp
CK283	ABP140-S4-STOP	TTCCTTTGAGATGCTTTCGAATTTCTTGATCAAATCTGCGACACCCTACATCGATGAATTCTCTGTCG	N-terminal “tagging” (pYM), reverse; includes STOP
CK457	ABP140-612COREf	AATGGCAAAGAAACTGAAAATGCCGAAAACGCTTCTCAACAAGCTTCCTTACCATTAAGTTGATC	Mutagenesis; insertion of pCORE
CK458	ABP140-747COREr	TTGAATGGCGGAGGTTGTTGATGACGTGGTGTCGCCGGTTGTATCGAGCTCGTTTTCGACACTGG	Mutagenesis; insertion of pCORE
CK459	ABP140-Drna-DPf	AATGGCAAAGAAACTGAAAATGCCGAAAACGCTTCTCAACAAGCTGATACAACCG	Mutagenesis; ΔRNA
CK460	ABP140-Drna-DPr	TTGAATGGCGGAGGTTGTTGATGACGTGGTGTCGCCGGTTGTATCAGCTTGTTGA	Mutagenesis; ΔRNA
CK461	ABP140-509seqfor	CATCTGAACCAGCCGAAGA	sequencing
CK291	ABP140-831-COREf	GCCATTCAAGAAGTGAATGATTTGGAAGTTGTTGATGACTCTTGTTCCTTACCATTAAGTTGATC	Mutagenesis; insertion of pCORE
CK292	ABP140-831-COREr	CTGAGTTAACGCTTTCAAATGCTCCCTATTATGCTGTTGATCAATGAGCTCGTTTTCGACACTGG	Mutagenesis; insertion of pCORE
CK293	ABP140-uugDa-DPf	TTCAAGAAGTGAATGATTTGGAAGTTGTTGATGACTCTTGTttgGGCATTGATC	Mutagenesis; CUUAGGC -> uugGGC
CK294	ABP140-uugDa-DPr	TAACGCTTTCAAATGCTCCCTATTATGCTGTTGATCAATGCCcaaACAAGAG	Mutagenesis; CUUAGGC -> uugGGC
CK295	ABP140-762for	CACCACGTCATCAACAACCT	sequencing
CK306	ABP140N17-S3	GTCGCAGATTTGATCAAGAAATTCGAAAGCATCTCAAAGGAAGAACGTACGCTGCAGGTCGAC	C-terminal truncation (pYM); fwd
CK489	ABP140-201-S3	GACGTAAATGAAGAGTTTGAGAATGAACCAGAAACAATTAACAGTcgtACGCTGCAGGTCGAC	C-terminal truncation (pYM); fwd
CK490	ABP140-402-S3	GAAAATACTGGCGCTGAAGTTCTTGCAAGTAGTGTTGAAGAATCCcgtACGCTGCAGGTCGAC	C-terminal truncation (pYM); fwd
CK479	ABP140-612-S3	AATGGCAAAGAAACTGAAAATGCCGAAAACGCTTCTCAACAAGCTcgtACGCTGCAGGTCGAC	C-terminal truncation (pYM); fwd
CK480	ABP140-750-S3	AACGCTAATGTCGACGACAGCACCAAAACCGGTGAAAATGATGATcgtACGCTGCAGGTCGAC	C-terminal truncation (pYM); fwd
CK481	ABP140-831-S3	ATTCAAGAAGTGAATGATTTGGAAGTTGTTGATGACTCTTGTCTTcgtACGCTGCAGGTCGAC	C-terminal truncation (pYM); fwd
CK482	ABP140-17pOMfor	GTCGCAGATTTGATCAAGAAATTCGAAAGCATCTCAAAGGAAGAAtgcAGGTCGACAACCCTTAAT	internal tagging after aa 17 (pOM)
CK484	ABP140-17pOMrev	TTTGAGAGGCTTTGATGAACTGTTTGTATCAACGGTAGCATCGCCgcgGCCGCATAGGCCACT	internal tagging after aa 17 (pOM)
JW24	TIF4632-S2	GAATTAAAAAGGAAAAAGACTAGCTTATCGTTTCTAAAAGAAAATCTTTTAatcgatgaattcgagctcg	C-terminal tagging (pYM); reverse
JW25	TIF4632-S3	CCAAGAGCTAATATGTTCGACGCATTAATGAATAACGATGGGGACAGTGATcgtacgctgcaggtcgac	C-terminal tagging (pYM); forward
JW30	TIF4632-internal	CGTGAAGGAATTGAGGGAAA	tagging control, forward
JW03	EDC3-S3	TTCCAAAACTGTGATCTTTTCGTCACTGACGGGTCCCTGCTATTAGATTTGCGTACGCTGCAGGTCGAC	C-terminal tagging (pYM); forward

Primer	Designation	Sequence	Purpose
JW04	EDC3-S2	ACCGTATGCTTATACGTATCTATCCAGTTTAGGCTAAAGTAATTCTTGGTTTAATCGATGAATTCGAGCTCC	C-terminal tagging (pYM); reverse
JW14	EDC3-internal	CGTCGGAAGTTATTGAAAGCA	tagging control, forward
CK246	sar1-delfor	CTTTTCTAGAAACATCATTATAACTAACAATATATAATTGGAATAcagctgaagcttcgtacgc	deletion (pUG); forward
CK247	sar1-delrev	GAATTCATGTGAATGTCATATAAAGGGTATAGATGTATACGTCAAgcataggccactagtggatctg	deletion (pUG); reverse
CK251	sar1-deltestfor	AACGCGTTGACCAGAAAACT	165 bp before START
CK230	URA3-ext-b	CATGGCAATTCCCGGGGATCgtgattctgggtagaagatcg	Allele Replacement
CK231	URA3-ext-a'	CATGGTGGTCgaCTGGAATTatcccaatacaacagatcacg	Allele Replacement
CK232	URA3-int-a	cttgacgttcgttcgactgatgagc	Allele Replacement
CK233	URA3-int-b	gagcaatgaacccaataacgaaatc	Allele Replacement
CK236	SEC21-A'	AATTCCAGtcGACCACCATGGACAAAAGCCAAGAAGCGATA	Allele Replacement
CK237	SEC21-B	GATCCCCGGGAATTGCCATGCTATTGATAACAAAAGAAGGGATTAAC	Allele Replacement
CK238	SEC27-A'	AATTCCAGtcGACCACCATGAAGACACCCAATCGAAACAA	Allele Replacement
CK239	SEC27-B	GATCCCCGGGAATTGCCATGATACACCGGCGAAGAAGAAA	Allele Replacement
JW001	PUB1-S3	CCGGTTATGTCTGAGCAACAACAGCAACAGCAGCAACAGCAGCAACAACAACGTACGCTGCAGGTCGAC	C-terminal tagging (pYM); forward
JW002	PUB1-S2	GCCTCTCTTTCTTCTTTCTTTTTGTTTCATTCCACTTTTCTTCATAATATTTAATCGATGAATTCGAGCTCC	C-terminal tagging (pYM); reverse
JW015	PUB1-internal	TGTCTGAGCAACAACAGCAA	tagging control, forward
CK273	HOG1-delfor	GGAACAAAGGGAAAACAGGGAAAACTACAACTATCGTATATAATAcagctgaagcttcgtacgc	deletion (pUG); forward
CK318	HOG1-delrev2	AAAAAGAAGTAAGAATGAGTGGTTAGGGACATTAAAAAAACACGTgcataggccactagtggatctg	deletion (pUG); reverse
CK278	HOG1-deltestfor2	TTTGTATAGTGGAAGAGGAATTTGC	160 bp before START
CK240	Sho1-delfor	TCAACGCCATCTTTTCAGAAACACCAAAAATCACGTTTTCAAAATcagctgaagcttcgtacgc	deletion (pUG); forward
CK241	Sho1-delrev	TTTTTTCCTTTGACTCGAGAATCCATGCTATAAGATTGTTAATCAgcataggccactagtggatctg	deletion (pUG); reverse
CK248	sho1-deltestfor	GAGCCTCGTTTTCAGTGAGG	176 bp before START
CK316	SKO1-delfor	CATTCCAAATACACCTGCCCAGTCTCTAGACCCTGCTTAATCATTcagctgaagcttcgtacgc	deletion (pUG); forward
CK317	SKO1-delrev	CGAAAGCATCAGATAGAAGACTATTTAAGAACCCCGTCGCTATCTCGgcataggccactagtggatctg	deletion (pUG); reverse
CK313	SKO1-deltestfor	CCAAAGGGGTTCAACGTAAA	224 bp before START
CK327	SLT2-pUGdelfor	AAAATAGTAGAAATAATTGAAGGGCGTGTATAACAATTCTGGGAGcagctgaagcttcgtacg	deletion (pUG); forward
CK328	SLT2-pUGdelrev	TCTATGGTGATTCTATACTTCCCCGGTTACTTATAGTTTTTTGTCgcataggccactagtggatctg	deletion (pUG); reverse
CK331	slt2-deltestfor	CTACGTATGCGGCGATTTTT	315 bp before START
CK369	CNB1-pUGdelfor	ACTCAATGGTGATCAGAATCCATAGAAGCATTTTTATTTCTTAAAcagctgaagcttcgtacg	deletion (pUG); forward
CK370	CNB1-pUGdelrev	TTAAAAATATTGGCATACCATAAATGAATGAAGTGTCCCCTAGTCgcataggccactagtggatctg	deletion (pUG); reverse
CK373	CNB1-deltestfor	GAAGGCCGGGTATCATCTTA	155 bp before START
CK334	ypk1-pUGdelfor	TCAAAGTTCCTCTCATATCAACAAACATTAATACAGTTCCTGAAAcagctgaagcttcgtacg	deletion (pUG); forward
CK335	ypk1-pUGdelrev	TTATATAAAGTATGTCATGAGTAAACTAGTTGATAATGTATTCACTAAGTgcataggccactagtggatctg	deletion (pUG); reverse
CK339	ypk1-deltestfor	ACGAGCCAACGGTAATCAAC	214 bp before START
CK376	CMK1-pUGdelfor	TATATAATATTGGAAGACACCAGAAAAAATAACGAGTCAATTACTcagctgaagcttcgtacg	deletion (pUG); forward
CK377	CMK1-pUGdelrev	TCATTGAAGATTTATTCGCCAGTGTGGTAAAACGGCATACTGTTAgcataggccactagtggatctg	deletion (pUG); reverse
CK378	CMK2-pUGdelfor	ACCTTTTCTTCTATCACATCGCCAATATAAATATAGACACCAAAAcagctgaagcttcgtacg	deletion (pUG); forward
CK379	CMK2-pUGdelrev	TAAATATTATATACGAATTTATGTACACGAATTCAAGTCCGTAATgcataggccactagtggatctg	deletion (pUG); reverse

Primer	Designation	Sequence	Purpose
CK381	CMK1-deltestfor	CGAAAGCCACATCGACTACA	108 bp before START
CK382	CMK2-deltestfor	CCACCCATTGCTGTTTCTCT	143 bp before START
JW114	gcn2-delfor	TTTTTTTTCA ATAATTTTCC GTTCCCCTTA ACACATACTA TGTATAA cagctgaagcttcgtacg	deletion (pUG); forward
JW115	gcn2-delrev	TTTACCTTTA ACTGATGCGT TATAGCGCCG CACAGATCTT TAAAGGC gcataggccactagtggatctg	deletion (pUG); reverse
JW116	gcn2-deltestfor	CCCAACATCACTTTACACGAA	deletion control; forward
JW118	ire1-delfor	TAAAAAAACA GCATATCTGA GGAATTAATA TTTTAGCACT TTGAAAA cagctgaagcttcgtacg	deletion (pUG); forward
JW119	ire1-delrev	CATTAATGCA ATAATCAACC AAGAAGAAGC AGAGGGGCAT GAACATG gcataggccactagtggatctg	deletion (pUG); reverse
JW120	ire1-deltestfor	GGAGATCAATGAGCCAACTT	deletion control; forward
CK427	cmd1-A'	AATTCCAGtcGACCACCATGCCCGCGTAAGAAGGTGTTTA	Allele Replacement
CK428	cmd1-B	GATCCCCGGGAATTGCCATGCCAGTGGTCCCAAAGAAAAA	Allele Replacement
JW110	cmd1-delfor	ATCGAACTACAAAGAAAGAGCTTAGTTAATACAAATAAAAAAGTACAcagctgaagcttcgtacg	deletion (pUG); forward
JW111	cmd1-delrev	GAATGGTAAGGGTAAGATAGCGGGAGCAAAAAATCACAAGGATGCACgcataggccactagtggatctg	deletion (pUG); reverse
JW112	cmd1-deltestfor	TTCAAGCACCCTCTTTTCCA	deletion control; forward
JW113	cmd1-deltestrev	TGCGTGTGGTTGTCAAACTT	deletion control; reverse
CK076	pat1-pUGdelfor	AGGTTTTAACCGGAAGTAAGAGCAGCAAGAAGCACTAGCAcagctgaagcttcgtacgc	deletion (pUG); forward
CK077	pat1-pUGdelrev	TTATGAAAAAAAAAGGATAACAAACTTATATAAACTTATAgcataggccactagtggatctg	deletion (pUG); reverse
CK078	pat1-deltestfor	ACCGGTTGATCCTACTCGTG	deletion control; forward
CK079	pat1-deltestrev	GTGATCGACGTACCATGACG	deletion control; reverse
CK061	scd6-pUGdelfor	AGGATGTCGTAGAAGAAGCATTCATCGAAAAACAGCAGCAAGGCAcagctgaagcttcgtacgc	deletion (pUG); forward
CK062	scd6-pUGdelrev	CTGAATGATATACTTAATTTACATAGAAACATCATTgcataggccactagtggatctg	deletion (pUG); reverse
CK065	scd6-deltestfor	ACGTGGAGGCAGTCAGAAAG	82 bp before START
CK066	scd6-deltestrev	CGGATGGAAGAAGCCATAAA	221 bp after STOP
CK470	scd6-S3	AGACCAGCCAACCAGTTTTCGCAACCTCCTTCCAACGTTGAATTTCGTACGCTGCAGGTCGAC	C-terminal tagging (pYM); forward
CK471	scd6-S2	TACATACTGAATGATATACTTAATTTACATAGAAACATCATTTTAATCGATGAATTCGAGCTCG	C-terminal tagging (pYM); reverse
CK472	scd6-tagtestfor	TGAACGTTGACACCTTTGGA	238 bp before STOP
CK492	PAT1-S3	TGGGGTTGGTGTATCGCGATGGTGAAATATCAGAACTAAAGcgtACGCTGCAGGTCGAC	C-terminal tagging (pYM); forward
CK493	PAT1-S2	AAAAAATACATGCGTAAGTACATTAAAATTACAGGAAAAATCTTAATCGATGAATTCGAGCTCG	C-terminal tagging (pYM); reverse
CK462	PAT1-1939-COREf	AATTTGATCACCATTTTGATTTCTCGTGCCGCATTAATCAAGCAATCCTTACCATTAAGTTGATC	Mutagenesis; insertion of pCORE
CK463	PAT1-1939-COREr	TGTGGAGATTTCAGGAGAGGAAAGAATATTAGATCTTGATGAATCGAGCTCGTTTTCGACACTGG	Mutagenesis; insertion of pCORE
CK485	PAT1-E647A-DPf-2	TTTGATTTCTCGTGCCGCATTAATCAAGCAAGcTTCATCAAGATCTAATATTCTTTCCTCTCCTG	Mutagenesis; *pat1-E647A*
CK465	PAT1-D658V-DPr	TATCATAAATCTCATTCCATGTGGAGATTaCAGGAGAGGAAAGAATATTAGATCTT	Mutagenesis; *pat1-E647A*
CK466	PAT1-2054seqrev	TCCCTTGGAGGGAAAATCAG	sequencing
CK068	dhh1-S2	AAGCGTATCTCACCACAGTAGTTATTTTTTCTTAGATATTCTTTAATCGATGAATTCGAGCTCG	C-terminal tagging (pYM); forward
CK086	dhh1-S3-2	GAACATTTCATGGCGATGCCACCTGGTCAGTCACAACCCCAGTATCGTACGCTGCAGGTCGAC	C-terminal tagging (pYM); reverse
CK070	dhh1-tagtestfor	CAAGCGATACCTCAGCAACA	tagging control, forward
CK071	dhh1-tagtestrev	AATAAAAACGGTGCGCAAAT	tagging control, reverse
CK430	pub1-pUGdelfor	GTTCATAATAAGAAGATTACCACATCTACTCTTTGTTCGATTCCAcagctgaagcttcgtacg	deletion (pUG); forward
CK431	pub1-pUGdelrev	TCTTTATTCTTTCTTTTTGTTTCATTCCACTTTTCTTCATAATATgcataggccactagtggatctg	deletion (pUG); reverse

Primer	Designation	Sequence	Purpose
CK432	pub1-deltestfor	CCGTCTTTCCTTGTCCTTCA	207 bp before START
CK422	CMD1-S3	TCAGGCGAGATCAACATTCAACAATTCGCTGCTTTGTTATCTAAAcgtACGCTGCAGGTCGAC	C-terminal tagging (pYM); forward
CK423	CMD1-S2	GTAAGGGTAAGATAGCGGGAGCAAAAAATCACAAGGATGCACCTAatcGATGAATTCGAGCTCG	C-terminal tagging (pYM); reverse
CK426	CMD1-tagtestfor	GTGAATTGGCCACTGTGATG	352 bp before STOP
CK429	cmd1-tagtestrev	ATTTGCGTGTGGTTGTCAAA	106 bp after STOP
CK467	EDC3-pUGdelfor	ATCCATGCTCTCAAGACAATACAGTAATTCGTAAAAGAAACCATAcagctgaagcttcgtacg	deletion (pUG); forward
CK468	EDC3-pUGdelrev	ATGCTTATACGTATGTATCCAGTTTAGGCTAAAGTAATTCTTGGTgcataggccactagtggatctg	deletion (pUG); reverse
CK469	EDC3-deltestfor	ACCCTGGTATCAAGCGTCAC	339 bp before START
CK383	ROM2-pUGdelfor	ATTACTGCTGACTTAATTGGACAATTCATCTCTTTTCCTGCGGTTcagctgaagcttcgtacg	deletion (pUG); forward
CK384	ROM2-pUGdelrev	TTTTTATTCTAAAGAAAATAAGGAAAGTCTATATACGTTGCTATCgcataggccactagtggatctg	deletion (pUG); reverse
CK385	YCK2-pUGdelfor	TTCTACTGAACACAGCATATAAGCCAAGAAAATAGTTTTCCAAAAcagctgaagcttcgtacg	deletion (pUG); forward
CK386	YCK2-pUGdelrev	GACGGTGGTGGGAATGATTACAAAAAACCTCCTCCGTTTTCTATTgcataggccactagtggatctg	deletion (pUG); reverse
CK387	MHP1-pUGdelfor	GCACTTAAATACGCAAAATATACAAGATAGCCCTACAACTGCTCCcagctgaagcttcgtacg	deletion (pUG); forward
CK388	MHP1-pUGdelrev	CGAAACCCAATACAAAAAAGAGATTAAAAAATTAAGAGAAATCCCgcataggccactagtggatctg	deletion (pUG); reverse
CK389	CYR1-pUGdelfor	TGCGAAACGAGCTAAAGCAACAGCAAACGAAATCCCTAGGTCGAAcagctgaagcttcgtacg	deletion (pUG); forward
CK390	CYR1-pUGdelrev	AATATGAAACGAGTAACAGGGTGGTACATAATTTACGAACAGAACgcataggccactagtggatctg	deletion (pUG); reverse
CK391	DOT6-pUGdelfor	AGCTTCCGTGCACGTTCCAGTCTTCCCTCCCTTCTCTGCTCCGTGcagctgaagcttcgtacg	deletion (pUG); forward
CK392	DOT6-pUGdelrev	TGATATTTTTTTATTTTTATTTTTTTTTCATTTTAAGTTTTCCCCgcataggccactagtggatctg	deletion (pUG); reverse
CK393	Ybr238c-pUGdelfor	ATATTTCTTACTCTAATTGCTTTTCTATCTTGCAAATCTGATCCTcagctgaagcttcgtacg	deletion (pUG); forward
CK394	Ybr238c-pUGdelrev	TTTTGTTCTGTAGAGAAAGAAGGTGAAAAGTGAAGGATATTAACTgcataggccactagtggatctg	deletion (pUG); reverse
CK395	Yol087c-pUGdelfor	AGAAGAGCAAGCCAATAAAAAGCCGGAGAAAATAGAAAGGTAATAcagctgaagcttcgtacg	deletion (pUG); forward
CK396	Yol087c-pUGdelrev	AAAACTCCAAATTCAGACCCCAAAATATAATTTAAATAAACATTAgcataggccactagtggatctg	deletion (pUG); reverse
CK397	IRA2-pUGdelfor	TGATATCAACTAAACTGTATACATTATCTTTCTTCAGGGAGAAGCcagctgaagcttcgtacg	deletion (pUG); forward
CK398	IRA2-pUGdelrev	TACAGATAGATATTGATATTTCTTTCATTAGTTTATGTAACACCTgcataggccactagtggatctg	deletion (pUG); reverse
CK399	SSP120-pUGdelfor	CAAGACCTAAAATTTTTTCATCCCTGTTCTATTAAAATTGTGGAAcagctgaagcttcgtacg	deletion (pUG); forward
CK400	SSP120-pUGdelrev	CTTGAATATTTTCTCAGTCTCAACTATTCATCTTGACCAAGTCCAgcataggccactagtggatctg	deletion (pUG); reverse
CK401	ROM2-deltestfor	TGGTATGGAAGTCCGAGGTC	255 bp before START
CK402	YCK2-deltestfor	GAACGTGGTTGTGTTTCGTG	124 bp before START
CK403	MHP1-deltestfor	TACAAGCAAATGCTGCGTTC	146 bp before START
CK404	CYR1-deltestfor	TCTTGCTGCAGTTCACAACC	99 bp before START
CK405	DOT6-deltestfor	CCGTGTTTCCTCCTTTTCAC	90 bp before START
CK406	Ybr238c-deltestfor	TATGCCATGGACATCTCGAA	235 bp before START
CK407	Yol087c-deltestfor	GCCATTCCTAACGAGGAAAC	99 bp before START
CK408	IRA2-deltestfor	AGACCGAAAAAGCGAAAACA	211 bp before START
CK409	SSP120-deltestfor	AGCTCAGGCAAATTGAGCAT	203 bp before START
CK152	PEP4-realfor	TTGCTGCAAAAGTCCACAAG	FISH probe, forward
CK191	PEP4-FISHrev	TAATACGACTCACTATAGGGAGCGCCTAAACCGATACCTTCA	FISH probe, reverse; includes T7
CK154	YPL279C-realfor	CCGACCGTTCTCTGGTCTAA	FISH probe, forward

Primer	Designation	Sequence	Purpose
CK192	YPL279C-FISHrev	TAATACGACTCACTATAGGGAGACTCAAAGTGCCGCAAAATC	FISH probe, reverse; includes T7
CK156	YEL057C-realfor	GCGAGGTTGGAGTAGTCAGC	FISH probe, forward
CK193	YEL057C-FISHrev	TAATACGACTCACTATAGGGAGCGGACCAGGAAAGAAAATTG	FISH probe, reverse; includes T7
CK158	DAN1-realfor	AATTGCCAAGGCTGTTTTTG	FISH probe, forward
CK194	DAN1-FISHrev	TAATACGACTCACTATAGGGAGTGGAGCACAAGACTGCAAAC	FISH probe, reverse; includes T7
CK160	CDA1-realfor	CACACACGTGGTCACATGAA	FISH probe, forward
CK195	CDA1-FISHrev	TAATACGACTCACTATAGGGAGTTGCACTGACAACGAAGAGG	FISH probe, reverse; includes T7
CK162	HXT2-realfor	TCGTGCTATGGCTATTGCTG	FISH probe, forward
CK196	HXT2-FISHrev	TAATACGACTCACTATAGGGAGGATGCTTGAAGGCGAAAAAC	FISH probe, reverse; includes T7
CK164	OPT2-realfor	TTTCACACAGGGTGGTTTCA	FISH probe, forward
CK197	OPT2-FISHrev	TAATACGACTCACTATAGGGAGTGGTGGCGAGTAGCTTTGAT	FISH probe, reverse; includes T7
CK166	MOH1-realfor	CGTGAGCTTCATCACCTACG	FISH probe, forward
CK198	MOH1-FISHrev	TAATACGACTCACTATAGGGAGTACCCTTTTCCAGGATCGTC	FISH probe, reverse; includes T7
CK168	YPL277C-realfor	CTCTTTCGGCTTGAGGTCAC	FISH probe, forward
CK199	YPL277C-FISHrev	TAATACGACTCACTATAGGGAGCCATGTCCAATTGCTTTTCC	FISH probe, reverse; includes T7
CK170	AMS1-realfor	ACCCACATGGAGTGGTGAAT	FISH probe, forward
CK200	AMS1-FISHrev	TAATACGACTCACTATAGGGAGTAGCATCAGTGACCGCAGTT	FISH probe, reverse; includes T7
CK172	YFL068W-realfor	AACGCAAACGCTGAAAAACT	FISH probe, forward
CK201	YFL068W-FISHrev	TAATACGACTCACTATAGGGAGGACTACCACTGCCAGCATCA	FISH probe, reverse; includes T7
CK174	CHS5-realfor	AAGAAGCAACGGGACAGAAA	FISH probe, forward
CK202	CHS5-FISHrev	TAATACGACTCACTATAGGGAGGGAACTCATTGAAGGCATCC	FISH probe, reverse; includes T7
CK176	CSR2-realfor	CCCGCTTAATTTGGTGAGAA	FISH probe, forward
CK203	CSR2-FISHrev	TAATACGACTCACTATAGGGAGACCGCGTCTTGGTTTATTCA	FISH probe, reverse; includes T7
CK178	YAR064W-realfor	GGACTTTTGTCAGCCACGTC	FISH probe, forward
CK204	YAR064W-FISHrev	TAATACGACTCACTATAGGGAGGAACTCAAGTCTGCGGAGGA	FISH probe, reverse; includes T7
CK182	VPS13-realfor	CAAACTCAGCGCAATCCTTT	FISH probe, forward
CK205	VPS13-FISHrev	TAATACGACTCACTATAGGGAGTTTCAATCCCTTCCTTTAGCC	FISH probe, reverse; includes T7
CK184	CRN1-realfor	ATTGAAGCCAGAGCCAGTGT	FISH probe, forward
CK206	CRN1-FISHrev	TAATACGACTCACTATAGGGAGGCAAACGTGCACCTACAAAA	FISH probe, reverse; includes T7
CK186	HBT1-realfor	CAAGACCTTCAGCTCGAACC	FISH probe, forward
CK207	HBT1-FISHrev	TAATACGACTCACTATAGGGAGTTACCAGCCTGTTCCTCACC	FISH probe, reverse; includes T7
CK126	ABP1-FISHfor	CGATTGGAATGAGCCTGAAT	FISH probe, forward
CK127	ABP1-FISHrev	TAATACGACTCACTATAGGGAGAATAGCATGACGCTGACGTG	FISH probe, reverse; includes T7
CK130	ABP140-FISHfor	CAGGCGATCAGAATGCAGTA	FISH probe, forward
CK131	ABP140-FISHrev	TAATACGACTCACTATAGGGAGATATGCGCGACGAGAAAACT	FISH probe, reverse; includes T7
CK284	ABP140-fishfor2	CTCAAAGGAAGAAGGCGATG	FISH probe, forward
CK285	ABP140-fishrev2	TAATACGACTCACTATAGGGAGTCATTTTCACCGGTTTTGGT	FISH probe, reverse; includes T7
CK307	yeGFP-FISHfor	GGTGCTGGAGCAATTCTGTC	FISH probe, forward

Primer	Designation	Sequence	Purpose
CK308	yeGFP-FISHrev	TAATACGACTCACTATAGGGAGCATGGGTAATACCAGCAGCA	FISH probe, reverse; includes T7
CK049	HAC1-nor-for	TCGCAATCGAACTTGGCTAT	Northern Probe
CK054	HAC1-nor-rev2	ATCTGCAGCTCCCATGAAGT	Northern Probe
CK473	ABP140-realfor	ACCGAGGAATCTGACGTTTG	qPCR
CK474	ABP140-realrev	GCCTGCTGGACTTGTTCTTC	qPCR
CK475	PGK1-realfor	TTCTCTGCTGATGCCAACAC	qPCR
CK476	PGK1-realrev	CAGCCAGCTGGAATACCTTC	qPCR
common	Kan&HIS-Primer	tgggcctccatgtcgctgg	internal tagging control, reverse
common	TRP-Primer	GCTATTCATCCAGCAGGCCTC	internal tagging control, reverse
BZ055	pUG73-LEU2rev	ctaacgtgcttgcctcttcc	internal tagging control, reverse
BZ056	pUG72-URA3rev	ggacagaaaattcgccgata	internal tagging control, reverse
CK320	pUG72-URA3160rev	cacggtgcaacactcacttc	internal tagging control, reverse
CK495	ActA-XbaI-for	agtTCTAGAATGTTGATTTTAGCTATGTTGGCTATTGGTGTTTTTTCTTTGGGTGCTTTTATT	pYM-N7-ActA cloning
CK496	ActA-XbaI-rev	actTCTAGAGCGTTATTCTTTCTCAATTGGATAATTTTAATAAAAGCACCCAAAGAAAAA	pYM-N7-ActA cloning
CK516	BamHI-Cit1for	AGAAGGATCCGAAAATAAGGCAAAACATATAGCAA	mitoGFP cloning
CK517	NotI-Cit1rev	AGAAGCGGCCGCACTATAGTGGCGAGCATTCAATAG	mitoGFP cloning

7.1.3.3 Plasmids

Table 7.5: Plasmids used in this study

Plasmid	Description	Source
pUG6	loxP-kanMX4-cassette	J. Hegemann
pUG72	loxP-URA3 cassette	J. Hegemann
pUG73	loxP-LEU2 cassette	J. Hegemann
pSH63	Cre-recombinase, TRP1	J. Hegemann
pSH47	Cre-recombinase, URA3	J. Hegemann
pYM6	9myc-TRP1-cassette	E. Schiebel
pYM12	yeGFP-kanMX4-cassette	E. Schiebel
pFA6a-NAT	natNT2-cassette	M. Knop
pYM26	yeGFP-TRP1-cassette	M. Knop
pYM29	EGFP-TRP1-cassette	M. Knop
pYM43	RedStar2-natNT2-cassette	M. Knop
pYM51	eqFP611-kanMX4-cassette	M. Knop
pYM51-NAT	eqFP611-natNT2-cassette	this study
	PvuII-BglII fragment from pYM51 containing eqFP611 was inserted into PvuII-BglII-restricted pYM43	
pYM-N7	natNT2-pADH-cassette	M. Knop
pYM-N7-ActA	natNT2-pADH-ActA-cassette	this study
	CK495/496 was inserted into XbaI site of pYM-N7 downstream of ADH1-promoter to introduce ActA incl. N-terminal ATG in frame with downstream ATG on S4-Primer	
pYM-N9	natNT2-pADH-yeGFP-cassette	M. Knop
pYM-4GFP-Kan	4xGFP-kanMX4-cassette	C. Taxis
pOM60	kanMX4-yeGFP-cassette	M. Trautwein
pFA6a-HBH-TRP1	HBH-TRP1-cassette	P. Kaiser
pCORE	kanMX4-URA3-cassette	M.A. Resnick
pSM1960	Sec63-RFP expression, *URA3*	S. Michaelis
pSM1959	Sec63-RFP expression, *LEU2*	S. Michaelis
pG14-MS2-GFP	MS2-GFP expression, *LEU2*	P. Chartrand
Cit1-GFP	mitoGFP expression, *LEU2*	this study
	CK516/517 product on genomic DNA (first 38 aa of Cit1p) was inserted into BamHI/NotI restricted pG14-MS2-GFP to yield Cit1N-GFP	
pMYY3-1	*sar1-D32G* expression, *TRP1*	A. Nakano
pHS47	*cmd1-3* expression, *URA3*	E. Schiebel
pRS406	chromosomal integration	P. Hieter

7.1.3.4 Antibodies

Table 7.6: Antibodies used in this study

Antibody	Dilution	Source
Rabbit anti-Sec61p, polyclonal	1:1,000 WB	R. Schekman/M.Spiess
Rabbit anti-Chs5p, polyclonal, affinity purified	1:500 WB	M. Trautwein
Mouse anti-Pgk1p, monoclonal	1:1,000 WB	Molecular Probes
Goat anti-Mpk1p, yN-19, polyclonal	1:1,000 WB	Santa Cruz Biotechnology
Rabbit anti-phospho-p44/42 MAP kinase (Thr202/Tyr204)	1:1,500 WB	Cell Signaling
Rabbit anti-GFP, polyclonal purified	1:1,000 WB; 1:400 IF, 1:200 FISH/IF	Torrey Pines
Mouse anti-Myc-epitope, 9E10, monoclonal	1:1,000 WB	Sigma
Goat anti-rabbit-HRP	1:30,000 WB	Pierce
Goat anti-mouse-HRP, polyclonal purified	1:10,000 WB	Pierce
Rabbit anti-goat-HRP	1:40,000 WB	Pierce
Goat anti-rabbit-Alexa680	1:10,000 WB	Molecular Probes

Antibody	Dilution	Source
Goat anti-mouse-Alexa680	1:10,000 WB	Molecular Probes
Goat anti-rabbit-IRDye800	1:10,000 WB	Rockland
Goat anti-rabbit-IRDye800	1:10,000 WB	Rockland
ImmunoPure Streptavidin, HRP-conjugated	1:6,600 WB	Thermo Scientific
Sheep anti-digoxigenin-AP F_{ab}-fragment	1:5,000 FISH	Roche
anti-Dig-POD F_{ab}-fragment	1:750 FISH/IF	Roche
AlexaFluor488 chicken anti-rabbit-	1:200 FISH/IF	Invitrogen
Goat anti-rabbit IgG	EM	BBInternational
Rabbit anti-Myc-epitope	EM	Abcam

7.1.3.5 Web resources

Resource	URL	Application
Entrez Pubmed	http://www.ncbi.nlm.nih.gov/sites/entrez?db=pubmed	literature searches
SGD	http://www.yeastgenome.org/	genomic sequences; data mining
Proteome	https://portal.biobase-international.com/cgi-bin/portal/login.cgi	data mining
BioGrid	http://thebiogrid.org/	data mining
Euroscarf	http://web.uni-frankfurt.de/fb15/mikro/euroscarf/index.html	plasmid sequences
NEB enzyme finder	http://www.neb.com/nebecomm/EnzymeFinder.asp	cloning
ExPASy Translate Tool	http://www.expasy.ch/tools/dna.html	cloning
Primer3	http://fokker.wi.mit.edu/primer3/input.htm	primer design
Reverse complement	http://www.bioinformatics.org/sms/rev_comp.html	primer design
NCBI Blast	http://blast.ncbi.nlm.nih.gov/Blast.cgi	Blast
RNAfold	http://rna.tbi.univie.ac.at/cgi-bin/RNAfold.cgi	RNA secondary structure prediction
RNAbindR	http://bindr2.gdcb.iastate.edu/RNABindR/	RNA-binding domain prediction
FunSpec	http://funspec.med.utoronto.ca/	MIPS enrichment
DAVID	http://david.abcc.ncifcrf.gov/home.jsp	functional clustering
Harlequin	http://harlequin.jax.org/polyA/	yeast 3'UTR lengths
Yeast_translation	www.stanford.edu/yeast_translation/data.shtml	yeast translation profiles
Yeast GFP database	http://yeastgfp.yeastgenome.org/getOrf.php?orf=YOR239W	yeast GFP fusion localization
ImageJ	http://rsb.info.nih.gov/ij/plugins/index.html	image analysis
Beckman	http://www.beckmancoulter.com/resourcecenter/labresources/centrifuges/rotorcalc.asp	g to rpm conversion

7.1.4 Biochemical methods[2]

7.1.4.1 Determination of yeast cell density

1 OD_{600} corresponds to 1.5×10^7 yeast cells per ml on the spectrophotometer Ultrospec 3100 *pro* (Amersham Biosciences). For OD_{600} measurements, cells were diluted to yield an OD_{600} of no more than 0.7. Unless otherwise indicated, logarithmically growing cells were harvested at an OD_{600} between 0.3 and 0.7.

7.1.4.2 Preparation of yeast total cell extract

15 ml of yeast culture were harvested and the cells resuspended in 150 µl 6 x Laemmli buffer. Approximately 120 µl of glass beads were added. After vigorous vortexing for 5 min, samples were incubated for 5 min at 65°C followed by an additional 1 min of vortexing. Cell debris and glass beads were sedimented (2 min, 10,000 g) and the supernatant was transferred to a fresh reaction tube. For subsequent analysis by SDS-PAGE and immunoblotting, 2-5 µl of the lysate were loaded per lane.

For comparison of protein expression levels, Laemmli buffer was replaced by lysis buffer (LowDTT). The lysates were normalized to equal total protein concentration using the Biorad DC protein assay. Routinely, 30 µg of total protein were loaded per lane.

6 x Laemmli Buffer	Lysis Buffer (LowDTT)
62.5 mM Tris/HCl (pH 6.8)	20 mM Tris/HCl (pH 8.0)
5 % 2-Mercaptoethanol	5 mM EDTA
10 % glycerol	1 mM DTT
2 % SDS	1% SDS
bromophenolblue	

7.1.4.3 Protein determination

Protein concentrations of detergent-free solutions were determined using the Biorad protein assay, which is based on the Bradford method (Bradford, 1976). Bovine γ-globulin served as protein standard. For detergent-containing solutions, the detergent-compatible Biorad DC protein assay was used, which is based on the Lowry method (Lowry et al., 1951). In this case, bovine serum albumin served as standard. All determinations were performed according to the manufacturer's recommendations.

[2] To a large part, the Methods section has been taken from the dissertation of my predecessor on this project, Mark Trautwein (Trautwein, 2004). Changes have only been made where necessary.

7.1.4.4 Trichloro acetic acid precipitation

TCA precipitations of proteins were conducted essentially as described (Bensadoun & Weinstein, 1976). One-tenth volume of 100% (w/v) TCA (4°C) was added to the ice-cold protein solution. After incubation on ice for 30 min, the sample was centrifuged for 15 min (20,000 g, 4°C). The pellet was washed with 1 ml acetone (-20°C) and sedimented again. After aspiration of the acetone, the pellet was dried for approximately 5 min at 65°C and dissolved in a smaller volume of 100 mM Tris/HCl pH 8.0.

7.1.4.5 SDS-PAGE

For the discontinuous, denaturing SDS polyacrylamide gel electrophoresis (Davis, 1964; Ornstein, 1964; Laemmli, 1970), minigels (8 cm x 6.5 cm x 0.075 cm) were used. In all instances, the percentage of the stacking gel was 4%. The percentage of the separation gel was chosen according to the analytical problem. The protein samples to be analyzed were complemented by 1/3 volume of 6 x Laemmli buffer, incubated at 65°C for 5-15 min and spun shortly. Formaldehyde-crosslinked samples were boiled for 30 min at 95°C to revert the crosslinking. The separation was performed at constant current (25 mA). Examples of standard gel compositions are given below.

SDS Running Buffer

25 mM Tris

192 mM glycine

0.1% SDS

Table 7.7: Pipetting scheme for 10% SDS gels.

	10% Separation Gel	4% Stacking Gel
Acrylamide 29.2% / Bisacrylamide 0.8%	20 ml	5 ml
1.5 M Tris/HCl pH 8.0	15 ml	---
0.5 M Tris/HCl pH 6.8	---	7,5 ml
10% SDS	300 µl	150 µl
dH_2O	19.5 ml	17.1 ml
TEMED	40 µl	30 µl
10% APS	400 µl	200 µl

Table 7.8: Pipetting scheme for 12.5% SDS gels.

	12.5% Separation Gel	4% Stacking Gel
Acrylamide 29.2% / Bisacrylamide 0.8%	25 ml	5 ml
1.5 M Tris/HCl pH 8.0	15 ml	---
0.5 M Tris/HCl pH 6.8	---	7,5 ml
10% SDS	300 µl	150 µl
dH_2O	19.5 ml	17.1 ml
TEMED	40 µl	30 µl
10% APS	400 µl	200 µl

7.1.4.6 Silver staining of polyacrylamide gels

Silver staining was performed essentially as described (Rabilloud et al., 1988). In short, after gel electrophoresis, the gel was incubated in fixative for 10 min, then washed twice in water (5 min). The gel was briefly incubated in a 0.02% thiosulfate solution (1/100 from stock; 1 min). After two brief washes in water (20 s), the gel was stained in 0.1% silver nitrate solution for 10 min, and rinsed three times with water. The staining was completed by addition of developer. Once the desired staining intensity was reached, the reaction was stopped by addition of 10% acetic acid. All washing steps were carried out with 50 ml of solution. All solutions were prepared freshly, with exception of those given in bold below.

Fixative

70% v/v methanol

0.1 ml formaldehyde (37 %) / 100 ml

Developer

3% w/v $NaCO_3$

0.0004% w/v $Na_2S_2O_3$ (20 µl of 2% stock / 100 ml)

0.1 ml formaldehyde (37%) / 100 ml

Thiosulfate Stock Solution

2% w/v $Na_2S_2O_3$

Stop Solution

10% acetic acid

7.1.4.7 Immunoblots

Proteins were usually transferred onto membranes using the wet-blot method (Towbin et al., 1979). Alternatively, for low molecular weight proteins (< 80 kDa), the faster semi-dry method was employed (Kyhse-Andersen, 1984). In either method, a sandwich is assembled consisting of the gel, the membrane, and gel blotting paper on each side. The proteins were electrotransferred in transfer

buffer (wet-blot: 3 h at RT, 30 V/250 mA; semi-dry: 45 min at RT, 15 V/2 A) onto nitrocellulose membranes with 0.45 µm pore size (Whatman).

After the transfer, the nitrocellulose was stained in Ponceau S solution for 1 min (optionally). Background was removed by washes in water. Complete destaining was accomplished by incubation in TBS. Unspecific binding sites were blocked by incubation in 5% milk (non-fat milk powder in TBS; 0.02% NaN_3) for 1 h; alternatively, 5% BSA in TBS was used (Streptavidin-HRP, anti-phospho-Slt2). The membrane was decorated with primary antibodies that were generally diluted in 5% milk for 3 h at RT or over night at 4°C. The membrane was washed repeatedly in TBST (1 x 15 min, 3 x 5 min). The secondary antibody coupled to horseradish peroxidase or an Alexa dye was diluted in TBST and incubated for 1 h at RT. If an antibody coupled to an Alexa dye was used, all subsequent steps were carried out in the dark. After repeated washes in TBST, signals were detected using either ECL (GE Healthcare) according to the manufacturer's recommendations or directly with the LiCor Odyssey system. Chemoluminescence was reported on ECL Hyperfilm (GE Healthcare) after different exposure times.

Transfer buffer:	20 x TBS
25 mM Tris	60 g Tris/HCl (pH 7.4)
192 mM glycine	160 g NaCl
0.25% SDS	4 g KCl
20% methanol	ad 1 l with H_2O

Ponceau S	TBST
0.2% w/v Ponceau S	1 x TBS
3% trichloro acetic acid	0.1% v/v Tween-20

7.1.4.8 Polysome profile analysis

Polysome preparations were done according to de la Cruz et al. (1997) on 4-47% sucrose gradients prepared with a Gradient Master (Nycomed Pharma; de la Cruz et al., 1997). In short, 200 ml of yeast cells were grown to an OD_{600} of 0.5-0.7. After temperature shift or application of the indicated stress, cycloheximide was added to a final concentration of 100 µg/ml, and the culture immediately placed into ice water. The cells were harvested at 4°C, washed once with 10 ml cold breaking buffer, and resuspended in 0.5 ml cold breaking buffer supplemented with 1 mM DTT and 0.1 mM PMSF. 500 µl glass beads were added to the tube, and the cells lysed by vortexing for 15 min at 4°C. The lysate was cleared by a short centrifugation (2 min, 10,000 g) and the supernatant transferred to a fresh tube. For storage, 10% v/v glycerol were added and the lysates stored at -20°C. A_{260} was measured in a

1:100 dilution and 8 units layered on top of a 7-47% sucrose gradient containing 50 mM Tris-Ac (pH 7.0), 50 mM NH_4Cl, 12 mM $MgCl_2$ and 1mM DTT. Settings of the Gradient Master were according to the manufacturer's recommendations for short SW41 gradients: Time: 1:58 min; Angle: 81.5°; Speed: 16. The samples were spun in a TST41.14 rotor for 3 h and 32,000 rpm at 4°C. Gradient analysis was performed using a gradient fractionator (Labconco) and the Ächta FPLC system (Amersham Pharmacia Biotech) and continuously monitored at A_{254}.

Breaking Buffer	10 x Gradient Buffer
10 mM Tris/HCl (pH 7.4)	500 mM Tris/HCl (pH 7.0)
100 mM NaCl	120 mM $MgCl_2$
30 mM $MgCl_2$	10 mM DTT
100 µg/ml cycloheximide	500 mM NH_4Cl
200 µg/ml heparin	

7.1.4.9 HBH purification

HBH purification was carried out according to the published protocol (Tagwerker et al., 2006), with several modifications. In short, 2 x 1.5 l of YPD yeast culture were grown to OD_{600} of 1.3-2.1 and shifted for 1 h to 37°C. Cells were fixed by addition of 42 ml 37% formaldahyde to each flask and incubated at RT for 10 min, gently shaking. The fixation was stopped by addition of 225 ml 3 M NH_3CO_3 and incubation at RT for 5 min, again under gentle agitation. Cells were harvested (SLC-4000, 5,000 rpm, 3 min, 4°C. Pellets of 3 l culture were pooled (appr. 10 ml), washed once in 25 ml ice-cold dH_2O and sedimented by centrifugation (5 min, 3,220 g, 4°C). Pellets were brought into suspension by addition of 2 ml dH_2O, dropped into liquid nitrogen and the beads stored at -80°C until they were processed further.

Lysis was performed in a bead beater with 40 ml Buffer 1 per 10 ml pelleted yeast for 3 min under constant cooling with ice; afterwards, the chamber was left to cool on ice for 3 min. The lysate was filtered to remove glass beads and cellular debris removed by a slow spin (10 min, 3,220 g, RT). The supernatant was then cleared by centrifugation in a SS-34 rotor (10 min, 5,000 rpm, RT), yielding supernatant SN1 and pellet P1. SN1 was spun again in the SS-34 rotor (10 min, 20,000 rpm, RT), yielding supernatant SN2 and pellet P2. P2 was then solubilized in 13 ml Buffer D. A Bradford protein determination was carried out with 1 µl sample.

The P2 fraction was incubated O/N at RT with 40 µl Ni-NTA slurry/mg total protein (15 ml 50% slurry washed in Buffer 1). The suspension was then transferred into a PolyPrep column (Biorad) and washed repeatedly (3 x 3.3 CV Buffer 1, 2 x 5 CV Buffer 2, 2 x 5 CV Buffer 3, 1 x 2 CV Buffer 4), and the bound protein eluted in 2.5 CV Ni-Elution buffer 5 (2 x 7.5 ml + 1 x 4 ml). The pH of the

elution was adjusted back to pH 8.0-8.5 with 1/20 volume 1 M Tris/HCl (pH 9.4) and then incubated O/N at RT with 2 µl Streptavidin-slurry/mg total protein (1.5 ml 50% slurry, washed with Buffer 1). The suspension was transferred into a PolyPrep column, washed repeatedly (4 x 10 CV Buffer 6, 1 x 10 CV Buffer 7), and finally transferred into a Protein LoBind Tube (Eppendorf) with 1 ml Buffer 7. Of the resulting slurry, 25 µl were prepared for SDS-PAGE. For this, the supernatant was removed and the beads resuspended in 20 µl 10 mM EDTA in formamide, incubated at 95°C for 10 min, spun shortly, and 20 µl of the supernatant mixed with 20 µl 2 x Laemmli. After 30 min incubation at 95°C, 10 µl were loaded for Western Blotting, 20 µl if the gel was silver stained.

The remainder of the slurry was subjected to ELC digest. From here on, only HPLC-grade solutions and Protein LoBind tubes were used. First, the beads were washed three times in 1 ml 50 mM Tris/HCl (pH 8.0), 0.1% SDS. A volume of 50 to 100 µl was left in the tube and 0.25 µl 1 mg/ml ELC added. After 2 h shaking at 37°C, another 0.25 µl 1 mg/ml ELC were added, and the digest was continued O/N (37°C, shaking). The supernatant was removed and the beads extracted two times with 50 mM Tris/HCl (pH 8.0), 0.1% SDS (1 x 200 µl, 1 x 100 µl). The three samples were pooled and dried in the Speed-Vac. The peptides were resuspended in 400 µl BS and loaded twice on a HILIC TopTip PolyLC spin column (PolyLC Inc.) that had been equilibrated with 3 x 50 µl ES and 3 x 50 µl BS. The column was washed (3 x 50 µl BS) and the peptides eluted four times with 25 µl ES. All elutions were pooled and dried in the Speed-Vac. The peptides were resuspended in 50 µl 50 mM NH_4HCO and subjected to trypsin digst with 0.5 µl 1 mg/ml trypsin (Promega) for 6 h at 37°C. Mass spectrometric analysis using LC-MS/MS (Orbitrap) was carried out by Suzette Moes in the lab of Paul Jenö.

Buffer 1
50 mM NaP_i (pH 8.0)
8 M Urea
300 mM NaCl
0.5% Tween-20
20 mM Imidazole

Buffer D
50 mM NaP_i (pH 8.0)
8 M Urea
300 mM NaCl
1% digitonin
20 mM Imidazole

Buffer 2
50 mM NaP_i (pH 6.4)
8 M Urea
300 mM NaCl
0.5% Tween-20

Buffer 3
50 mM NaP_i (pH 6.4)
8 M Urea
300 mM NaCl
0.5% Tween-20
20 mM Imidazole

Buffer 4	Buffer 5
50 mM NaP_i (pH 6.4)	50 mM NaAc (pH 4.3)
8 M Urea	8 M Urea
300 mM NaCl	300 mM NaCl
0.5% Tween-20	0.5% Tween-20
40 mM Imidazole	

Buffer 6	Buffer 7
50 mM Tris/HCl (pH 8.0)	50 mM Tris/HCl (pH 8.0)
8 M Urea	8 M Urea
300 mM NaCl	300 mM NaCl
2% SDS	0.2% SDS

BS	ES
85% acetonitril	85% acetonitril
10 mM NH_4Ac/formic acid (pH 3.5)	10 mM NH_4Ac/ formic acid (pH 3.5)

7.1.4.10 RNA isolation from cytosolic and membrane-enriched fractions

Separation of cytosolic and membrane-enriched fractions was carried out as described (Stoltenburg et al., 1995; Frey, 2002; Baum et al., 2004). 1.5 l of yeast culture were grown to logarithmic phase and shifted for 1 h to the non-permissive temperature when necessary. Cycloheximide was added to a final concentration of 100 µg/ml and the culture immediately placed into ice water. The cells were harvested at 4°C, washed once in 25 ml cold EP buffer, resuspended in 1 ml cold EP buffer supplemented with 1 mM DTT and 0.1 mM PMSF and slowly pipetted into liquid nitrogen, allowing small beads to form. Cell beads were either stored at –70°C or immediately processed.

Lysis of cells occurred under liquid nitrogen in a mortar placed on ice in which the cells were ground for approximately 30 min. Lysis efficiency was verified under the microscope. The resulting fine powder was stored at -70°C and aliquots removed under constant cooling with liquid nitrogen.

For cell fractionation, 500 µl of ground yeast powder was supplemented with 500 µl cold EP buffer containing 1 mM DTT, 0.1 mM PMSF, and 5 µl/ml RNasin ribonuclease inhibitor (Promega; EP+++). After vortexing to completely dissolve the frozen powder, the suspension was spun to remove cellular debris (5 min, 1,000 g, 4°C). 50 µl of the S1 supernatant were retained for SDS-PAGE, the rest was centrifuged to yield a P13 pellet and a S13 supernatant (10 min, 13,000 g, 4°C). S13 was spun again to remove residual membranes (15 min, 20,000 g, 4°C). The cleared supernatant was either layered directly on a sucrose gradient for polysome profile analysis, or 100 µl extracted with

TRIzol (Invitrogen) according to the manufacturer's recommendations. The P13 pellet was washed once with EP+++ (3 min, 20,000 g, 4°C) and either resuspended in 200 µl EP buffer supplemented with 2% polyoxyethylenlaurylether ("Nikkol", Sigma) and used for polysome profile analysis, or resuspended in 100 µl of EP+++;. 10 µl of the P13 fraction were retained for SDS-PAGE, the remainder was extracted with TRIzol and the RNA analyzed by Northern blot or on Affymetrix GeneChips.

7.1.4.11 Flotation of PBs

Flotation of ER membranes was performed essentially as described previously (Schmid et al., 2006). The equivalent of 50 OD_{600} units was converted into spheroplasts at 37°C and lysed by dounce homogenization in 3 ml of EP buffer supplemented with 1 mM DTT and PMSF. After removal of cellular debris (5 min, 300 g), membranes were pelleted by centrifugation (10 min, 13,000 g), resuspended in 2 ml of EP buffer containing 50% sucrose, and layered on top of 2 ml 65% sucrose in EP buffer. Two additional 5 ml and 2 ml cushions (40% and 0% sucrose) were layered on top. The step gradient was spun in a TST41.14 rotor for 16 h and 28,000 g at 4°C. After centrifugation, 1 ml fractions were collected from each of the cushions and all interphases and TCA precipitated. The samples were analyzed by SDS-PAGE and immunoblot using monoclonal mouse anti-Myc antibodies (9E10, Sigma) and polyclonal rabbit anti-Sec61 antibodies (a gift from R. Schekman and M. Spiess).

EP Buffer

20 mM Hepes/KOH (pH 7.6)

100 mM sorbitol

100 mM KAc

5 mM $Mg(Ac)_2$

1 mM EDTA

100 µg/ml cycloheximide

7.1.5 Molecular biological methods

Standard techniques for nucleic acid manipulations were used throughout this study (Sambrook et al., 1989).

7.1.5.1 Transformation of *E. coli*

Routinely, *E. coli* cells were transformed chemically. Usually, 50 µl chemically competent cells (which were available in the laboratory) were thawed on ice and mixed with 0.3 µl plasmid DNA or with 5 µl of a ligation reaction. The cells were heat-shocked for 30 s at 42°C and immediately placed on ice. SOC medium (240 µl) was added to the cells. The mixture was incubated on a shaker for 30 min at 37°C before the cells were plated out on selection plates. When a plasmid with ampicillin resistance was transformed, this last incubation step was omitted.

7.1.5.2 Plasmid preparation from *E. coli*

Plasmid preparations from *E. coli* were performed according to the alkaline lysis method described by Birnboim and Doly, with minor modifications (Birnboim & Doly, 1979). Routinely, 1.5 ml of an overnight culture were harvested (5 min, 16,000 g, RT). Cells were carefully resuspended in 300 µl buffer P1 and 300 µl buffer P2 was added. After incubation for 5 min at RT, 300 µl of buffer P3 were added to stop the lysis. The solution was cleared by two centrifugation steps (10 min, 16,000 g, RT). The plasmid DNA in the supernatant was precipitated by addition of 600 µl isopropanol and subsequent centrifugation (10 min, 16,000 g, RT). The resulting pellet was washed with 1 ml 70% ethanol and spun again (5 min, 16,000 g, RT). The pellet was dried at 65°C for about 5 min and then dissolved in 20 µl H_20 and stored at –20°C.

In cases when very pure DNA was required, the Qiagen plasmid mini kit was used according to the supplier's recommendations.

Buffer P1	Buffer P2	Buffer P3
20 mM Tris/HCl pH 8.0	0.2 M NaOH	3 M KAc pH 5.5
10 mM EDTA	1% SDS	
100 µg/ml RNase		

7.1.5.3 Determination of nucleic acid concentration

The concentration of nucleic acids was determined using a spectrophotometer (Ultrospec 3100 *pro*, Amersham Biosciences) or the NanoDrop (Thermo Scientific). The nucleic acids were diluted in dH_2O, and the absorption at 260 nm was determined. It was assumed that a unit of absorption at 260 nm corresponds to 50 µg/ml double-stranded DNA or 40 µg/ml single-stranded RNA.

7.1.5.4 Restriction digest of DNA

Plasmid preparations were analyzed by restriction digest and agarose gel electrophoresis with subsequent ethidium bromide staining. The guidelines for enzymatic digests provided by the suppliers of restriction endonucleases (NEB or Roche) were followed. For cloning purposes, restriction digests were purified with the PCR purification kit (Qiagen), and DNA fragments were eluted from agarose gels using the Gel extraction kit (Qiagen) according to the manufacturer's recommendations.

7.1.5.5 Cloning

DNA fragments for (sub-)cloning were obtained either by restriction digest of plasmid DNA or by PCR amplification from genomic yeast DNA. For protein expression in yeast, the p4XX vector series was used (Christianson et al., 1992; Mumberg et al., 1995). In case of PCR amplification, suitable restriction sites were included in the primers. Purified vector DNA and purified DNA insert were ligated using the rapid ligation kit (Roche) following the manufacturer's recommendations. If a unique restriction site was used, the digested vector was dephosphorylated with rAPid alkaline phosphatase (Roche) to prevent religation. Positive clones were identified by colony PCR or restriction digest and verified by DNA sequencing.

7.1.5.6 Polymerase chain reaction (PCR)

To produce DNA fragments for DNA cloning or homologous recombination, polymerase-chain-reaction was used (Mullis et al., 1986). The proof-reading Expand High Fidelity System (Roche) was used for preparative production of DNA. A typical reaction contained 37 µl H_20, 5 µl 10 x reaction buffer, 5 µl 2 mM dNTPs, 2 x 1 µl 10 mM oligonucleotide primer and 1 µl template DNA. Usually, 35 cycles of amplification were performed. The annealing temperature was typically at 54°C, and 1 min/kb was allowed for elongation.

7.1.5.7 Quantitative reverse-transcription-PCR (RT-PCR)

For qPCR, total RNA was isolated from yeast essentially as described (Schmitt et al., 1990). In short, yeast cells were grown to logarithmic phase and 25 OD_{600} were harvested. Cells were resuspended in 0.8 ml AE buffer, 80 µl 20% SDS and 0.8 ml PCI were added, and the tube vortexed for 10 s. After incubation for 4 min at 65°C, tubes were chilled at -70°C for 30 s and then centrifuged (2 min, 10,000 g, RT). The upper aqueous phase was transferred to a fresh tube and extracted with 400 µl TRIzol LS (Invitrogen) and 100 µl chloroform. After phase separation by centrifugation, the upper aqueous phase was again transferred to a fresh tube and one-tenth volume of 3 M NaAc (pH 5.2) was added. The RNA was precipitated with two volumes 100% EtOH at -20°C, washed with 70% EtOH, and the pellet resuspended in 500 µl RNase-free water. RNA clean-up and qPCR were carried out with Philippe Demougin at the Life Sciences Training Facility (LSTF). In short, 5 µg of RNA were treated

with Turbo DNase (*TURBO* DNA-free™ Kit, Ambion), cleaned up on Zymo-Spin™ columns (Zymo Research), and reverse transcribed using random nonamers and the Eurogentec Core Kit (RT-RTCK-03). The resulting cDNA was used as a template for the qPCR reaction and incorporation of SyBR green monitored on a Corbett Rotor-Gene Q.

7.1.5.8 DNA-sequencing

DNA sequencing was performed by a company (Microsynth).

7.1.5.9 Glycerol stocks

For the preparation of *E. coli* glycerol stocks, 750 µl of an overnight culture were mixed with 500 µl 50% glycerol and stored at –70°C. For the preparation of yeast glycerol stocks, yeast cells streaked out as a patch and grown on appropriate plates. The plates were incubated until a dense lawn of cells was obtained. The cells were transferred into 800 µl 15% glycerol with a sterile glass pipette and stored at –70°C.

7.1.5.10 Chromosomal manipulations of yeast cells

To delete or tag genes in yeast cells or to place them under an exogenous promoter, PCR-generated cassettes were integrated into the genome as has been described (Knop et al., 1999; Gueldener et al., 2002; Janke et al., 2004; Gauss et al., 2005; Tagwerker et al., 2006). Briefly, preparative PCR was performed on template plasmids with primers having 45 bp 5'-overhangs homologous to the desired target site in the yeast genome. The PCR-product was transformed directly into yeast cells without further purification. Cells were selected for with the corresponding auxotrophy or resistance marker, and correct integration was confirmed by analytical colony PCR. Wherever possible, expression of the appended tag was checked by immunoblotting on total yeast lysates. If required, the chromosomal manipulation was sequenced. In this case, a fragment containing the desired manipulation was amplified from genomic yeast DNA using the proof-reading Expand PCR system (Roche) and used as a template for the sequencing reaction.

Alleles were transferred into our preferred strain background by PCR-based allele replacement (Erdeniz et al., 1997) or integrated into the genomic locus using the pRS vector series (Sikorski & Hieter, 1989). Site-directed mutagenesis on the chromosome was carried out using the delitto perfetto method (Storici et al., 2001). In short, a cassette carrying the counter-selectable marker *URA3* was first integrated at the target site and later replaced by a fragment carrying the desired mutation. Integrants were selected by growth on 5-FOA and then sequenced to confirm the successful manipulation.

7.1.5.11 Preparation of genomic yeast DNA

Crude yeast DNA was obtained by rapid phenol/chloroform extraction (Hoffman & Winston, 1987). For this, 5 ml of yeast culture were grown to saturation. The cells were harvested and resuspended in 200 µl buffer A. 200 µl glass beads and 200 µl PCI were added. After vigorous vortexing for 5 min, 200 µl H_2O were added. Phase separation was accomplished by centrifugation (5 min, 10,000 g). The aqueous phase was transferred to a fresh reaction tube and 1 ml 100% EtOH (RT) added to precipitate the DNA, which was pelleted by centrifugation for 5 min (16,000 g). The resulting pellet was dried at 65°C for about 5 min and resuspended in 40 µl H_2O. Routinely, 0.5 µl genomic DNA were used per PCR reaction.

Buffer A

10 mM Tris/HCl pH 8.0

100 mM NaCl

1 mM EDTA

2% Triton X-100

1% SDS

7.1.5.12 Yeast transformation

Yeast cells were transformed by a highly efficienct lithium acetate transformation method (Gietz et al., 1995). Cells were grown over night to early log phase. 5 OD_{600} of cells were harvested and washed once in sterile water. The cells were incubated for 5 min at 30°C in 100 mM LiAc. Subsequently, they were resuspended in 360 µl transformation mix and vortexed for 1 min. A heat shock was employed for 15-40 min at 42°C, after which the cells were pelleted (5 s, 16,000 g). The cell pellet was resuspended in 300 µl sterile water and 170 µl aliquots were plated on appropriate selection plates. If kanamycin or nourseothricin resistance cassettes were transformed, cells were first incubated in YPD for at least 3 h at RT before plating on the corresponding plates. Fast growing colonies were chosen for a second round of selection. Sometimes, replica plating was necessary to allow for the selection of stable transformants.

Transformation mix

240 µl 50% (w/v) PEG (AMW 3,350)

36 µl 1 M LiAc

50 µl 2 mg/ml single-stranded salmon sperm DNA

5 µl of PCR product or 0.25 µl plasmid DNA, ad 360 µl with H_20

7.1.5.13 Analytical PCR of yeast colonies

Analytical PCR of yeast colonies was performed to confirm chromosomal manipulations of yeast cells or to determine the mating type after mating or sporulation. Generally, a forward primer binding 100-300 bp upstream of the desired integration event was combined with a reverse primer located on the integrated cassette, so that a product of the correct size was only amplified if the integration had taken place. A typical reaction contained 18.5 µl H_2O, 2.5 µl 10 x reaction buffer, 2.5 µl 2 mM dNTPs, 2 x 0.5 µl 10 µM oligonucleotide-primer, 0.15 µl *Taq* DNA-polymerase (Roche) and a small portion of a yeast colony. Usually, the annealing temperature was set at 54°C, and 1 min/kb was allowed for elongation. Generally, 40 cycles were used for amplification. Routinely, 20 µl of the reaction were analyzed by agarose gel electrophoresis. For mating type PCR, standard primers were used(Huxley et al., 1990), and 10 µl of the reaction were resolved on a 1.2% agarose gel.

7.1.5.14 Digoxigenin-labeling of RNA-antisense probes

Labeled RNA antisense probes were generated by *in vitro* transcription in the presence of labeled nucleotides. First, a PCR was performed on genomic DNA with primers containing a T7 promoter. Primers were chosen to yield fragments of around 800 bp. In the rare cases where the corresponding gene contained an intron, these regions were spared. The PCR product was purified with the Pellet Paint Co-Precipitant (Novagen) and used as a template for *in vitro* transcription with the Ambion MEGAscript T7 kit. A ratio of 1:5.6 of Dig-11-UTP:UTP was used. The integrity of the probe was checked by formaldehyde agarose gel electrophoresis. After quantification, the probe was adjusted to working concentration (0.5 µg/ml in FISH hybridization buffer, see recipe below), divided into aliquots, and kept at –70°C. Excess probe was stored as a highly concentrated stock at 35 µg/ml.

7.1.5.15 Fluorescent *in situ* hybridization (FISH)

FISH with digoxigenin-labeled antisense probe was performed essentially as described previously (Takizawa et al., 1997). Cells were grown over night to logarithmic phase and shifted for 1 h to the non-permissive temperature, if necessary. Cells were fixed directly in liquid medium by addition of 540 µl 37% formaldehyde to 5 ml culture and incubation for 1 h at RT under gentle agitation. Cells were washed twice in PBS (3 min, 1,000 g, RT) and resuspended in 1 ml 100 mM KP_i (pH 7.0), 1.2 M sorbitol. 2 µl β-mercaptoethanol were added. After incubation for 5 min at RT, the cells were spheroplasted by addition of 4 µl zymolyase T-100 suspension (10 mg/ml) for 20 min at 37°C. Cells were washed three times with 100 mM KP_i (pH 7.0), 1.2 M sorbitol (3 min, 1,000 g) and resuspended in 250 µl of the same buffer. An aliquot was allowed to settle on poly-lysine treated multi-well slides for 30 min. The slides were immersed in 50% formamide/5 x SSC for 5-10 min. For prehybridization, cells were incubated with hybridization mix in a humid chamber containing 50% formamide/5 x SSC for 3 h. The hybridization mix was replaced by new mix containing the digoxigenin-labelled antisense

probe at 0.5 µg/ml and the slides incubated at 37°C over night in a humid chamber. Slides were then immersed in 0.2 x SSC for 1 h at 37°C. Blocking solution was applied for 30 min at RT. F_{ab}-fragments of antibodies directed against digoxigenin and covalently coupled to alkaline phosphatase (Roche) were diluted 1:5,000 in blocking solution and applied to the cells for 1 h at 37°C. Slides were washed 3 x 5 min in washing buffer, then washed 2 x 5 min in detection buffer. The HNPP/Fast Red TR mix (Roche) was applied for 23 min at RT, after which slides were washed with water (1 x 10 min, 3 x 5 min). 3 µl Citifluor AF1 (supplemented with 1 µg/ml DAPI to stain the nuclei) was pipetted onto each well. Sildes were sealed by nail polish and stored at -70°C. Pictures were taken by Axiocam MRm on an Axioplan 2 fluorescence microscope with an eqFP611 filter using Axiovision software. Image processing was performed with Adobe Photoshop CS2.

Washing buffer
100 mM Tris/HCl pH 7.5
150 mM NaCl
0.05% Tween-20

Detection buffer
100 mM Tris/HCl pH 8.0
100 mM NaCl
10 mM $MgCl_2$

Hybridization Mix
50% formamide
5 x SSC
1 mg/ml yeast tRNA
100 µg/ml heparin
1x Denhardt's reagent
0.1% Tween-20
0.1% Triton X-100
5 mM EDTA

Blocking solution
5% horse serum
100 mM Tris/HCl pH 7.5
150 mM NaCl

HNPP/Fast Red TR mix
10 µl HNPP (10 mg/ml in DMF)
10 µl Fast Red TR solution
1 ml detection buffer
prepared freshly and filtered through
a 0.2 µm nylon membrane

Fast Red TR solution
25 mg/ml in H_2O
stable for up to four weeks

7.1.5.16 Fluorescent *in situ* hybridization / immunofluorescence (FISH/IF)

If FISH was to be combined with immunofluorescence, the following adjustments to the protocol were made. Cells were fixed, spheroplasted, and settled on slides as described in the standard FISH protocol. Before washing the slides in 50% formamide/5 x SSC, an additional fixation step was included: Slides were first immersed in ice-cold methanol for 6 min, then transferred into ice-cold

acetone for 30 s and dried at RT for 3-5 min. The prehybridization and hybridization steps were carried out according to the standard FISH protocol, except that wells were coated with Sigmacote (Sigma). After hybridization, slides were washed twice for 10 min with 0.5 x SSC pre-warmed to 42°C. Wells were washed with 15 µl PBT (1 x 5 min) and blocked with PBTB for 10 min. Incubation with anti-DIG-POD (Roche, 1:750 in PBTB) and anti-GFP (Torrey Pines, 1:200) was carried out for 1 h at 37°C in a humid chamber. Wells were then washed repeatedly with PBTB (6 x 5 min) and subsequently incubated with preabsorbed chicken anti-rabbit-IgG-Alexa488 (Invitrogen, 1:200 in PBS) for 1 h at 37°C in a humid chamber. After repeated washing steps (3 x 5 min PBTB, 1 x 5 min PBT, 1 x 5 min PBS), 10 µl tyramide solution (PerkinElmer, 1:100 in Amplification Solution) were added to each well and incubated for 1 h at 37°C in a humid chamber. Slides were washed with PBS (6 x 5 min), and 3 µl Citifluor AF1 (supplemented with 1 µg/ml DAPI to stain the nuclei) was pipetted onto each well. Sildes were then sealed by nail polish and stored at –70°C. Pictures were taken on a Leica SP5 confocal microscope. Image processing was performed with ImageJ (NIH, open source).

PBT	PBTB
1 x PBS	1 x PBS
0.1 Tween-20	0.1 Tween-20
1 mg/ml yeast tRNA	1 % fat free milk powder

Preabsorbed secondary antibody

Remaining spheroplasts were washed three times in PBS and resuspended in 1 ml PBS. 5 µl chicken anti-rabbit-IgG-Alexa488 were added, the tube wrapped in aluminum foil and rotated over night at 4°C; the supernatant was stored in the dark at 4°C and directly used for FISH/IF.

7.1.5.17 Northern blot analysis

Cells were grown over night to logarithmic phase and shifted for 1 h to the non-permissive temperature, where necessary. Cells were harvested, frozen in liquid nitrogen and stored at –20°C until further analysis. Total RNA was extracted using TRIzol (Invitrogen) according to the protocol provided by the manufacturer. The RNA was resolved on low-formaldehyde 1.2% agarose gels. To cast the gels, 0.6 g agarose were boiled in 43.5 ml H_2O. After cooling to about 60°C, 5 ml 10 x MOPS and 1.5 ml 37% formaldehyde (pH > 4) were added in the fume hood. Equal amounts of RNA (30 µg per lane) were mixed with 5 x RNA sample buffer and heated to 65°C for 15 min. The samples were placed on ice and 20 µl were immediately loaded per lane. Electrophoresis was performed in 1 x MOPS at 50 V for 3 h. After electrophoresis, the gel was first washed in DEPC-H_2O (3 x 5 min), and then in 10 x SSC (1 x 15 min). The RNA was transferred over night in 10 x SSC onto Hybond N+ membrane (GE Healthcare) by capillary blot as described previously (Sambrook et al., 1989). The RNA

was crosslinked to the damp membrane with a UV Stratalinker 1800 (Stratagene) set to autocrosslink mode. To verify equal loading, the membrane was stained with methylene blue, washed in DEPC-treated water, and photographed for documentation. To prepare Northern blot probes, the AlkPhos direct labeling kit (GE Healthcare) was used according to the manufacturer's recommendations. Briefly, a heat-stable alkaline phosphatase was directly crosslinked to a heat-denatured PCR product. After hybridization at 60°C, alkaline phosphatase activity was detected using CDP-Star substrate (Amersham Biosciences) and the chemoluminescence was reported on ECL Hyperfilm (GE Healthcare).

10 x MOPS
230 mM MOPS/NaOH pH 7.0
50 mM NaAC
10 mM EDTA

5 x RNA Sample Buffer
11.6 µl H_2O
8 µl 500 mM EDTA pH 8.0
72 µl 37 %formaldehyde
308 µl formamide
200 µl 100 %glycerol
400 µl 10 x MOPS
+ bromophenolblue

RNA Running Buffer
1 x MOPS
0.74% formaldeyde

10 x SSC
150 mM TriNa-citrate-dihydrate/HCl (pH 7.0)
1.5 M NaCl

Methylene Blue Stain
0.5 M NaAc/HAc, pH 5.5
0.04% methylene blue

For all solutions, DEPC-treated H_2O was used, and recommendations for working with RNA were followed (Sambrook et al., 1989).

7.1.5.18 Microarray

Microarrays were carried out with Philippe Demougin at the Life Sciences Training Facility (LSTF) at the Biozentrum. In short, total RNA was subjected to on-column clean-up (Qiagen RNeasy) and eluted in 32 µl RNase-free water. Integrity of the RNA was assessed on an Agilent 2100 Bioanalyzer using the RNA Nano Kit; RNA samples were consistently awarded a RNA integrity number (RIN) of 10 or higher.

Biotin labeling of RNA was performed as described in the GeneChip Expression Analysis Technical Manual (Affymetrix, 2001). Double-stranded cDNA was synthesized with the One-Cycle cDNA Synthesis Kit (Affymetrix), starting from 3.2 µg of total RNA. The material was purified with the Sample Cleanup Module (Affymetrix).

The purified cDNA was used as template for an *in vitro* transcription to synthesize cRNA in the presence of a biotin-conjugated ribonucleotide analog reaction using the IVT labeling kit (Affymetrix). Approximately 40 µg of labeled cRNA from each reaction were purified with the Sample Cleanup Module, and average size of the cRNA molecules was assessed on RNA Nano 6000 Chips (Agilent). The cRNA targets were incubated at 94°C for 35 min in the provided Fragmentation buffer and the resulting fragments of 50–150 nucleotides again monitored with the Bioanalyzer. All synthesis reactions were carried out in a PCR machine (T1 Thermocycler; Biometra) to ensure the highest possible degree of temperature control.

The hybridization cocktail (85 µl) containing fragmented biotin-labeled target cRNA at a final concentration of 0.05 µg/µl was transferred into Yeast Genome 2.0 Arrays (Affymetrix) and incubated at 45°C on a rotator in a hybridization oven 640 (Affymetrix) for 16 h at 60 rpm. The arrays were washed and stained on a Fluidics Station 450 (Affymetrix) by using the Hybridization Wash and Stain Kit (Affymetrix). To increase the signal strength, the antibody amplification protocol was used (FS450_0003). The GeneChips were processed with an Affymetrix GeneChip Scanner 3000 7G (Affymetrix). DAT image files of the microarrays were generated using GeneChip Operating Software (GCOS 1.4; Affymetrix). Data was filtered with the GeneSpring software (Agilent) to remove all non-*S. cerevisiae* ORFs, and the data analyzed with Microsoft Excel.

7.1.6 Cell biological methods

7.1.6.1 Pre-treatment of microscopy slides

To increase cell adherence, microscopy slides were routinely pre-treated with either poly-lysine, Sigmacote or concanavalin A (ConA). For poly-lysine treatment of multi-well slides, 15 µl of poly-lysine solution (20 µg/ml in water) were pipetted onto each well and incubated for 5-10 min at RT. Slides were then rinsed extensively with water, let dry and used immediately. Coating with Sigmacote (Sigma) was carried out according to the supplier's recommendations. For ConA coating, 10 µl of ConA solution (1 mg/ml in water) were spread on a slide to cover an area of appr. 1 cm^2 and allowed to dry. Long-term storage at RT generally improved the adherent properties of ConA-coated slides.

7.1.6.2 Fluorescence microscopy of GFP fusion proteins in living cells

Cells were grown over night to logarithmic phase in YPD or in the appropriate selection medium. If yeast cells carried an *ade2* marker that caused them to accumulate red dye in the vacuoles, the medium was supplemented with 50 mg/l adenine to suppress cellular autofluorescence. Cells were shifted for 1 h to non-permissive temperature, if necessary. A 1 ml aliquot was taken from liquid culture, and subjected to a specific stress if required. Cells were then harvested (30 s, 16,000 g, RT), resuspended in 40 µl HC complete that was complemented with glucose unless stated otherwise; if stresses were applied, the HC medium was complemented accordingly. 3 µl of cell suspension were spread on slides that had been pre-treated with ConA, and directly visualized under an Axioplan 2 fluorescence microscope from Zeiss using the GFP and eqFP611 filters. Pictures were taken by Axiocam MRm using Axiovision software. Image processing was performed with Adobe Photoshop CS2. For time-course analysis, cells were fixed in the presence of 3.7% formaldehyde for 1 h under gentle agitation. Cells were incubated in 100 mM KP_i (pH 6.5) for 10 min at RT, harvested, and resuspended in a smaller volume. Cells were allowed to settle for 30 min on a multi-well slide that had been pre-treated with poly-lysine. The slides were briefly washed in PBS, and 3 µl Citifluor AF1 (supplemented with 1 µg/ml DAPI to stain the nuclei) was pipetted onto each well. Sildes were then sealed by nail polish and stored at –20°C until they were inspected under the microscope. For counting, pictures were taking randomly, exported to Photoshop, inverted, and the tonal range adjusted using the levels dialog box to facilitate counting; all pictures from the same experiment were treated equally. A minimum of one hundred cells from at least two independent experiments was counted for each condition. In the quantification graphs, the size of the box is determined by the 25th and 75th percentiles, the whiskers represent the 5th and 95th percentiles, the horizontal line and the little square mark the median and the mean, respectively.

7.1.6.3 Actin cytoskeleton staining

Actin cytoskeleton staining was performed essentially as described previously (Adams & Pringle, 1991). Cells were grown over night to logarithmic phase and fixed directly in liquid medium by addition of 37% formaldehyde to a final concentration of 3.7% and incubation for 30 min at RT under gentle agitation. Cells were washed twice with PBS containing 1 mg/ml BSA (3 min, 1,000 g, RT). The cell pellet was resuspended in 25 µl PBS containing 1 mg/ml BSA and 5 µl of rhodamine-phalloidin (Molecular Probes, 300U/1.5 ml MeOH) were added. After incubation for 1 h at RT in the dark, cells were washed three times and resuspended in 500 µl PBS containing 1 mg/ml BSA. An aliquot was allowed to settle for 30 min on poly-lysine-treated multi-well slides. The slides were washed briefly in PBS, Citifluor AF1 was added, and the coverslips were sealed with nail-polish. Slides were stored at -20°C. Rhodamine fluorescence was observed by epifluorescence microscopy using the Cy3 channel on an Axioplan 2 fluorescence microscope from Zeiss. Pictures were taken by Axiocam MRm using Axiovision software. Image processing was performed with Adobe Photoshop CS2.

7.1.6.4 Analysis of budding pattern and staining of cell wall chitin

Analysis of the budding pattern and staining of cell wall chitin was carried out as described previously (Lord et al., 2002). A stationary liquid culture was diluted and grown for at least 16 h to logarithmic phase. Cells were fixed directly in the growth medium by adding 540 µl 37% formaldehyde to 5 ml of yeast culture, followed by an incubation for 1 h at RT under gentle agitation. Cells were washed twice in H_2O, resuspended in 250 µl 1 mg/ml calcofluor white solution and incubated for 5 min at RT. The cells were washed twice with H_2O, resuspended in 1 ml H_2O and stored at 4°C (up to several months). To facilitate budding pattern analysis, a small aliquot was squashed between slide and coverslip to bring the bud scars into one focal plane. Cells were observed under an Axioplan 2 fluorescence microscope from Zeiss using the DAPI filter. Pictures were taken by Axiocam MRm using Axiovision software. Image processing was performed using Adobe Photoshop CS2.

7.1.6.5 Mitochondrial live staining

For mitochondrial live staining, yeast cells were incubated with Rhodamine B (hexyl ester) (Molecular Probes) according to the supplier's recommendations. In short, 100 nM Rhodamine B (1:1000 from 0.1 M stock in DMSO) were added to 1 ml of yeast liquid culture and incubated for 20 min at RT. Cells were washed in 100 mM KP_i (pH 6.5) to remove excess dye and visualized on ConA-treated cells under the Axioplan 2 epifluorescence microscope from Zeiss using the Cy3 filter. Pictures were taken by Axiocam MRm using Axiovision software. Image processing was performed using Adobe Photoshop CS2. Alternatively, cells were transformed with a plasmid carrying mito-GFP and the GFP fluorescence monitored directly.

7.2 Abbreviations

5-FOA	5-fluoroorotic acid
A_{260}	absorbance at 260 nm
aa	amino acid
Ac	acetate
AMW	average molecular weight
AP	alkaline phosphatase
APS	ammonium persulfate
ARE	AU-rich element
ARF1	ADP ribosylation factor 1
ATP	adenosine-5'-triphosphate
bp	base pair
BSA	bovine serum albumin
cDNA	complementary DNA, generated by reverse transcription of RNA
C. elegans	*Cenorhabditis elegans*
CFW	calcofluor white
CHX	cycloheximide
ConA	concanavalin A
COPI	coat protein 1
COPII	coat protein 2
CV	column volume
CWI	cell wall integrity
DAPI	4',6-Diamidino-2-phenylindole dihydrochloride
DEPC	diethyl pyrocarbonate
dH_2O	water bidest.
DMSO	dimethylsulfoxide
DNA	desoxyribonucleic acid
DNase	DNA-hydrolyzing enzyme
dNTPs	desoxynucleotide triphosphates
DTT	dithiothreitol
ECL	enhanced chemoluminescence
E. coli	*Escherichia coli*
EDTA	ethylenediaminetetraacetic acid
EGFP	enhanced GFP
EGP body	eIF4E, eIF4G, and Pab1p-containing body
eIF	eukaryotic translation initiation factor
ELC	endoproteinase Lys-C
EM	electron microscopy

eqFP611	*Entacmaea quadricolor* fluorescent protein, emission maximum at 611 nm
ER	endoplasmic reticulum
EtOH	ethanol
FISH	fluorescent *in situ* hybridization
FISH/IF	fluorescent *in situ* hybridization combined with immunofluorescence
FITC	fluoresceine-isothiocyanate
g	gravitational acceleration constant
GAP	GTPase-activating protein
GDP	guanosin-5'-diphosphate
GEF	guanine nucleotide exchange factor
GFP	green fluorescent protein
GPI	glycosylphosphatidylinositol
GTP	guanosine-5'-triphosphate
GTPase	GTP hydrolyzing enzyme
HAST	Hda1p-affected subtelomeric
HBH	6xHis – biotin – 6xHis
HEPES	N-[2-Hydroxyethyl]piperazine-N'-[2-ethanesulfonic acid]
HRP	horseradish peroxidase
IF	immunofluorescence
IP	immunoprecipitation
IRES	internal ribosomal entry site
kb	kilo base
K. lactis	*Kluyveromyces lactis*
KP_i	potassium phosphate buffer
LatA	latrunculin A
LB	lysogeny broth
LC-MS	liquid chromatography coupled to mass spectrometry
MAP kinase	mitogen-activated protein kinase
MAS	membrane association score
MeOH	methanol
Met-tRNAi	initiator transfer RNA
MIPS	Munich Information Center for Protein Sequences
miRNA	micro RNA
MOPS	3-(N-Morpholino)propanesulfonic acid
mRNA	messenger RNA
mRNP	messenger RNA/protein containing complex
MRP	mitochondrial RNA processing
MS	mass spectrometry
MT	microtubule

MW	molecular weight
NaP_i	sodium phosphate buffer
n.d.	not determined
Ni-NTA	Nickel-Nitrilo tetra-actetic acid agarose
NMD	nonsense-mediated decay
OD_{600}	optical density at 600 nm
O/N	over night
ORF	open reading frame
PAGE	polyacrylamide gel electrophoresis
PB	P body
PBS	phosphate-buffered saline
PCI	phenol:chloroform:isoamylalcohol 25:24:1
PCR	polymerase chain reaction
PEG	polyethylene glycol
PM	plasma membrane
PMSF	phenylmethylsulfonylfluoride
qPCR	quantitative PCR
RBP	RNA-binding protein
RFP	red fluorescent protein
RNA	ribonucleic acid
RNAi	RNA interference
RNase	RNA-hydrolyzing enzyme
rpm	revolutions per minute
RT	room temperature
RT-PCR	reverse transcription followed by PCR
S. cerevisiae	*Saccharomyces cerevisiae*
SDS	sodium dodecyl sulfate
SG	stress granule
SRE	smaug response element
SRP	signal recognition particle
TAM body	temporal asymmetric MRP body
TBS	Tris-buffered saline
TC	ternary complex
TCA	trichloro acetic acid
TEMED	N,N,N‘,N‘-Tetramethylethylenediamin
TGN	trans-Golgi network
Tris	Tris(hydroxymethylaminomethane)
tRNA	transfer RNA
ts	temperature-sensitive

uORF	upstream ORF
UPR	unfolded protein response
UTP	uridine-5'-triphosphate
UTR	untranslated region
WB	Western blot
wt	wild-type
yeGFP	yeast codon-optimized GFP

According to the suggestions of the IUPAC-IUB Joint Commission on Biochemical Nomenclature (1983), the One-Letter or the Three-Letter code were used for amino acids.

7.3 Literature

Adams, A.E. & Pringle, J.R., 1991. Staining of actin with fluorochrome-conjugated phalloidin. *Methods Enzymol.*, 194:729-31.

Affymetrix, 2001. *GeneChip Expression Analysis Technical Manual*.

Aizer, A. et al., 2008. The dynamics of mammalian P body transport, assembly, and disassembly in vivo. *Mol Biol Cell.*, 19(10):4154-66.

Anderson, P. & Kedersha, N., 2006. RNA granules. *J Cell Biol.*, 172(6):803-8.

Andoh, T. et al., 2006. Visual screening for localized RNAs in yeast revealed novel RNAs at the bud-tip. *Biochem Biophys Res Commun.*, 351(4):999-1004.

Andrei, M.A. et al., 2005. A role for eIF4E and eIF4E-transporter in targeting mRNPs to mammalian processing bodies. *RNA*, 11(5):717-27.

Aragon, A.D. et al., 2006. Release of extraction-resistant mRNA in stationary phase Saccharomyces cerevisiae produces a massive increase in transcript abundance in response to stress. *Genome Biol.*, 7(2):R9.

Arava, Y. et al., 2003. Genome-wide analysis of mRNA translation profiles in Saccharomyces cerevisiae. *Proc Natl Acad Sci U S A.*, 100(7):3889-94.

Aronov, S. et al., 2007. mRNAs encoding polarity and exocytosis factors are cotransported with the cortical endoplasmic reticulum to the incipient bud in Saccharomyces cerevisiae. *Mol Cell Biol.*, 27(9):3441-55.

Aronov, S. & Gerst, J.E., 2004. Involvement of the late secretory pathway in actin regulation and mRNA transport in yeast. *J Biol Chem.*, 279(35):36962-71.

Asakura, T. et al., 1998. Isolation and characterization of a novel actin filament-binding protein from Saccharomyces cerevisiae. *Oncogene*, 16(1):121-30.

Ashe, M.P., De Long, S.K. & Sachs, A.B., 2000. Glucose depletion rapidly inhibits translation initiation in yeast. *Mol Biol Cell.*, 11(3):833-48.

Audhya, A. et al., 2005. A complex containing the Sm protein CAR-1 and the RNA helicase CGH-1 is required for embryonic cytokinesis in Caenorhabditis elegans. *J Cell Biol.*, 171(2):267-79.

Balagopal, V. & Parker, R., 2009. Polysomes, P bodies and stress granules: states and fates of eukaryotic mRNAs. *Curr Opin Cell Biol.*, 21(3):403-8.

Barbee, S.A. et al., 2006. Staufen- and FMRP-containing neuronal RNPs are structurally and functionally related to somatic P bodies. *Neuron*, 52(6):997-1009.

Barrett, L.E. et al., 2006. Region-directed phototransfection reveals the functional significance of a dendritically synthesized transcription factor. *Nat Methods.*, 3(6):455-60.

Batiza, A.F., Schulz, T. & Masson, P.H., 1996. Yeast respond to hypotonic shock with a calcium pulse. *J Biol Chem.*, 271(38):23357-62.

Baum, S., Bittins, M., Frey, S. & Seedorf, M., 2004. Asc1p, a WD40-domain containing adaptor protein, is required for the interaction of the RNA-binding protein Scp160p with polysomes. *Biochem J.*, 380(Pt 3):823-30.

Baxter, B.K. et al., 2005. Atg19p ubiquitination and the cytoplasm to vacuole trafficking pathway in yeast. *J Biol Chem.*, 280(47):39067-76.

Beelman, C.A. et al., 1996. An essential component of the decapping enzyme required for normal rates of mRNA turnover. *Nature*, 382(6592):642-6.

Beliakova-Bethell, N. et al., 2006. Virus-like particles of the Ty3 retrotransposon assemble in association with P-body components. *RNA*, 12(1):94-101.

Belostotsky, D., 2009. Exosome complex and pervasive transcription in eukaryotic genomes. *Curr Opin Cell Biol.*, 21(3):352-8.

Bensadoun, A. & Weinstein, D., 1976. Assay of proteins in the presence of interfering materials. *Anal Biochem.*, 70(1):241-50.

Berleth, T. et al., 1988. The role of localization of bicoid RNA in organizing the anterior pattern of the Drosophila embryo. *EMBO J.*, 7(6):1749-56.

Besse, F. & Ephrussi, A., 2008. Translational control of localized mRNAs: restricting protein synthesis in space and time. *Nat Rev Mol Cell Biol.*, 9(12):971-80.

Birnboim, H.C. & Doly, J., 1979. A rapid alkaline extraction procedure for screening recombinant plasmid DNA. *Nucleic Acids Res.*, 7(6):1513-23.

Bi, J. et al., 2007. Copb1-facilitated axonal transport and translation of kappa opioid-receptor mRNA. *Proc Natl Acad Sci U S A.*, 104(34):13810-5.

Böhl, F. et al., 2000. She2p, a novel RNA-binding protein tethers ASH1 mRNA to the Myo4p myosin motor via She3p. *EMBO J.*, 19(20):5514-24.

Boldogh, I.R., Fehrenbacher, K.L., Yang, H.C. & Pon, L.A., 2005. Mitochondrial movement and inheritance in budding yeast. *Gene*, 354:28-36.

Bonangelino, C.J., Chavez, E.M. & Bonifacino, J.S., 2002. Genomic screen for vacuolar protein sorting genes in Saccharomyces cerevisiae. *Mol Biol Cell.*, 13(7):2486-501.

Bonifacino, J.S. & Glick, B.S., 2004. The mechanisms of vesicle budding and fusion. *Cell*, 116(2):153-66.

Bonilla, M. & Cunningham, K.W., 2002. Calcium release and influx in yeast: TRPC and VGCC rule another kingdom. *Sci STKE*, 2002(127):pe17.

Bonilla, M. & Cunningham, K.W., 2003. Mitogen-activated protein kinase stimulation of Ca(2+) signaling is required for survival of endoplasmic reticulum stress in yeast. *Mol Biol Cell.*, 14(10):4296-305.

Bonilla, M., Nastase, K.K. & Cunningham, K.W., 2002. Essential role of calcineurin in response to endoplasmic reticulum stress. *EMBO J.*, 21(10):2343-53.

Bonnerot, C., Boeck, R. & Lapeyre, B., 2000. The two proteins Pat1p (Mrt1p) and Spb8p interact in vivo, are required for mRNA decay, and are functionally linked to Pab1p. *Mol Cell Biol.*, 20(16):5939-46.

Bourens, M. et al., 2009. Mutations in the Saccharomyces cerevisiae kinase Cbk1p lead to a fertility defect that can be suppressed by the absence of Brr1p or Mpt5p (Puf5p), proteins involved in RNA metabolism. *Genetics*, 183(1):161-73.

Bouveret, E. et al., 2000. A Sm-like protein complex that participates in mRNA degradation. *EMBO J.*, 19(7):1661-71.

Bradford, M.M., 1976. A rapid and sensitive method for the quantitation of microgram quantities of protein utilizing the principle of protein-dye binding. *Anal Biochem.*, 72:248-54.

Brangwynne, C.P. et al., 2009. Germline P granules are liquid droplets that localize by controlled dissolution/condensation. *Science*, 324(5935):1729-32.

Brengues, M., Teixeira, D. & Parker, R., 2005. Movement of eukaryotic mRNAs between polysomes and cytoplasmic processing bodies. *Science*, 310(5747):486-9.

Buchan, J.R., Muhlrad, D. & Parker, R., 2008. P bodies promote stress granule assembly in Saccharomyces cerevisiae. *J Cell Biol.*, 183(3):441-55.

Buchan, J.R. & Parker, R., 2009. Eukaryotic stress granules: the ins and outs of translation. *Mol Cell.*, 36(6):932-41.

Bullock, S.L., 2007. Translocation of mRNAs by molecular motors: think complex? *Semin Cell Dev Biol.*, 18(2):194-201.

Burd, C.G., Matunis, E.L. & Dreyfuss, G., 1991. The multiple RNA-binding domains of the mRNA poly(A)-binding protein have different RNA-binding activities. *Mol Cell Biol.*, 11(7):3419-24.

Chang, F. & Peter, M., 2003. Yeasts make their mark. *Nat Cell Biol.*, 5(4):294-9.

Chang, L. et al., 2006. Assembling an intermediate filament network by dynamic cotranslation. *J Cell Biol.*, 172(5):747-58.

Chang, W. et al., 2008. Myo2p, a class V myosin in budding yeast, associates with a large ribonucleic acid-protein complex that contains mRNAs and subunits of the RNA-processing body. *RNA*, 14(3):491-502.

Chardin, P. et al., 1996. A human exchange factor for ARF contains Sec7- and pleckstrin-homology domains. *Nature*, 384(6608):481-4.

Chartrand, P. et al., 2002. Asymmetric sorting of ash1p in yeast results from inhibition of translation by localization elements in the mRNA. *Mol Cell.*, 10(6):1319-30.

Checkley, M.A. et al., 2010. P-body components are required for Ty1 retrotransposition during assembly of retrotransposition-competent virus-like particles. *Mol Cell Biol.*, 30(2):382-98.

Chowdhury, A., Mukhopadhyay, J. & Tharun, S., 2007. The decapping activator Lsm1p-7p-Pat1p complex has the intrinsic ability to distinguish between oligoadenylated and polyadenylated RNAs. *RNA*, 13(7):998-1016.

Christianson, T.W. et al., 1992. Vector systems for heterologous expression of proteins in Saccharomyces cerevisiae. *Gene*, 110(1):119-22.

Chritton, J.J. & Wickens, M., 2010. Translational repression by PUF proteins in vitro. *RNA*, [Epub ahead of print].

Cohen, R., 2005. The role of membranes and membrane trafficking in RNA localization. *Biol Cell.*, 97(1):5-18.

Coller, J., Gray, N. & Wickens, M., 1998. mRNA stabilization by poly(A) binding protein is independent of poly(A) and requires translation. *Genes Dev.* , 12(20):3226-35.

Coller, J. & Parker, R., 2005. General translational repression by activators of mRNA decapping. *Cell*, 122(6):875-86.

Coller, J.M. et al., 2001. The DEAD box helicase, Dhh1p, functions in mRNA decapping and interacts with both the decapping and deadenylase complexes. *RNA*, 7(12):1717-27.

Condeelis, J. & Singer, R.H., 2005. How and why does beta-actin mRNA target? *Biol Cell.*, 97(1):97-110.

Costanzo, M. et al., 2010. The genetic landscape of a cell. *Science*, 327(5964):425-31.

Coué, M., Brenner, S.L., Spector, I. & Korn, E.D., 1987. Inhibition of actin polymerization by latrunculin A. *FEBS Lett.*, 213(2):316-8.

Cougot, N., Babajko, S. & Séraphin, B., 2004. Cytoplasmic foci are sites of mRNA decay in human cells. *J Cell Biol.*, 165(1):31-40.

Cox, J.S. & Walter, P., 1996. A novel mechanism for regulating activity of a transcription factor that controls the unfolded protein response. *Cell*, 87(3):391-404.

Czaplinski, K. & Singer, R.H., 2006. Pathways for mRNA localization in the cytoplasm. *Trends Biochem Sci.*, 31(12):687-93.

Davis, B.J., 1964. DISC ELECTROPHORESIS. II. METHOD AND APPLICATION TO HUMAN SERUM PROTEINS. *Ann N Y Acad Sci.*, 121:404-27.

de Bettignies, G. et al., 1999. RGD1 genetically interacts with MID2 and SLG1, encoding two putative sensors for cell integrity signalling in Saccharomyces cerevisiae. *Yeast*, 15(16):1719-31.

De Filippi, L. et al., 2007. Membrane stress is coupled to a rapid translational control of gene expression in chlorpromazine-treated cells. *Curr Genet.*, 52(3-4):171-85.

de la Cruz, J., Iost, I., Kressler, D. & Linder, P., 1997. The p20 and Ded1 proteins have antagonistic roles in eIF4E-dependent translation in Saccharomyces cerevisiae. *Proc Natl Acad Sci U S A.*, 94(10):5201-6.

Decker, C.J. & Parker, R., 1993. A turnover pathway for both stable and unstable mRNAs in yeast: evidence for a requirement for deadenylation. *Genes Dev.*, 7(8):1632-43.

Decker, C.J. & Parker, R., 2006. CAR-1 and trailer hitch: driving mRNP granule function at the ER? *J Cell Biol.*, 173(2):159-63.

Decker, C.J., Teixeira, D. & Parker, R., 2007. Edc3p and a glutamine/asparagine-rich domain of Lsm4p function in processing body assembly in Saccharomyces cerevisiae. *J Cell Biol.*, 179(3):437-49.

Deloche, O. et al., 2004. A membrane transport defect leads to a rapid attenuation of translation initiation in Saccharomyces cerevisiae. *Mol Cell.*, 13(3):357-66.

Deng, Y., Singer, R.H. & Gu, W., 2008. Translation of ASH1 mRNA is repressed by Puf6p-Fun12p/eIF5B interaction and released by CK2 phosphorylation. *Genes Dev.*, 22(8):1037-50.

Dennis, G.J. et al., 2003. DAVID: Database for Annotation, Visualization, and Integrated Discovery. *Genome Biol.*, 4(5):P3.

Deshler, J.O., Highett, M.I. & Schnapp, B.J., 1997. Localization of Xenopus Vg1 mRNA by Vera protein and the endoplasmic reticulum. *Science*, 276(5315):1128-31.

Dever, T.E. et al., 1992. Phosphorylation of initiation factor 2 alpha by protein kinase GCN2 mediates gene-specific translational control of GCN4 in yeast. *Cell*, 68(3):585-96.

Diehn, M., Eisen, M.B., Botstein, D. & Brown, P.O., 2000. Large-scale identification of secreted and membrane-associated gene products using DNA microarrays. *Nat Genet.*, 25(1):58-62.

Drubin, D.G., Miller, K.G. & Botstein, D., 1988. Yeast actin-binding proteins: evidence for a role in morphogenesis. *J Cell Biol.*, 107(6 Pt 2):2551-61.

D'Souza-Schorey, C. & Chavrier, P., 2006. ARF proteins: roles in membrane traffic and beyond. *Nat Rev Mol Cell Biol.*, 7(5):347-58.

Dunckley, T. & Parker, R., 1999. The DCP2 protein is required for mRNA decapping in Saccharomyces cerevisiae and contains a functional MutT motif. *EMBO J.*, 18(19):5411-22.

Du, T.G., Schmid, M. & Jansen, R.P., 2007. Why cells move messages: the biological functions of mRNA localization. *Semin Cell Dev Biol.*, 18(2):171-7.

Duttagupta, R. et al., 2005. Global analysis of Pub1p targets reveals a coordinate control of gene expression through modulation of binding and stability. *Mol Cell Biol.*, 25(13):5499-513.

Elkon, R., Zlotorynski, E., Zeller, K.I. & Agami, R., 2010. Major role for mRNA stability in shaping the kinetics of gene induction. *BMC Genomics*, 11(1):259.

Erdeniz, N., Mortensen, U.H. & Rothstein, R., 1997. Cloning-free PCR-based allele replacement methods. *Genome Res.*, 7(12):1174-83.

Estrada, P. et al., 2003. Myo4p and She3p are required for cortical ER inheritance in Saccharomyces cerevisiae. *J Cell Biol.*, 163(6):1255-66.

Eulalio, A., Behm-Ansmant, I., Schweizer, D. & Izaurralde, E., 2007. P-body formation is a consequence, not the cause, of RNA-mediated gene silencing. *Mol Cell Biol.*, 27(11):3970-81.

Fan, J. et al., 2002. Global analysis of stress-regulated mRNA turnover by using cDNA arrays. *Proc Natl Acad Sci U S A.*, 99(16):10611-6.

Farabaugh, P.J., Kramer, E., Vallabhaneni, H. & Raman, A., 2006. Evolution of +1 programmed frameshifting signals and frameshift-regulating tRNAs in the order Saccharomycetales. *J Mol Evol.*, 63(4):545-61.

Fernandez, J. et al., 2002. Regulation of internal ribosomal entry site-mediated translation by phosphorylation of the translation initiation factor eIF2alpha. *J Biol Chem.*, 277(21):19198-205.

Ferraiuolo, M.A. et al., 2005. A role for the eIF4E-binding protein 4E-T in P-body formation and mRNA decay. *J Cell Biol.*, 170(6):913-24.

Fischer, N. & Weis, K., 2002. The DEAD box protein Dhh1 stimulates the decapping enzyme Dcp1. *EMBO J.*, 21(11):2788-97.

Fournier, M.L. et al., 2010. Delayed correlation of mRNA and protein expression in rapamycin-treated cells and a role for Ggc1 in cellular sensitivity to rapamycin. *Mol Cell Proteomics.*, 9(2):271-84.

Frank, J., 2003. Toward an understanding of the structural basis of translation. *Genome Biol.*, 4(12):237.

Franks, T.M. & Lykke-Andersen, J., 2008. The control of mRNA decapping and P-body formation. *Mol Cell.*, 32(5):605-15.

Franzusoff, A., Lauzé, E. & Howell, K.E., 1992. Immuno-isolation of Sec7p-coated transport vesicles from the yeast secretory pathway. *Nature*, 355(6356):173-5.

Frey, S., 2002. *Charakterisierung von Scp160p, einem mRNA- und ribosomenassoziierten Protein in Saccharomyces cerevisiae*. Heidelberg: Ruprecht-Karls-Universität Heidelberg.

Frey, S., Pool, M. & Seedorf, M., 1997. Scp160p, an RNA-binding, polysome-associated protein, localizes to the endoplasmic reticulum of Saccharomyces cerevisiae in a microtubule-dependent manner. *J Biol Chem.*, 276(19):15905-12.

García-Martínez, J., Aranda, A. & Pérez-Ortín, J.E., 2005. Genomic run-on evaluates transcription rates for all yeast genes and identifies gene regulatory mechanisms. *Mol Cell.*, 15(2):303-13.

García-Rodríguez, L.J., Gay, A.C. & Pon, L.A., 2007. Puf3p, a Pumilio family RNA binding protein, localizes to mitochondria and regulates mitochondrial biogenesis and motility in budding yeast. *J Cell Biol.*, 176(2):197-207.

Gauss, R., Trautwein, M., Sommer, T. & Spang, A., 2005. New modules for the repeated internal and N-terminal epitope tagging of genes in Saccharomyces cerevisiae. *Yeast*, 22(1):1-12.

Gaynor, E.C., Chen, C.Y., Emr, S.D. & Graham, T.R., 1998. ARF is required for maintenance of yeast Golgi and endosome structure and function. *Mol Biol Cell.*, 9(3):653-70.

Geiser, J.R. et al., 1991. Can calmodulin function without binding calcium? *Cell*, 65(6):949-59.

Gerber, A.P., Herschlag, D. & Brown, P.O., 2004. Extensive association of functionally and cytotopically related mRNAs with Puf family RNA-binding proteins in yeast. *PLoS Biol.*, 2(3):E79.

Gerst, J.E., 2008. Message on the web: mRNA and ER co-trafficking. *Trends Cell Biol.*, 18(2):68-76.

Gietz, R.D., Schiestl, R.H., Willems, A.R. & Woods, R.A., 1995. Studies on the transformation of intact yeast cells by the LiAc/SS-DNA/PEG procedure. *Yeast*, 11(4):355-60.

Gilbert, W.V., Zhou, K., Butler, T.K. & Doudna, J.A., 2007. Cap-independent translation is required for starvation-induced differentiation in yeast. *Science*, 317(5842):1224-7.

Gill, T., Aulds, J. & Schmitt, M.E., 2006. A specialized processing body that is temporally and asymmetrically regulated during the cell cycle in Saccharomyces cerevisiae. *J Cell Biol.*, 173(1):35-45.

Giorgi, C. & Moorem, M.J., 2007. The nuclear nurture and cytoplasmic nature of localized mRNPs. *Semin Cell Dev Biol.*, 18(2):186-93.

Gonzalez, I., Buonomo, S.B., Nasmyth, K. & von Ahsen, U., 1999. ASH1 mRNA localization in yeast involves multiple secondary structural elements and Ash1 protein translation. *Curr Biol.*, 9(6):337-40.

Goossens, A., Dever, T.E., Pascual-Ahuir, A. & Serrano, R., 2001. The protein kinase Gcn2p mediates sodium toxicity in yeast. *J Biol Chem.*, 276(33):30753-60.

Granneman, S., Petfalski, E., Swiatkowska, A. & Tollervey, D., 2010. Cracking pre-40S ribosomal subunit structure by systematic analyses of RNA-protein cross-linking. *EMBO J.*, [Epub ahead of print].

Grousl, T. et al., 2009. Robust heat shock induces eIF2alpha-phosphorylation-independent assembly of stress granules containing eIF3 and 40S ribosomal subunits in budding yeast, Saccharomyces cerevisiae. *J Cell Sci.*, 122(12):2078-88.

Gruber, A.R. et al., 2008. The Vienna RNA Websuite. *Nucleic Acids Res.*, 36(Web Server issue):W70-4.

Gu, W., Deng, Y., Zenklusen, D. & Singer, R.H., 2004. A new yeast PUF family protein, Puf6p, represses ASH1 mRNA translation and is required for its localization. *Genes Dev.*, 18(12):1452-65.

Gueldener, U. et al., 2002. A second set of loxP marker cassettes for Cre-mediated multiple gene knockouts in budding yeast. *Nucleic Acids Res.*, 30(6):e23.

Gygi, S.P., Rochon, Y., Franza, B.R. & Aebersold, R., 1999. Correlation between protein and mRNA abundance in yeast. *Mol Cell Biol.*, 19(3):1720-30.

Hafner, M. et al., 2010. Transcriptome-wide identification of RNA-binding protein and microRNA target sites by PAR-CLIP. *Cell*, 141(1):129-41.

Hartwell, L.H. & McLaughlin, C.S., 1969. A mutant of yeast apparently defective in the initiation of protein synthesis. *Proc Natl Acad Sci U S A.*, 62(2):468-74.

Hayashi, M. & Maeda, T., 2006. Activation of the HOG pathway upon cold stress in Saccharomyces cerevisiae. *J Biochem.*, 139(4):797-803.

Heath, V.L., Shaw, S.L., Roy, S. & Cyert, M.S., 2004. Hph1p and Hph2p, novel components of calcineurin-mediated stress responses in Saccharomyces cerevisiae. *Eukaryot Cell.*, 3(3):695-704.

He, W. & Parker, R., 2000. Functions of Lsm proteins in mRNA degradation and splicing. *Curr Opin Cell Biol.*, 12(3):346-50.

Hilgers, V., Teixeira, D. & Parker, R., 2006. Translation-independent inhibition of mRNA deadenylation during stress in Saccharomyces cerevisiae. *RNA*, 12(10):1835-45.

Hilliker, A. & Parker, R., 2008. Stressed out? Make some modifications! *Nat Cell Biol.*, 10(10):1129-30.

Hinnebusch, A.G., 2005. Translational regulation of GCN4 and the general amino acid control of yeast. *Annu Rev Microbiol.*, 59:407-50.

Hoffman, C.S. & Winston, F., 1987. A ten-minute DNA preparation from yeast efficiently releases autonomous plasmids for transformation of Escherichia coli. *Gene*, 57(2-3):267-72.

Hogan, D.J. et al., 2008. Diverse RNA-binding proteins interact with functionally related sets of RNAs, suggesting an extensive regulatory system. *PLoS Biol.*, 6(10):e255.

Hogg, J. & Collins, K., 2007. RNA-based affinity purification reveals 7SK RNPs with distinct composition and regulation. *RNA*, 13(6):868-80.

Hohmann, S., 2002. Osmotic stress signaling and osmoadaptation in yeasts. *Microbiol Mol Biol Rev.*, 66(2):300-72.

Holmes, L.E. et al., 2004. Loss of translational control in yeast compromised for the major mRNA decay pathway. *Mol Biol Cell.*, 24(7):2998-3010.

Holt, C.E. & Bullock, S.L., 2009. Subcellular mRNA localization in animal cells and why it matters. *Science*, 326(5957):1212-6.

Hoyle, N.P. et al., 2007. Stress-dependent relocalization of translationally primed mRNPs to cytoplasmic granules that are kinetically and spatially distinct from P-bodies. *J Cell Biol.*, 179(1):65-74.

Huang, C.F. et al., 2003. Role for Arf3p in development of polarity, but not endocytosis, in Saccharomyces cerevisiae. *Mol Biol Cell.*, 14(9):3834-47.

Huang, D., Sherman, B. & Lempicki, R., 2009. Systematic and integrative analysis of large gene lists using DAVID bioinformatics resources. *Nat Protoc.*, 4(1):44-57.

Huckaba, T.M., Lipkin, T. & Pon, L.A., 2006. Roles of type II myosin and a tropomyosin isoform in retrograde actin flow in budding yeast. *J Cell Biol.*, 175(6):957-69.

Hüttelmaier, S. et al., 2005. Spatial regulation of beta-actin translation by Src-dependent phosphorylation of ZBP1. *Nature*, 438(7067):512-5.

Hu, W., Petzold, C., Coller, J. & Baker, K.E., 2010. Nonsense-mediated mRNA decapping occurs on polyribosomes in Saccharomyces cerevisiae. *Nat Struct Mol Biol.*, 17(2):244-7.

Huxley, C., Green, E.D. & Dunham, I., 1990. Rapid assessment of S. cerevisiae mating type by PCR. *Trends Genet.*, 6(8):236.

Inada, M. & Guthrie, C., 2004. Identification of Lhp1p-associated RNAs by microarray analysis in Saccharomyces cerevisiae reveals association with coding and noncoding RNAs. *Proc Natl Acad Sci U S A.*, 101(2):434-9.

Irie, K. et al., 2002. The Khd1 protein, which has three KH RNA-binding motifs, is required for proper localization of ASH1 mRNA in yeast. *EMBO J.*, 21(5):1158-67.

Irion, U. & St Johnston, D., 2007. bicoid RNA localization requires specific binding of an endosomal sorting complex. *Nature*, 445(7127):554-8.

Jackson, C.L. & Képès, F., 1994. BFR1, a multicopy suppressor of brefeldin A-induced lethality, is implicated in secretion and nuclear segregation in Saccharomyces cerevisiae. *Genetics*, 137(2):423-37.

Jakymiw, A. et al., 2005. Disruption of GW bodies impairs mammalian RNA interference. *Nat Cell Biol.*, 7(12):1267-74.

Jambhekar, A. & Derisi, J.L., 2007. Cis-acting determinants of asymmetric, cytoplasmic RNA transport. *RNA*, 13(5):625-42.

Janke, C. et al., 2004. A versatile toolbox for PCR-based tagging of yeast genes: new fluorescent proteins, more markers and promoter substitution cassettes. *Yeast*, pp.21(11):947-62.

Janke, C. et al., 2004. A versatile toolbox for PCR-based tagging of yeast genes: new fluorescent proteins, more markers and promoter substitution cassettes. *Yeast*, 21(11):947-62.

Jansen, R.P. et al., 1996. Mother cell-specific HO expression in budding yeast depends on the unconventional myosin myo4p and other cytoplasmic proteins. *Cell*, 84(5):687-97.

Jansen, J.M., Wanless, A.G., Seidel, C.W. & Weiss, E.L., 2009. Cbk1 regulation of the RNA-binding protein Ssd1 integrates cell fate with translational control. *Curr Biol.*, 19(24):2114-20.

Jones, S. et al., 1999. Genetic interactions in yeast between Ypt GTPases and Arf guanine nucleotide exchangers. *Genetics*, 152(4):1543-56.

Kaufman, R.J. et al., 2002. The unfolded protein response in nutrient sensing and differentiation. *Nat Rev Mol Cell Biol.*, 3(6):411-21.

Kedersha, N.L. et al., 1999. RNA-binding proteins TIA-1 and TIAR link the phosphorylation of eIF-2 alpha to the assembly of mammalian stress granules. *J Cell Biol.*, 147(7):1431-42.

Kedersha, N. et al., 2005. Stress granules and processing bodies are dynamically linked sites of mRNP remodeling. *J Cell Biol.*, 169(6):871-84.

Khusial, P., Plaag, R. & Zieve, G.W., 2005. LSm proteins form heptameric rings that bind to RNA via repeating motifs. *Trends Biochem Sci.*, 30(9):522-8.

Kiebler, M.A. & Bassell, G.J., 2006. Neuronal RNA granules: movers and makers. *Neuron*, 51(6):685-90.

Kimata, Y. et al., 2007. Two regulatory steps of ER-stress sensor Ire1 involving its cluster formation and interaction with unfolded proteins. *J Cell Biol.*, 179(1):75-86.

Kim-Ha, J., Smith, J.L. & Macdonald, P.M., 1991. oskar mRNA is localized to the posterior pole of the Drosophila oocyte. *Cell*, 66(1):23-35.

Kirchhausen, T., 2000. Three ways to make a vesicle. *Nat Rev Mol Cell Biol.*, 1(3):187-98.

Knop, M. et al., 1999. Epitope tagging of yeast genes using a PCR-based strategy: more tags and improved practical routines. *Yeast*, 15(10B):963-72.

Kshirsagar, M. & Parker, R., 2004. Identification of Edc3p as an enhancer of mRNA decapping in Saccharomyces cerevisiae. *Genetics*, 166(2):729-39.

Kulkarni, M., Ozgur, S. & Stoecklin, G., 2010. On track with P-bodies. *Biochem Soc Trans.*, 38(Pt 1):242-51.

Kyhse-Andersen, J., 1984. Electroblotting of multiple gels: a simple apparatus without buffer tank for rapid transfer of proteins from polyacrylamide to nitrocellulose. *J Biochem Biophys Methods.*, 10(3-4):203-9.

Laemmli, U.K., 1970. Cleavage of structural proteins during the assembly of the head of bacteriophage T4. *Nature*, 227(5259):680-5.

Lambert, A.A., Perron, M.P., Lavoie, E. & Pallotta, D., 2007. The Saccharomyces cerevisiae Arf3 protein is involved in actin cable and cortical patch formation. *FEMS Yeast Res.*, 7(6):782-95.

Lange, S. et al., 2008. Simultaneous transport of different localized mRNA species revealed by live-cell imaging. *Traffic*, 9(8):1256-67.

Lang, B.D. & Fridovich-Keil, J.L., 2000. Scp160p, a multiple KH-domain protein, is a component of mRNP complexes in yeast. *Nucleic Acids Res.*, 28(7):1576-84.

Lang, B.D., Li, A.M., Black-Brewster, H. & Fridovich-Keil, J., 2001. The brefeldin A resistance protein Bfr1p is a component of polyribosome-associated mRNP complexes in yeast. *Nucleic Acids Res.*, 29(12):2567-74.

Lécuyer, E. et al., 2007. Global analysis of mRNA localization reveals a prominent role in organizing cellular architecture and function. *Cell*, 131(1):174-8.

Leeds, P., Peltz, S.W., Jacobson, A. & Culbertson, M.R., 1991. The product of the yeast UPF1 gene is required for rapid turnover of mRNAs containing a premature translational termination codon. *Genes Dev.*, 5(12A):2303-14.

Lee, K.S. et al., 1993. A yeast mitogen-activated protein kinase homolog (Mpk1p) mediates signalling by protein kinase C. *Mol Cell Biol.*, 13(5):3067-75.

Lee, M.C. et al., 2004. Bi-directional protein transport between the ER and Golgi. *Annu Rev Cell Dev Biol.*, 20:87-123.

Lerner, R.S. et al., 2003. Partitioning and translation of mRNAs encoding soluble proteins on membrane-bound ribosomes. *RNA*, 9(9):1123-37.

Li, Y. et al., 2000. Repression of ribosome and tRNA synthesis in secretion-defective cells is signaled by a novel branch of the cell integrity pathway. *Mol Cell Biol.*, 20(11):3843-51.

Lin, Y. et al., 2009. Protein acetylation microarray reveals that NuA4 controls key metabolic target regulating gluconeogenesis. *Cell*, 136(6):1073-84.

Liu, H.P. & Bretscher, A., 1989. Disruption of the single tropomyosin gene in yeast results in the disappearance of actin cables from the cytoskeleton. *Cell*, 57(2):233-42.

Liu, B. et al., 2010. The polarisome is required for segregation and retrograde transport of protein aggregates. *Cell*, 140(2):257-67.

Liu, J., Valencia-Sanchez, M.A., Hannon, G.J. & Parker, R., 2005. MicroRNA-dependent localization of targeted mRNAs to mammalian P-bodies. *Nat Cell Biol.*, 7(7):719-23.

Li, Z., Wang, L., Hays, T.S. & Cai, Y., 2008. Dynein-mediated apical localization of crumbs transcripts is required for Crumbs activity in epithelial polarity. *J Cell Biol.*, 180(1):31-8.

Li, A.M., Watson, A. & Fridovich-Keil, J.L., 2003. Scp160p associates with specific mRNAs in yeast. *Nucleic Acids Res.*, 31(7):1830-7.

Lodish, H. et al., 2003. *Molecular Cell Biology*. Fifth Edition ed. W. H. Freeman.

Long, R.M. et al., 2000. She2p is a novel RNA-binding protein that recruits the Myo4p-She3p complex to ASH1 mRNA. *EMBO J.*, 19(23):6592-601.

Long, R.M. et al., 1997. Mating type switching in yeast controlled by asymmetric localization of ASH1 mRNA. *Science*, 277(5324):383-7.

Lord, M., Chen, T., Fujita, A. & Chant, J., 2002. Analysis of budding patterns. *Methods Enzymol.*, 350:131-41.

Lowry, O.H., Rosebrough, N.J., Farr, A.L. & Randall, R.J., 1951. Protein measurement with the Folin phenol reagent. *J Biol Chem.*, 193(1):265-75.

Loya, A. et al., 2008. The 3'-UTR mediates the cellular localization of an mRNA encoding a short plasma membrane protein. *RNA*, 14(7):1352-65.

Mangus, D.A. & Jacobson, A., 1999. Linking mRNA turnover and translation: assessing the polyribosomal association of mRNA decay factors and degradative intermediates. *Methods*, 17(1):28-37.

Marc, P. et al., 2002. Genome-wide analysis of mRNAs targeted to yeast mitochondria. *EMBO Rep.*, 3(2):159-64.

Matlack, K.E. & Walter, P., 1995. The 70 carboxyl-terminal amino acids of nascent secretory proteins are protected from proteolysis by the ribosome and the protein translocation apparatus of the endoplasmic reticulum membrane. *J Biol Chem.*, 270(11):6170-80.

Matsumoto, T.K. et al., 2002. An osmotically induced cytosolic Ca2+ transient activates calcineurin signaling to mediate ion homeostasis and salt tolerance of Saccharomyces cerevisiae. *J Biol Chem.*, 277(36):33075-80.

Meignin, C. & Davis, I., 2010. Transmitting the message: intracellular mRNA localization. *Curr Opin Cell Biol.*, 22(1):112-9.

Melamed, D., Pnueli, L. & Arava, Y., 2008. Yeast translational response to high salinity: global analysis reveals regulation at multiple levels. *RNA*, 14(7):1337-51.

Michelitsch, M.D. & Weissman, J.S., 2000. A census of glutamine/asparagine-rich regions: implications for their conserved function and the prediction of novel prions. *Proc Natl Acad Sci U S A.*, 97(22):11910-5.

Mili, S. & Macara, I.G., 2009. RNA localization and polarity: from A(PC) to Z(BP). *Trends Cell Biol.*, 19(4):156-64.

Molina-Navarro, M.M. et al., 2008. Comprehensive transcriptional analysis of the oxidative response in yeast. *J Biol Chem.*, 283(26):17908-18.

Molin, C. et al., 2009. mRNA stability changes precede changes in steady-state mRNA amounts during hyperosmotic stress. *RNA*, 15(4):600-14.

Mollet, S. et al., 2008. Translationally repressed mRNA transiently cycles through stress granules during stress. *Mol Biol Cell.*, 19(10):4469-79.

Morris, D.K. & Lundblad, V., 1997. Programmed translational frameshifting in a gene required for yeast telomere replication. *Curr Biol.*, 7(12):969-76.

Muhlrad, D., Decker, C.J. & Parker, R., 1994. Deadenylation of the unstable mRNA encoded by the yeast MFA2 gene leads to decapping followed by 5'-->3' digestion of the transcript. *Genes Dev.*, 8(7):855-66.

Mullis, K. et al., 1986. Specific enzymatic amplification of DNA in vitro: the polymerase chain reaction. *Cold Spring Harb Symp Quant Biol.*, 51 Pt 1:263-73.

Mumberg, D., Müller, R. & Funk, M., 1995. Yeast vectors for the controlled expression of heterologous proteins in different genetic backgrounds. *Gene*, 156(1):119-22.

Mutka, S.C. & Walter, P., 2001. Multifaceted physiological response allows yeast to adapt to the loss of the signal recognition particle-dependent protein-targeting pathway. *Mol Biol Cell.*, 12(3):577-88.

Nakamura, A., Amikura, R., Hanyu, K. & Kobayashi, S., 2001. Me31B silences translation of oocyte-localizing RNAs through the formation of cytoplasmic RNP complex during Drosophila oogenesis. *Development*, 128(17):3233-42.

Nakamura, Y., Gojobori, T. & Ikemura, T., 2000. Codon usage tabulated from international DNA sequence databases: status for the year 2000. *Nucleic Acids Res.*, 28(1):292.

Nelson, K.K. & Lemmon, S.K., 1993. Suppressors of clathrin deficiency: overexpression of ubiquitin rescues lethal strains of clathrin-deficient Saccharomyces cerevisiae. *Mol Cell Biol.*, 13(1):521-32.

Nierras, C. & Warner, J., 1999. Protein kinase C enables the regulatory circuit that connects membrane synthesis to ribosome synthesis in Saccharomyces cerevisiae. *J Biol Chem.*, 274(19):13235-41.

Ohya, Y. & Botstein, D., 1994. Diverse essential functions revealed by complementing yeast calmodulin mutants. *Science*, 263(5149):963-6.

Ornstein, L., 1964. DISC ELECTROPHORESIS. I. BACKGROUND AND THEORY. *Ann N Y Acad Sci.*, 121:321-49.

Paquin, N. et al., 2007. Local activation of yeast ASH1 mRNA translation through phosphorylation of Khd1p by the casein kinase Yck1p. *Mol Cell.*, 26(6):795-809.

Parker, R. & Sheth, U., 2007. P bodies and the control of mRNA translation and degradation. *Mol Cell.*, 25(5):635-46.

Patil, C.K., Li, H. & Walter, P., 2004. Gcn4p and novel upstream activating sequences regulate targets of the unfolded protein response. *PLoS Biol.*, 2(8):E246.

Peyroche, A. et al., 1999. Brefeldin A acts to stabilize an abortive ARF-GDP-Sec7 domain protein complex: involvement of specific residues of the Sec7 domain. *Mol Cell.*, 3(3):275-85.

Peyroche, A. & Jackson, C.L., 2001. Functional analysis of ADP-ribosylation factor (ARF) guanine nucleotide exchange factors Gea1p and Gea2p in yeast. *Methods Enzymol.*, 329:290-300.

Pillai, R.S. et al., 2005. Inhibition of translational initiation by Let-7 MicroRNA in human cells. *Science*, 309(5740):1573-6.

Poon, P.P. et al., 1999. Retrograde transport from the yeast Golgi is mediated by two ARF GAP proteins with overlapping function. *EMBO J.*, 18(3):555-64.

Posas, F. & Saito, H., 1997. Osmotic activation of the HOG MAPK pathway via Ste11p MAPKKK: scaffold role of Pbs2p MAPKK. *Science*, 276(5319):1702-5.

Prescianotto-Baschong, C. & Riezman, H., 2002. Ordering of compartments in the yeast endocytic pathway. *Traffic*, 3(1):37-49.

Prinz, S. et al., 2007. Control of signaling in a MAP-kinase pathway by an RNA-binding protein. *PLoS One*, 2(2):e249.

Proft, M. & Struhl, K., 2002. Hog1 kinase converts the Sko1-Cyc8-Tup1 repressor complex into an activator that recruits SAGA and SWI/SNF in response to osmotic stress. *Mol Cell.*, 9(6):1307-17.

Ptacek, J. et al., 2005. Global analysis of protein phosphorylation in yeast. *Nature*, 438(7068):679-84.

Rabilloud, T., Carpentier, G. & Tarroux, P., 1988. Improvement and simplification of low-background silver staining of proteins by using sodium dithionite. *Electrophoresis*, 9(6):288-91.

Reijns, M.A., Alexander, R.D., Spiller, M.P. & Beggs, J.D., 2008. A role for Q/N-rich aggregation-prone regions in P-body localization. *J Cell Sci.*, 121(15):2463-72.

Reineke, L.C., Komar, A.A., Caprara, M.G. & Merrick, W.C., 2008. A small stem loop element directs internal initiation of the URE2 internal ribosome entry site in Saccharomyces cerevisiae. *J Biol Chem.*, 283(27):19011-25.

Rendl, L.M., Bieman, M.A. & Smibert, C.A., 2008. S. cerevisiae Vts1p induces deadenylation-dependent transcript degradation and interacts with the Ccr4p-Pop2p-Not deadenylase complex. *RNA*, 14(7):1328-36.

Riedl, J. et al., 2008. Lifeact: a versatile marker to visualize F-actin. *Nat Methods.*, 5(7):605-7.

Robinson, M.D., Grigull, J., Mohammad, N. & Hughes, T.R., 2002. FunSpec: a web-based cluster interpreter for yeast. *BMC Bioinformatics*, 3:35.

Robyr, D. et al., 2002. Microarray deacetylation maps determine genome-wide functions for yeast histone deacetylases. *Cell*, 109(4):437-46.

Romero-Santacreu, L., Moreno, J., Pérez-Ortín, J.E. & Alepuz, P., 2009. Specific and global regulation of mRNA stability during osmotic stress in Saccharomyces cerevisiae. *RNA*, 15(6):1110-20.

Rothman, J.E. & Wieland, F.T., 1996. Protein sorting by transport vesicles. *Science*, 272(5259):227-34.

Salgado-Garrido, J., Bragado-Nilsson, E., Kandels-Lewis, S. & Séraphin, B., 1999. Sm and Sm-like proteins assemble in two related complexes of deep evolutionary origin. *EMBO J.*, 18(12):3451-62.

Sambrook, J., Fritsch, E.F. & Maniatis, T., 1989. *Molecular cloning: A Laboratory Manual*. Second Edition ed. Cold Spring Habor Laboratory Press.

Schekman, R. & Orci, L., 1996. Coat proteins and vesicle budding. *Science*, 271(5255):1526-33.

Schmelzle, T., Helliwell, S.B. & Hall, M.N., 2002. Yeast protein kinases and the RHO1 exchange factor TUS1 are novel components of the cell integrity pathway in yeast. *Mol Cell Biol.*, 22(5):1329-39.

Schmid, M., Jaedicke, A., Du, T.G. & Jansen, R.P., 2006. Coordination of endoplasmic reticulum and mRNA localization to the yeast bud. *Curr Biol.*, 16(15):1538-43.

Schmitt, M.E., Brown, T.A. & Trumpower, B.L., 1990. A rapid and simple method for preparation of RNA from Saccharomyces cerevisiae. *Nucleic Acids Res.*, 18(10):3091-2.

Scrimale, T., Didone, L., de Mesy Bentley, K.L. & Krysan, D.J., 2009. The unfolded protein response is induced by the cell wall integrity mitogen-activated protein kinase signaling cascade and is required for cell wall integrity in Saccharomyces cerevisiae. *Mol Biol Cell.*, 20(1):164-75.

Serman, A. et al., 2007. GW body disassembly triggered by siRNAs independently of their silencing activity. *Nucleic Acids Res.*, 35(14):4715-27.

Shepard, K.A. et al., 2003. Widespread cytoplasmic mRNA transport in yeast: identification of 22 bud-localized transcripts using DNA microarray analysis. *Proc Natl Acad Sci U S A.*, 100(20):11429-34.

Sheth, U. & Parker, R., 2003. Decapping and decay of messenger RNA occur in cytoplasmic processing bodies. *Science*, pp.300(5620):805-8.

Sheth, U. & Parker, R., 2006. Targeting of aberrant mRNAs to cytoplasmic processing bodies. *Cell*, 125(6):1095-109.

Sheth, U., Pitt, J., Dennis, S. & Priess, J.R., 2010. Perinuclear P granules are the principal sites of mRNA export in adult C. elegans germ cells. *Development*, 137(8):1305-14.

Sidrauski, C. & Walter, P., 1997. The transmembrane kinase Ire1p is a site-specific endonuclease that initiates mRNA splicing in the unfolded protein response. *Cell*, 90(6):1031-9.

Sikorski, R.S. & Hieter, P., 1989. A system of shuttle vectors and yeast host strains designed for efficient manipulation of DNA in Saccharomyces cerevisiae. *Genetics*, 122(1):19-27.

Spang, A., Grein, K. & Schiebel, E., 1996. The spacer protein Spc110p targets calmodulin to the central plaque of the yeast spindle pole body. *J Cell Sci.*, 109(Pt9):2229-37.

Spang, A., Herrmann, J.M., Hamamoto, S. & Schekman, R., 2001. The ADP ribosylation factor-nucleotide exchange factors Gea1p and Gea2p have overlapping, but not redundant functions in retrograde transport from the Golgi to the endoplasmic reticulum. *Mol Biol Cell.*, 12(4):1035-45.

Squirrell, J.M. et al., 2006. CAR-1, a protein that localizes with the mRNA decapping component DCAP-1, is required for cytokinesis and ER organization in Caenorhabditis elegans embryos. *Mol Biol Cell.*, pp.17(1):336-44.

Squirrell, J.M. et al., 2006. CAR-1, a protein that localizes with the mRNA decapping component DCAP-1, is required for cytokinesis and ER organization in Caenorhabditis elegans embryos. *Mol Biol Cell.*, 17(1):336-44.

St Johnston, D., 2005. Moving messages: the intracellular localization of mRNAs. *Nat Rev Mol Cell Biol.*, 6(5):363-75.

Stahl, G. et al., 2004. Translational accuracy during exponential, postdiauxic, and stationary growth phases in Saccharomyces cerevisiae. *Eukaryot Cell.*, 3(2):331-8.

Stearns, T., Kahn, R.A., Botstein, D. & Hoyt, M.A., 1990. ADP ribosylation factor is an essential protein in Saccharomyces cerevisiae and is encoded by two genes. *Mol Cell Biol.*, 10(12):6690-9.

Stephens, S.B. et al., 2005. Stable ribosome binding to the endoplasmic reticulum enables compartment-specific regulation of mRNA translation. *Mol Biol Cell.*, 16(12):5819-31.

Stewart, M.S., Krause, S.A., McGhie, J. & Gray, J.V., 2007. Mpt5p, a stress tolerance- and lifespan-promoting PUF protein in Saccharomyces cerevisiae, acts upstream of the cell wall integrity pathway. *Eukaryot Cell.*, 6(2):262-70.

Stoecklin, G. et al., 2004. MK2-induced tristetraprolin:14-3-3 complexes prevent stress granule association and ARE-mRNA decay. *EMBO J.*, 23(6):1313-24.

Stoltenburg, R., Wartmann, T., Kunze, I. & Kunze, G., 1995. Reliable method to prepare RNA from free and membrane-bound polysomes from different yeast species. *Biotechniques*, 18(4):564-68.

Storici, F., Lewis, L.K. & Resnick, M.A., 2001. In vivo site-directed mutagenesis using oligonucleotides. *Nat Biotechnol.*, 19(8):773-6.

Sweet, T.J. et al., 2007. Microtubule disruption stimulates P-body formation. *RNA*, 13(4):493-502.

Swisher, K.D. & Parker, R., 2010. Localization to, and effects of Pbp1, Pbp4, Lsm12, Dhh1, and Pab1 on stress granules in Saccharomyces cerevisiae. *PLoS One*, 5(4):e10006.

Tadauchi, T., Matsumoto, K., Herskowitz, I. & Irie, K., 2001. Post-transcriptional regulation through the HO 3'-UTR by Mpt5, a yeast homolog of Pumilio and FBF. *EMBO J.*, 20(3):552-61.

Tadros, W., Westwood, J.T. & Lipshitz, H.D., 2007. The mother-to-child transition. *Dev Cell.*, 12(6):847-9.

Tagwerker, C. et al., 2006. A tandem affinity tag for two-step purification under fully denaturing conditions: application in ubiquitin profiling and protein complex identification combined with in vivocross-linking. *Mol Cell Proteomics.*, 5(4):737-48.

Takizawa, P.A. et al., 1997. Actin-dependent localization of an RNA encoding a cell-fate determinant in yeast. *Nature*, 389(6646):90-3.

Tanaka, K.J. et al., 2006. RAP55, a cytoplasmic mRNP component, represses translation in Xenopus oocytes. *J Biol Chem.*, 281(52):40096-106.

Tarun, S.Z.J. & Sachs, A.B., 1995. A common function for mRNA 5' and 3' ends in translation initiation in yeast. *Genes Dev.*, 9(23):2997-3007.

Teixeira, D. & Parker, R., 2007. Analysis of P-body assembly in Saccharomyces cerevisiae. *Mol Biol Cell.*, 18(6):2274-87.

Teixeira, D. et al., 2005. Processing bodies require RNA for assembly and contain nontranslating mRNAs. *RNA*, 11(4):371-82.

Terribilini, M. et al., 2007. RNABindR: a server for analyzing and predicting RNA-binding sites in proteins. *Nucleic Acids Res.*, 35:W578-W584.

Tharun, S. et al., 2000. Yeast Sm-like proteins function in mRNA decapping and decay. *Nature*, 404(6777):515-8.

Tharun, S., Muhlrad, D., Chowdhury, A. & Parker, R., 2005. Mutations in the Saccharomyces cerevisiae LSM1 gene that affect mRNA decapping and 3' end protection. *Genetics*, 170(1):33-46$.

Tharun, S. & Parker, R., 2001. Targeting an mRNA for decapping: displacement of translation factors and association of the Lsm1p-7p complex on deadenylated yeast mRNAs. *Mol Cell.*, 8(5):1075-83.

Thomas, M.G. et al., 2009. Mammalian Staufen 1 is recruited to stress granules and impairs their assembly. *J Cell Sci.*, 122(4):563-73.

Tourrière, H. et al., 2003. The RasGAP-associated endoribonuclease G3BP assembles stress granules. *J Cell Biol.*, 160(6):823-31.

Towbin, H., Staehelin, T. & Gordon, J., 1979. Electrophoretic transfer of proteins from polyacrylamide gels to nitrocellulose sheets: procedure and some applications. *Proc Natl Acad Sci U S A.*, 76(9):4350-4.

Trautwein, M., 2004. *The small GTPase Arf1p from Saccaromyces cerevisiae goes new ways - Novel roles in mRNA transport and in the formation of specialized vesicles from the Golgi*. Dissertation.

Trautwein, M., Dengjel, J., Schirle, M. & Spang, A., 2004. Arf1p provides an unexpected link between COPI vesicles and mRNA in Saccharomyces cerevisiae. *Mol Biol Cell.*, 15(11):5021-37.

Trautwein, M. et al., 2006. Arf1p, Chs5p and the ChAPs are required for export of specialized cargo from the Golgi. *EMBO J.*, 25(5):943-54.

Tritschler, F. et al., 2009. Structural basis for the mutually exclusive anchoring of P body components EDC3 and Tral to the DEAD box protein DDX6/Me31B. *Mol Cell.*, 33(5):661-8.

Tritschler, F. et al., 2008. Similar modes of interaction enable Trailer Hitch and EDC3 to associate with DCP1 and Me31B in distinct protein complexes. *Mol Cell Biol.*, 28(21):6695-708.

Tsai, N.P., Ho, P.C. & Wei, L.N., 2008. Regulation of stress granule dynamics by Grb7 and FAK signalling pathway. *EMBO J.*, 27(5):715-26.

Tsai, P.C. et al., 2008. Afi1p functions as an Arf3p polarization-specific docking factor for development of polarity. *J Biol Chem.*, 283(24):16915-27.

Ulbricht, R.J. & Olivas, W.M., 2008. Puf1p acts in combination with other yeast Puf proteins to control mRNA stability. *RNA*, 14(2):246-62.

Unsworth, H. et al., 2010. mRNA escape from stress granule sequestration is dictated by localization to the endoplasmic reticulum. *FASEB J.*, [Epub ahead of print].

Van Wuytswinkel, O. et al., 2000. Response of Saccharomyces cerevisiae to severe osmotic stress: evidence for a novel activation mechanism of the HOG MAP kinase pathway. *Mol Microbiol.*, 37(2):382-97.

Vasudevan, S. & Peltz, S.W., 2001. Regulated ARE-mediated mRNA decay in Saccharomyces cerevisiae. *Mol Cell.*, 7(6):1191-200.

Verna, J. et al., 1997. A family of genes required for maintenance of cell wall integrity and for the stress response in Saccharomyces cerevisiae. *Proc Natl Acad Sci U S A.*, 94(25):13804-9.

Wach, A., Brachat, A., Pöhlmann, R. & Philippsen, P., 1994. New heterologous modules for classical or PCR-based gene disruptions in Saccharomyces cerevisiae. *Yeast*, 10(13):1793-808.

Walter, P. & Blobel, G., 1981. Translocation of proteins across the endoplasmic reticulum III. Signal recognition protein (SRP) causes signal sequence-dependent and site-specific arrest of chain elongation that is released by microsomal membranes. *J Cell Biol.*, 91(2 Pt 1):557-61.

Wang, C.W., Hamamoto, S., Orci, L. & Schekman, R., 2006. Exomer: A coat complex for transport of select membrane proteins from the trans-Golgi network to the plasma membrane in yeast. *J Cell Biol.*, 174(7):973-83.

Wang, Y. et al., 2002. Precision and functional specificity in mRNA decay. *Proc Natl Acad Sci U S A.*, 99(9):5860-5.

Weber, V. et al., 1997. Purification and nucleic-acid-binding properties of a Saccharomyces cerevisiae protein involved in the control of ploidy. *Eur J Biochem.*, 249(1):309-17.

Wickens, M., Bernstein, D.S., Kimble, J. & Parker, R., 2002. A PUF family portrait: 3'UTR regulation as a way of life. *Trends Genet.*, 18(3):150-7.

Wilczynska, A. et al., 2005. The translational regulator CPEB1 provides a link between dcp1 bodies and stress granules. *J Cell Sci.*, 118(5):981-92.

Wilhelm, J.E., Buszczak, M. & Sayles, S., 2005. Efficient protein trafficking requires trailer hitch, a component of a ribonucleoprotein complex localized to the ER in Drosophila. *Dev Cell.*, 9(5):675-85.

Yahara, N., Ueda, T., Sato, K. & Nakano, A., 2001. Multiple roles of Arf1 GTPase in the yeast exocytic and endocytic pathways. *Mol Biol Cell.*, pp.12(1):221-38.

Yanagitani, K. et al., 2009. Cotranslational targeting of XBP1 protein to the membrane promotes cytoplasmic splicing of its own mRNA. *Mol Cell.*, 34(2):191-200.

Yang, S., Ayscough, K.R. & Drubin, D.G., 1997. A role for the actin cytoskeleton of Saccharomyces cerevisiae in bipolar bud-site selection. *J Cell Biol.*, 136(1):111-23.

Yang, H.C. & Pon, L.A., 2002. Actin cable dynamics in budding yeast. *Proc Natl Acad Sci U S A.*, 99(2):751-6.

Yang, R., Wek, S.A. & Wek, R.C., 2000. Glucose limitation induces GCN4 translation by activation of Gcn2 protein kinase. *Mol Cell Biol.*, 20(8):2706-17.

Yoshimoto, H. et al., 2002. [Online] Available at: http://www.stanford.edu/group/cyert/CNCRZ.tab2.txt [Accessed 21 April 2010].

Yoshimoto, H. et al., 2002. Genome-wide analysis of gene expression regulated by the calcineurin/Crz1p signaling pathway in Saccharomyces cerevisiae. *J Biol Chem.*, 277(34):31079-88.

Zeitelhofer, M., Macchi, P. & Dahm, R., 2008. Perplexing bodies: The putative roles of P-bodies in neurons. *RNA Biol.*, 5(4):244-8.

Zewail, A.H., 2008. *Physical Biology: From Atoms to Medicine*. Imperial College Press.

Zhang, S., Guo, Y. & Boulianne, G., 2001. Identification of a novel family of putative methyltransferases that interact with human and Drosophila presenilins. *Gene*, (280(1-2):135-44).

Zhu, W. et al., 1996. Bcl-2 mutants with restricted subcellular location reveal spatially distinct pathways for apoptosis in different cell types. *EMBO J.*, 15(16):4130-41. ActA localization to mitos.

Zipor, G. et al., 2009. Localization of mRNAs coding for peroxisomal proteins in the yeast, Saccharomyces cerevisiae. *Proc Natl Acad Sci U S A.*, 106(47):19848-53.